

# **DESIGN OF A SEMI-AUTOMATED LIDAR POINT CLASSIFICATION FRAMEWORK**

**KRISTA AMOLINS**

**April 2016**



**TECHNICAL REPORT  
NO. 302**

**DESIGN OF A SEMI-AUTOMATED  
LIDAR POINT CLASSIFICATION  
FRAMEWORK**

Krista Amolins

Department of Geodesy and Geomatics Engineering  
University of New Brunswick  
P.O. Box 4400  
Fredericton, N.B.  
Canada  
E3B 5A3

April 2016

© Krista Amolins, 2016

## PREFACE

This technical report is a reproduction of a dissertation submitted in partial fulfillment of the requirements for the degree of Doctor of Philosophy in the Department of Geodesy and Geomatics Engineering, April 2016. The research was supervised by Dr. David Coleman, and funding was provided by the Natural Sciences and Engineering Research Council of Canada (NSERC).

As with any copyrighted material, permission to reprint or quote extensively from this report must be received from the author. The citation to this work should appear as follows:

Amolins, Krista (2016). *Design of a Semi-Automated LiDAR Point Classification Framework*. Ph.D. dissertation, Department of Geodesy and Geomatics Engineering, Technical Report No. 302, University of New Brunswick, Fredericton, New Brunswick, Canada, 237 pp.

## **ABSTRACT**

Data from airborne light detection and ranging (LiDAR) systems are becoming more commonplace and are being used in applications other than traditional remote sensing and GIS applications, such as for archaeological surveys. However, non-expert LiDAR users face challenges when working with LiDAR data or derived products. Anecdotal evidence suggests that many users may not have much knowledge of how a LiDAR product was derived or the qualities of the original LiDAR point cloud. In addition, suitable processing software may not be accessible due to cost or may require extensive training and familiarity with the tools for users to achieve their desired results.

This thesis addresses some of the challenges non-expert LiDAR users may face by developing a semi-automated point classification framework that does not require expert user input to classify individual points within the point cloud. The Canadian Airborne LiDAR Acquisition Guideline, released by Natural Resources Canada in 2014, was used as a guide in the development process. The framework consists of a multi-stage classification process that can be applied using LiDAR point clouds exclusively or using LiDAR data integrated with other types of data. Code developed as part of this thesis to implement the framework is hosted in a repository on Bitbucket.

The first stage is a ground point identification process that requires little or no operator input to classify ground points within a LiDAR point cloud. It achieved greater than 95% accuracy in sample tests, as compared to available classified ground data. Subsequent stages add or refine classification of points within the

point cloud. If only LiDAR data are used, points are classified as building/structure, low vegetation, medium vegetation, high vegetation, unpaved ground, road or paved surface, or points above paved surface. Points that do not meet the criteria for any of the classes are left unclassified. Additional data can be introduced at any stage to improve processing time; add classes, for example, water; or refine results.

Recommendations for future research include making greater use of 3D data structures, making greater use of point level information, and improving methods used to refine classification results.

## **DEDICATION**

For all those who never doubted I would get to the end, and

For those dear to my heart who passed away too soon.

## **ACKNOWLEDGEMENTS**

I would like to thank my supervisor, Dr. David Coleman, for all his advice and support throughout the long process of completing this research, for giving me the opportunity to try my hand at teaching – which let me dive more deeply into the subject of LiDAR than I otherwise would have, and for allowing me to sometimes devote more of my time to student politics than to my research.

I would also like to thank the Natural Sciences and Engineering Research Council for their financial support; New Brunswick Department of Public Safety for providing LiDAR data for Fredericton; and DJ Lehto at GeoDigital International for sharing data for both testing and fun.

Finally, I would like to thank my family, for believing in me and supporting me through all the years that I was so far from home.

# TABLE OF CONTENTS

	Page
Abstract.....	ii
Dedication.....	iv
Acknowledgements.....	v
Table of Contents.....	vi
List of Figures .....	x
List of Tables.....	xiv
List of Abbreviations .....	xv
1. INTRODUCTION.....	1
1.1. Research Purpose .....	3
1.2. Thesis Objectives.....	7
1.3. Thesis Organization .....	8
2. OVERVIEW OF CONCEPTS AND DISCUSSION OF RELATED LITERATURE .....	12
2.1. Fundamentals.....	12
2.1.1. Principles of Airborne LiDAR.....	13
2.1.2. Research Definitions .....	14
2.1.3. Data Handling Techniques.....	15
2.2. Surface Generation .....	20
2.2.1. Digital Terrain Models .....	21
2.2.2. LiDAR Data Interpolation .....	23
2.3. Classification Methods.....	25
2.3.1. Basic Filtering.....	26
2.3.2. Classification of LiDAR Data .....	28
2.3.3. Augmenting Classification with LiDAR Data .....	31
2.3.4. Identifying Features.....	33
2.4. Data Fusion and Integration .....	36
2.5. Comparison of Existing Standards and Guidelines .....	38
2.5.1. Canadian LiDAR Acquisition Guideline .....	39
2.5.2. Australian Acquisition Specifications.....	44



2.5.3. USGS NGP Lidar Guidelines and Base Specification .....	45
2.5.4. Comparative Strengths and Weaknesses.....	47
2.6. Summary of Relevant Concepts .....	48
3. METHODS AND DATA SETS .....	50
3.1. Data Measures .....	50
3.1.1. Height Measures .....	51
3.1.2. Non-Height Measures .....	53
3.2. Data Sources .....	60
3.2.1. Data for the City of Fredericton, N.B. ....	60
3.2.2. Online LiDAR Databases .....	64
3.3. Chapter Summary.....	66
4. GROUND POINT IDENTIFICATION .....	67
4.1. Purpose for Ground Extraction.....	67
4.2. Ground Detection Techniques.....	70
4.2.1. Pixel Connectedness .....	72
4.2.2. Point Neighbourhood .....	76
4.2.3. Wavelet Detail Mask .....	80
4.2.4. Preliminary Ground Points.....	83
4.3. Surface comparison technique .....	84
4.4. Ground Point Classification and Refinement.....	88
4.5. Testing and Accuracy .....	91
4.5.1. Accuracy Assessment.....	93
4.6. Summary of GPI Process .....	98
5. CLASSIFICATION OF SINGLE SOURCE LIDAR DATA SETS.....	100
5.1. Preliminary Classification .....	103
5.1.1. Terrain Ruggedness Index Thresholding .....	103
5.1.2. Multiple Returns and Height Measures Masking.....	107
5.1.3. Limitations.....	108
5.2. Building Classification .....	112
5.3. Uncertainty and Declassification .....	115
5.4. High Vegetation Classification .....	117
5.5. Roads, Low Vegetation and Objects Above Road.....	119
5.6. Reminders and Accuracy .....	121
5.6.1. Sample Classification Results.....	124
5.6.2. Classification Accuracy Assessment .....	126

5.7. Summary of MSPC Process.....	136
6. CLASSIFICATION OF LIDAR DATA USING MULTIPLE DATA SOURCES.....	137
6.1. Existing Tools .....	138
6.2. Assessing Data Integration.....	140
6.3. Augmented Ground Extraction .....	142
6.4. Water Classification.....	146
6.5. Building Footprints.....	150
6.6. Road Centrelines.....	154
6.7. Multi-Temporal Data .....	158
6.8. Summary of Integrated Classification.....	163
7. CONCLUSION AND RECOMMENDATIONS .....	165
7.1. Ground Point Identification.....	167
7.2. Classification of Single LiDAR Data Sets .....	169
7.3. Classification of LiDAR Data using Multiple Data Sources .....	171
7.4. Recommendations for Future Work.....	174
References.....	177
A. Pseudocode for GPI and MSPC implementation .....	193
A.1. Ground Point Identification Process .....	194
A.1.1. Pixel Connectedness .....	194
A.1.2. Point Neighbourhood .....	195
A.1.3. Wavelet Detail Mask.....	198
A.1.4. Preliminary Ground .....	199
A.1.5. Surface comparison technique .....	200
A.2. Multi-Stage Point Classification .....	201
A.2.1. Preliminary Classification .....	202
A.2.2. Building Classification .....	204
A.2.3. Uncertainty.....	205
A.2.4. High Vegetation .....	207
A.2.5. Roads and Low Vegetation .....	208
A.2.6. Object Above Roads .....	209
A.2.7. Water Classification .....	209
A.3. Utility Scripts .....	210
A.3.1. Fill .....	211
A.3.2. Grid.....	212
A.3.3. Clean.....	213

B.	Additional Images.....	215
B.1.	Measure Illustrations.....	216
B.1.1.	Height Measures .....	216
B.1.2.	Non-Height Measures .....	218
B.2.	GPI Output Samples .....	222
C.	Integration Assessments.....	226
C.1.	Raster-to-Raster.....	227
C.2.	Raster-to-Point.....	230
C.3.	Point-to-Point .....	232
C.4.	Horizontal Adjustment .....	235

Curriculum Vitae

## LIST OF FIGURES

1.1	Flowchart for the point classification framework .....	9
2.1	Search area definitions: a) cell boundaries; b) circle inscribed in cell; c) circle of equal area; d) circle circumscribing cell. Green points fall within search area; red points fall outside search area. ....	16
2.2	Effect of grid resolution on ground detection under forest canopy. Minimum value in cell using a) 1 m b) 3 m and c) 5 m resolution. ....	18
3.1	Example of three band ground-vegetation ratio representation. ....	57
3.2	Interpolation of all LiDAR points in the Odell Park study area. ....	62
4.1	Flowchart for the Ground Point Identification process. ....	71
4.2	Four combined binary raster layer images show bands where terrain elevation gradually increases and isolated groups of cells belonging to non-terrain objects at lower terrain elevations. ....	74
4.3	Results of the Pixel Connectedness method using two different slope thresholds: a) 10° and b) 15°. ....	76
4.4	Probability curves for Point Neighbourhood method. ....	78
4.5	Results of the Point Neighbourhood method: a) probabilities calculated using Eq. 4.1; b) probabilities calculated using Eq. 4.2. ....	79
4.6	Results of Wavelet Detail Mask: a) wavelet details; b) masked areas contain no data while unmasked areas contain locally flat surfaces. ....	82
4.7	a) Initial ground raster with data gaps. b) Initial ground raster after gaps have been filled. ....	83
4.8	Surface comparison technique for obtaining a ground raster from a set of input ground surfaces. ....	85
4.9	Example of the output from the surface comparison technique using six input surfaces and two iterations. The resolution is 5 m. ....	87
4.10	Ground point classification and refinement process. ....	89
4.11	Sample interpolation at 2 m resolution of final ground point classification results. ....	91
4.12	Limitations in quantifying ground classification accuracy: a) point representation and b) raster representation of locations of points classified as ground by <i>LAStools</i> <sup>TM</sup> (blue), by the GPI process (orange) and by both (brown) or neither (white) method; and interpolation of ground elevation from c) <i>LAStools</i> <sup>TM</sup> results and d) GPI process results. ....	94
4.13	Location and point cloud representation of Segment 6412, within the Odell Park study area. ....	96
5.1	Flowchart for the Multi-Stage Point Classification process. Although both TRI and MMM masks may be generated for comparison, only one is used to generate a height infused building raster. ....	102

5.2	Example of a) TRI image and b) corresponding TRI mask. ....	105
5.3	Example of preliminary building classification using TRI Thresholding method. The circled area highlights small building under vegetation that remain unclassified. ....	106
5.4	Example of preliminary building classification using MMM method. ....	108
5.5	Example of a) Multiple return interpolation; b) difference between maximum and minimum values; c) minimum HAG; and d) the resulting MMM mask. In all images, black represents areas where the conditions were met. ....	109
5.6	Point cloud representation of the Centre Block of Parliament Hill in Ottawa, from data provided by GeoDigital International [Lehto, 2012a].	111
5.7	Example of building classification process from MMM results: a) classified potential building polygons; b) building mask infused with elevation values. ....	114
5.8	Illustration of uncertainty measure: a) percentage of non-ground, non-building points in a 3 x 3 window; b) percentage of ground points in a 3 x 3 window; c) resulting uncertainty mask; and d) uncertainty mask overlaid on a raster interpolation of elevation. ....	116
5.9	Example of high and medium vegetation classification results with building roof elevation included to provide context. ....	118
5.10	Example of a ground intensity histogram. Exact shape will be different for each data set. ....	120
5.11	Example of road surface, low vegetation, vehicle and other above road feature classification results. ....	121
5.12	Example of building edge classification results. In the upper image, non-edge roof points are in red; in the lower image, these points have been removed to make the edge points more visible. ....	123
5.13	Raster representation of point classification results for tile 2487_7439. ....	125
5.14	Enlarged section of classification results for tile 2487_7439. ....	126
5.15	Building classification results for Sample 7966. Top: Manual. Middle: MSPCb. Bottom: LAStools. ....	130
5.16	Building classification results for Sample 6606. Top: Manual. Middle: MSPCb. Bottom: LAStools. ....	131
5.17	Building classification results for Sample 1095. Top: Manual. Middle: MSPCb. Bottom: LAStools. ....	132
5.18	Classification results for Sample 3341. Top: Full classification using the MSPC process. Bottom: LAStools. The circled area is an example of roof points classified as vegetation by <i>LAStools</i> <sup>TM</sup> . ....	133
5.19	Classification results for Sample 3059. Top: Full classification using the MSPC process. Bottom: LAStools. ....	134
5.20	Classification results for Sample 2910. Top: Full classification using the MSPC process. Bottom: LAStools. The circled area is an example of roof points classified as ground by <i>LAStools</i> <sup>TM</sup> . ....	135

6.1	Interpolations of data from Christina River Basin, PA: a) April minimum values; b) April maximum values; c) July minimum values; d) July maximum values. ....	145
6.2	Augmented ground extraction: a) ground surface extracted from leaf-off data and b) ground points extracted from leaf-on data using leaf-off surface. ....	146
6.3	Elevation interpolation of Ottawa LiDAR data set as classified by GeoDigital: a) non-ground points and b) ground points. ....	148
6.4	Illustration of water classification using polygons, with road and building features overlaid on extracted and interpolated ground and water classes. ....	150
6.5	Elevation-infused building masks derived from a) LiDAR data and b) footprints. ....	153
6.6	Building classification results, using a) LiDAR data only and b) LiDAR data and building footprints. ....	153
6.7	Example of road surface classification results: a) using intensity threshold value of 100, all ground classes; b) using a 3 m road centreline buffer, all ground classes; c) using intensity threshold value of 100, road surface only; and d) using a 3 m road centreline buffer, road surface only. ....	156
6.8	Polyline buffers that could be used to classify streams (3 m), roads (3 m) and trails (1 m) overlaid on a) classification results and b) elevation interpolation. ....	157
6.9	Elevation differences, April data subtracted from July data. ....	159
6.10	a) Sample of 2006 LiDAR data. b) Sample of 2011 data. Some notable differences, such as building construction and destruction and tree removal, are circled. ....	161
6.11	Elevation differences, 2006 data subtracted from 2011 data. Circled areas correspond to circled areas in Figure 6.10. ....	162
B.1	Sample height above ground surface. a) DSM b) DEM c) Difference between DSM and DEM. ....	216
B.2	Sample maximum minus minimum surface. a) Maximum values b) minimum values c) Difference between maximum and minimum. ....	217
B.3	a) Sample terrain ruggedness index and two masks from TRI: count of adjacent pixels with TRI less than b) 1.0 and c) 1.5. ....	217
B.4	Sample local point density image from Ottawa data. ....	218
B.5	Sample terrain slope representation for Ottawa data. ....	219
B.6	Sample multiple return density. ....	219
B.7	Sample intensity image. ....	220
B.8	Example of a land cover map derived from LiDAR data showing ground, buildings, and high vegetation. ....	221
B.9	Results from ground detection techniques: a) Pixel Connectedness, 10°; b) Pixel Connectedness, 15°; c) Point Neighbourhood, negative quadratic equation; d) Point Neighbourhood, linear equation; e) Preliminary Ground Points, filled; e) Wavelet Detail Mask, threshold $\pm 0.15$ . ....	223

B.10	Results from an application of the surface comparison technique using the surfaces in Figure B.9. a) Count criterion; b) standard deviation criterion; and c) output surface, the average of input surfaces where criteria are met. .....	224
B.11	Raster products from two iterations of the ground point classification and refinement process. a) Initial input, 5 m resolution; b) filled input; c) interpolation of ground points classified in first iteration, 2 m resolution; d) filled interpolation, input to second iteration; e) interpolation of points classified in second iteration; and f) filled surface.....	225
C.1	Result of subtracting LiDAR elevations from SNB elevations. Orange/red means SNB values are higher; blue means LiDAR values are higher.....	228
C.2	Close-up of from Figure C.1, with building footprints and SNB points added.....	229
C.3	LiDAR points within 1.5 m of Monument 7127 and their errors. ....	234
C.4	Observed horizontal offsets between a LiDAR-derived image and vector data sets. ....	236
C.5	Improved horizontal alignment can be observed after a transformation is applied to the LiDAR-derived image.....	237

## LIST OF TABLES

4.1	Summary of ground detection techniques.....	72
4.2	Error matrix for all points in randomly selected polygons.....	96
4.3	Error matrix for Polygon 6412. ....	96
5.1	Sample classification results for tile 2487_7439, without building edge classification. ....	124
5.2	Sample classification results for tile 2487_7439, with building edge classification. ....	125
6.1	Ground and building classification accuracy using MSPCb. ....	127
6.2	Ground and building classification accuracy using <i>LAStools</i> <sup>TM</sup> . ....	128
A.1	Classification Codes used in MSPC .....	202
C.1	Summary of differences for surface elevation subtracted from monument elevation.....	231
C.2	LiDAR points around Monument 7027 .....	233
C.3	LiDAR points around Monument 7127 .....	234



## LIST OF ABBREVIATIONS

ALS	airborne laser scanning
CGVD2013	Canadian Geodetic Vertical Datum of 2013
CGVD28	Canadian Geodetic Vertical Datum of 1928
CHM	canopy height model
CoF	City of Fredericton
CRB	Christina River Basin
DEM	digital elevation model
DSM	digital surface model
DTDB98	Digital Topographic Data Base - 1998
DTM	digital terrain model
FVA	fundamental vertical accuracy
GPI	ground point identification
GPS	global positioning system
GVR	ground-vegetation ratio
HAG	height above ground
ICSM	Australian Intergovernmental Committee on Surveying and Mapping
IDW	inverse distance weighting
LAS	laser file format
LiDAR	light detection and ranging
LPD	local point density
MaxMin	maximum minus minimum
mHAG	minimum height above ground
MMM	multiple returns and height measures masking
MRD	multiple return density
MSPC	multi-stage point classification
NAVD88	North American Vertical Datum of 1988
nDSM	normalized digital surface model
NDVI	normalized difference vegetation index

NES	National Elevation System
NPD	nominal point density
NPS	nominal point spacing
NRCan	Natural Resources Canada
RGB	red, green, blue
SAR	synthetic aperture radar
SNB	Service New Brunswick
TIN	triangulated irregular networks
TRI	Terrain Ruggedness Index
USGS NGP	U.S. Geological Survey National Geospatial Program
UTM	Universal Transverse Mercator
3D	three-dimensional

*"La dernière chose qu'on trouve on faisant un ouvrage, est de savoir celle qu'il faut mettre par première." "The last thing one finds out when constructing a work is what to put first."  
~ Blaise Pascal*

## **CHAPTER 1**

### **INTRODUCTION**

Light detection and ranging (LiDAR) is a tool whose importance in remote sensing has been growing since the mid-1990s. It is primarily considered a source of elevation data, with digital elevation models (DEMs) derived from LiDAR data collected through airborne laser scanning (ALS) now being used in numerous applications. Anecdotal evidence, including conference presentations (e.g., [Wittner et al. 2013]); data catalogues offering "LiDAR DEMs" with 5 m resolutions (e.g., Halifax Regional Municipality [n.d.]); and comments in the literature (e.g., Bewley et al. [2005]; Gesch [2009]; Graham [2010]), however, suggests that users may not have much knowledge of how the LiDAR product they are using was derived or the qualities of the original LiDAR point cloud.

One factor that may limit non-expert LiDAR users' knowledge and understanding of the data is differing product standards. In July 2012, Natural Resources Canada (NRCan) released a first draft of Canadian LiDAR acquisition guidelines [Natural Resources Canada, 2012]. After consultation with LiDAR user and client communities, a second draft of this document was released in October 2013 and the final version released in 2014 [Natural Resources Canada, 2014]. Henceforth, these will be referred to as the NRCan guidelines. The stated objectives of the NRCan guidelines include presenting standardized criteria for

data acquisition and derived products, and encouraging data ownership models that permit data sharing. If the NRCan guidelines are followed by all parties involved in collecting, managing, and processing LiDAR data, future products will have the potential to be integrated with other data more easily. However, they cannot necessarily be applied retroactively to existing LiDAR data sets because some of the required information may be missing or the data may not have been collected in a manner that is compatible with the new guidelines.

Another factor that may limit the uptake of LiDAR data is the availability of suitable processing software. Although numerous commercial software packages are available for visualizing and processing LiDAR data, for example *Terrasolid* [Terrasolid Oy, n.d.], *LP360* [QCoherent Software LLC, n.d.], *MARS* [Merrick & Company, n.d.] and the LAS Dataset toolset in *ArcGIS for Desktop* [Esri Inc., 2014], these can be cost-prohibitive for many potential users. Free software is often limited to viewers or has been developed for a specific purpose, such as forestry [Idaho LiDAR Consortium, n.d.]. A subset of tools in the *LAStools* [rapidlasso GmbH, n.d.] package is open source; however, the tools for classification and product derivation must be licenced. In all cases, the software may require extensive training and familiarity with the tools for users to achieve their desired results.

Making reference to the NRCan guidelines, this thesis addresses the challenges non-expert LiDAR users may have when working with the data by developing a semi-automated point classification framework that does not require expert user input to classify individual points within the point cloud. The

framework consists of a multi-stage classification process that can be used exclusively with LiDAR point clouds or with LiDAR data integrated with other types of data.

## **1.1. RESEARCH PURPOSE**

As mentioned, although there are a number of software packages available for visualizing and processing LiDAR data, these packages are not accessible to all users due to cost or complexity. The packages also may not allow data from additional sources, such as municipal data catalogues, to be used to augment the classification process. There is therefore a need for a software package that is simple to use, will classify points to the desired level of completeness, and can incorporate additional data when they are available.

One purpose for developing this LiDAR point classification framework is to create a method for processing and interpreting LiDAR data that is simple to use. Technological developments in recent years have increased the quantity and quality of available LiDAR data, and this in turn has led to the recognition that these data can be used for more than just generating DEMs. Specifically, extracting and modelling buildings and other complex features from LiDAR data are major areas of research, for example, Haala and Brenner [1999], Mumtaz and Mooney [2009], Saeedi et al. [2009], and Kabolizade et al. [2010].

The inherent three-dimensional (3D) nature of LiDAR point clouds makes them ideal bases for 3D modelling. Advances and innovations in LiDAR systems, including, for example, an increase in the amount of data recorded per emitted

pulse, returned pulse intensity recorded along with range, and increased pulse repetition rates and scanners with multiple lasers operating simultaneously have increased the potential point density ([Wehr and Lohr, 1999; Mallet and Bretar, 2009; Morsdorf et al., 2009]). They have also contributed to the amount of information contained in, and therefore that can be extracted from, LiDAR point clouds. However, other inherent characteristics, such as high data volume and quasi-random sampling of ground and surfaces, create challenges for processing and interpreting the data, including the challenge of having to handle very large volumes of data.

It is not uncommon for researchers in other fields to discuss findings that rely on LiDAR-derived DEMs while failing to speak to the vertical accuracy of the DEMs, the spatial characteristics of the original point cloud, or the process through which the ground surface was extracted, all of which may impact heavily on the research findings (e.g., Hiltz [2012]; Mouland et al. [2012]). This is likely due to a widespread perception that LiDAR data provide a highly detailed and sufficiently accurate representation of the ground surface, even under vegetation cover, regardless of how the data were collected or what form that representation takes. A process that is simple to apply, in the sense that it does not require expert user input, can help researchers gain an understanding of the LiDAR data.

Another purpose for developing this LiDAR point classification framework is to create a point classification process that will classify LiDAR data to a desired level of completeness. For LiDAR data, the lowest level of classification

completeness is ground and non-ground. This is sufficient for applications where only the ground surface is required, such as watershed analysis. A more complete classification of LiDAR data is needed to extract information for other applications, such as building extraction (classify building points within the non-ground subset); biomass estimation (classify tree canopy points with the non-ground subset); or road network modelling (classify road points within the ground subset).

There are many approaches to classifying LiDAR data. Some involve first interpolating the elevation (or intensity) measurements to a regular grid, which allows them to be easily combined with aerial or satellite imagery. Others involve working directly with the point cloud, but produce results that show the scene reduced to two-dimensional patches that are marked as part of the ground surface or of an object of interest. In either case, the inherent 3D nature of the data is being underused. While single returns are generated from pulses that fall in open areas, multiple returns are generated in vertically structured areas and contain more detailed information that can be exploited. For example, identifying double returns from rooftop edges helps to delineate more exactly the location of a building. A point classification process retains all of the 3D information captured within a LiDAR point cloud.

A final purpose for developing this LiDAR point classification framework is to create a process that can incorporate additional data when they are available and can augment single-source LiDAR data. Studies have suggested that LiDAR is the most cost-effective technology for acquiring elevation data for floodplain

mapping [US National Research Council, 2007] yet each LiDAR point cloud is wholly unique. Even small, and unavoidable, variations in trajectory, platform orientation, laser scan angle, and other flight parameters result in a distinct sampling of the same terrain and features that cannot be assumed to be suitable for floodplain mapping, or any specific application. Incorporating data from additional sources may help to ascertain the suitability of a LiDAR data set. It can also produce products that combine the unique temporal and spatial characteristics of each data set.

The products that result from merging data from disparate data sets may allow faster processing or provide greater detail, whether vertical, horizontal, or object-oriented, than the individual components and can allow trends and patterns to be observed over time as technology evolves. In this context, disparate data sets could mean data sets collected using different sensor types (e.g., LiDAR data and remote sensing imagery), different sensor parameters (e.g., imagery from different satellites), different collection parameters (e.g., separate LiDAR flights), or any or all of the above. The data sets could have different spatial resolutions, different accuracies, and could be in different coordinate systems. The source differences must be identified, assessed, and resolved before the data can be successfully merged and used in combination. This includes the effects of variations on point spacing and point density, and, in turn, the effects of variations in point spacing and point density on point cloud processing and derived products.

Combining multispectral imagery with LiDAR data is perhaps the most



prevalent integration technique, at least when the objective is classification (e.g., Mancini et al. [2009]; Salah et al., 2009; [Guo et al., 2011]). Although airborne LiDAR data have some advantages over aerial and satellite imagery, the imagery also have advantages over airborne LiDAR data. Combining newer LiDAR data sets with older DEMs and contour lines, rather than simply replacing the old with the new to fill in gaps, increase the resolution, or update reference data, is also becoming more common than in the past (e.g. Reiss [2002]; [Zhang J. , 2010]; Schindler et al. [2011]). LiDAR survey firms, enabled by LiDAR equipment manufacturers offering "a full line of aerial digital cameras" [Optech, n.d.], may collect imagery simultaneously with LiDAR data. A process in which additional data may be incorporated at any stage can lead to an end product that combines the best properties of each available data source.

## **1.2. THESIS OBJECTIVES**

To reiterate, there is a need for a software package that is simple to use, will classify points to the desired level of completeness, and can incorporate additional data when they are available. In order to extract information from the LiDAR point cloud, a complete, in the context of the specific application, and accurate classification of LiDAR data is needed. Classification levels and accuracy for each level are defined in Section 4 of the NRCan guidelines; however, for a building assessment application, for example, "complete" may require only ground and building classification.

To make use of the unique temporal and spatial characteristics of disparate

data sets, namely LiDAR data with ancillary data, in such a way that the classification results are enhanced in terms of completeness or accuracy, source differences must be identified, assessed, and resolved before the data can be successfully integrated.

Hence, the objectives of this thesis are to:

1. Develop a ground point identification (GPI) process that achieves 95% point classification accuracy.
2. Develop a semi-automated multi-stage point classification (MSPC) process to classify points as "building/structure", "medium vegetation" and "high vegetation", and separate ground points into "low vegetation", "road (or paved) surface", and "other ground". High point classification accuracy for all classes should be visually verifiable and, where adequate truth exists for point classification, numerically as 90% correct or better.
3. Propose and develop measures to assess the quality of data integration results.
4. Develop, implement, and test strategies for integrating disparate data sets, specifically additional elevation data and feature vector data, into the LiDAR point classification framework.

### **1.3. THESIS ORGANIZATION**

In order to achieve these objectives and satisfy the purpose that underlies them, the remainder of this thesis is organized into six chapters. The flowchart in Figure 1.1 shows the relationship between the objectives stated above and the

thesis chapters.

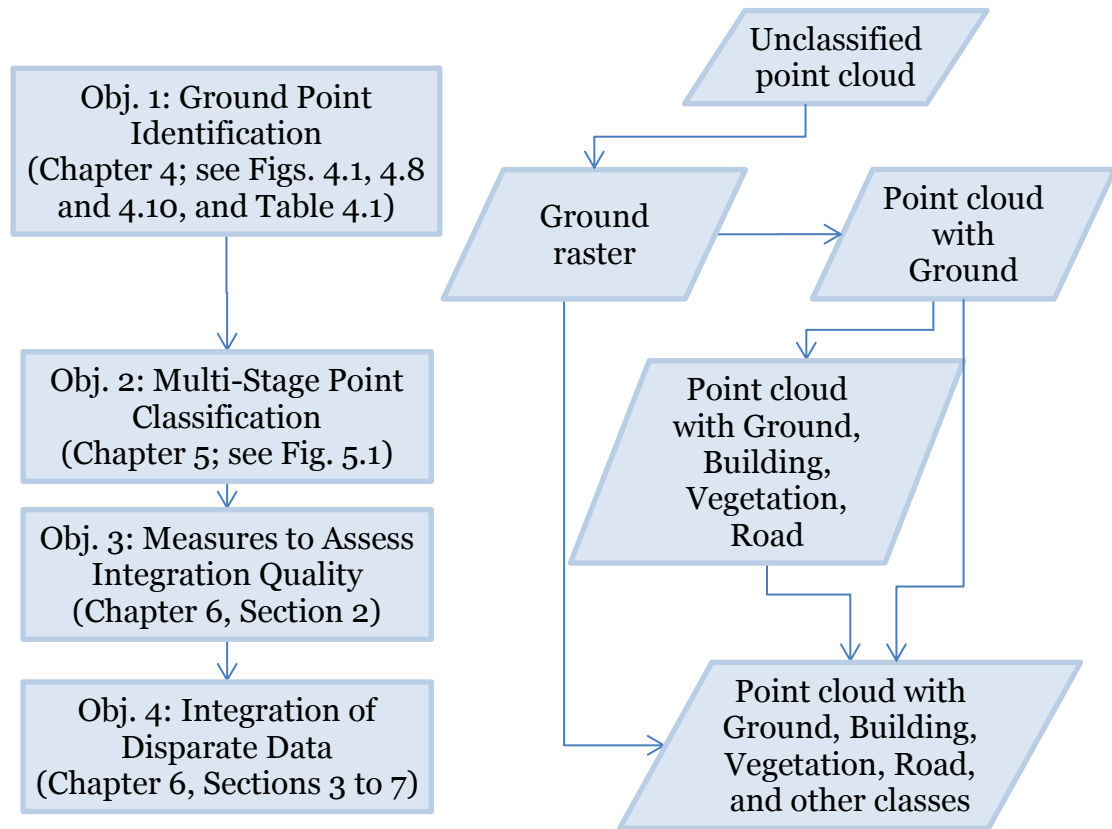


Figure 1.1  
Flowchart for the point classification framework.

The chapters are summarized as follows:

Chapter 2 gives an overview of literature relevant to the research. This includes successes and limitations of existing classification methods, examples of LiDAR data integration, and the comparison of the NRCAN guidelines to guidelines from other countries.

Chapter 3 presents a discussion of the measures and methods that were used in this research, in the context of the NRCAN guidelines. It also describes the data sets used in testing.

Chapter 4 details the ground point identification process developed by the author, including an accuracy assessment. GPI is comprised of ground detection techniques, a surface comparison technique, and a point classification process. The GPI process can be fully automated or the user may choose to set parameters for the ground detection techniques employed, select different surfaces to include in the comparison, and adjust what is deemed to be a significant change in the point classification.

Chapter 5 describes the multi-stage classification process developed by the author to classify LiDAR points into seven additional classes using a single LiDAR data set. It also includes accuracy assessments. The MSPC process can be fully automated, require the user to select between two measures in the initial stage and set one threshold in a later stage, or allow manual refinement and adjustment of parameters.

Chapter 6 discusses using other data sources to improve classification results and/or processing time, including factors to consider when combining data from multiple sources, and also briefly discusses to potential benefits of multi-temporal LiDAR data.

Chapter 7 gives conclusions and recommendations, with a review and analysis of accomplished tasks with respect to the measurable objectives, and provides recommendations for future work.

With the exception of data visualization and the application of a few basic GIS functions, particularly vector data manipulation, all of the work carried out as part of this research made use of code developed by the author in the C

programming language. This includes code to implement and test the ground point identification process and the multi-stage point classification process. Due to space and readability considerations, the core functionality of the developed code is included as pseudocode in Appendix A. The full code can be found in a repository on Bitbucket<sup>1</sup> at <https://bitbucket.org/kamolins/thesiscode>.

---

<sup>1</sup> Bitbucket is a code management and collaboration service. Cloud hosting is free for individuals. <https://bitbucket.org/>

*"Pereant, inquit, qui ante nos nostra  
dixerunt." "Confound those who have made  
our comments before us."*

*~ Aelius Donatus*

## **CHAPTER 2**

### **OVERVIEW OF CONCEPTS AND DISCUSSION OF RELATED LITERATURE**

This chapter contains an overview of concepts, literature, and resources directly related to the research in this thesis. The first section briefly presents principles of LiDAR, provides definitions for important terminology as used in this research, and discusses data management techniques that were employed. The next sections discuss examples from literature on surface generation, data classification, and data integration. The final section provides a comparison of existing LiDAR acquisition guidelines.

#### **2.1. FUNDAMENTALS**

As previously mentioned, those who use LiDAR data may only use elevation products derived from LiDAR and may not have any knowledge of the properties of the point cloud. Yet, understanding basic principles of LiDAR is critical to understanding the limitations of any derived products. A brief overview of the principles of airborne LiDAR, along with definitions of terminology and data handling techniques as used in the thesis, is therefore presented here.

### **2.1.1. Principles of Airborne LiDAR**

The basis of LiDAR systems is laser ranging. In pulse-based systems, which are used for ALS, a laser pulse is emitted from the sensor. Any object within the laser footprint may generate a reflection, also called a return. If two or more surfaces are separated by a large enough distance in the range direction, each will generate a discrete return [Petrie and Toth, 2008]. These multiple returns can provide data from within tree canopies and can be helpful in locating boundaries between features.

Each pulse emitted from the sensor has the same height (energy level or intensity) and width. The returning pulses, however, will be distorted in various ways. Different materials have different reflectivity properties: snow and vegetation, for example, will reflect more of the energy back to the sensor than asphalt and concrete [Wehr and Lohr, 1999]. The intensity of each return is recorded along with the distance to the target. When LiDAR data are displayed using intensity values instead of, or as modulators of, elevation values, more feature details may be visible.

Detailed platform position and orientation measurements are taken throughout a survey so that the collected range and scan angle data can be accurately transformed into three dimensional coordinates. Although pulses are emitted at a constant rate and the scanning mechanism moves in a known pattern, small variations in platform speed, position, orientation, etc., as well as variations in terrain and feature height will cause deviations from the theoretical as to where pulses actually fall [Baltsavias, 1999b].

### **2.1.2. Research Definitions**

Deviations from the theoretical also exist, in a certain sense, in the terminology. While the use of some terms is consistent across the literature, the use of other terms can vary according to personal preference, institutional preference, suitability, or other factors. For this reason, key terms for the research in this thesis are defined here:

Classification: "the action or process of classifying something according to shared qualities or characteristics" [Apple Dictionary, n.d.].

Extraction: "the action of taking out something, esp. using effort or force." ORIGIN late Middle English: via Old French from late Latin *extractio(n-)*, from Latin *extrahere* 'draw out' [Apple Dictionary, n.d.].

Filtering: "removing unwanted measurements, as in the case of finding ground surface from a mixture of ground and vegetation measurements" [Axelsson, 1999]

This research focuses on point cloud classification, that is, on retaining the full point cloud while injecting into it information about the features. A classified point cloud will have points marked as ground, building, vegetation, and/or other classes. Any of these classes can be extracted from the point cloud, for example, to create a ground surface representation or a point cloud containing only building points. Information is extracted from the point cloud for use in the classification process but the final product is the classified point cloud and not



any derived products. Similarly, points may be filtered out of a class but remain in the point cloud.

### **2.1.3. Data Handling Techniques**

One of the greatest challenges when working with LiDAR is the very large volume of data, which are not necessarily organized in a way that allows the characteristics of a single point to be analyzed in the context of all geographically neighbouring points. A standard file exchange format for LiDAR data is the American Society of Photogrammetry and Remote Sensing (ASPRS) LASer (LAS) file format specification [LAS Working Group, n.d.]. The latest version, LAS 1.4, approved in November 2011, includes many changes and additions to address the challenges of accessing, manipulating, and storing large volumes of data and information without altering the point cloud. It also allows for the inclusion of supplemental information, such as red, green, blue and near-infrared colourization values obtained from auxiliary optical sensors, to be stored for each point, and defines 18 standard point classes, including four specific to power transmission structures [Graham, 2012a].

Although the LAS specification provides a standard for data storage, additional data handling techniques are needed to work with the data. Two basic data handling techniques were employed for ground point identification and all further classification in this work: regular interpolation and voxel sorting.

### 2.1.3.1. Regular Interpolation

For LiDAR data, "regular interpolation" is a process of aggregating the point data into a two-dimensional grid of equal-sized cells. The search area for selecting points to aggregate for each cell can be defined in number of different ways, including:

1. The boundaries of the cell.
2. The perimeter of a circle inscribed in the cell.
3. The perimeter of a circle of area equal to that of the cell.
4. The perimeter of a circle circumscribing the cell.

Each of these is illustrated in Figure 2.1. The first search area definition is most appropriate when the output is a count, such as local point density, an extrema, or otherwise is a value representing the cell area. The other search area definitions are more appropriate when values are being averaged in some way or otherwise are meant to best represent the cell as a discrete point. The larger circular search areas ensure that there are fewer points do not fall inside any search area but also create overlaps between the search areas of adjacent cells.

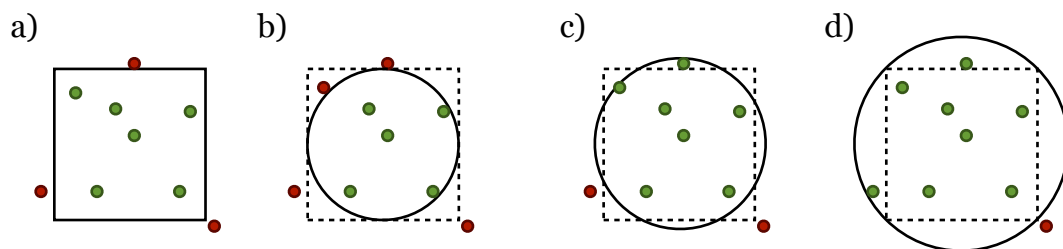


Figure 2.1

Search area definitions: a) cell boundaries; b) circle inscribed in cell; c) circle of equal area; d) circle circumscribing cell. Green points fall within search area; red points fall outside search area.

Regardless of the definition of the search area, the grid resolution selected for the interpolation can affect the results significantly. "Higher" and "lower" resolutions are relative to each data set and the distribution of points within the data set. In version 2 of the NRCan guidelines [2014], which are further described later in this chapter, there is a stated expectation that pulses are uniformly distributed throughout the collection area. This is to be verified by creating a grid with cell sizes twice the nominal pulse spacing (i.e., by using a relatively low resolution) and ensuring that at least 90% of cells contain at least one last return point. A lower percentage of cells could indicate clustering of last returns and an uneven data collection. The standard pulse spacing specified in the NRCan guidelines is 1 pulse per m<sup>2</sup>. The recommended resolution for raster products derived from a point cloud is 1 m.

A higher grid resolution can provide more detail and accuracy at the individual cell level than a lower resolution, but is also more likely to leave gaps in the resulting interpolated raster due to an increased probability that no points fall within the search area for a given cell. Lower grid resolutions, in contrast, tend to smooth out data, which can be advantageous in some circumstances. For example, part of the test area in Fredericton includes a forest that was too dense in many places for the laser to penetrate openings in the vegetation down to the ground. Figure 2.2 shows a sample of the minimum elevations in each cell at 1 m, 3 m, and 5 m resolutions. In the 1 m interpolation, many of the minimum values are "non-ground" points and so the ground surface is mostly obscured. In the 5 m interpolation, the resolution is low enough that many of those non-

ground points are eliminated, resulting in a smoother surface where the ground under the forest is mostly visible.

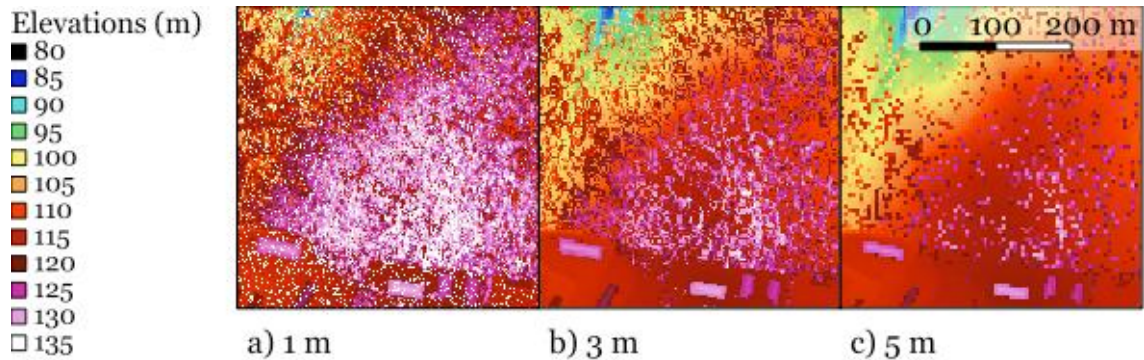


Figure 2.2

Effect of grid resolution on ground detection under forest canopy. Minimum value in cell using a) 1 m b) 3 m and c) 5 m resolution.

When the interpolation does not represent the minimum or maximum value or a count of points within the search area, some function must be applied to obtain a single value that represents all of the points in the search area. The values to be interpolated could be elevation, intensity, or some other attribute contained in the point data. One option is to calculate a simple average,  $\bar{v}$ , from the point values:

$$\bar{v} = \frac{1}{n} \sum_n v_i \quad (3.1)$$

where  $n$  is the number of points in the search area and  $v_i$  is the value of the  $i$ th point. This option is simple to implement but places equal weight on every point in the search area, regardless of the distance from the centre.

A commonly used alternative is inverse distance weighting (IDW). The basic form for IDW is:

$$v = \begin{cases} \sum_n w_i v_i / \sum_n w_i, & \text{if } d_i \neq 0 \text{ for all } i \\ v_i, & \text{if } d_i = 0 \text{ for some } i \end{cases}$$

$$w_i = d_i^{-p} \tag{3.2}$$

where  $n$  is the number of points in the search area,  $v_i$  is the value of the  $i$ th point,  $d_i$  is the distance to the  $i$ th point, and  $p$  is a number greater than zero [Shepard, 1968]. The interpolation method deemed most suitable for the circumstances was used where interpolated surfaces were required to test the ground point identification (GPI) and multi-stage point classification (MSPC) processes.

### **2.1.3.2. Voxel Sorting**

Interpolation leads to a loss of information because it reduces the data to what is commonly referred to as “2.5 dimensions” — one  $z$  value for each regularly spaced  $x$  and  $y$  coordinate pair. Data structures or techniques that maintain the three dimensions, such as using volume pixels (voxels), should be applied [Mosa et al., 2012] to preserve the inherently 3D information in the point cloud. Although voxels are not mentioned in the NRCan guidelines, voxel sorting can be used to preserve the 3D data while organizing it in such a way to allow faster access to all points within a specified neighbourhood. It is akin to the indexing performed by software such as *LP360*<sup>TM2</sup> and *LAStools*<sup>TM</sup>, but it applies the concept of voxels: equal volume, three-dimensional divisions of space [Stoker, 2009]. The space is divided into rows, columns, and layers,

---

<sup>2</sup> *LP360*<sup>TM</sup> is a licenced software product of QCoherent Software LLC.

creating voxels of specific length, width, and height. All the points within the cloud are then sorted into their respective voxels by layer (z), row (y), column (x) and transferred into a new file. By recording the number of points within each voxel along with the coordinates and the starting index for each voxel, all points near specified coordinates can be quickly and easily located in the sorted file.

The dimensions of the voxels can be equal (cube) or different (rectangular prisms). As currently implemented in the code developed for this thesis work (which is included as pseudocode in `o`), smaller voxels require a longer time to complete the sorting but this is offset by faster processing when point neighbourhoods are examined because there are fewer points in the smaller voxels.

## **2.2. SURFACE GENERATION**

Research involving LiDAR data ranges from generic ground/non-ground separation for DEM generation to highly specialized detection and modelling, for example, of power lines and curbstones. The methods a researcher proposes to accomplish his or her objectives may use only LiDAR data, imagery augmented by LiDAR data, or LiDAR data augmented by imagery or other types of data. Some algorithms are designed to work directly with 3D point clouds (e.g., Shan and Sampath [2005]; Brodu and Lague [2011]) and perhaps small local neighbourhoods (e.g., Chehata et al. [2009]), but the majority create intermediate surfaces (e.g., Forlani et al. [2006]; Miliareisis and Kokkas [2007]; Antonarakis et al. [2008]; Alexander et al. [2011]) as there is a need to identify

the structure within a point cloud before target features can be identified. The intermediate surfaces are usually representations of the ground surface but Guan et al. [2014] partitioned the point cloud into equal-sized cells and generate multi-directional cross-section-planes for each cell.

Common surfaces created are upper surfaces, or digital surface models (DSMs); ground surfaces, or digital terrain models (DTMs); and normalized DSMs (nDSMs, called height above ground or HAG in this thesis), which are calculated as the difference between DSMs and DTMs. All three types of surfaces are generated from LiDAR point clouds as part of the research in this thesis. The next sections give an overview of DTMs and an overview of LiDAR data interpolation, as found in the literature.

### **2.2.1. Digital Terrain Models**

The first use of the term DTM has been attributed to Charles L. Miller's work in the 1950s [Miller and Laflamme, 1958]. A DTM can be defined as “an ordered array of numbers that represents the spatial distribution of terrain characteristics” [Doyle, 1978]. Data used to create a DTM could be acquired from various sources, such as ground surveys, stereomodels from aerial or satellite imagery, existing maps, altimeters, or laser scanners. Two “competing” methods of representing the data are grids and triangulated irregular networks (TINs). Grids are conceptually simpler and may be simpler to generate, manipulate and integrate with other data, whereas TINs adapt to the roughness of the terrain, and are therefore arguably the more efficient alternative [Fowler

and Little, 1979], although they may also be more prone to including errors from the data.

The objective in Li [1994] was to investigate the accuracy of DTMs generated from different data models, namely contours and grids, both alone and enhanced with feature-specific data such as points along ridges and break lines. It was found that greater accuracies were achieved when the feature-specific data were included. Similarly, Florinsky [1998] found that an increased amount of information could be extracted when DTMs were combined with imagery. Before combining data sets, however, issues such as DTM resolution, accuracy, and precise superpositioning need to be resolved.

Podobnikar et al. [2000] studied integrating elevation data from different sources, including contour lines and hydrographic line and polygon data, into an existing DEM to produce one at a higher resolution. Their process includes both visual examination and statistical testing of the data to be integrated to ensure their suitability. In contrast, Reiss [2002] described an opposite approach, using photogrammetric data and methods along survey data to verify the accuracy of LiDAR data.

Podobnikar [2005] and Warriner and Mandlbürger [2005] further explored and proposed methods for generating high-quality DTMs using data from various sources, recognizing that each source has its own advantages and disadvantages and so can potentially be used as a check and/or to complement other data sources. These two papers are discussed in further detail in Section 2.4.



### **2.2.2. LiDAR Data Interpolation**

One problem that persists with point data is the question of optimum sampling, whether they are LiDAR data or data from other point sources. Sufficient points need to be acquired to represent the surface with the desired degree of accuracy, yet what is “sufficient” depends on the terrain. Algorithms have been developed to determine the optimum number of sample elevation points, for example, in a stereomodel [Ayeni, 1982]. A LiDAR data point cloud, however, consists of pseudo-randomly sampled points in three dimensions. The spacing of points in both the along-track and across-track directions is a function of the laser scan pattern but is affected by flight parameters and terrain variation [Baltsavias, 1999a]. Moreover, while any point is likely to lie in close spatial proximity to the points immediately preceding and following it in the data file, the scan pattern makes it very difficult to quickly determine if there are other points in the cloud that are similarly close. The simplest method of overcoming the problem of pseudo-random sampling is to resample the data to a regular grid; however, some information is consequently lost and there is no guarantee that key feature points will be sampled.

Zinger et al. [2002] investigated the effects of three different methods of interpolation: triangle-based linear interpolation, triangle-based nearest neighbour interpolation, and kriging. They were specifically interested in determining which method produced the best results, as determined by correlation with a reference DSM, for data from urban areas, where edges are critical since they define building outlines, roads, and other urban features. They

found that kriging produced slightly better results (approximately 1% higher correlation) than linear interpolation but acknowledged that results are dependent on the parameters chosen and also that the reference DSM may be missing details retained in the interpolations, which would negatively impact correlation.

Goulden et al. [2014] similarly investigated the effects of different interpolation methods, but also the effects of spatial resolution and specifically on watershed areas and stream networks. From their analysis, they determined that the features present in a scene must be taken into consideration when choosing the spatial resolution for a DEM, but also the purpose for using the DEM as lower resolution DEMs may provide adequate information while being easier to process.

In Cho et al. [2004], the authors used a pseudo-grid in an attempt to avoid the loss of information that comes with interpolating point data to a grid. Instead of aggregating the point data that fall within each grid cell, the cells functioned as bins that store the data of each individual point. This approach has the benefits of grid cell adjacency and also of full point detail; however, it is more complicated to process and manipulate.

More recently, some research has involved the use of voxels (volume pixels). If voxels are used simply as point aggregators, some loss of information may still occur, but less than when rasterization is applied. However, voxels can also be used to help reduce the number of points under consideration. For example, Jwa et al. [2009] used voxels in the first step of a process to detect and reconstruct

powerlines. A Hough transform and an Eigenvalue computation were applied to the points within each voxel to detect linear features and thereby identify potential powerline points.

Voxels have also been used in forestry applications. Hosoi et al. [2013] divided terrestrial LiDAR data points collected around a tree into voxels and then, starting from manually selected seed stem or large branch voxels, classified neighbouring voxels as stem, large branch, or small branch in an iterative process. The set of classified voxels were then merged to create a solid model of the tree. Voxels were also used by Musselman et al. [2013] to create a model but from airborne LiDAR data points and to represent the canopy structure rather than an individual tree. A traversal algorithm was then applied to the voxel space for rays of varying slopes and directions as a way to estimate how solar beams are transmitted through the canopy.

In Chen et al. [2014], multiple scales were used to improve detection and reconstruction of building roofs. A large scale (cell size two to three times the average point spacing) was used in the identification of non-ground points, from which building seed regions are detected. A small scale (cell size half the average point spacing) was used to avoid losing of data and detect building features. They found that this approach could be applied successfully in complex urban environments.

### **2.3. CLASSIFICATION METHODS**

LiDAR data are being utilized to classify land cover and land use. Height

information from the points can be used to discriminate between ground and non-ground, and to further discriminate between buildings and vegetation. Objects and features can be visually identified within LiDAR data, whether they are displayed as a 3D point cloud or rasterized, and from both elevation and intensity values. To make different terrain and feature characteristics more easily visible, different surfaces can be derived from the data, such as bare-earth DTMs, DSMs, HAG, slope, aspect, and others, and assigning sets of these surfaces to red, green, and blue colour channels to create an image [Stoker, 2010]. However, the patterns that are recognizable to the human eye often have subtle variations that create challenges for automated object and feature recognition. The following sections discuss examples of filtering methods, classification approaches and feature identification.

### **2.3.1. Basic Filtering**

Filtering entails removing unwanted points. One filtering task that is common to most LiDAR classification and interpretation processes is separating ground from non-ground points [Axelsson, 1999]; whether it is the ground points that are being filtered or the non-ground points depends on the end goal for the filtering. Generally, a sudden change in elevation can be expected when moving from ground to object (positive slope) or from object to ground (negative slope) and this concept is commonly exploited in data filtering algorithms.

The main problem with slope-based filtering is that it performs poorly in areas where the terrain is steep, particularly if it is covered by vegetation. This is

observed in Sithole and Vosselman [2004], which compares the performance of filtering methods from eight different participants in a variety of settings. The comparison also showed that all of the tested methods produced errors in complex urban areas, but performed well in smooth, rural areas.

Various approaches have been devised for resolving the problem of poor performance on sloped terrain, for example, Kraus and Pfeifer [2001], which combined filtering and terrain interpolation in one process; Sithole [2001], which used a filter that adapts to the slope of the terrain so that it can be applied to steeper terrain; Shan and Sampath [2005], which applied a one-dimensional filter to a scan line in one direction and then the reverse direction; and Yuan et al. [2009], which applied a threshold to a point and a planar surface constructed from neighbouring points.

Polat et al. [2015] introduced a decimation step, which they found could be applied either before or after an adaptive TIN filtering process with comparably high results, in terms of correlation with a reference DEM. The approach used by Bartels and Wei [2006] applied a second order Daubechies wavelet filter to separate features from hilly terrain, while Lu et al. [2009] used a conditional random field model and machine learning to train the classifier.

In Pingel et al. [2013], a progressive morphological filter was applied to a minimum surface derived from LiDAR points. A slope tolerance and a maximum window radius that represents the size of the largest non-terrain feature to be removed were used to flag cells as either bare earth or object. A DEM was derived from the bare earth cells, and then the LiDAR points were classified as

ground or non-ground based on their distance from the derived DEM.

The point cloud is often interpolated to a regular grid during filtering, including in some of the approaches cited above, but many examples can also be found where the filtering process is point-based. Sithole and Vosselman [2003] used a raw point cloud segmentation approach in which points are connected into line segments through height differences or slope and then connected into surfaces. Surfaces and their composite points are classified as bare earth, detached object (bridge, overpass), or attached object (building, vegetation). Yao et al. [2009] and Moosmann et al. [2009] also used methods that operate directly on the point cloud. The former employed clustering techniques, while the latter treated points as nodes in a graph. Point-based filtering methods avoid loss of information and accuracy that occurs when 3D point clouds are transformed into 2.5D representations, but also require more complex procedures.

### **2.3.2. Classification of LiDAR Data**

After separating points into ground and non-ground, further filtering or classification can be used to identify subclasses within each set: grass, roads, bare earth in the set of “ground points”; and buildings and trees in the set of “non-ground points.” A significant amount of research, some of which is cited below, has been conducted on identifying attributes of the different subclasses that, individually or in combination, make them separable within a LiDAR point cloud. Height information from LiDAR data was very early seen to be useful for

augmenting classification based on images (e.g., [Haala and Walter, 1999]) but there have also been ongoing attempts to make use only of the information contained within a point cloud.

Height information is the most reliable information contained in a point cloud. Nevertheless, the ability to record both first and last returns allows two basic surfaces to be derived, a DSM and an approximative DTM, as well as a third surface, HAG, which can all provide information supplementary to height. HAG is calculated from the difference between the first return and last return surfaces and shows areas of “change,” such as vegetation and building edges. Arefi et al. [2003] used these surfaces to classify buildings and trees through a process that involves maximum likelihood classification and morphological filtering.

Studies have shown that pulse intensity data may also be suitable for classification. For example, Song et al. [2002] conducted a separability analysis for four types of materials (asphalt, grass, house roof, and tree) and three different intensity interpolations (inverse distance weighting before and after filtering and kriging) and found that separability was high enough to allow for land-cover classification. However, Yoon et al. [2008] found that, while the intensity from most materials was dependent on the range, this was not the case for vegetation and consequently there was not sufficient separability in intensity values to allow for land cover classification. Hopkinson [2007] found that there was a linear relationship between intensity values and peak pulse power concentration and that it was possible to derive a correction model to normalize

across variable power concentrations of different surveys. Wang and Glenn [2009] applied a normalization factor to the intensity values before using a threshold to separate vegetation and non-vegetation (bare ground) and achieved an 85% overall accuracy.

In Garcia-Gutierrez et al. [2009; 2011], thirty-three measures were derived from intensity, height, point return information, and other characteristics of the point cloud. Among the ten measures chosen for use in the pixel-based classifier were intensity minimum, mean, and skewness. The classifier identified pixels as water, marsh, grass and bare earth, middle vegetation, high vegetation, roads and railways, or urban zones.

Intensity information has also been assessed for a highly specialized classification: temperate, lowland alluvial sediment with the potential to preserve the cultural and environmental archaeological record. Challis et al. [2011] found that, although the intensity values could not be used to predict preservation potential, there was correlation with key soil parameters and LiDAR intensity data were useful in qualitative assessments.

One final type of information contained within a LiDAR point cloud is the point return information. Airborne LiDAR survey systems can record separate returns for each separable surface within the laser footprint. The LAS file format supports up to 15 recorded returns per pulse [Graham, 2012]. Some filtering processes make use of point return information, for example Ma et al. [2015], which in essence discarded all but single and last returns before applying slope based filtering to separate ground from non-ground.



Niemeyer et al. [2014] used a set of measures derived from the LiDAR point information, including from point return numbers and point density, in a process involving conditional random fields that classified points as grassland, road, gabled roof, low vegetation, façade, flat roof, or tree. The measure that they found was the most important was HAG.

### **2.3.3. Augmenting Classification with LiDAR Data**

Satisfactory results can be achieved using only point clouds, but numerous examples can be found of point clouds being used to augment image-based classification processes with height information. The images may be acquired from aerial or satellite platforms, and may be multispectral, hyperspectral, or even synthetic aperture radar (SAR) data. In broad terms, multispectral and hyperspectral imagery help to separate objects or land covers based on spectral characteristics, while SAR imagery offers surface texture and LiDAR data are primarily used as elevation data. Examples of combinations of LiDAR data with hyperspectral data include Voss [2008] and Dalponte et al., [2008], which both aimed to classify tree species; and Goodenough et al. [2008], which combined LiDAR, hyperspectral, and SAR data to classify land covers in a forested area as water, swamp, herb, shrub, or forest and claimed to achieve an overall classification accuracy of 84%.

Typically, when multiple data sources are used, a DSM is derived (and/or an HAG, and/or a DTM), with a grid resolution to match the resolution of the imagery, and used as an additional “spectral” band in the classification. Syed et

al. [2005] used three multi-spectral bands from aerial imagery together with HAG from LiDAR data in an object-based process that classified pixels into a vegetation/non vegetation hierarchy. Bartels et al. [2006] used LiDAR data and imagery that were collected simultaneously, specifically using first returns, last returns, LiDAR intensity, plus RGB and near infra-red bands. The classification process marked pixels as building, vegetation, car, or ground with an 85% overall accuracy. Yoon et al. [2006] used the same bands derived from LiDAR but derived a normalized difference vegetation index (NDVI) from the imagery. The classification process involved clustering, and marked pixels as building, grass, road, soil, tree, or water. The process in Yu et al. [2009b] was two-staged. The first stage classified pixels as impervious, vegetation, or water based on the imagery. The second stage used HAG from the LiDAR data to subdivide the first stage classes based on height as well as morphological properties.

The images that underlie the classification may also be generated from the LiDAR data themselves: in Zhou [2013] the results of an object-based classification using LiDAR intensity and elevation imagery were found to be comparable to those obtained using multispectral and LiDAR elevation imagery. Land cover was classified into tree, pavement, grass, or building. The overall accuracy for LiDAR data alone was found to be 90.67%, while the overall accuracy for LiDAR data with aerial imagery was found to be 92%.

Parent et al. [2015] developed a detailed set of rules for deriving a 1 m resolution land cover map from LiDAR data and multispectral imagery. The land covers depicted in the map are deciduous trees, coniferous trees, medium-height

vegetation, low vegetation, water, riparian wetlands, buildings, and low impervious cover. The measures calculated included maximum and minimum height and understory detection from the LiDAR data, and NDVI and reflectivity from the imagery. The overall accuracy was over 90%.

#### **2.3.4. Identifying Features**

LiDAR point clouds are a natural source for 3D data, and buildings can be readily detected in point clouds, but the irregular spacing of the data is problematic. Many algorithms have been proposed for extracting building models from point clouds, or from imagery augmented by point cloud data. Some of these rely on a library of building types, while others detect and characterize roof planes - either way, the aim is to determine “approximately” the shape of the building and its location, not the nature of individual points.

Elaksher and Bethel [2002] used a region growing technique, starting from candidate building points that are at least 5 m above the surrounding terrain, to find roof regions from which region borders can be extracted. Rottensteiner and Briese [2002] also used region growing, starting from planar patches that are found by segmenting the DSM. Texture analysis was applied in Zhang et al. [2009], by using gray level co-occurrence matrix after morphological filtering was applied to the DSM; and Samadzadegan et al. [2009b], by calculating various measures on first and last return elevation and intensity images.

The results of building detection and classification processes are affected by the scale of the object relative to the size of the window in which data points are

being compared as well as by overhanging vegetation. To overcome the scale issue, Vu et al. [2009] used a multi-scale process and both elevation data from LiDAR and spectral data from aerial imagery. To overcome the vegetation issue, Zhou et al. [2009] used clustering based on HAG to find objects and shape regularity to determine if an object is a tree or a building.

Progressive refinements can be introduced to improve final results. Many of the works cited above involve multiple stages of filtering and/or classification to reach the final product. Another example is Mao et al. [2009], in which vegetation points were filtered out by using LiDAR intensity data, along with aerial images, before clustering is used to classify building surface points and building wall points. A different approach, "double-fusion," was used in Demir et al. [2009]: aerial imagery was fused with LiDAR data, and then the results of four different building detection methods were fused to produce a final result with improved completeness and correctness over the individual results. In Alexander et al. [2011], a decision tree classifier was used, with possible classes being building with flat roof, building with pitched roof, grass, road, trees, and shrubs. Their results illustrated the challenges of correctly classifying points at buildings edges: many of these points seemed to have been classified as trees and some points at the edges of flat roofs seemed to have been classified as pitched roofs.

A different approach was used in Yu et al. [2011] The point cloud was segmented into objects by first extracting terrain and calculating HAG values, then identifying clusters of points as individual objects. In the results, each

building had its own classification, rather than having one classification for all buildings. Li et al. [2012] also used a segmentation approach to classification, but for the purpose of segmenting individual trees in a forested area. Lehrbass and Wang [2012] aimed to improve mapping of urban tree cover by first using the LiDAR data to correct relief displacement of trees in aerial imagery and then using HAG derived from the LiDAR data together with the imagery to outline tree cover.

In urban areas, additional data are often available, such as multispectral imagery and 2D ground plans, that can help in classifying features. An early example of methods proposed for incorporating two types of data, namely multispectral imagery and ground plans for buildings, with LiDAR data was in Haala and Brenner [1999]. The multispectral imagery was combined with a HAG and the ground plans with a DSM. They found that such integrations significantly improved image classification and strongly recommend integrating LiDAR data during the automatic generation of urban data sets. Rottensteiner et al. [2004] noted that the complementary nature of the data – aerial imagery offer higher resolution, while LiDAR data are not (as) affected by shadows, occlusions, or poor contrast – was most beneficial in building detection, roof plane detection, and determination of roof boundaries. Al-Durgham et al. [2012] however, argued that many building algorithms still required user interaction and did not address the issue of varying point densities. Their approach used planar surfaces and minimum bounding rectangles to extract building outlines.

The scenes tested in Kada and McKinley [2009] did not have vegetation

overhanging buildings and the data available included existing grounds plans and so the process could be focused on reconstructing roof-structures. The method split each footprint into sections and fit roof shapes to each piece. In a similar approach, Kim et al. [2013] used a "mean planar filter" to separate points that lie in a plane from boundary points. Buildings were then extracted through a combination of height filtering, supervised classification using aerial imagery, and area-based filtering. Buildings can also be further classified by type, as in Meng et al. [2012], where an approach was used that first combined LiDAR data with aerial photography to detect buildings and green space versus parking space, and then derived additional measures from road polygons to identify buildings as residential or non-residential.

Other features that can be identified and extracted include roads. Clode et al. [2007] used intensity and height in the initial classification, then added local point density, and finally vectorized the road features. Samadzadegen et al. [2009a] applied both a minimum distance and a maximum likelihood classifier to first and last return intensity and range, obtaining two classes for roads (asphalt and cement), plus building, grassland, tree, and parking classes. The results were then fused. Although roads were not the only feature classified in Mancini et al. [2009], it did propose an approach for extracting road and roundabout features based on the classification results.

## **2.4. DATA FUSION AND INTEGRATION**

Many of the examples cited above combine data from multiple sources – in

some cases using data from one source to improve data from another source – but few explore in any detail the processes required to combine disparate data sets effectively. This section describes two papers that discuss integration in great detail: Papasaika and Baltsavias [2009] and Warriner and Mandlburger [2005].

In their paper proposing a method for fusing LiDAR and photogrammetric DEMs, Papasaika and Baltsavias identify six reasons for fusing DEMs, any or all of which may apply:

1. To combine DEMs produced by different technologies, which implies different strengths and weaknesses.
2. To update existing DEMs with newer data, perhaps for change detection purposes.
3. To increase the accuracy of DEMs.
4. To densify DEMs.
5. To fill gaps in DEMs.
6. To increase the total coverage area by mosaicking DEMs.

These reasons could all be extended to apply to any geographic data, not just LiDAR and photogrammetric DEMs.

As part of their fusion method, Papasaika and Baltsavias evaluate the quality of the result but require knowledge about the technology used to create the DEM, the date when the data were acquired, the resolution of DEM, and a global measure of accuracy. They apply a mathematical approach to fusion based on an accuracy analysis of each DEM and similarities or differences between DEMs.

Although the process examines local quality, often in a 3x3 window, the final solution has only a global measure of accuracy.

Warriner and Mandlbürger have a far simpler fusion process: select the highest accuracy data. At boundaries between DTMs, blending can be applied to provide a smoother transition. Along with the fusion product, they also generate a quality indicator and quality map showing which areas have what accuracy and accompany it with a header file that gives more information about the accuracies. This largely automatic process is designed for specific data products and specific needs, namely integrating 2 m resolution LiDAR-derived DTMs into an existing database containing lower resolution elevation products and where all the data sources need to be available and selectable. Although their solution is not broadly applicable to data integration, aspects of it are, in particular blending at boundaries and quality assessment.

The following section examines existing standards and guidelines for LiDAR data acquisition and processing, which are an important factor in successfully integrating data sets.

## **2.5. COMPARISON OF EXISTING STANDARDS AND GUIDELINES**

Integration is a common theme in at least three documents detailing LiDAR standards for different countries:

"[The collection of numerous lidar data sets across the nation] have used a



variety of specifications and required a diverse set of products, resulting in many incompatible data sets and making cross-project analysis extremely difficult." Preface to the U.S. Geological Survey National Geospatial Program (USGS NGP) Lidar Guidelines and Base Specification [US Geological Survey, 2010].

"Inconsistent and diverse product specifications, and variable data quality are often making it difficult to integrate data sets to address regional, state and national issues." Preface to the Australian Intergovernmental Committee on Surveying and Mapping (ICSM) LiDAR Acquisition Specification and Tender Template [Australian Intergovernmental Committee on Surveying & Mapping, 2010].

"The lack of LiDAR acquisition guidelines contributes to inconsistent data quality and impedes data sharing and data integration within and across jurisdictions in Canada." Preface to the Canadian Airborne LiDAR Acquisition Guideline [Natural Resources Canada, 2014].

The commonality in all of these is the need for consistency in data collection parameters and deliverables to facilitate integration – but a balance must be struck between enough specifications and too many restrictions. Each of these documents is summarized in the sections below, followed by a comparative analysis of strengths and weaknesses.

### **2.5.1. Canadian LiDAR Acquisition Guideline**

The first draft of the NRCan guidelines was circulated in July 2012. They were based on the Australian document, cited above, but were to be developed specific

to the Canadian reality. Arguably, the technical specifications did not change significantly from version 1.0 to version 2.0, in terms of numerical details for the specifications that were in version 1.0. However, in the version 2.0 draft, released in October 2013, the purpose of the document is explicitly stated as being not only to provide consistency in data collection but also "to create a baseline for discussion between new and experienced LiDAR data users and LiDAR service providers" [Natural Resources Canada, 2013, p. 5]. It provides additional clarification of some specifications; introduces new specifications, such as point density guidelines; acknowledges that the specifications may need to be relaxed or enhanced to meet the specific needs of a client; and encourages clients to communicate fully with LiDAR service providers and rely on their expertise.

The project planning and contracting section gives an outline of what information should be included when an acquisition project is put out to tender. Any landscape characteristics that may affect the data at any stage before delivery must be described; this is important for those bidding to be able to plan properly. In version 2.0 of the NRCan guidelines, a recommendation is added that a description of the intended use of the project deliverables be included so that LiDAR service providers might provide guidance based on their experience with similar applications.

The general survey specifications section describes the accuracy, datums, and map projection to be used, which are presumably chosen to match the most commonly used standards so LiDAR data do not need to be transformed before

integration. A note is included about delivering orthometric heights in the new Canadian Geodetic Vertical Datum of 2013 (CGVD2013) after November 2013. Data and documentation for survey control must be supplied, which allows for independent quality checks. The collection requirements, including point spacing, maximum scan angle, flight line overlap, and environmental conditions help ensure full coverage at a sufficiently high resolution (point density). One of the additions to the general specifications is a suggestion that data be collected with leaf-on conditions, where this would not reduce the accuracy below what is required for the application for which the data are being collected, to increase the utility of the data for other applications.

Perhaps the most significant improvement in version 2.0 over version 1.0 is an expanded discussion of point spacing and spatial distribution. Whereas in version 1.0, the required nominal point spacing was 2 pulses per square metre, version 2.0 makes allowances for different application requirements and defines three specifications, low pulse spacing (1 pulse per 2 m<sup>2</sup>), standard pulse spacing (1 pulse per 1 m<sup>2</sup>) and high definition pulse spacing (2 pulses per 2 m<sup>2</sup>). Nominal point spacing (NPS) is calculated from first returns only. Corresponding nominal point densities (NPD), which include multiple returns, are defined for both open areas (equal to NPS) and vertically structured areas (three times as many points as NPS). Version 2.0 also includes a methodology for verifying the spatial distribution of points that is present in the Australian guidelines but were not present in version 1.0 of the NRCan guidelines.

The point cloud specifications require fully compliant LAS format v1.2 or v1.3.

The LAS format is one of the most commonly used formats for LiDAR data. A variety of software tools are available that can display, and/or process the data, including version 10.1 and higher of *ArcGIS™<sup>3</sup> for Desktop*. Basic classification types are defined as well as levels of classification with defined classification accuracies. Ground must always be classified at a 95% accuracy or greater. These definitions provide greater transparency in overall quality. Ensuring a minimum accuracy in ground classification means that more reliable products, such as bare earth DEMs, can be derived.

There are two notable changes from version 1.0. First, in version 2.0 it is recommended that both ellipsoidal and orthometric heights be provided, rather than just ellipsoidal, and that geoid heights be included if ellipsoidal heights are not a deliverable. This facilitates integration of the LiDAR data with other height data. Second, Classification Level 1, "Automated and Semi-Automated Classification" in version 1.0, is split into two levels in version 2.0. Classification Level 1 becomes "Ground/Non-Ground" and is the bare minimum level of classification required. Classification Level 2, "Standard Classification", can be fully or semi-automated and has points classified as ground, vegetation, buildings/structures, low/high points and noise, and water.

The derived data specifications describe how intensity images, DSM, DEM, and canopy height model (CHM) are to be generated, although the only data product that must be part of the deliverables in all acquisitions is the DEM. Version 2.0 provides more detail as to how these products should be generated.

---

<sup>3</sup> ArcGIS is a licenced software product of Esri Inc.

The DEM should be generated from points classified as ground only, the DSM from the highest return, of any class, within each grid cell, and the CHM as the difference between the DSM and the DEM. Intensity images may be one of three types, either INT-LAST, from last returns only, INT-FIRST, from first returns only, or INT-SUM, the total of intensity values of all returns within a grid cell. Each of these products should be at a 1 m resolution and should follow a file naming convention that follows National Elevation System (NES) conventions, ensuring national consistency. The convention includes information about the what, when, how, and where relevant to the data, all in the file name. This is very important for organizing large collections of data and referencing data coverage.

The specifications regarding the data delivery recommend that data sets should be supplied as single files where possible. If the data need to be tiled, the recommended size is 1 km x 1 km tiles. Global Positioning System (GPS) data for all base stations are to be supplied, which allows for independent verification of positions.

The project plan must include verification procedures and calibration checks. An accuracy report must be completed and accepted by the client before classification proceeds, and must include absolute and relative accuracy achieved, flight trajectories as shapefiles, and all information related to determining and checking accuracy. The final project report is to discuss all processes followed. Detailing all of these procedures and results ensures that care is taken in processing the raw data into a 3D point cloud and that all relevant information is available after the data are delivered. It also provides the

necessary information for independent verification.

The quality assurance requirements detail processes for determining vertical and horizontal accuracy and list maximum demonstrated erroneous classification values for each of the levels of classification for both ground and other classes. Classification accuracy tests are to be presented in an error matrix reporting errors of omission and commission generated from randomly selected points. Checks must also be made for consistency in the data.

### **2.5.2. Australian Acquisition Specifications**

Much of the NRCan guidelines are copied word for word from the Australian version [Australian Intergovernmental Committee on Surveying & Mapping, 2010], hereafter referred to as the ICSM guidelines, although version 2.0 of the NRCan guidelines were reformatted and are not in tabular format, as the ICSM guidelines are. Some of the differences in the guidelines are clearly country-specific, such as referring to the Australian equivalent of the NES, which is the National Elevation Framework Data Portal (NEDF-Portal), and specifying datums, projection, and geoid model appropriate to Australia. The ICSM guidelines document does not have a section describing its purpose and scope but is otherwise divided similarly to the NRCan guidelines, with sections for a tender template, general LiDAR specifications, point cloud specifications, derivative data specifications, data supply specifications, project planning and reporting specifications, and quality assurance specifications.

The reason for other differences between the ICSM guidelines and version 1.0

of the NRCan guidelines may be less clear. They may be due to an attempt to "Canadianize" the NRCan guidelines, or there may be other causes. The ICSM guidelines provide more detail on survey control than the NRCan guidelines and specify that files should be limited in size to 2 GB – and that data should be delivered on DVD or external hard drive. The ICSM guidelines describe an additional derived product, a Foliage Cover Model; require a Quality Assurance Plan that complies with ISO 9001; and progress reports every two weeks that include a plan for the next two weeks

The most significant difference is in the quality assurance section. The ICSM guidelines stipulate that the vertical accuracy must be tested using a TIN constructed from LiDAR bare earth, yet the accuracy validation must be performed before classification, and testing against bare earth requires some classification. It is unclear how this accuracy validation is to be conducted.

The ICSM guidelines are also version 1.0. In contrast, the USGS NGP guidelines, summarized below, are at version 13.

### **2.5.3. USGS NGP Lidar Guidelines and Base Specification**

Unlike the ICSM guidelines and version 1.0 of the NRCan guidelines, which are in tabular format, the USGS NGP document [US Geological Survey, 2010], hereafter referred to as NGP guidelines, are in a report format. This made it more difficult to locate specifications and compare the document to the other two documents. (Version 2.0 of the NRCan guidelines are also in a report format but follow the same organizational flow as version 1.0 and have clear section

divisions and headings.) Among the changes in version 1.1 of the NGP guidelines, released in October 2014, was some reorganization and re-formatting of the document, including placing some information in tables [Heidemann, 2014].

Some of the notable differences are that the NGP guidelines discourage achieving nominal pulse spacing through overlap or multiple passes, preferring that single flight lines achieve the required spacing. Relative accuracies must be no more than  $\pm 7$  cm within swaths and no more than  $\pm 10$  cm between swaths in the overlap. "Relative accuracy" is not explicitly defined within the document but is assumed to be a measure between points expected to be at the same elevation. FVA must be  $\pm 24.5$  cm, as opposed to  $\pm 30$  cm and the NGP guidelines require supplemental vertical accuracy be tested for each landcover type that makes up more than 10% of the area.

Each flight line should have a unique ID and any flight line file larger than 2GB must be split into segments. All collected flight lines must be delivered, including calibration flight lines, and all collected points must be delivered; full data delivery allows the client to make a full assessment of the collection activities conducted on their behalf. The "withheld" flag or class 11 may be used to identify outliers, blunders, noise, and otherwise unreliable points. (Use of the withheld flag of class is more clearly described in version 2.0 of the NRCan guidelines.)

A final notable difference is a requirement for 98% classification accuracy for all points, except those that are withheld. Fewer classifications must be included



than in the NRCan and ICSM guidelines, namely: processed but unclassified, bare-earth ground, noise, water, ignored ground, and withheld.

Each set of guidelines is supposed to meet the needs of a particular country or government agency, yet they all concern the same type of data. The next section presents a brief comparative analysis of the three set of guidelines.

#### **2.5.4. Comparative Strengths and Weaknesses**

Overall, the NGP guidelines provide much greater detail and more explicit requirements and seem, comparatively, quite restrictive. The high requirement for classification accuracy may require significant, and time-consuming, manual processing. and the stipulation that files must be split at 2 GB could potentially require breaks at more unnatural places in the file than if some discretion could be used. Yet such detail can also be helpful: the procedure for checking spatial distribution, which was missing from version 1.0 of the NRCan guidelines but included in version 2.0, is important to have because the LiDAR point distribution will never be uniform in the strict sense and without clarification such a requirement could lead to disputes. The main weakness, comparatively, in the NGP guidelines is the format: there is a lot of text to read through, making it difficult to locate similar or related content in different sections.

The ICSM guidelines also have "good" detail, such as the point distribution check, and "bad" detail, such as requiring a progress report every two weeks and specifying how data are to be delivered. One of the main weaknesses of the first draft of the NRCan guidelines was that some of the good details had been

omitted. Stipulating too many things, even when the documents are called "guidelines" and there is some relaxation of requirements in certain conditions, can take away the flexibility data suppliers and clients need to adapt to project-specific circumstances. Not making enough stipulations, however, permits too much flexibility, which leads to greater integration challenges.

Many of the qualitative additions and changes in the second version of the NRCan guidelines seem to have been made to emphasize the degree of flexibility that exists within the guidelines. Specifications touching on data compatibility, for example file format and vertical and horizontal accuracies, are requirements. In contrast, specifications touching on data content, for example point spacing and level of classification, are merely recommendations. The result is a more robust document that should serve the needs of both providers and consumers of LiDAR data.

## **2.6. SUMMARY OF RELEVANT CONCEPTS**

The concepts introduced and discussed in this chapter form the foundation for the research detailed in this thesis. An understanding of the principles of LiDAR, in particular as applied to ALS, is necessary for understanding the possibilities and limitations in classification, and the similarities and differences between LiDAR data and other data types that might challenge or facilitate integration. Clear definitions of terminology used are necessary for understanding methods and analysis of results.

The body of literature related to the use of LiDAR data in classification,

whether on their own or in combination with other data, continues to grow. The papers cited above provide examples of methods and techniques employed, of successes and failures and lessons learned that can be – and were – built upon or otherwise used as inspiration for the methods and techniques used in this research. The two papers described in Section 2.4 were particularly useful in developing the methods and measures employed in Chapter 6 when integrating other types of data with LiDAR data.

Finally, as noted above, the NRCAN guidelines helped provide a structure to combine the dual goals of LiDAR point data classification and integration of disparate data sets. An overview of the guidelines and how they compare with other similar documents gives context to the references of the guidelines throughout this thesis. The next chapter describes measures used in the GPI and MSPC processes developed in this research and how the NRCAN guidelines relate to these measures, and provides details regarding the data used in testing.

*"Quidquid agis, prudenter agas, et respice finem." "Whatever you do, do it warily, and take account of the end."*

*~ from Gesta Romanorum*

## **CHAPTER 3**

### **METHODS AND DATA SETS**

Both the ground point identification (GPI) and multi-stage point classification (MSPC) processes developed as part of this research and described in later chapters rely on certain data handling techniques for handling a large volume of LiDAR data and employ certain measures to determine spatial context for individual points. The two main handling techniques, namely point interpolation and voxel sorting, were described in Section 2.1. This chapter describes the measures employed to determine spatial context (Section 3.1), where appropriate in the context of the NRCan guidelines. It also describes the different data sets that were used to test the GPI and MSPC processes that were developed (Section 3.2).

#### **3.1. DATA MEASURES**

Interpolating and sorting are helpful techniques in managing LiDAR data and can also provide some spatial context. To obtain additional spatial context from the point cloud data, several different measures were applied in the GPI and MSPC processes detailed in Chapters 4 and 5 and the modified MSPC methods described in Chapter 6. A few of the measures were also used to assess local

quality of data from different sources, which is an important factor to consider when fusing data sets [Papasaika and Baltsavias, 2009]. Sample illustrations for each of the measures can be found in Appendix B, Section B.1.

### **3.1.1. Height Measures**

Height measures are straightforward measures in terms of calculations that require at most a reference height surface from which to calculate values. The following sections describe the height measures used in this research.

#### **3.1.1.1. Height Above Ground (HAG)**

HAG is more commonly known as an nDSM, which is the difference from a first return or other surface model to the reference ground [Stoker, 2010]. Although it is usually derived as a raster product, HAG can also be calculated for individual LiDAR points as the difference between the point's z value and the reference ground. HAG values are almost always positive but negative values can occur, for example, where the ground surface value is the average elevation for a group of points. The reference ground can be a DEM derived from the LiDAR data, as per the specifications in the NRCan guidelines, or can be from another elevation data source. In this research, if the reference ground had any gaps, for example, corresponding to building footprints, those gaps were filled before HAG was calculated so that values could be obtained for all points.

One variation of HAG that was developed and used for the MSPC process was minimum HAG (mHAG). This measure was similar in principle to HAG but used

a minimum value interpolation for the surface model, and calculated the height difference only for the minimum value in each grid cell rather than the entire point cloud.

### **3.1.1.2. Maximum minus Minimum (MaxMin)**

MaxMin was another measure developed and used for the MSPC process. It is a raster measure calculated as the difference between the maximum elevation and the minimum elevation in a grid cell. MaxMin is near zero for solid surfaces, namely for ground and buildings. Small variations in terrain elevation within a cell will produce small non-zero MaxMin values.

Sloped building rooftops can produce small to moderate non-zero MaxMin values, depending on the slope angle and the size of the cell. For a 1 m cell resolution and roof slopes no more than 45 degrees, MaxMin values will be 1 m or less within the area of the rooftop. At the edges of building rooftops and other non-terrain features, MaxMin values can be much larger, up to the height of the building. The values may also be large where pulses were able to pass through openings in vegetation and are akin to the CHM described in the NRCan guidelines. The MaxMin values may represent the full height of the vegetation, if a cell contains points both from the top of the vegetation and from the ground.

### **3.1.1.3. Terrain Ruggedness Index (TRI)**

TRI is a measurement developed by Riley et al. [1999] to express the amount of elevation difference between adjacent cells and is calculated as:

$$TRI = \sqrt{\sum_{i=0}^8 (z_0 - z_i)^2} \quad (3.1)$$

where  $z_0$  is the elevation of the centre cell and the  $z_i$ 's are the elevations of the eight surrounding cells. Riley et al. applied TRI to a grid at 1 km resolution and therefore their ruggedness scale, which defined flat terrain as having a TRI up to 80 m, is too coarse to use with LiDAR data. The general principle, however, of larger TRI values corresponding to larger variation in terrain elevation within the cell area, and smaller TRI values corresponding to flatter terrain within the cell area, is applicable at grid resolutions appropriate for LiDAR data.

### **3.1.2. Non-Height Measures**

LiDAR point clouds contain more than just elevation information. The following sections describe measures based on other characteristics that were used in this research.

#### **3.1.2.1. Local Point Density (LPD)**

Although arguments have been made regarding the capabilities of modern photogrammetric methods, such as those given in Leberl et al. [2010], LiDAR data have much higher point densities than point data generated through most other means and therefore provide much greater detail. Yet NPDs, which simply divide the total number of points by the area covered, can be misleading in terms of the actual distribution and density of points: the presence of multiple returns

will increase the NPD, while data voids, which do occur over water, will decrease the NPD. In contrast, images representing point density give a better indication of point distribution and density by showing the degree of detail available over an area of interest.

LPD represents the number of single and first (or last) returns in each cell, normalized by the area of the cell and is similar in concept to the spatial distribution specification described in the NRCan guidelines. Any voids, large or small, in the data can be seen in the LPD image, as well as overlap between flight lines. This can be helpful in determining an appropriate resolution for derived raster products that balances the detailed information provided by higher resolutions against the need for nearly complete coverage of the area of interest.

### **3.1.2.2. Multiple Return Density (MRD)**

MRD is another point density representation. It is similar to LPD, in that it is a normalized and localized point count; the difference is that, where LPD counts only single and first returns, MRD counts all returns that are not single or first. Multiple returns only occur where the laser footprint contained multiple surfaces at separable distances, primarily in areas of vegetation, where the laser pulse may be partially reflected from leaves, branches, boles, and/or the ground. Other examples include building rooftop and ground and electrical wire(s) and ground. The higher an MRD value, the less solid the feature. The highest surfaces are excluded (e.g., building rooftop), but all lower surfaces (e.g., ground at foot of building) are included in the MRD image. Since no processing is required to generate an MRD image, it can be used as a quick approximation of a



land cover map.

### **3.1.2.3. Intensity**

Intensity is the recorded strength of the return pulse. Many factors besides material reflectivity affect recorded intensity, including multiple returns, sensor configuration, and flying height. Intensity values therefore should not be used as the sole basis for classification and any application of intensity measures must be adapted to each data set, or even to each survey segment. For example, in a 2007 LiDAR survey over Fredericton that was conducted over four days, the intensity ranges varied from day-to-day even when the same area was flown. Intensity may indicate possible range bias where substances reflecting a higher percentage of the laser pulse energy appear to be at higher elevations than substances reflecting a lower percentage of the laser pulse energy [Csanyi and Toth, 2007].

The NRCan guidelines describe three types of intensity images: the intensity of the last returns only, the intensity of the first returns only, and the total intensity of all returns in each cell. No specific guidelines are given for calculating the intensity when multiple last returns or first returns fall in the same cell. Using or at least examining different intensity images may provide more information than a single intensity image and this could include images where different methods are used to combine intensity values from multiple points.

#### **3.1.2.4. Ground-vegetation ratio (GVR)**

The greatest advantage of LiDAR remains its ability to penetrate openings in vegetation but the laser cannot penetrate the vegetation itself. One lone, deciduous tree in late fall/early spring may not obscure the ground to any significant degree because there would be plenty of large openings between the bare branches. In contrast, a dense cluster of coniferous trees may block a large percentage of pulses from reaching the ground year-round because the branches and needles are tightly clustered with few openings. Ratios of non-ground to total returns have been used in forestry applications, e.g., Hudak et al. [2006]. GVR is a modification of such ratios, developed as part of this research, that represents the occurrence of ground points as compared to vegetation points across a study area as an indication of how well the laser pulses were able to penetrate openings in the vegetation. It is used in the MSPC process to mark areas of uncertainty, but it can also be used as a visualization technique.

The process of obtaining a GVR image that was developed involves deriving rasters to represent the percentage of total points that are classified as vegetation in a local area, the percentage of total points that are classified as ground in a local area, and a normalizing factor, for example the LPD as a percentage of the maximum LPD in the scene. Each derived raster is then assigned to a different RGB colour channel to obtain a single image. By assigning the ground point measure to the red channel, the vegetation point measure to the green channel and the normalizing factor to the blue channel, as in Figure 3.1, areas that contain mostly ground points will appear red and areas that

contain mostly vegetation points will appear green.

- Red channel: ground point measure
- Green Channel: vegetation point measure
- Blue Channel: normalizing factor

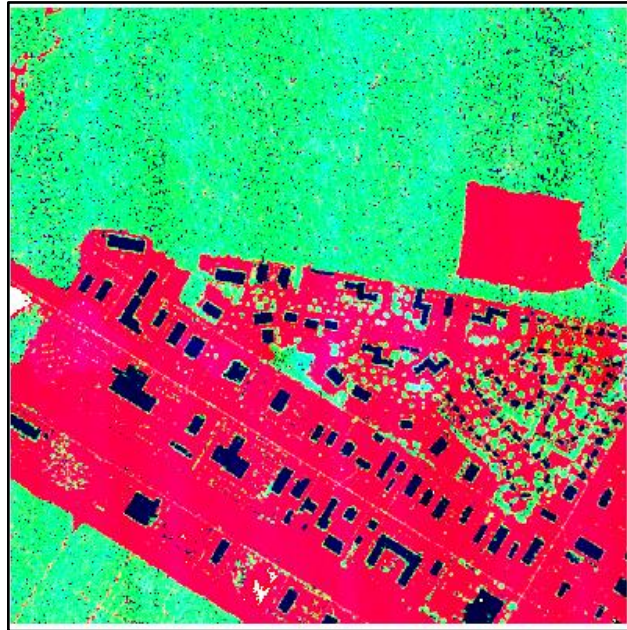


Figure 3.1

Example of three band ground-vegetation ratio representation.

The addition of the normalizing factor pulls areas with high point counts towards the blue spectrum (i.e., green towards cyan or red towards magenta) while areas where there are relatively few points appear black. The mapping used above also capped maximum input values at 0.5; any higher values in the band were assigned the maximum output value. This had the effect of highlighting overlaps: any areas with high percentages (close to 50%) of both ground and vegetation points, such as along the edges of trees, appear yellow. It must be noted, however, that this is a subjective measure and the results are highly dependent on correct ground and vegetation classification.

### **3.1.2.5. Slope**

When a laser pulse is normal to the target surface, it illuminates a circular area with a diameter roughly dependent on the beam divergence and the distance from the sensor to the target; typical footprints range from 30 cm to 2 m [Fowler et al., 2007]. When the laser pulse is not normal to the target surface, some of the energy hits the target sooner and is reflected back sooner, elongating the return pulse and creating an elliptical footprint. A number of factors influence when the sensor records a return so, theoretically, the point position recorded could be anywhere within the distorted footprint and not necessarily at the point where the pulse was aimed.

A laser pulse may not be normal to the target surface due to the scan angle and/or due to sloped terrain. Goulden [2009] examines the error in LiDAR observations due to terrain slope. The uncertainty as to where exactly within the laser footprint the pulse return was generated means LiDAR data are subject to greater errors on sloped surfaces. Papasaika and Baltsavias [2009] consider terrain slope in their accuracy analysis, along with aspect and roughness. The steeper the angle, the greater the distortion and the lower the accuracy. By calculating the slope in the neighbourhood of a specific point, equations can be derived for the shape of the laser footprint [Sheng, 2008], giving an uncertainty ellipse for the planimetric position of the return pulse.

Deriving a visual representation of the terrain slope over the whole area of interest can help to identify areas where the vertical accuracy may be most affected. The slope image could also be used to check for ground classification

errors: small areas with high slope values may indicate small non-terrain objects that were not successfully separated from the terrain points.

### **3.1.2.6. Land Cover Map**

Although land cover is not a metric that can be calculated as the other measures, a land cover map can be used to locate open areas. This is important because the NRCan and other guideline documents discussed above all specify that the fundamental vertical accuracy (FVA) of LiDAR data is to be checked in flat, open areas, where there is a high probability that the laser pulse was returned from a ground point that is at or very close to the same elevation as the measured ground control.

Land cover maps can also be used to locate areas where there may be uncertainty in the derivation of a bare-earth DEM, for example because of a dense tree canopy, and may also provide an explanation for any larger errors or differences between data from different sources than were expected. A land cover map may be derived from any data source that includes non-ground information, but one advantage of deriving a land cover map from LiDAR data is the possibility of seeing any overlapping covers, such as where ground points have been detected under vegetation. A land cover map enhanced with an intensity image, to create more classes, can provide a quick visual aid to identify where material reflectivity may have affected measurements along with an aid to identify covered terrain. An example of a land cover map derived from LiDAR data can be found in Appendix B.

The following section describes the data sources used to test the LiDAR point

classification framework.

### **3.2. DATA SOURCES**

There is a trend towards making data "open" at all levels of government from federal (e.g., Government of Canada Open Data Portal<sup>4</sup>), to provincial (e.g., New Brunswick's GeoNB site<sup>5</sup>) to municipal (e.g., City of Fredericton Open Data [City of Fredericton, n.d.] and Open Data Ottawa<sup>6</sup>). Open data sites provide free access to geographic and other types of data sets in various formats. As well, a few portals exist to help users access LiDAR data. The primary data sources used for this research are from Fredericton, N.B., and include three LiDAR surveys; provincial and municipal elevation point data; provincial control monument data; and municipal feature data. Yet it is always prudent to test processes with data that are markedly different from the data used during the development of those processes. The next sections describe and provide technical details, as far as they are known and are relevant to this research, regarding the data for Fredericton and other areas used in the development and testing of the LiDAR point classification framework.

#### **3.2.1. Data for the City of Fredericton, N.B.**

The principal LiDAR data set used in this research was collected over Fredericton, N.B. A number of other data sets were obtained for the City of

---

4 Government of Canada Open Data Portal <http://www.data.gc.ca>

5 GeoNB <http://www.snb.ca/geonb1/e/index-E.asp>

6 City of Ottawa Open Data Catalog <http://data.ottawa.ca/en/>

Fredericton to compare to this data since LiDAR data are not yet available everywhere and there is still value in historical data.

### **3.2.1.1. Fredericton 2011 LiDAR Data**

The principal LiDAR data set used in this research was collected over Fredericton, N.B., in the summer of 2011 by Leading Edge Geomatics, Ltd. for the New Brunswick Department of Public Safety and provided to UNB for research purposes. The data were delivered in tiles, each 1 km x 1 km, in the New Brunswick Double Stereographic projection with orthometric heights referenced to the Canadian Geodetic Vertical Datum of 1928 (CGVD28). The labelling convention for the tiles is `eeee_nnnn`, where `eeee` is the Easting coordinate in km and `nnnn` is the Northing coordinate in km of the south-west corner of the tile. Figure 3.2 shows the main test area, an area encompassing most of Odell Park where there is dense vegetation and steep terrain. The elevation point data have been interpolated to a regular grid at 1 m resolution. The four tiles are labelled, clockwise from top-left, `2486_7439`, `2487_7439`, `2487_7438`, and `2486_7438`. Road centrelines and building footprints have been overlaid on the raster for reference.

Nominal point density for the tiles, based on examination of a small sample, is below 2 points per metre<sup>2</sup>. The data points were reportedly classified as ground, low vegetation, and high vegetation, but examination of sample data revealed inconsistencies in the classification.

This data set was collected to replace one collected in 2007 for the same agencies for the purpose of flood mapping. A loose screw on the mirror of the

sensors during collection introduced inconsistencies in the data [Mofford, 2012], rendering it unsuitable for integration and many other applications.

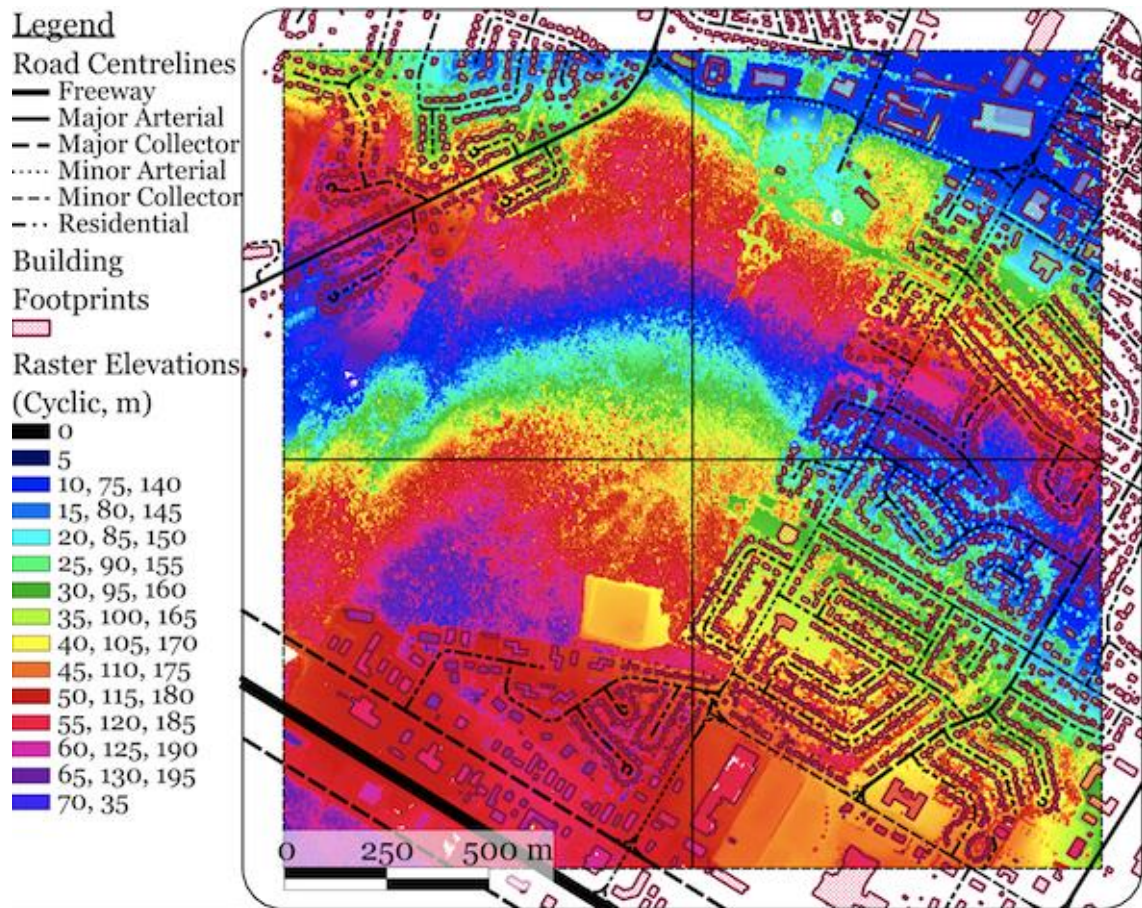


Figure 3.2

Interpolation of all LiDAR points in the Odell Park study area.

### 3.2.1.2. Fredericton 2006 LiDAR Data

Initial investigations, exploration of horizontal adjustment for data integration, and the potential of multi-temporal data made use of a data set collected over Fredericton, N.B., in May of 2006 by the Applied Geomatics Research Group at the Nova Scotia Community College. The data were delivered in the original flight lines, in the Universal Transverse Mercator (UTM)



projection, zone 19 N. The vertical reference has been reported as ellipsoidal heights [Hopkinson, 2013]. Nominal point density for the data is approximately 2.5 point per metre<sup>2</sup>. The data were not classified.

### **3.2.1.3. Fredericton Elevation Data**

There are two types of elevation data that were used in this research: elevation point data and control monument data. One of the elevation point sources is the Digital Topographic Data Base - 1998 (DTDB98), available from Service New Brunswick (SNB) [2010]. The New Brunswick Digital Terrain Model, part of the DTDB98, consists of point elevations, either as regularly spaced profiles or as a filtered data set that was created through a random densification process [Pegler, 2001] and contains elevation mass points, check points, spot heights and random densified points. The DEM data were collected photogrammetrically from 1:33,000-scale leaf-free aerial photography, and points are expressed to the nearest 1.0 m in x and y and the nearest 0.1 m in z. The stated accuracy is  $\pm 2.5$  m for well-defined features [Service New Brunswick, 2010].

The other elevation point source is the City of Fredericton (CoF) open data site [City of Fredericton, n.d.]. It is newer than the SNB data, having been collected as part of the generation of CoF's 2002 orthophotos. It has a nominally higher point density than the SNB data but its accuracy is unknown. Z values are expressed to the nearest 0.1 m.

The control monument network database for the province of New Brunswick is a database of surveyed points. Many are expressed to centimetre or millimetre

precision. Each database record includes associated attributes for the point, such as geoid/ellipsoid separation [Service New Brunswick, 2002].

#### **3.2.1.4. Fredericton Feature Data**

The data content available from open data sites varies. Municipal data sites are likely to include feature data such as road centrelines, building footprints, and water bodies, as well as elevation data, but details in the corresponding metadata are often lacking. The feature data downloaded from the CoF site include road centrelines, building polygons, trails, and stream lines. Little information is available regarding the accuracy or currency of these data sets.

#### **3.2.2. Online LiDAR Databases**

A few on-line portals exist to help users access LiDAR data. One is the Center for LiDAR Information Coordination and Knowledge (CLICK)<sup>7</sup>, operated by the U.S. Geological Survey. Another is lidardata.com<sup>8</sup>, which claims to be “The World’s Largest Lidar Data Warehouse”. Information related to the shape and the area are accessible by simply clicking on a shape in CLICK; LiDARDATA.com does not seem to provide any additional information from the GIS. Neither system offers any data for New Brunswick.

A third portal is OpenTopography.org<sup>9</sup> [Krishnan et al., 2011]. Along with free access to nearly 500 billion LiDAR data points covering a total area of 85, 757

---

<sup>7</sup> Center for LiDAR Information Coordination and Knowledge (CLICK)  
<http://lidar.cr.usgs.gov>

<sup>8</sup> Lidardata.com Data Browser <http://lidardata.com>

<sup>9</sup> NSF OpenTopography Facility <http://opentopography.org>

km<sup>2</sup>, the site provides links to data management, manipulation, and visualization tools. Two data sets from the Christina River Basin in Pennsylvania collected as part of the Critical Zone Observatory LiDAR project [Guo, 2011] were downloaded from this portal. They are described below.

#### **3.2.2.1. Christina River Basin 2010**

As noted above, additional data were downloaded from OpenTopography.org for a small area in the Christina River Basin (CRB) in Pennsylvania. Significantly more technical details are known about these data than about the Fredericton data because an accompanying report was also available for download. The data were collected as part of the Critical Zone Observatory LiDAR Mapping Project. Leaf-off data were collected in April 2010 and leaf-on data were collected in July 2010 for the same area. The data are in UTM projection, zone 17 N, with orthometric heights referenced to the North American Vertical Datum of 1988 (NAVD88). The nominal point densities for both data sets are slightly above 10 points per m<sup>2</sup> [Guo, 2011].

#### **3.2.2.2. Additional Data for Testing**

The final two LiDAR data sets that were used in this research were provided directly to the author for testing purposes. They were collected and ground classified by GeoDigital International, Inc. [Lehto, 2012b]. One data set is from Ottawa, Ont., in UTM projection, zone 18 N, and the other is from Oklahoma. No additional information is known about these data sets. Feature data were

downloaded from the Open Data Ottawa<sup>10</sup> catalogue to use together with the Ottawa LiDAR data, including water body polygons, building footprints, and street centrelines.

### **3.3. CHAPTER SUMMARY**

While the NRCan guidelines are primarily intended for LiDAR data acquisition, the specifications can also be useful when processing data. In this chapter, two data management techniques and a set of measures used in the ground point identification and multi-stage point classification process developed in this research are described in the context of the NRCan guidelines as applicable. The data sets used for testing are also described. The following chapter details the ground point identification process.

---

<sup>10</sup> City of Ottawa Open Data Catalog <http://data.ottawa.ca/en/>

*"All things are artificial, for nature is the art of God."*

*~ Sir Thomas Browne*

## **CHAPTER 4**

### **GROUND POINT IDENTIFICATION**

This chapter describes the GPI process that was developed as part of this research. First, the purpose and context of ground extraction are explained (Section 4.1), then the ground detection techniques, extracted ground surface comparison technique, and point classification and refinement processes developed in this research are described (Section 4.2 to 4.4). Finally, an accuracy assessment of the ground point identification process is presented based on test data from the City of Fredericton (Section 4.5). Pseudocode for the GPI process implementation can be found in Appendix A, Section A.1.

#### **4.1. PURPOSE FOR GROUND EXTRACTION**

Frequently, LiDAR data users are only interested in the ground surface [Lehto, 2012a] for infrastructure planning, terrain and hydrological modelling, ground monitoring, or other purposes. Several examples can be found in research where the phrase “using LiDAR” could be replaced with “using high resolution and high accuracy bare earth elevation data” or, in other words, where the method of collecting the data is not important to the application (e.g., [Hiltz, 2012; Mouland et al., 2012; Wittner et al., 2013]). Identifying and extracting the

ground surface was therefore chosen as the basis for all further manipulation and utilization of LiDAR data in this research. The terms "identification" and "extraction" are used here instead of "segmentation" because the ground surface is always treated as one object even when it is being represented by unconnected pixel patches or point clusters. In contrast, segmentation according to Yao et al. [2009] refers to the partition of a set of measurements into smaller and coherent subsets for the purpose of recognizing object-classes.

Automatic ground extraction at high resolution and high accuracy remains a challenge because there are so many possible variations within a relatively small area. For example, even in "flat" areas, allowances must be made for roads that are raised in the centre for drainage; curb stones that are lower at crossings for accessibility; natural bumps and depressions in open fields; and other small fluctuations in elevation due to natural and artificial causes. Sudden changes in elevation, which generally indicate non-ground objects, could instead be part of a cliff face or a retaining wall. There are also cases where different definitions of what is considered ground will produce different results: bridges, overpasses, and tunnels are all part of the natural ground for part of their distance then rise above or fall below it.

The variety of surface objects that make up a typical landscape – such as large and small buildings; hedges and trees; and small urban objects, including cars and other vehicles, electrical and telephone lines, and street lights and signs – and the varying point densities involved combine to produce almost infinite possibilities for point cloud scenes from which the goal is to extract all ground

points and only ground points, or, conversely, to filter out all non-ground points. A human examining the point cloud and/or derived products can interpret most scenes, but it is tedious and time consuming to manually classify the point cloud. Even then, the human operator would have difficulty separating any ground points from vegetation in a forest on a hill, such as is the case in Odell Park in Fredericton.

Ground extraction or ground filtering was one of the earliest problems explored (e.g., [Axelsson, 1999; Briese and Pfeifer, 2001; Kraus and Pfeifer, 2001; Zhang et al., 2003]) and many examples can be found of algorithms and techniques for extracting ground with good – or excellent – results. However, many methods require expertise to define the model parameters required to produce reliable extractions of ground surfaces while solutions designed not to require operator expertise can fail to produce acceptable results under conditions that were not present in the data with which the solutions were tested. Classification methods using parametric models often perform very well with the training data and data that are very similar but may perform relatively poorly with new data (e.g., [Caceres and Slatton, 2007; Dalponte et al., 2008]). Theoretically, and as demonstrated by Demir et al. [2009], the most successful approaches may be those that combine a number of different measures or the results from multiple classifiers.

The ground point identification process that was developed, henceforth referred to as GPI and illustrated in Figure 4.1, applies four ground extraction techniques that require little or no operator input but have different strengths

and weaknesses. Two of the techniques are raster-based and two are point-based. As applied through GPI, all four produce raster outputs that represent the extracted ground surface. A raster-based comparison technique is used to obtain a single raster representation of ground elevation that is then used to identify ground points within the point cloud and classify points as ground or non-ground. A final ground surface can be extracted from the classified point cloud however the classified point cloud is the primary product of GPI. The following sections describe the detection techniques, surface comparison technique, and point classification process that comprise GPI.

## **4.2. GROUND DETECTION TECHNIQUES**

Four separate ground detection techniques were devised for the GPI process developed in this research. Each technique has its own strengths and weaknesses, some of which are inherent to the data format on which the technique operates and some particular to the technique. The primary techniques, namely Pixel Connectedness and Point Neighbourhood, require more processing time or power but can be used independently of the other techniques, albeit with lower overall accuracy; the secondary techniques, namely Wavelet Detail Mask and Preliminary Ground Points, require relatively little processing but should not be used on their own. These techniques are summarized in Table 4.1 and described in the following section. Sample outputs from each of the techniques can be seen in Appendix B, Figure B.9.



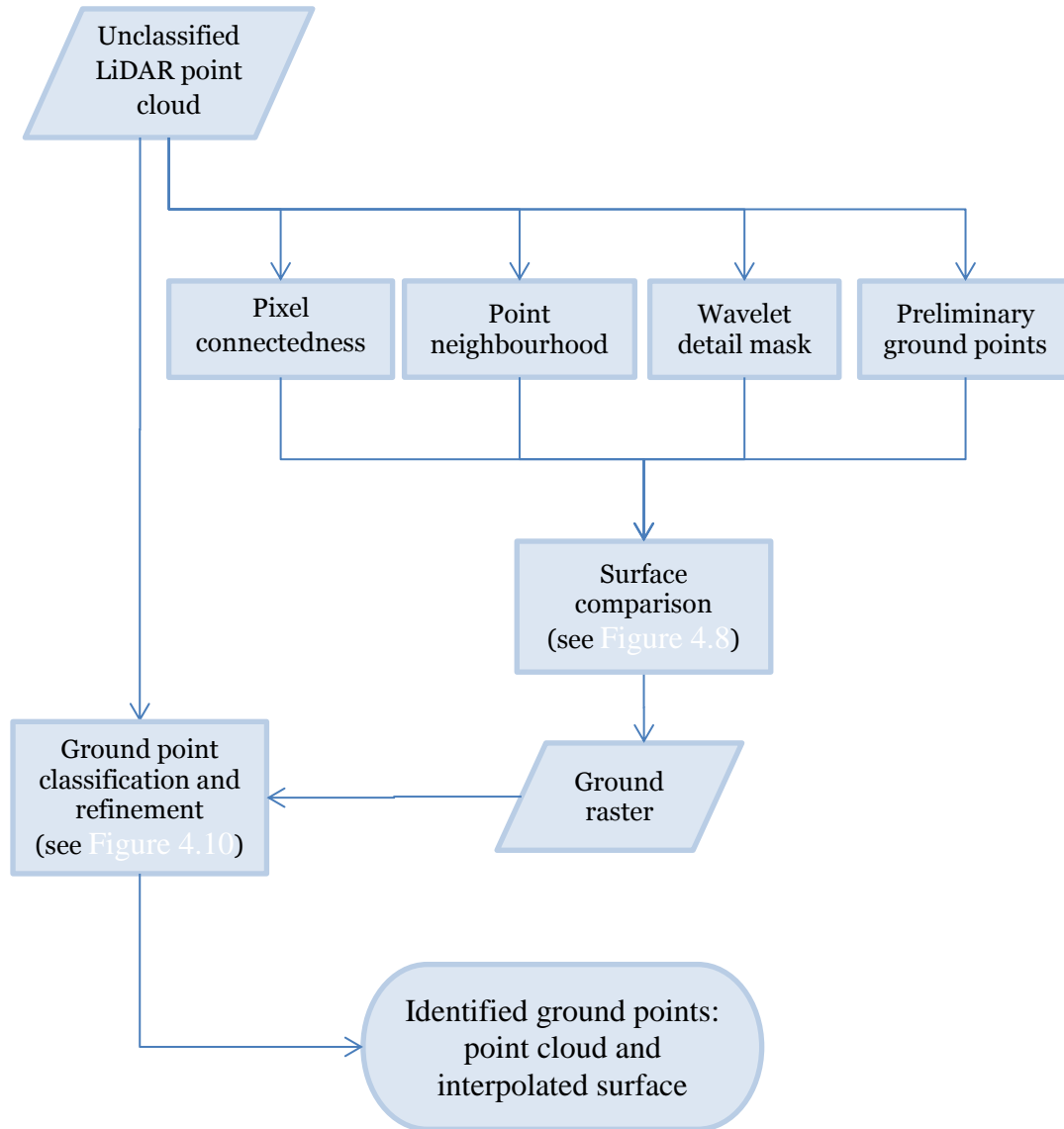


Figure 4.1

Flowchart for the Ground Point Identification process.

Table 4.1  
Summary of ground detection techniques.

<b>Name, Type</b>	<b>Parameter</b>	<b>Automatic</b>	<b>Manual</b>
Pixel Connectedness, Raster-based	Ground seed pixels	Lowest vertical layer with at least 0.5% coverage	User selects seed pixels or provides control point coordinates
	Slope threshold	Run multiple times at 5° intervals	Estimate of maximum terrain slope
Point Neighbourhood, Point-based	Ground seed points	Random selection from last returns	User selects seed points
	Percent threshold	50%	User's desired probability
Wavelet Detail Mask, Raster-based	Detail threshold	+/- 0.15 m	User's estimate of minimum height difference for non-ground
Preliminary Ground Points, Point-based	Height above reference ground	+/- 1 m	User's estimate of allowable height difference

#### 4.2.1. Pixel Connectedness

The Pixel Connectedness technique is raster-based. The goal of this technique is to reliably identify and exclude non-terrain objects from an initial potential ground surface leaving a raster with, ideally, holes where buildings or other solid objects are located and elevation values very close to true ground elevation in open areas as well as where penetrable objects (trees) are located. This is accomplished by growing a ground surface from a set of seed ground pixels by looking for pixels that are connected planimetrically and do not have an excessive vertical separation to known ground pixels. It requires an initial

potential ground surface, a set of ground seed pixels, and a slope threshold. The pseudocode for this technique can be found in Appendix A, Section A.1.1. As a raster-based technique, Pixel Connectedness exploits the regular grid pattern of rasters both for performing operations and for establishing spatial context between features. However, there is some loss of information in the conversion from a point cloud to a raster.

Ground seed pixels are obtained by dividing the 3D scene into a set of equally spaced vertical layers and then selecting a suitable seed layer. In the division, a binary raster is generated for each vertical layer, with the value 0 representing "no points in cell" (0-value cells) and 1 representing "at least one point in cell" (1-value cells). Figure 4.2 combines the binary images for four consecutive layers in one image to illustrate the effects using a 1 m resolution both planimetrically and vertically. In areas of open terrain, consecutive images will creep up slopes, with some overlap. Non-terrain objects appear as small isolated groups of cells.

Selection of the seed layer can be automatic or manual. To avoid having non-terrain objects in the seed layer, the seed layer should be one of the lowest vertical layers. The lowest layer will contain 1-value cells corresponding to the lowest points in the file. However, due to sensor errors, noise in the data, multipath reflections, or other effects, the lowest points may not necessarily correspond to actual ground point elevations or there may be too few to make the lowest layer an effective choice for ground seed pixels.

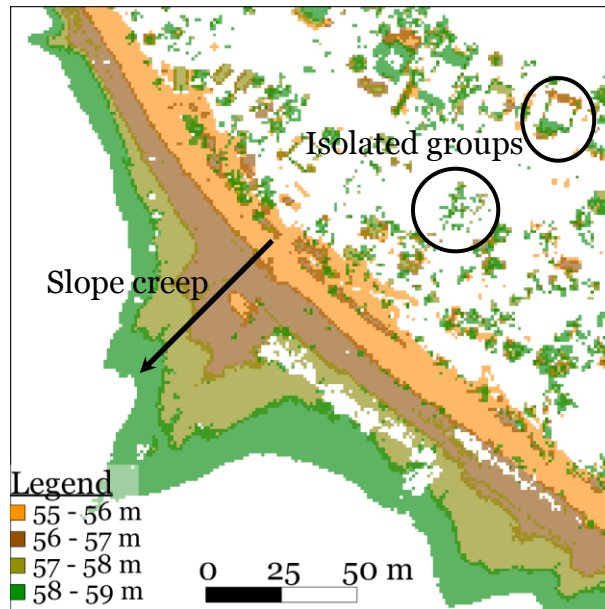


Figure 4.2

Four combined binary raster layer images show bands where terrain elevation gradually increases and isolated groups of cells belonging to non-terrain objects at lower terrain elevations.

The lowest layer with, for example, at least 0.5% 1-value cells could be automatically chosen as the seed layer, or the layers could be visually inspected and one chosen manually. If no layers are deemed suitable to use as the ground seed layer, patches or even single pixels could be chosen, or the user could input ground seeds by clicking on (a) point(s) on the potential ground surface or providing control point coordinates from open areas. Regardless of how the ground seed pixels are chosen, minimum elevation values are derived for each from the point cloud.

The initial potential ground surface is a raster of minimum values derived from the point cloud that will include buildings and some trees. The true ground surface is extracted from the potential ground surface through an iterative process. Any pixels that are touching a pixel identified as "ground" from the seed

pixels or a previous iteration are flagged and the slope from the identified ground pixel to the flagged pixel is calculated. If the slope is less than the specified threshold angle, the flagged pixel becomes part of the ground. This process can be re-run by manually selecting different seed pixels.

One slope threshold is used for the entire area and it must be selected based on the properties of the area. The maximum threshold that should be used for high resolution data is higher than what should be used for lower resolution data because "ground-to-rooftop" slope value from 1 m away, for example, is a much larger angle than the corresponding "ground-to-rooftop" slope value from 5 m away. In general, higher thresholds (e.g., 30°) may fail to eliminate more objects, while lower thresholds (e.g., 5°) may eliminate some terrain features or fail to find ground pixels at all if the slope of the terrain itself exceeds the threshold, as may be the case in rugged terrain or around stream beds.

Using a single threshold makes the technique inflexible in varying terrain. To overcome this inflexibility, the process can be run multiple times with different thresholds and the results combined in the surface comparison step of the GPI, described in Section 4.3. Figure 4.3 shows two examples of Pixel Connectedness results, using different slope thresholds. In (b), a large building was not properly excluded by the process. In this particular instance, this is a side effect of the low resolution (5 m) and a smoothing operation that was applied to the potential surface before the Pixel Connectedness method was applied.

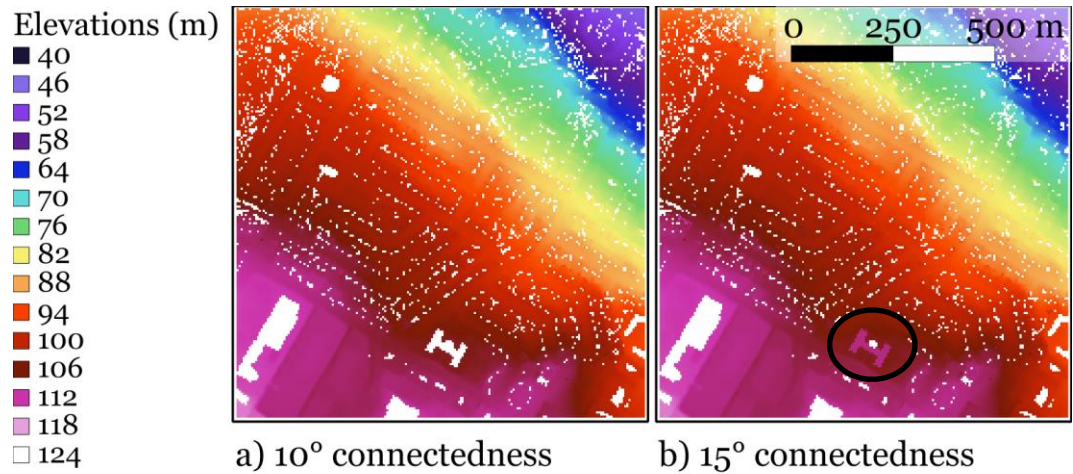


Figure 4.3

Results of the Pixel Connectedness method using two different slope thresholds:

a) 10° and b) 15°.

This method is not directionally biased so any feature attached to the ground on at least one side will become part of the ground surface. Examples of attached objects include bridges, which start and end on roads at ground level; and structures with ramped access to the top. These objects may need to be identified and removed manually if they do not meet the user's definition of "ground."

#### 4.2.2. Point Neighbourhood

The Point Neighbourhood method is point-based. The basic premise is to grow a set of ground points from a set of ground seed points. Since it operates on the point cloud itself rather than a raster interpolation, this method better preserves the 3D information. However, the point cloud must be sorted or indexed in such a way that the number of points considered as possible neighbours is minimized. The seed points can be chosen automatically and at

random, with a condition imposed that they must be last returns to minimize the probability that they are not ground points. The pseudocode for this technique can be found in Appendix A, Section A.1.2.

For each last or single return point within the neighbourhood of a ground seed point, a probability is calculated that it is also a ground point. In effect, this is not an independent measure of whether the point being tested is a ground point but rather is a measure of whether the point should be identified as a ground point given its distance from a known ground point. The three probability functions used are:

$$p = 100 - 50 r \quad (4.1)$$

$$p = 100 - 25 r^2 \quad (4.2)$$

$$p = (5 r - 10)^2 \text{ for } r \leq 2, \quad (4.3)$$

where  $p$  is the probability, in percent, and  $r$  is distance measure in metres. All three functions were chosen to have 100% probability when  $r$  equals 0 m and 0% probability at 2 m metres (see Figure 4.4), since near points are very likely to belong to the same class but too much uncertainty exists within a point cloud to determine the class of one point based only on the class of another point beyond a couple of metres. Simple functions were chosen to limit the computational complexity of the algorithm.

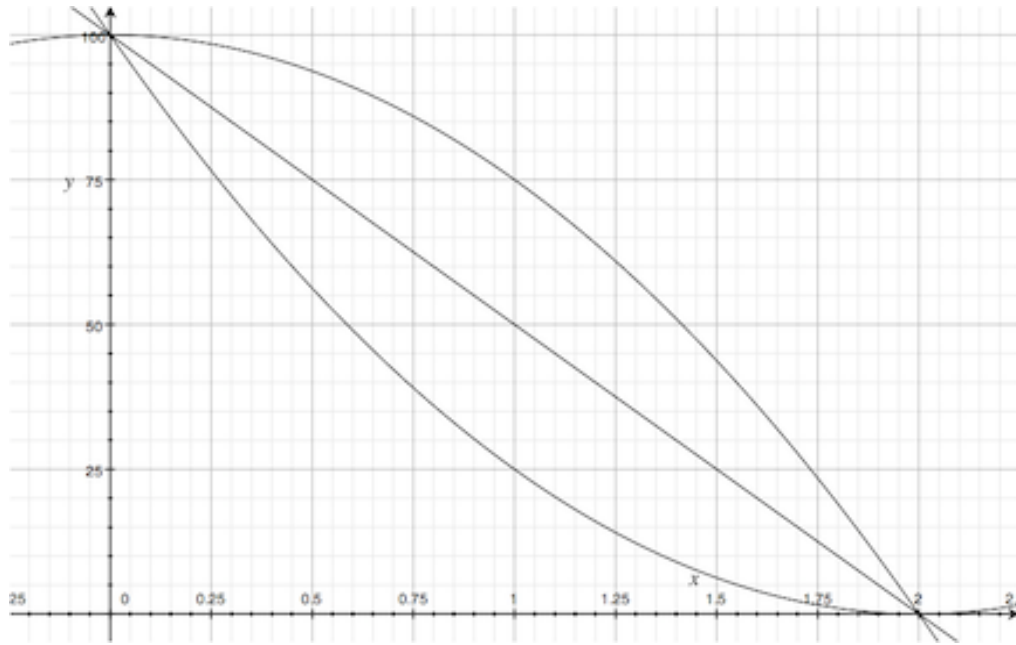


Figure 4.4

Probability curves for Point Neighbourhood method.

If the probability calculated for a point is greater than the set threshold percent, the point is marked as "ground." The initial threshold is set at 50% but can be set to a higher value to reduce the numbers points being marked as ground. Each of the functions is more or less "forgiving" of combined differences in planar ( $d$ ) and vertical ( $z$ ) distance (the  $r$  value) between a reference point and the target point, with Eq. 4.2 assigning the highest probability for a given  $r$  and Eq. 4.3 assigning the lowest probability. The distance measures are:

$$r = \Delta z + \Delta d/2 \quad (4.4)$$

for Eq. 4.1 and Eq. 4.2 and

$$r = \Delta z + \Delta d/3 \quad (4.5)$$

for Eq. 4.3, where

$$\Delta z = |z - z_0| \quad (4.6)$$

$$\Delta d = \sqrt{(x - x_0)^2 + (y - y_0)^2} \quad (4.7)$$

The  $\Delta z$  values are given a larger weight than the  $\Delta d$  values so that points with



large  $\Delta z$  and small  $\Delta d$  have lower probabilities than points with small  $\Delta z$  and large  $\Delta d$ .

The result of this process is a point cloud where points are marked either "ground" or "non-ground." Because the operation is applied directly to points, it gives a better representation of the actual ground sampling. However, it can only be applied when the point cloud has at least a minimum point density: if the point density is too low (i.e., less than 1 pt/m<sup>2</sup>), there is a risk that no points will be found within any neighbourhood even in flat, open terrain. This limitation applies under dense vegetation, even for point clouds that otherwise have a sufficiently high point density, because of the difficulty penetrating to the ground and the resulting sparseness of ground points. Figure 4.5 shows examples of the results, using Eq. 4.1 and Eq. 4.2.

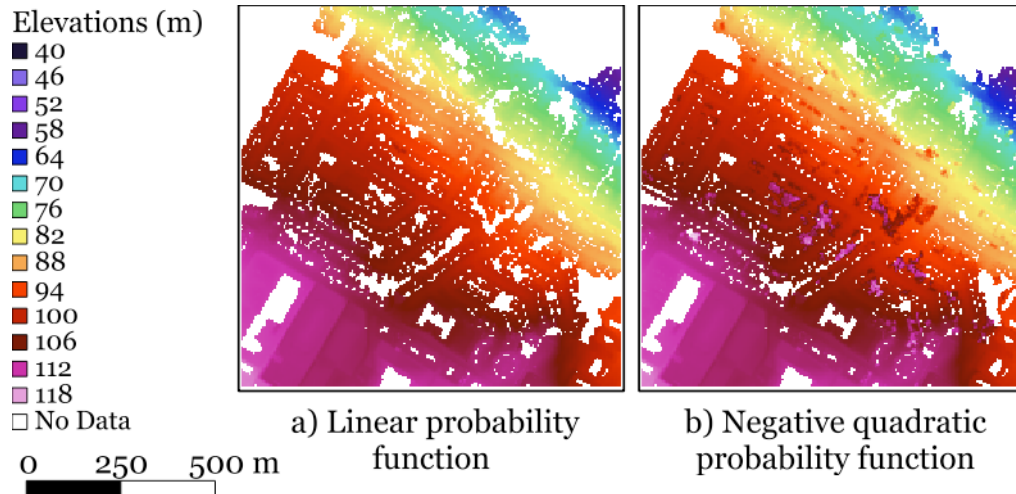


Figure 4.5

Results of the Point Neighbourhood method: a) probabilities calculated using Eq. 4.1; b) probabilities calculated using Eq. 4.2.

As implemented, the maximum distance for which a probability is calculated is 2 m. This value could be revised to accommodate sparser point clouds but,

when performing one-to-one comparisons, in the absence of other contextual information, there is more uncertainty about the relationship between points as the distance increases. Eq. 4.2 has, in fact, a tendency to mark vegetation as "ground" because the distance measure combined with the probability function will assign high probabilities to low vegetation points almost directly above ground points, and then higher vegetation points are also touched.

These probability calculations might seem counter-intuitive: if the terrain is sloped, then the calculations should allow for a greater elevation difference at larger planimetric distance, rather than the other way around. However, that approach would also assign higher probabilities to small non-ground objects at larger planimetric distances. By only allowing either  $\Delta z$  or  $\Delta d$  to be "large", only the points within a constrained neighbourhood are evaluated as possible ground points.

### **4.2.3. Wavelet Detail Mask**

The Wavelet Detail Mask method is a secondary method, meaning that it should not be used as a stand-alone method. It seeks out areas in a raster with no sudden changes in elevation by creating a mask to remove areas where there are sudden changes in elevation, or in other words, where there are terrain and feature details. The pseudocode for this technique can be found in Appendix A, Section A.1.3. Wavelet functions as applied to images produce an approximation image, or an image at a lower resolution, and a detail image; reversing the process restores the original image. The detail image is so-called because it

contains the details that were removed from the original image to create the approximation. When a non-decimating wavelet filter is applied, the approximation image stays at the original resolution and the detail image is simply the difference between the original image and the approximation. The results are therefore suitable for direct comparison with other images.

Areas in the detail image where the values are close to zero correspond to areas where there was very little difference between values in the window of the wavelet filter, or, in other words, flat areas. Areas in the detail image where the values are large ("large" being relative to scale) correspond to areas where there were large differences between the values in the wavelet filter window, or, in other words, areas where the surface is rough. For example, with LiDAR data, high vegetation will generally produce large detail values. Large detail values also occur at building edges and on sloped roofs.

To obtain the wavelet detail mask, the minimum LiDAR data values are interpolated to a regular grid and then a wavelet filter is applied to the interpolation. The wavelet filter that is used in this method is derived from a  $B_3$  cubic spline profile (as described in [Núñez et al., 1999]):

$$\frac{1}{256} \begin{bmatrix} 1 & 4 & 6 & 4 & 1 \\ 4 & 16 & 24 & 16 & 4 \\ 6 & 24 & 36 & 24 & 6 \\ 4 & 16 & 24 & 16 & 4 \\ 1 & 4 & 6 & 4 & 1 \end{bmatrix} \quad (4.8)$$

The mask is created from the resulting detail image, using thresholds to mark areas where there are abrupt changes in elevation. To mask all but the smallest variations, the initial threshold is  $\pm 0.15$  m.

The areas outside the mask are assumed to be ground, although flat roofs of large buildings are also outside the mask. Figure 4.6 shows an example of a wavelet detail image (Figure 4.6a) and the result of masking the elevation interpolation to produce a raster that shows only areas assumed to be ground (Figure 4.6b). Note that, contrary to the assumption, a large, flat building roof is in the unmasked area.

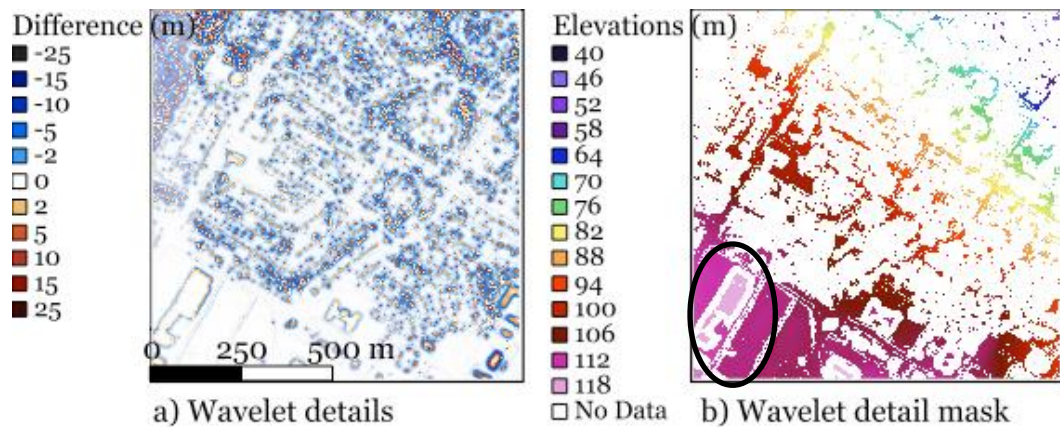


Figure 4.6

Results of Wavelet Detail Mask: a) wavelet details; b) masked areas contain no data while unmasked areas contain locally flat surfaces.

Depending on the roughness of the scene overall, a relatively small area might be unmasked and so this method may not be sufficient in and of itself to get a good ground approximation. It can, however, add support to the findings from other methods by confirming ground locations and elevations. A modification of the surface comparison technique, which will be described in Section 4.3 below, is to use the results of applying the wavelet detail mask as an override for the simple count measure, provided at least one of the other rasters in the surface comparison is a filled raster so that any flat rooftops remaining in the wavelet detail mask can be eliminated through value comparison.

#### 4.2.4. Preliminary Ground Points

The Preliminary Ground Points method is also a secondary method, as it depends on having an initial, preliminary ground raster, such as might be obtained using the Pixel Connectedness method, and so cannot be used independently. The initial ground raster should not have any gaps in data where buildings are located or where there are dense trees. Figure 4.7 illustrates the effect of filling an initial ground raster. As the name should imply, the ground representation does not need to be perfect: it only needs to be free of obviously too-high cells, i.e., above-ground elevation values.

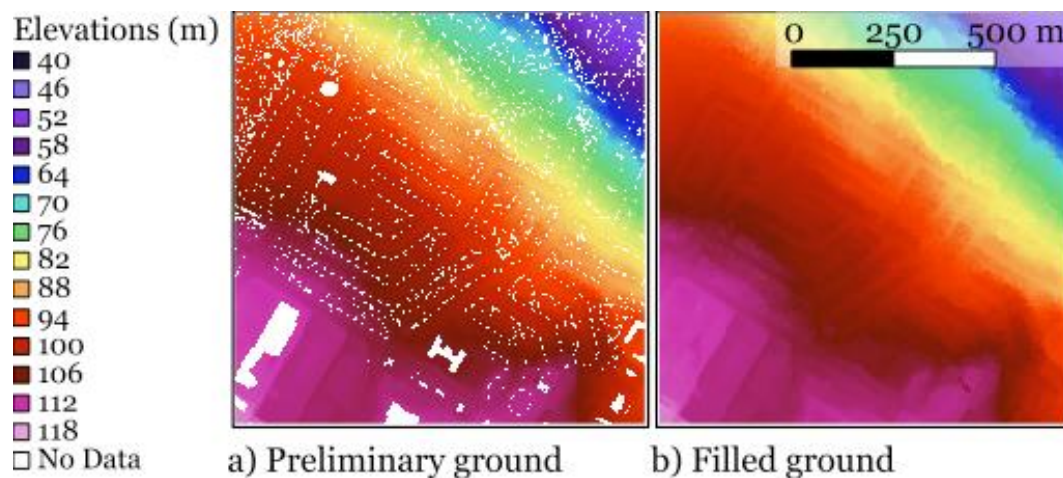


Figure 4.7

a) Initial ground raster with data gaps. b) Initial ground raster after gaps have been filled.

The method itself is point-based: any points with a HAG (determined by subtracting the ground raster value from the point elevation value) less than 1 m are marked as preliminary ground points. Points that are a reasonable distance below the initial ground surface are also marked as preliminary ground, which has the effect of pulling the initial surface down. This is a common approach

(e.g., [Kraus and Pfeifer, 1998; Briese and Pfeifer, 2001; Schickler and Thorpe, 2001]) to ground extraction, starting with a general surface and excluding points that are too high above while weighting points below more heavily to pull the surface down to the true ground surface. The pseudocode for this technique can be found in Appendix A, Section A.1.4. The preliminary ground points can be used to create a new ground raster and the process can be repeated if there are any substantial changes between the initial surface and the new surface or simply to further refine the estimate.

### **4.3. SURFACE COMPARISON TECHNIQUE**

Because of the complexity of any scene captured by ALS, the overall ground extraction solution has to be adaptable and must consider changes at various scales to determine if anomalies are a natural ground features or artificial objects. Each of the four methods described in the preceding section can be repeated, with variations, to refine to a certain extent the ground rasters that are produced but none can definitely find all ground in all cases. Combining the results from each, in an effective manner, can help overcome the limitations of each and produce a usable final result.

The surface comparison technique described here, and illustrated in Figure 4.8 and Appendix B, Figure B.10, is raster-based and therefore has the same underlying issues as any raster-based method, namely that it allows for a quick comparison even for very large areas, but there is a loss of information. The output from the point-based methods described above must be interpolated to a

grid to allow them to be compared to the output from the raster-based methods.

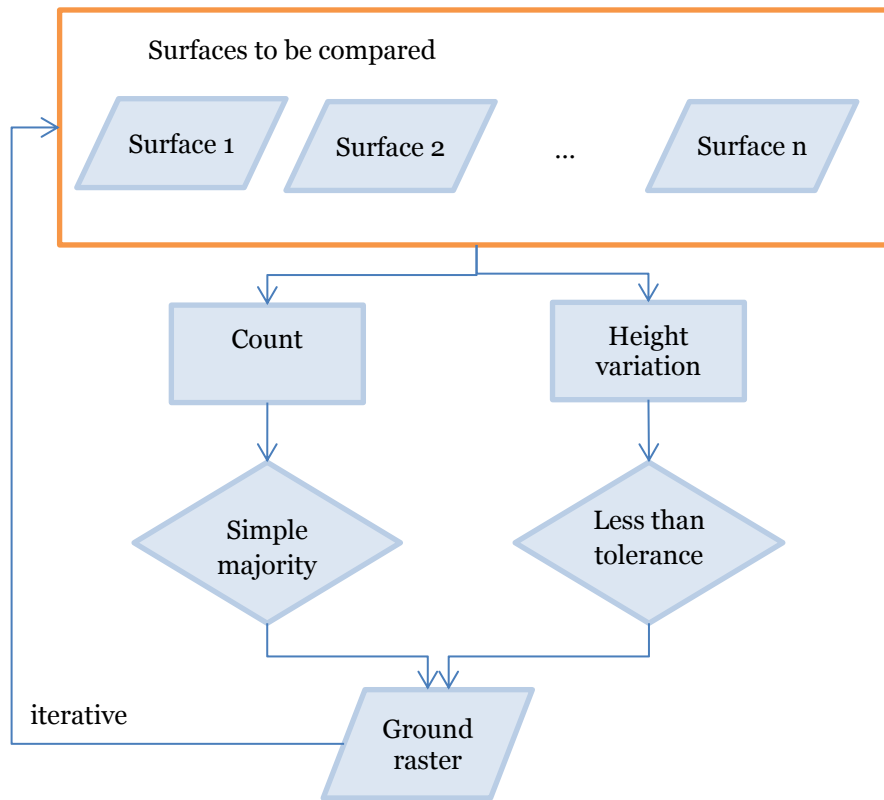


Figure 4.8

Surface comparison technique for obtaining a ground raster from a set of input ground surfaces.

Any number of surfaces can be compared using this technique, provided that in the input surfaces empty cells indicate no ground. Two local measures are used in the comparison to determine whether the (approximate) ground elevation has been found. The first measure is a simple count of how many of the rasters that are being compared have a value in a particular cell. With this measure, no assessment is made as to whether the value is actually ground. If a simple majority of the rasters contains a value, that cell can be considered a potential ground pixel.

The second measure is the standard deviation of values for the cell, however many values there might be. This is calculated only for cells where the count criterion is satisfied. Although a similarity in values for a particular cell does not guarantee that all of them are at or near ground, differences between values that are larger than the cell resolution suggest that non-ground features are present in one or more of the input surfaces. Provided that at least one method found a true ground value, or at least one of the surfaces being compared was filled to get a rough ground approximation below objects, the standard deviation where non-ground values were found will be greater than the set tolerance and so the higher, above-ground values will be rejected.

The surface comparison technique was tested by the author using two iterations and six input surfaces. The script used to implement the comparison technique can be found in Appendix A, Section A.1.5, as pseudocode. In the first iteration, the surfaces that were compared were:

1. Results from the Point Neighbourhood technique using Eq. 4.1 interpolated to a regular grid.
2. Results from the Point Neighbourhood technique using Eq. 4.3 interpolated to a regular grid.
3. Results from Pixel Connectedness technique using a  $15^\circ$  threshold.
4. Results from Pixel Connectedness technique using a  $10^\circ$  threshold.
5. Results from Preliminary Ground Points technique based on filled surface obtained through the Pixel Connectedness technique, interpolated to a regular grid.



6. Results from Wavelet Detail Mask technique using a threshold of  $\pm 0.15$ .

In the second iteration, the results from the first iteration replaced (2), since it was deemed to be most likely to contain non-ground. The results from one test area, namely the south-east tile in the Odell Park study area, are shown in Figure 4.9. The raster contains the average of values in cells where both of the two conditions described above, i.e., the count condition (simple majority) and standard deviation condition (below set tolerance), were met and no data in cells where one or both conditions failed.

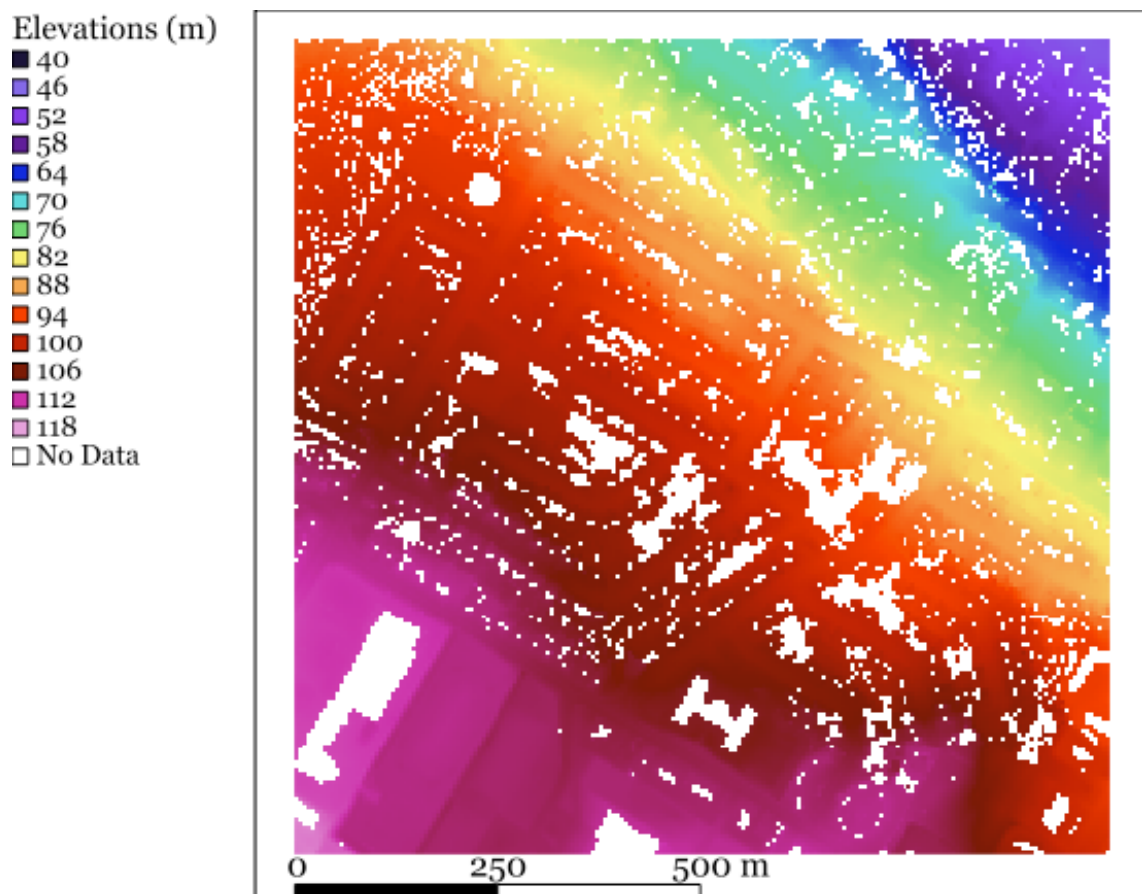


Figure 4.9

Example of the output from the surface comparison technique using six input surfaces and two iterations. The resolution is 5 m.

#### **4.4. GROUND POINT CLASSIFICATION AND REFINEMENT**

In the test results in Figure 4.9, as compared to the lower-right tile in Figure 3.2, it can be seen that ground points were detected under trees and large buildings were eliminated using the ground detection techniques and surface comparison technique described above. However, although a raster output may be suitable for some applications, the goal and the requirement in the NRCan guidelines is to classify points, not simply produce a ground raster. The comparison technique is therefore just a means to get an approximation of the ground through raster methods, which can then be refined through a combination of raster and point methods. The three main steps used in the refinement process, illustrated in Figure 4.10, are: interpolate, fill, and classify. The pseudocode for the fill and interpolate steps can be found in Appendix A, Section A.1.6 and for the classify step in Appendix A, Section A.1.4.

The output from the surface comparison technique is an interpolated raster that has no-data cells where buildings and dense vegetation are located. To ensure that all of the points in the point cloud can be compared to non-empty values in the raster, an iterative process is applied to fill the gaps based on the values in connected cells. The further away a no-data pixel is from data values, the less reliable the resulting fill value will be – but it is also less likely that there are ground data points in the area. Once all the no-data cells have been filled to produce an initial reference ground surface, the same technique as in the Preliminary Ground Points technique is applied to classify ground points.

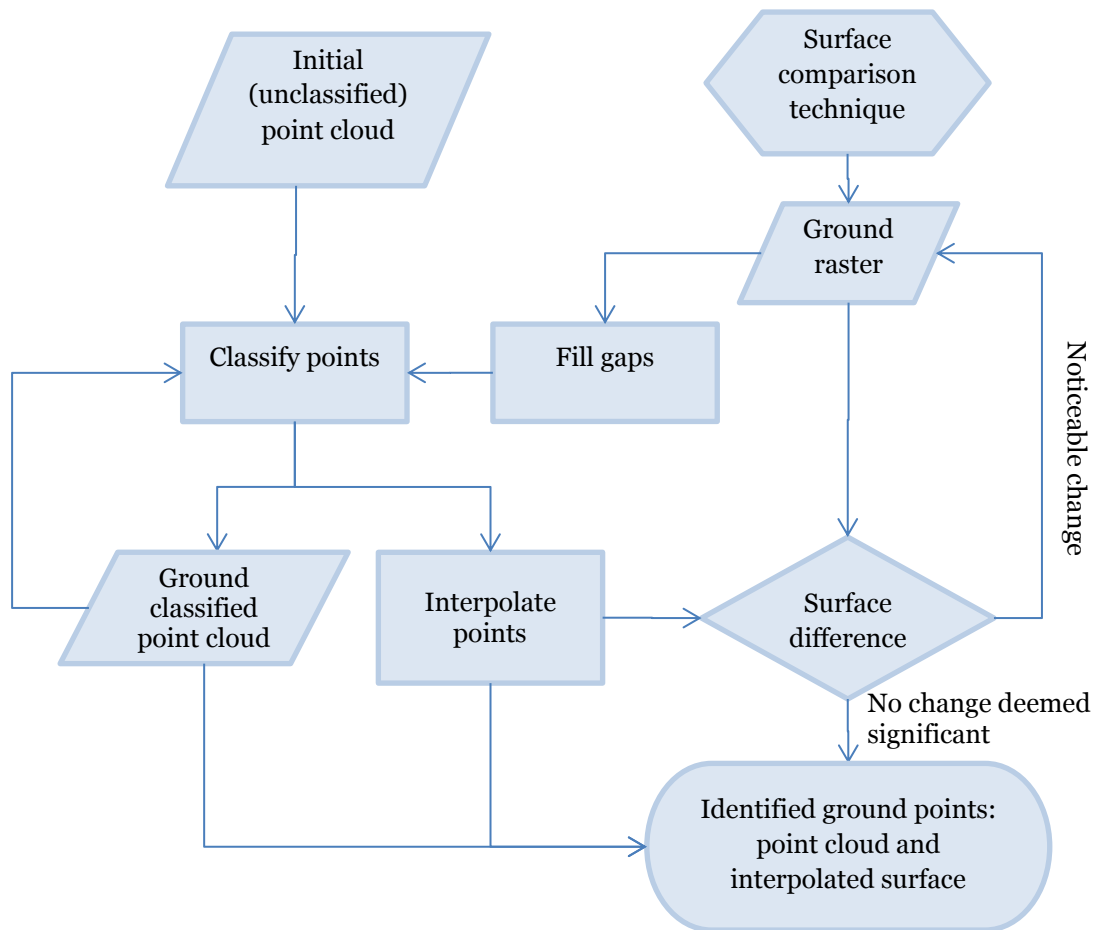


Figure 4.10

Ground point classification and refinement process.

A new reference surface is then created by interpolating the classified ground points to a raster at a resolution appropriate to the point density. Any points classified as ground that were below the initial reference ground surface will pull the new surface down. If there are noticeable changes between the initial reference surface and the new reference surface, the refinement process will be repeated: any holes in the new surface are filled, points are classified against the filled raster, and a reference surface is created for comparison. An example of the surfaces can be seen in Appendix B, Figure B.11.

The final GPI test results for tile 2487\_7438 (Odell Park study area, south-east tile) from the 2011 LiDAR data set are shown in Figure 4.11, interpolated to a regular grid for display purposes. The differences between it and Figure 4.9 are due to differences in resolution. The output of the surface comparison technique cannot be at a higher resolution than the resolution of the input surfaces because the technique is entirely raster based. A 5 m resolution was chosen for testing the ground detection techniques (Section 4.2) and the surface comparison technique (Section 4.3) because of the improved ground detection under forest canopy at this resolution, as illustrated in Figure 2.2, and consequently the example output shown in Figure 4.9 has a 5 m resolution.

In contrast, the ground point classification and refinement process can take an input raster at any resolution and output a raster at any resolution because the classification step of the process is point based. Repeated iterations of the process will minimize any negative effects on classification due to the initial input raster resolution and once classified, the points can be interpolated at any resolution. The resolution of Figure 4.11 is 2 m because this is a more appropriate resolution for the point density of the data set than 5 m.

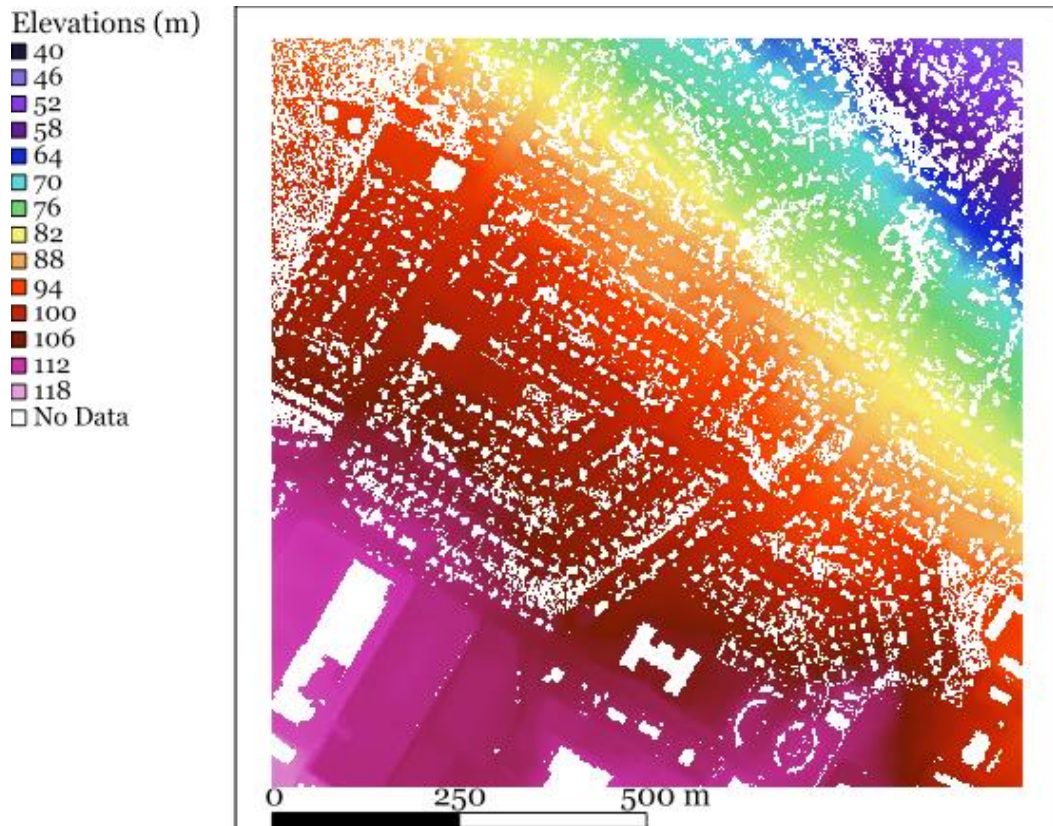


Figure 4.11

Sample interpolation at 2 m resolution of final ground point classification results.

#### 4.5. TESTING AND ACCURACY

The stated objective was to develop a ground point identification process that achieves 95% point classification accuracy. This should be achieved under various conditions without the need for any operator input, or without the need for operator input that requires technical knowledge. To test the results of the GPI process, seven tiles were chosen from the 2011 Fredericton LiDAR data to represent a variety of terrain, vegetation, and building conditions. Four of the selected tiles, as shown in Figure 3.2, encompass most of Odell Park and the

adjacent residential and commercial properties; one is a section of Garden Creek where there are no artificial structures; one is a section of UNB campus and residential properties to the north-west (the intersection of Beaverbrook and Windsor is at the north-west corner of the tile); and one is part of the City Plat and includes a section of the Saint John River.

The exact same parameters that are listed in Section 4.3 for testing the surface comparison technique, and, by extension, the four different ground detection techniques, were applied to all seven tiles. Seed pixels for the Pixel Connectedness technique and seed points for the Point Neighbourhood technique were chosen randomly for each tile. Once the second iteration of the surface comparison technique was completed for each tile, three iterations of the described point classification and refinement process were applied to each tile. Significant differences were observed after the first iteration due to the change of resolution between the interpolations (from 5 m for the input ground raster from the surface comparison technique to 2 m for the output raster). Differences observed after the second iteration were only around features edges and were almost all less than 0.5 m. Samples of the test output images can be found in Appendix B.

The final resolution for the extracted ground raster was chosen as 2 m because of low overall NPD for all of the tiles and the presence of dense vegetation, which further lowers the NPD for ground-only points. However, the extracted ground raster is a secondary product of GPI. The classification of points as ground within the point cloud is the primary product of the GPI.

### 4.5.1. Accuracy Assessment

The 2011 Fredericton data, as obtained from the data provider, were classified as ground (class 2) and a few other classes. Unfortunately, it is unclear what definitions were used for the other classes. For example, some points classified as "5", which is the code for "high vegetation" in the LAS format specifications, are very close to ground level. Since manually classifying a large enough number of points to conduct a reliable accuracy assessment was not feasible, the ground classification tool that is part of the *LAStools*<sup>™</sup> package was used in an attempt to get a comparable classification. The *LAStools*<sup>™</sup> package was chosen because it was free to use for research purposes at the time of testing. However, the classification was only partially successful: the widely-accepted *LAStools*<sup>™</sup> ground classification tool, called *lasground*, found some ground points that the GPI process did not, and vice versa. Furthermore, *lasground* requires the user to either select one of "forest or hills", "town or flats", "city or warehouses", or "metropolis", none of which adequately describe the areas being tested; or manually set four different parameters. This requirement makes it difficult for a user who is not familiar with the parameters of *lasground* to use the tool.

The difficulties in obtaining true ground are illustrated in Figure 4.12a and 4.12b, which are a point representation and a raster interpolation, respectively, of the location of ground points from a sample area under vegetation. The blue points or pixels show the locations where only the *LAStools*<sup>™</sup> method identified ground points, orange points or pixels show the locations where only the GPI process identified ground points, and brown points or pixels are the locations

where both methods identified ground points. White pixels in Figure 4.12b are the locations where no ground points were identified by either method. Non-ground points were omitted from Figure 4.12a. Figure 4.12c and 4.12d, which are raster interpolations of the elevation values of identified ground points, show no anomalies in ground elevation between the two, suggesting that: (1) both methods may be equally valid and (2) neither is capable of finding all the ground points under dense vegetation that exist in the point cloud.

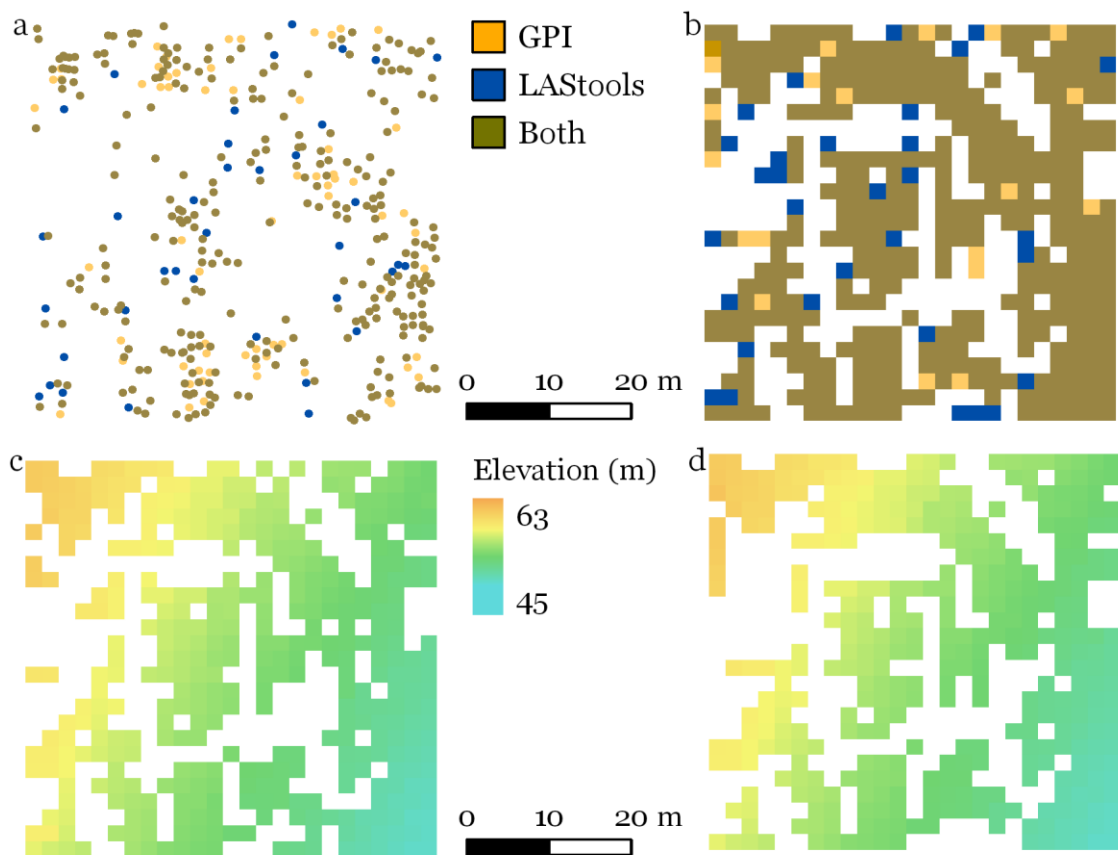


Figure 4.12

Limitations in quantifying ground classification accuracy: a) point representation and b) raster representation of locations of points classified as ground by *LAStools*<sup>TM</sup> (blue), by the GPI process (orange) and by both (brown) or neither (white) method; and interpolation of ground elevation from c) *LAStools*<sup>TM</sup> results and d) GPI process results.



The NRCan guidelines require classification accuracy to be reported in an error matrix. Although true accuracy cannot be determined without true ground, an assessment can be conducted against the *LAStools* results. To achieve this, the test tiles were divided into 50 m x 50 m segments and approximately 1% were randomly selected for assessment. The selected segments contained 151,245 points, or 1.26% of all the points in the test tiles. Table 4.2 is the error matrix for all of the points in the randomly selected segments, while Table 4.3 is the error matrix for Segment 6412, which is around E 2486375 N 7438725 in a densely forested part of Odell Park. The location and point cloud for Segment 6412 are shown in Figure 4.13.

As compared to the *LAStools*<sup>TM</sup> ground (forest or hills setting), which is not necessarily true ground, all measures of accuracy are above 95% for the aggregate sample. As Polygon 6412 illustrates, however, accuracy is lower for GPI ground versus *LAStools*<sup>TM</sup> ground. Similar results occur with all of the sample segments that include a significant amount of high vegetation. Without closely examining all of the points in these sample segments, it is not possible to determine whether it is the *LAStools*<sup>TM</sup> classification or the GPI classification that is in error, yet a visual examination and quick analysis of the Segment 6412 results show that the differences fall into one of three cases.

Table 4.2  
Error matrix for all points in randomly selected polygons.

	<b>GPI ground</b>	<b>GPI non-ground</b>	<b>User's accuracy</b>
<b>LAStools ground</b>	62079	1748	<b>97.26%</b>
<b>LAStools non-ground</b>	3115	84303	<b>96.44%</b>
<b>Producer's accuracy</b>	<b>95.22%</b>	<b>97.97%</b>	<b>96.78%</b>

Table 4.3  
Error matrix for Polygon 6412.

	<b>GPI ground</b>	<b>GPI non-ground</b>	<b>User's accuracy</b>
<b>LAStools ground</b>	157	0	<b>100.00%</b>
<b>LAStools non-ground</b>	38	5087	<b>99.26%</b>
<b>Producer's accuracy</b>	<b>80.51%</b>	<b>100.00%</b>	<b>99.28%</b>



Figure 4.13

Location and point cloud representation of Segment 6412, within the Odell Park study area.

First, there are *LAStools*<sup>™</sup> non-ground points that are spatially very close to a surface interpolated from the *LAStools*<sup>™</sup> ground points and would likely be classified as ground if different parameter values had been set for the *lasground* tool. Second, of the 38 GPI ground points that are non-ground points in the *LAStools*<sup>™</sup> results, seven are within 15 cm of the interpolated ground and another fifteen are between 15 cm and 30 cm. This is within the fundamental vertical accuracy of LiDAR measurements specified in the NRCan guidelines. Third, of the nine GPI ground points that are more than 0.5 m above the interpolated ground, most are located around a small discontinuity in the surface. In the GPI algorithm, the classification of all of these points was flagged as being of lower confidence than points closer to the surface.

As a further attempt to test the accuracy of GPI, other data sets that had passed through a classification process used by commercial data producers were obtained from GeoDigital International [Lehto, 2012b]. One data set was from an area of downtown Ottawa, Ont., and the other from Oklahoma. Upon examination of the data, however, it was found that while points classified as "ground" were true ground, the unclassified points included a large number of points that were within 0.3 m of ground, or, in other words, that were within the target vertical accuracy for LiDAR and that might normally be assumed to be ground points. This uncertainty in ground point classification precludes the calculation of a meaningful error matrix. The measures that are meaningful are user's accuracy for ground (matched GPI ground versus all GeoDigital ground points) and producer's accuracy for non-ground (matched GPI non-ground

versus all GPI non-ground points). For both the Ottawa and Oklahoma data sets, greater than 99% is achieved for these measures.

There are similarities between the Ottawa and Oklahoma scenes and the Fredericton scenes. The Ottawa data cover a portion of the city's downtown, including Parliament hill. It is similar to the tested Fredericton tile covering the City Plat. However, the buildings in the Ottawa data are larger and in many cases more complex than the ones in Fredericton data. They are also surrounded by less vegetation. Most of the vegetation in the Ottawa scene is along the river, where there is also a steep terrain slope. The Oklahoma data cover an area outside Tulsa. They are similar to the data from Odell Park or Garden Creek, but the terrain is flatter (approximately 15 m change in elevation as compared to approximately 40 m or more) and the vegetation less dense. While more extensive accuracy testing over a wider range of terrain conditions would be valuable, the assessments that were completed show that the ground classification accuracy of GPI as compared to other ground classification processes is sufficiently high to meet the requirements in the NRCan guidelines in mixed urban scenes with varying terrain and areas of high vegetation. Furthermore, visual inspection of the classification results did not reveal any significant errors.

## **4.6. SUMMARY OF GPI PROCESS**

In this chapter, a process was described for identifying and classifying ground points in a point cloud. The process is comprised of a set of detection techniques,

a surface comparison technique, and a point classification and refinement process. Four detection techniques were described, each of which produces a ground surface raster within the GPI process. The ground surfaces are compared and a ground raster extracted from the comparison. The ground raster is then used to identify ground points within the original point cloud and classify all points as either ground or non-ground. In the next chapter, a multi-stage point classification process is described that starts with the GPI output and progressively identifies additional classes in the point cloud.

*"The physician can bury his mistakes, but the architect can only advise his client to plant vines."*

*~ Frank Lloyd Wright*

## **CHAPTER 5**

### **CLASSIFICATION OF SINGLE SOURCE LIDAR DATA SETS**

Ground extraction may be sufficient for applications where only terrain information is needed, but only extracting ground points effectively discards a significant amount of the collected information and there are many applications, such as augmented reality and street view navigation, where there is a need for detailed representations of buildings and other objects. Although airborne LiDAR often cannot provide very much information about building façades, if the point cloud is accurately classified it can be used to estimate building footprints as well as obtain height information for buildings and other objects that may not be available from other data sources, such as satellite imagery (see, for example, [Haala and Brenner, 1999; Zhou et al., 2009; Kabolizade et al., 2010; Chase et al., 2011]).

When the only data available are in a single point cloud, there are limits to what is achievable with automated classification and a multi-stage process is necessary. The *LAStools*<sup>™</sup> software, for example, employs three stages: ground extraction, calculation of HAG, and classification of buildings and vegetation. Clusters of points at least 2 m above ground are considered objects and buildings are separated from vegetation using planarity conditions. The user, however, needs to be able to categorize the scene or be familiar enough with the effects of

varying different parameters on ground extraction results to select appropriate values [Isenburg, n.d.]. Building classification can also be performed in *LP360*<sup>TM</sup> but, again, the user needs to be able to specify appropriate parameters.

This chapter describes the process developed in this thesis, illustrated in Figure 5.1 and henceforth referred to as MSPC for "multi-stage point classification," to classify points in a LiDAR point cloud. The stages of MSPC are:

1. Ground surface extraction (from the output of the process described in Chapter 4) and high and low noise identification.
2. Preliminary classification (Section 5.1), to identify potential vegetation and building points.
3. Building classification (Section 5.2).
4. Identification of areas of uncertainty and de-classification of points within those areas (Section 5.3).
5. High vegetation classification (Section 5.4).
6. Separation of low vegetation and roads or other paved surfaces (Section 5.5).
7. Identification of vehicles and other objects above road surfaces (Section 5.5).

With the exception of Stage 1, which offers a choice between two measures, and Stage 6, which requires a threshold to be set, the MSPC does not require user input and therefore does not require the user to have any expert knowledge. Pseudocode for the MSPC process implementation can be found in Appendix A, Section A.2.

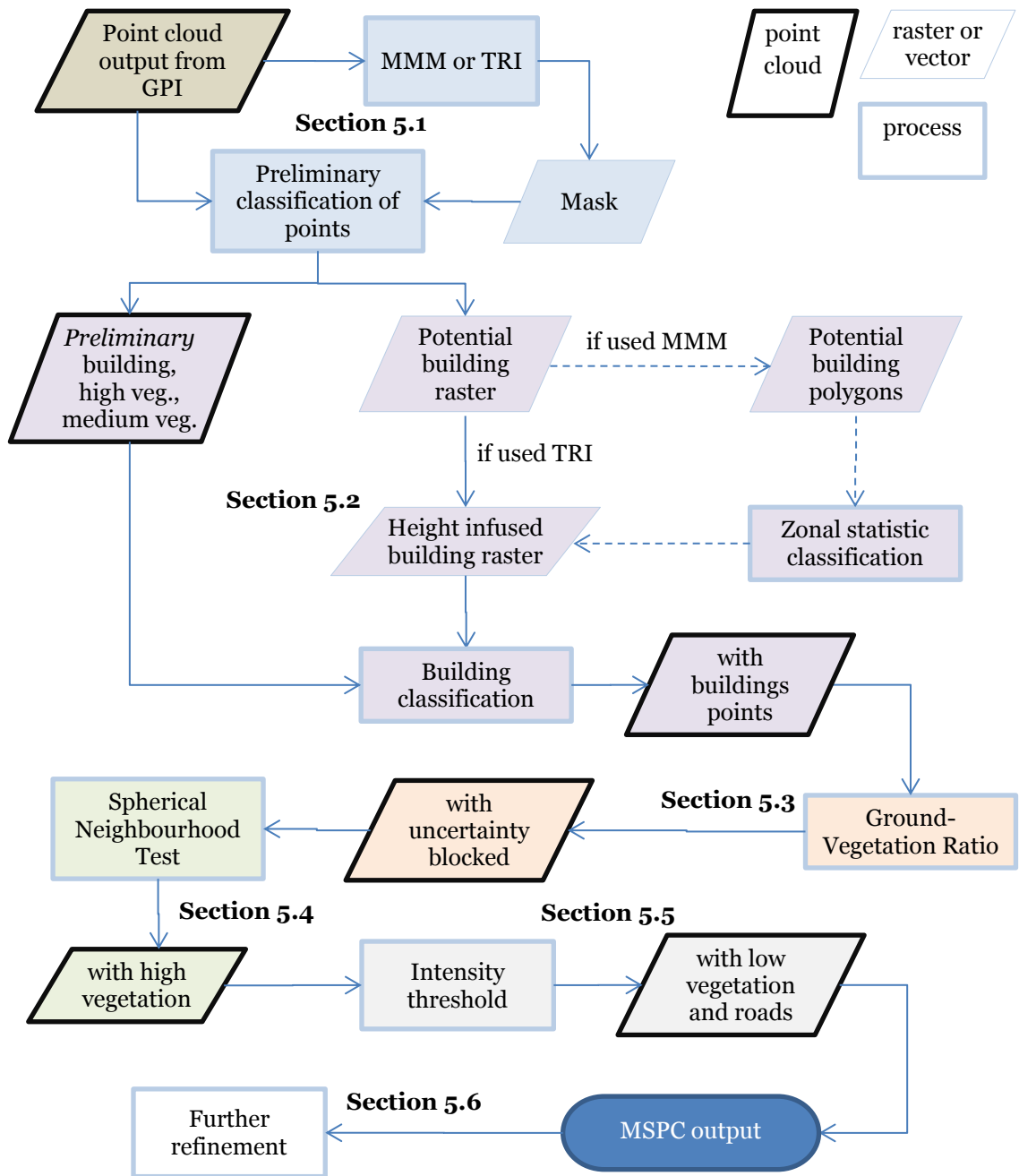


Figure 5.1

Flowchart for the Multi-Stage Point Classification process. Although both TRI and MMM masks may be generated for comparison, only one is used to generate a height infused building raster.



## **5.1. PRELIMINARY CLASSIFICATION**

The primary classes present in a typical urban scene are ground, building, and high vegetation. Buildings in general have identifiable characteristics, such as height, shape, and roof planarity, while vegetation and other objects can have greatly varying characteristics. The goal of the preliminary classification stage is to separate (likely) building points from non-building. The pseudocode for preliminary classification can be found in Appendix A, Section A.2.1

Because of variations in how scenes are captured during LiDAR surveys and similarities in the way objects appear in the point cloud, particularly when there is limited spatial context, no assumptions can be made about the accuracy of the preliminary classification; it is simply a starting point for further classification and a means to derive spatial context in the form of rasters from the point cloud. Two approaches were developed and tested in this work: Terrain Ruggedness Index (TRI) Thresholding and Multiple Returns and Height Measures Masking (MMM).

### **5.1.1. Terrain Ruggedness Index Thresholding**

TRI, proposed by Riley et al. [1999], is a measure of changes in surface elevation (described in Section 3.1.1.3). Larger TRI values mean greater variation in elevations within the window but the values are scale dependent: the range of index values and the interpretation of the values changes with the resolution of the raster. Ideally, to use TRI to identify potential buildings, the resolution should be 1 m. TRI can be applied to different raster interpolations. From tests

conducted on different interpolations it was determined that for the TRI thresholding approach the best representation for capturing all surface variations, particularly where there is dense vegetation, is one created using IDW rather than one created through averaging or maxima selection. However, where a scene contains buildings with recessed entrances, a maximum surface is a better choice so that any points captured from the ground within these recesses would not interfere with the rooftop points above the recesses.

TRI images, such as the one shown in Figure 5.2a, have too much variability to be used directly. Instead, a threshold is applied to locate flat pixels: for a 1 m resolution raster, flat pixels are defined as those having a TRI value below 5. Isolated pixels that differ in value from the surrounding pixels after the threshold is applied, also called "salt and pepper noise," are identified by examining the adjacent eight pixels and changing the value to match the surrounding pixels to produce a cleaner image.

If in the cleaned image a pixel is not touching any flat pixels, the corresponding surface is, by definition, "rough" and the preliminary classification algorithm labels any non-ground points in rough areas as "vegetation." If a pixel is touching many flat pixels (more than six), the corresponding surface and surrounding neighbourhood are deemed to be relatively flat. Figure 5.2b shows the resulting mask corresponding to Figure 5.2a, where the colour black represents flat neighbourhoods and the colour green represents rugged neighbourhoods.

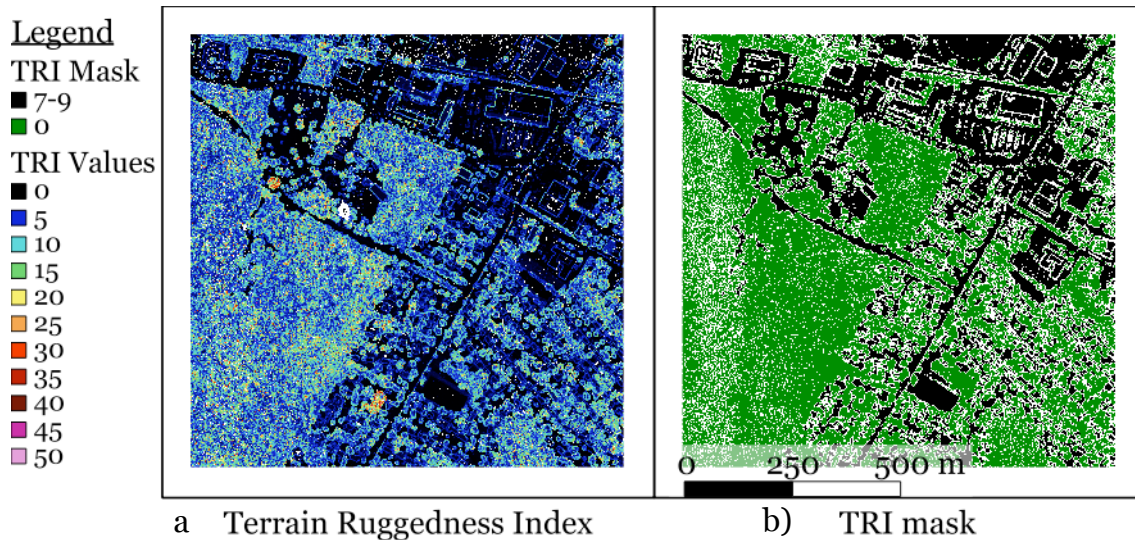


Figure 5.2

Example of a) TRI image and b) corresponding TRI mask.

At this stage of the MSPC, it is preferable to have errors of omission rather than errors of commission for each of the preliminary classes. Points erroneously omitted from a preliminary class may be added to a class in later stages. HAG is the deciding factor for classifying non-ground points:

1. Last return points in flat neighbourhoods that are more than 2 m above ground are classified as "preliminary building points."
2. Points in rough areas that are between 0.3 and 2 m above ground are classified as "preliminary medium vegetation points."
3. Those points that are more than 2 m above ground are classified as "preliminary high vegetation points."

Points that do not satisfy the criteria for any of the three preliminary classes, and have not been previously identified as ground, are left unclassified. The restriction that only last returns can be preliminary buildings points is applied because buildings should be solid. Although the measure does exclude first

returns that occur at rooftop edges, there is significant uncertainty associated with such points and therefore they should not be included in preliminary classification.

Figure 5.3 shows an example of preliminary building classification results along with building footprint shapes obtained from CoF open data site, overlaid on an elevation raster. It should be noted that, to better illustrate the point classification results in this image, a raster was generated showing where points classified as preliminary building were located. It is therefore not fully representative of the point cloud classification. A similar approach was used for other figures in this chapter.

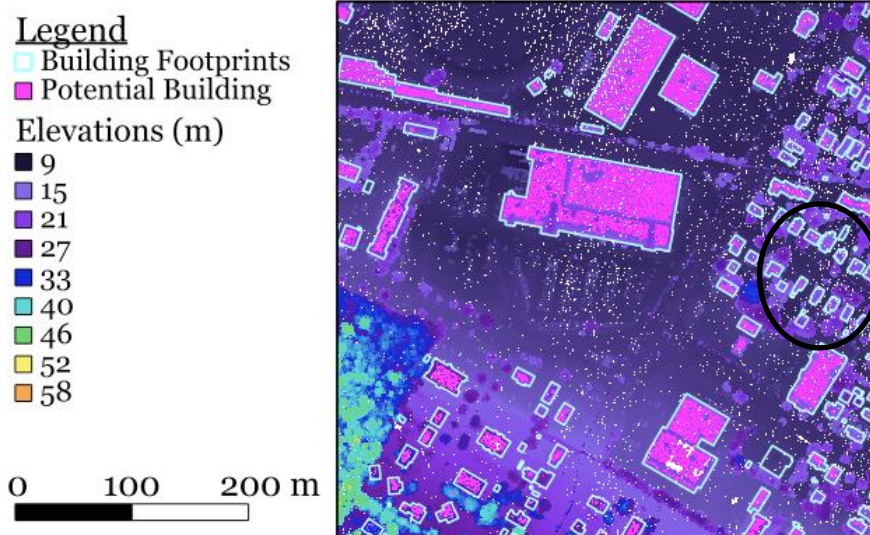


Figure 5.3

Example of preliminary building classification using TRI Thresholding method. The circled area highlights small building under vegetation that remain unclassified.

### **5.1.2. Multiple Returns and Height Measures Masking**

As can be seen in Figure 5.3, the TRI method may fail to detect small buildings surrounded by high vegetation; in contrast, using the MMM method, as shown in Figure 5.4, produces results that correspond more completely to the building footprints. The MMM method seeks to overcome the TRI limitations by looking for solid regions that are above ground and have little range in elevation between highest and lowest points. The mask is produced by combining three measures:

1. An interpolation of multiple return counts (or an MRD), where a zero value means no pulses were split by edges or by partial penetration of openings in vegetation (Figure 5.5a).
2. The difference between the highest and lowest points, where a value less than 1 m for a 1 m image resolution means that the maximum slope within the cell is no greater than the slope of a typical slanted roof (Figure 5.5b).
3. HAG for the minimum point, where a value greater than 1 m means that there is an object above ground level (Figure 5.5c).

As with the TRI mask, salt and pepper noise is removed in the images representing each of the three measures by examining the eight adjacent pixels for each potential noise pixel. Then the images are combined to find neighbourhoods where all three conditions hold. Figure 5.5 illustrates the process of creating the mask. In each of the images, white represents areas where the condition failed. Figure 5.5d is the resulting mask. The same height

conditions are applied as described above to classify preliminary medium vegetation, high vegetation, and building points.

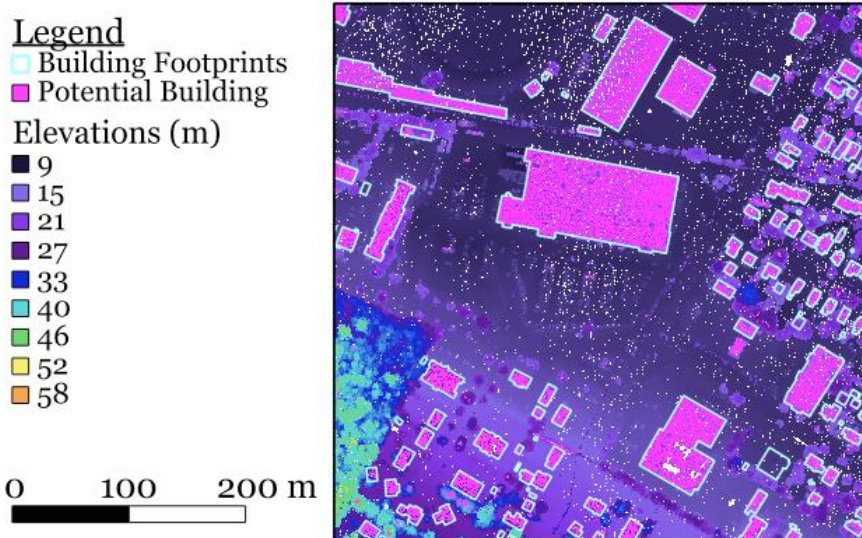


Figure 5.4

Example of preliminary building classification using MMM method.

### 5.1.3. Limitations

Neither of the approaches described in the previous two sections perform perfectly. The TRI method is largely successful in avoiding false building detection within areas of vegetation yet performs poorly in residential areas with mature tree cover where only a small portion of house roofs may be visible. It performs best in scenes where there is clear separation between buildings and vegetation. The MMM method performs very well in detecting building points (as compared to building footprints), even detecting small houses partially obstructed by trees, yet it also detects false buildings in areas of dense, high, narrow vegetation (i.e., tall hedges). It will perform best where such vegetation does not exist or can be easily detected.

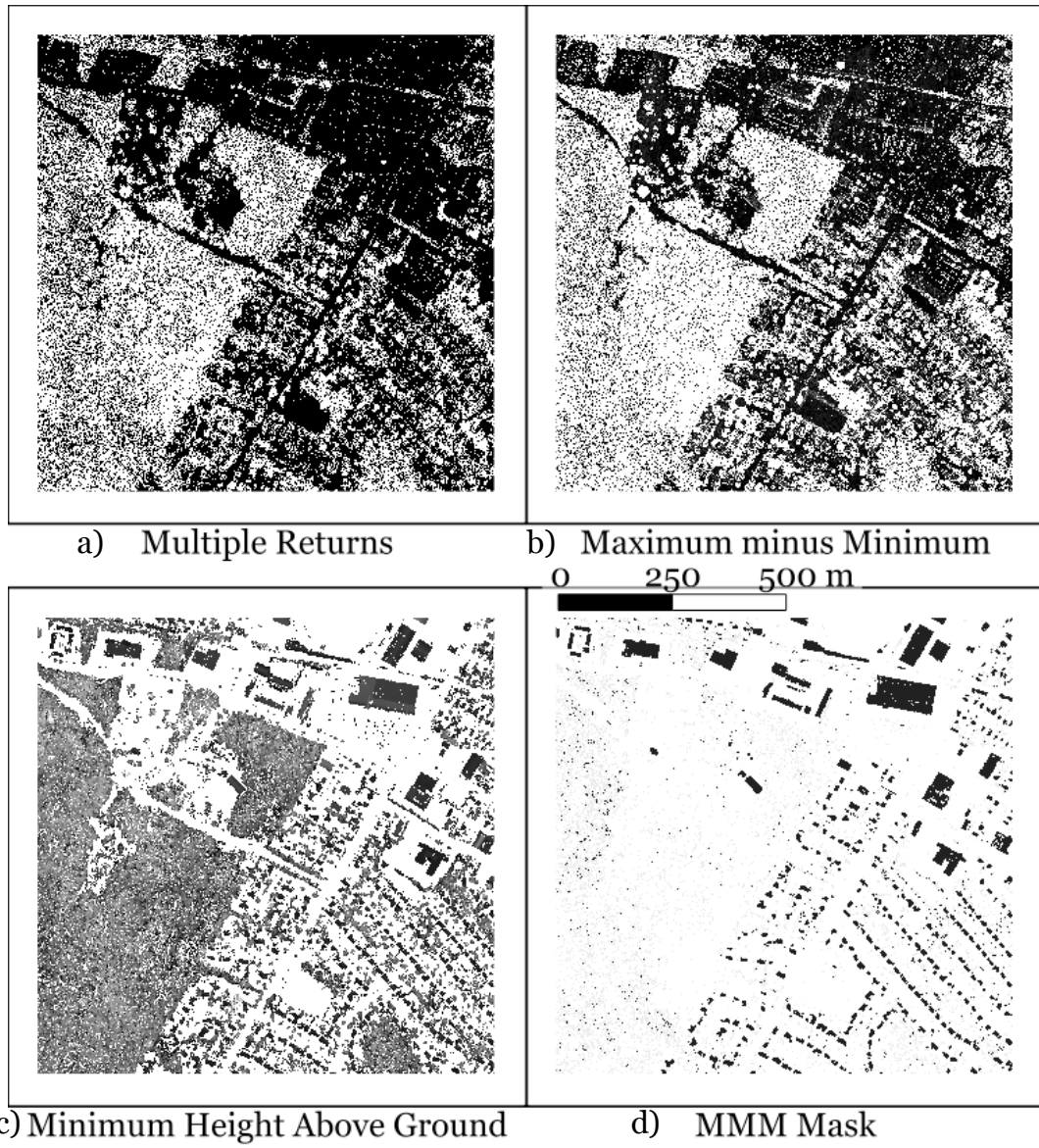


Figure 5.5

Example of a) Multiple return interpolation; b) difference between maximum and minimum values; c) minimum HAG; and d) the resulting MMM mask. In all images, black represents areas where the conditions were met.

While most buildings conform to basic shapes, there are almost endless variations possible for even small, simple houses that will always create challenges and cause failures in automatic building detection. Large buildings present even more variations, and creative architecture. As an illustration of the challenges, Figure 5.6 shows two views of a point cloud representation of the Centre Block on Parliament Hill in Ottawa from the data provided by GeoDigital International [Lehto, 2012b]. The single building has multiple level rooftops, steeply pitched roofs, the round Library of Parliament, and the tall Peace Tower. Even the flag flying from the Peace Tower is visible in the point cloud. The MMM method is able to detect more of the building than the TRI method, but the round shape and irregular roof structure of the Library of Parliament just do not follow normal rules for buildings and present a challenge for any automated classification approach.



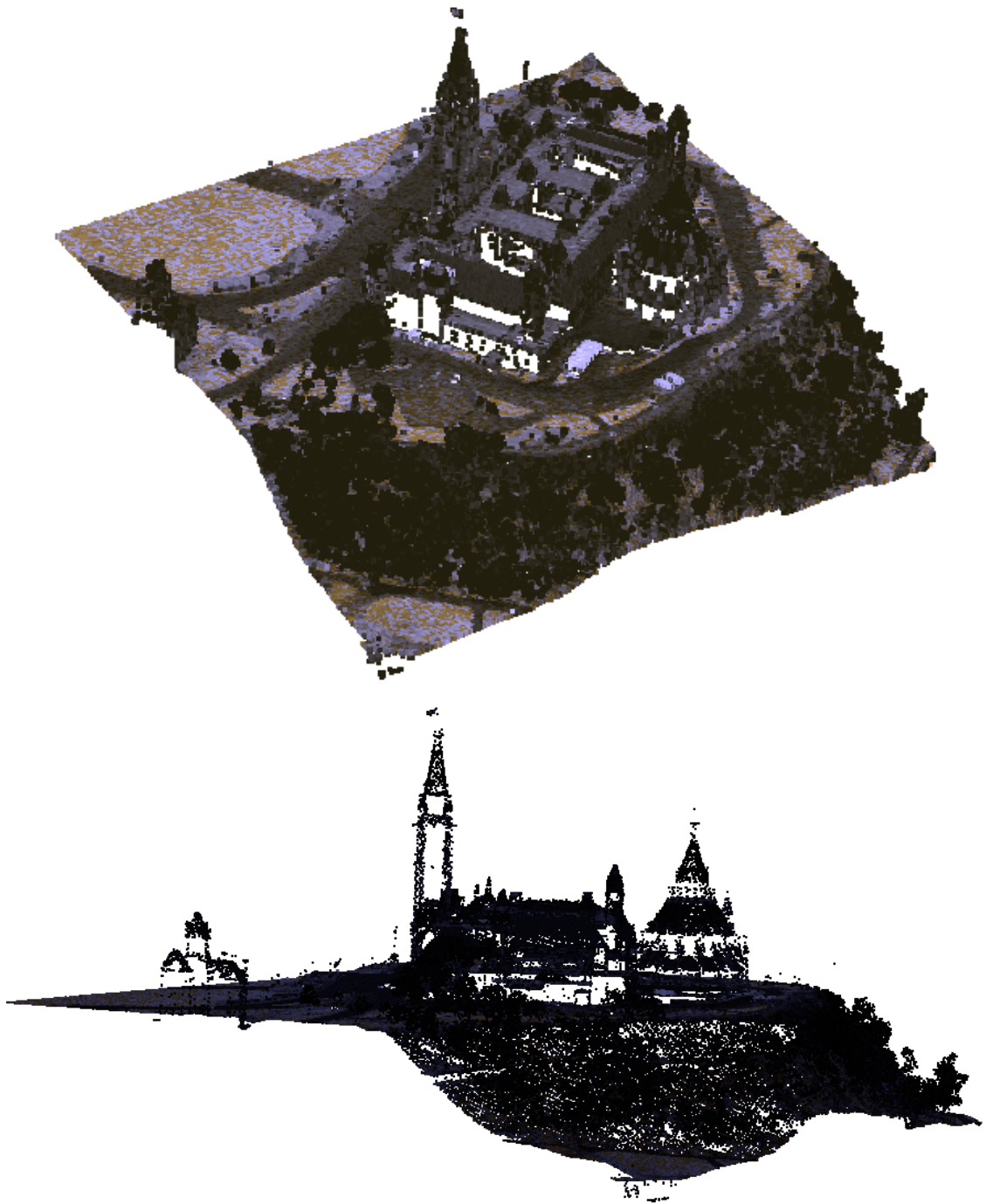


Figure 5.6

Point cloud representation of the Centre Block of Parliament Hill in Ottawa, from data provided by GeoDigital International [Lehto, 2012a].

## 5.2. BUILDING CLASSIFICATION

The goal of the preliminary classification is to separate potential building points from non-building points; the next step is to find actual buildings. The pseudocode for building classification can be found in Appendix A, A.2.2. This is accomplished in the MSPC process using a building mask infused with elevations based on the results of the preliminary classification. If the TRI thresholding method captures the buildings in a scene sufficiently well, the mask can be derived directly from the potential building points.

If the MMM method is to be used, some processing is required to eliminate as many false positives as possible before the mask is derived. First, a binary image with 1 m resolution is created from the points classified as potential buildings by the MMM method. Isolated pixels both outside and inside of larger shapes are removed based on the value of the eight adjacent pixels to produce a cleaner image and the results are vectorized to obtain potential building polygons. Zonal statistics are then calculated from the minimum HAG raster, including number of pixels, sum of values, and mean value of pixels within the polygon. When the raster has a 1 m resolution, the number of pixels is equivalent to the total area of the polygon.

The zonal statistics are used to classify the polygons. Although there will be some variability in statistics between different data sets, the polygon classifications are generally applicable. The classes based on area are:

- (1) Class A: area > 100 m<sup>2</sup> (very large building)
- (2) Class B: 60 m<sup>2</sup> < area ≤ 100 m<sup>2</sup> (large building)

(3) Class C:  $\text{area} < 8 \text{ m}^2$  (too small to identify)

The classes based on both area and HAG are:

(4) Class D:  $21 \text{ m}^2 \leq \text{area} \leq 60 \text{ m}^2$  and  $8.0 \text{ m} < \text{HAG} < 11.0 \text{ m}$  (largish high building, probably)

(5) Class E:  $21 \text{ m}^2 \leq \text{area} \leq 60 \text{ m}^2$  and  $\text{HAG} < 8.0 \text{ m}$  (largish normal building, probably)

(6) Class F:  $12 \text{ m}^2 \leq \text{area} \leq 20 \text{ m}^2$  and  $\text{HAG} < 6.0 \text{ m}$  (normal house, probably)

(7) Class G:  $8 \text{ m}^2 \leq \text{area} \leq 11 \text{ m}^2$  and  $\text{HAG} < 6.0 \text{ m}$  (fragment of house, probably)

The smaller the count, the greater the uncertainty about what the polygon represents and there are likely to be polygons on the wrong side of the last four thresholds: there is too much variability in how LiDAR points are collected, as well as in captured features, to allow for clear boundaries that can be used to conclusively separate all features.

Once the polygons are classified, a raster is created based on the classes defined above, excluding Class C, and finally the raster is infused with elevation values. The reason for converting back to raster is to obtain localized heights on the roofs, rather than some summary of heights for the shape, to have a better chance of classifying points on sloped roofs. Figure 5.7 shows an example of the classified polygons (a) and the mask infused with elevation values (b).

In the figures, a Class D polygon (circled, top right) and two Class F polygons (circled, centre) are actually hedges, but this could only be determined through

close examination of the point cloud. Although the mask derivation process can be run automatically, to improve the results the user could intervene to omit Classes F and G when creating the mask to remove more polygons that represent trees, although this risks also excluding some smaller buildings. Class D could be omitted because these could also be dense trees or hedges. Alternatively, a user could examine the polygon classifications manually to determine which polygons to keep.

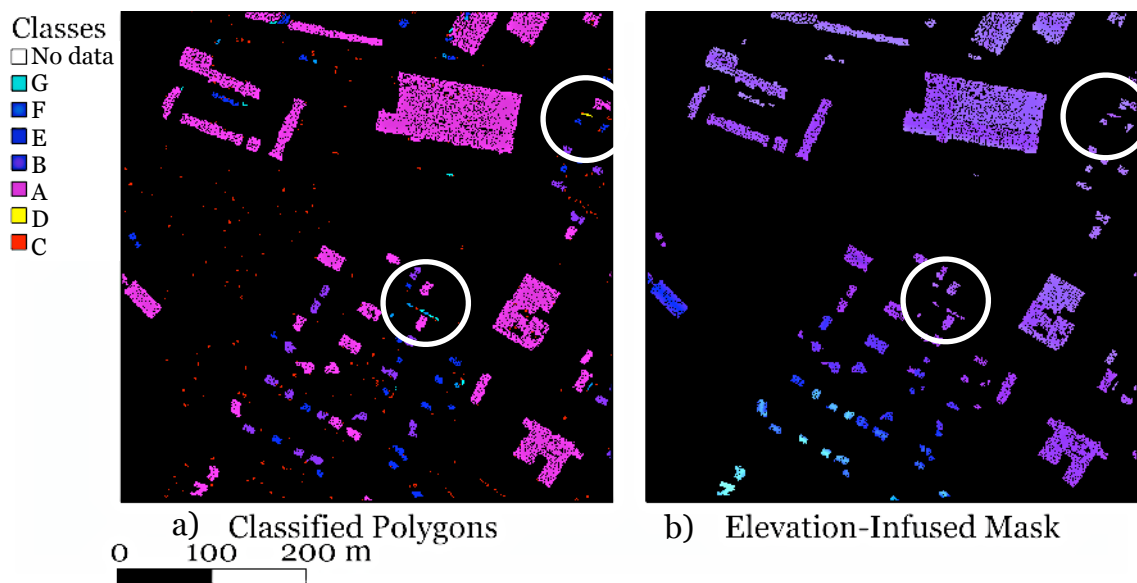


Figure 5.7

Example of building classification process from MMM results: a) classified potential building polygons; b) building mask infused with elevation values.

Whether the building mask is derived from the TRI results or the MMM results, the building classification process is completed by conducting a point classification where points that are less than 1 m above the mask elevation are deemed to be building points. This excludes high overhanging tree points, while including any wall points that are at least 0.3 m above ground if the mask extends to the edge of the building.

### **5.3. UNCERTAINTY AND DECLASSIFICATION**

Building points can be classified without too much difficulty because buildings have characteristics that can be defined in code and/or otherwise, aside from the exceptions noted in Section 5.1.3. Points belonging to any other features, however, present complications. Rather than risk misclassifying such points, in the MSPC process areas with the greatest classification uncertainty are blocked out by applying an uncertainty measure and points within those areas remain unclassified to allow greater confidence in the points that are classified. The pseudocode for this stage can be found in Appendix A, Section A.2.3.

The measure used to map areas of uncertainty is a ground-vegetation ratio, which is described in Section 3.1.2. The purpose of the ratio, as illustrated in Figure 5.8, is to find areas where there is a certainty of ground classification (Figure 5.8a) and areas where, given the preliminary and building classification results, there is a certainty of objects that are above ground and not (yet) identified as buildings (Figure 5.8b). Uncertainty occurs where there is both a significant percentage of points in the window that are ground and a significant percentage of points that are not building (Figure 5.8c). In the figure, the value for "significant" was set at 10%. This uncertainty measure blocks most power lines, the edges of vegetation, and some building edges, as can be seen in Figure 5.8d. Any points within an area of uncertainty are not classified or declassified in the MSPC process.

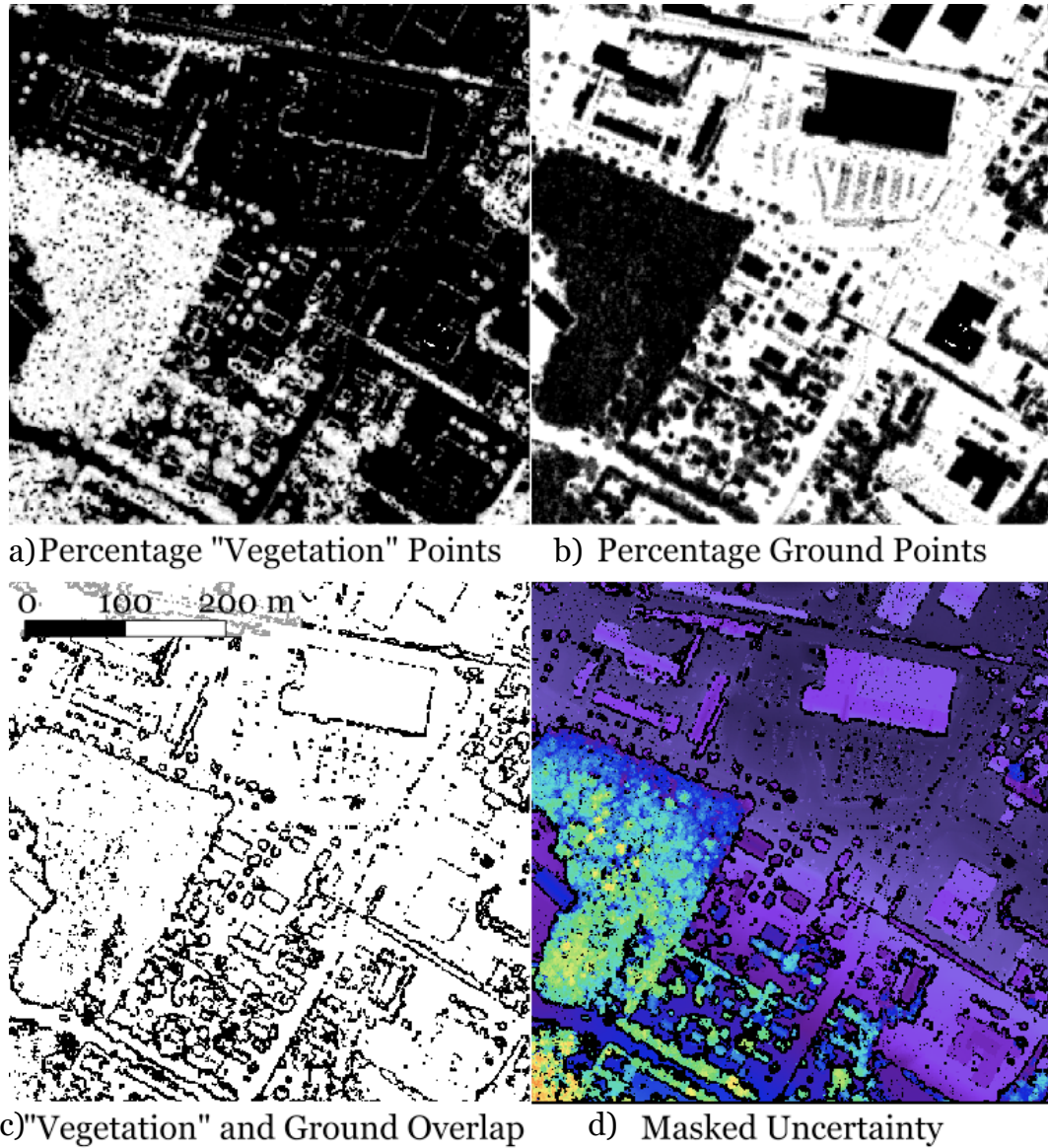


Figure 5.8

Illustration of uncertainty measure: a) percentage of non-ground, non-building points in a 3 x 3 window; b) percentage of ground points in a 3 x 3 window; c) resulting uncertainty mask; and d) uncertainty mask overlaid on a raster interpolation of elevation.

## 5.4. HIGH VEGETATION CLASSIFICATION

By this, the fifth stage of the MSPC process (see Figure 5.1), points have been classified as ground and buildings, marked as being in an area of uncertainty, or identified as preliminary vegetation. If the uncertainty measure described in the previous section is fully successful the points still classified as "preliminary vegetation" points should be true vegetation but that is not always the case. To increase the degree of certainty for vegetation, two criteria are applied in the MSPC process. The pseudocode for high vegetation classification can be found in Appendix A, Section A.2.4. First, the points in a 2 m spherical neighbourhood around a preliminary vegetation point are tested and at least 50% have to be of the same class, i.e., preliminary vegetation. The 2 m distance is based on the height for the high vegetation classification in the NRCan guidelines. This criterion removes points around the edges of vegetation (and buildings), leaving points in the "preliminary vegetation" class for which there is a high level of confidence that they are truly vegetation rather than other non-building objects.

The second criterion is that a point that has been marked as preliminary vegetation has to be within range (1 m) of other such points. Any points satisfying both criteria are classified as high vegetation. The NRCan guidelines simply stipulate that "high vegetation" is more than 2 m above ground and "medium vegetation" is 0.3 m to 2 m above ground. During testing of the high vegetation classification process, fewer than 3% of points marked as preliminary vegetation in the second stage of the MSPC process (Section 5.1) were found to be between 0.3 to 2 m above ground, and most of these were located on roads or

in parking lots (vehicles), adjacent to buildings (raised decks, walls), or within areas of high vegetation. Therefore, for this classification process, the "medium vegetation" class was used for preliminary vegetation points for which a majority of neighbouring points were also preliminary vegetation but that were more than 1 m away from any such neighbours, along with any vegetation points between 0.3 and 2 m above ground. This change to the definition of "medium vegetation" provides an extra measure of certainty for the "high vegetation" class. Although it is possible that more errors of omission will occur as a result of the changed definition, there are fewer errors of commission in the high vegetation class than there would be without the change. Figure 5.9 shows an example of the results of vegetation classification.

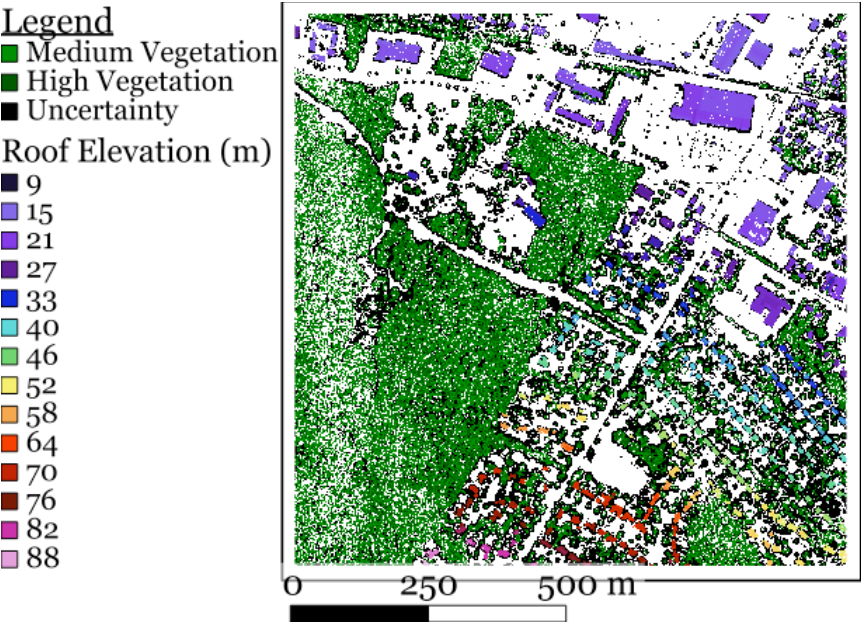


Figure 5.9

Example of high and medium vegetation classification results with building roof elevation included to provide context.



## **5.5. ROADS, LOW VEGETATION AND OBJECTS ABOVE ROAD**

"Ground" consists of roads and other paved surfaces; grass and other low vegetation cover; and bare soil. The material reflectivity, which is captured in the point intensity values, is used in the MSPC process as a better means to separate these groups than elevation. Asphalt generally has low reflectivity while vegetation has high reflectivity, but there is no absolute threshold: unhealthy (dry) grass may have low reflectance while faded asphalt and gravel may have high reflectance. Furthermore, when multiple returns are generated from a pulse, the total energy is split between the returns so even highly reflective materials may generate returns with low intensity values. Multiple returns are therefore excluded from either class (ground or low vegetation) in the MSPC process to avoid misclassification. The pseudocode for this stage can be found in Appendix A, Section A.2.5.

The threshold that is used must be chosen arbitrarily, but depends, to a certain extent, on the sensor that was used to collect the data and on the scene. Figure 5.10 is an example, for illustration purposes, of an intensity value histogram for single returns classified as ground. (It is depicted as a scatter plot rather than as a vertical bar graph for readability purposes.) In this particular data set, there is a plateau in point counts from values around 70 to 110 then an increase up to the peak at around 145. Different data sets will have different ground intensity histograms. In this and similar scenes, the threshold to split between road and grass lies somewhere in the plateau, at a high enough value so that most road points will be classified as road, and at a low enough value so that

few low vegetation points are classified as road. The threshold value is arbitrarily chosen within the range of plateau values.

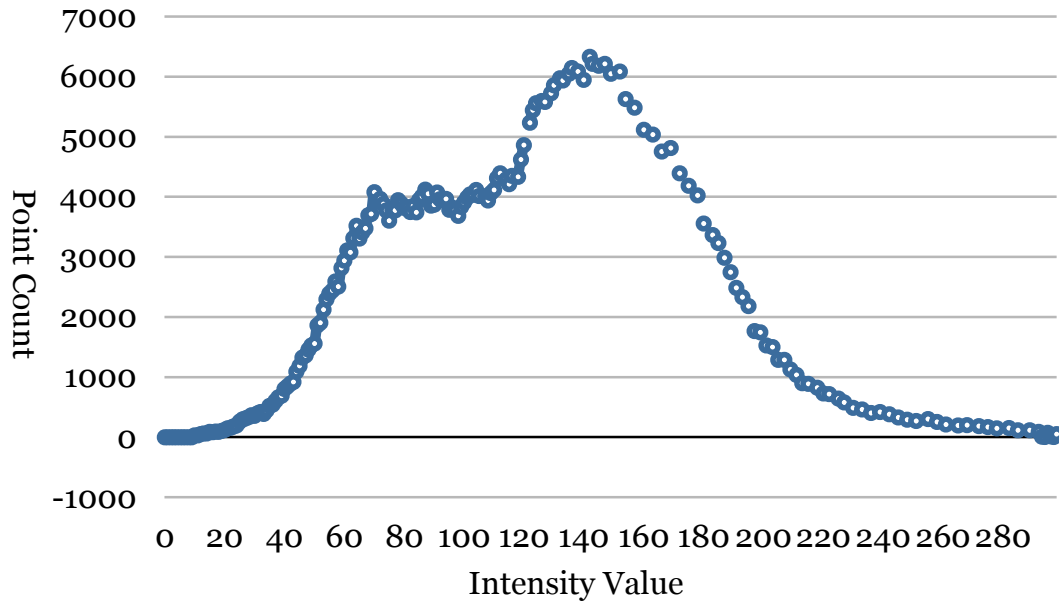


Figure 5.10

Example of a ground intensity histogram. Exact shape will be different for each data set.

Points in the ground set with an intensity value below the threshold are classified as road points. Vehicles are then located within the point cloud by creating a binary road mask and identifying points within the mask that are 0.3 to 2 m above ground. Points that are within the mask that are more than 2 m above ground are classified as "other objects above the road surface." The pseudocode for this stage can be found in Appendix A, Section A.2.6. The height threshold was chosen based on an estimate of typical car height. Some vehicles will be higher, such as trucks and buses, but mostly the threshold will separate overhanging trees, overhead wires and signs, streetlights, and other such features that are in the space directly above a road or paved surface. Figure 5.11

shows an example of "road" and "low vegetation", and "vehicle" and "other object" classification.

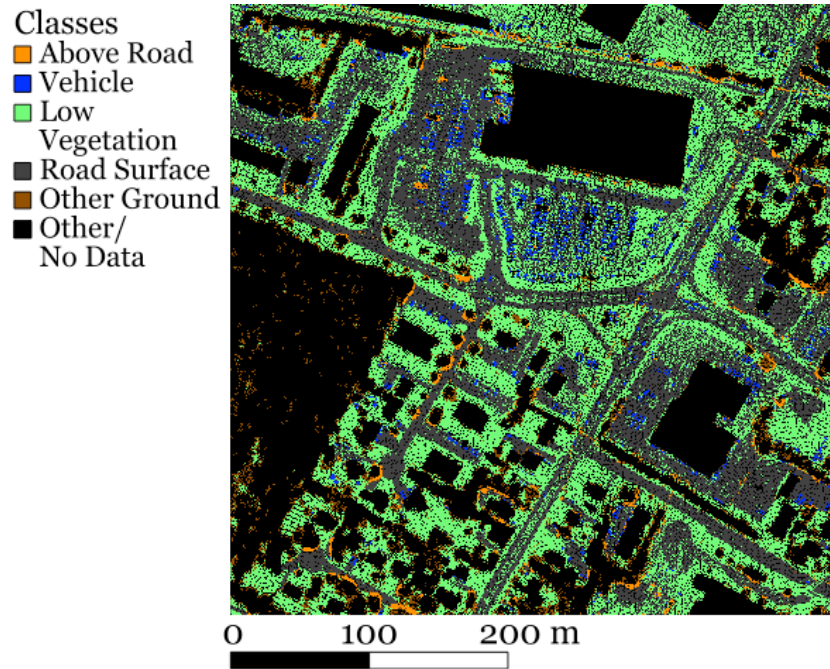


Figure 5.11

Example of road surface, low vegetation, vehicle and other above road feature classification results.

## 5.6. REMAINDERS AND ACCURACY

A large number of points remain unclassified after the MSPC process described above is complete, because in the development of the process errors of omission were preferred over errors of commission. Sample results are described in Section 5.6.1 and quantified in Table 5.1. Pseudocode for the implementation of the MSPC process can be found in Appendix A.

Any stage of the classification process can be rerun, with masks of greater certainty or changed restrictions, to slowly reduce the errors of omission.

Processing time will vary for each stage depending on the size and number of points in the area being processed and on whether the stage employs raster-based techniques or point neighbourhood techniques (and on the hardware capabilities). In testing using the Fredericton data, processing time for each stage was on the order of seconds or tens of seconds. The only decisions that the user must make are whether to use the TRI or MMM technique in preliminary classification and intensity threshold to use to differentiate between roads and low vegetation. Criteria could be developed to make these decisions based on the data, thereby allowing the MSPC process to be fully automated.

Yet, there is a limit to how many of the points can be accurately classified without resorting to manual classification, as the variability in where points fall with respect to feature locations and in intensity values precludes being able to create any definite rule base. In addition, no attempt was made to classify water solely from the point cloud in the MSPC process. Often, water bodies return no data due to the way water reflects and/or absorbs the laser energy. Where returns *are* generated, the points do not have any distinctive properties that allow them to be separated from ground points. Different approaches have been applied by researchers to handle water points or wet areas, for example Cook et al. [2009], Höfle et al. [2009], Wang et al. [2009], and Wu et al. [2009]. A method for classifying water points using data from other sources is proposed in Chapter 6.

One final classification step that was tested was to identify building edges (potential wall points). This step is not part of the MSPC process because it

depends on having all building points classified and a reliable roof height, and furthermore because the generation of such points is highly dependent on the orientation of the airborne platform with respect to the building. In the test that was conducted, points below the building height and more than 0.3 m above ground were marked as edges, as were points up to 1 m above building height that were not last returns, which had the effect of outlining buildings where pulses were split into multiple returns at the roof edge. Figure 5.12 shows an example of a point cloud representation of the building edge point classification.

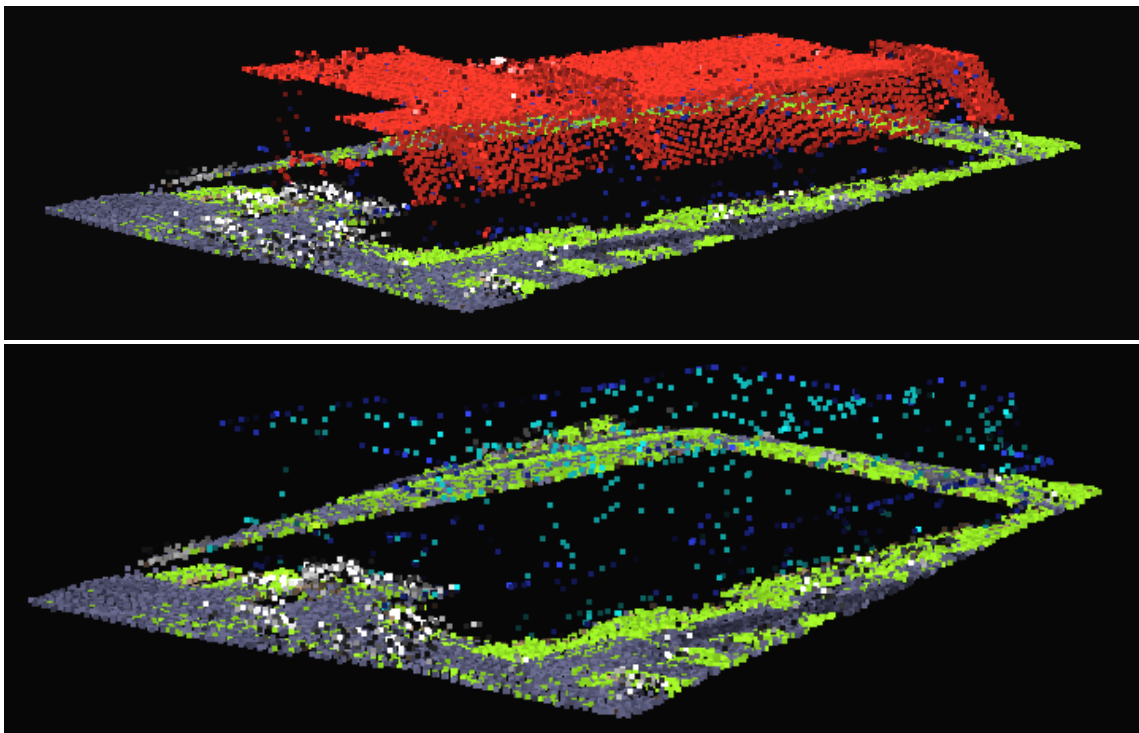


Figure 5.12

Example of building edge classification results. In the upper image, non-edge roof points are in red; in the lower image, these points have been removed to make the edge points more visible.

### 5.6.1. Sample Classification Results

Tables 5.1 and 5.2 contain the numeric results from testing the MSPC process described in the previous sections on tile 2487\_7439 of the Fredericton data (Odell study area, north-east tile). Figures 5.13 and 5.14 are raster representations of the classification results. Approximately 25% of the points are in an area of uncertainty or otherwise remain unclassified. The edge classification criteria operated on all except ground points, on the assumption that the building mask did not extend far beyond the actual building area and any points within the mask must therefore belong to the building.

Table 5.1

Sample classification results for tile 2487\_7439, without building edge classification.

<b>class</b>	<b>count</b>	<b>%</b>	<b>class</b>	<b>count</b>	<b>%</b>
<b>low vegetation</b>	273,471	15.15%	<b>medium vegetation</b>	212,922	11.79%
<b>road surface</b>	195,556	10.83%	<b>high vegetation</b>	413,993	22.93%
<b>other ground</b>	88,655	4.91%	<b>area of uncertainty</b>	156,867	8.69%
<b>vehicle</b>	11,145	0.62%	<b>not classified</b>	295,535	16.37%
<b>object above road</b>	30,551	1.69%	<b>high noise</b>	20	0.00%
<b>building</b>	126,478	7.01%	<b>low noise</b>	2	0.00%

Table 5.2

Sample classification results for tile 2487\_7439, with building edge classification.

class	count	%	class	count	%
low vegetation	273,350	15.14%	medium vegetation	212,609	11.78%
road surface	195,510	10.83%	high vegetation	413,622	22.91%
other ground	88,655	4.91%	area of uncertainty	153,653	8.51%
vehicle	10,291	0.57%	not classified	292,912	16.23%
object above road	30,199	1.67%			
building	116,894	6.48%	building edge	17,478	0.97%

- Classification
- Medium Vegetation
  - High Vegetation
  - Building Edge
  - Building
  - Over Road
  - Vehicle
  - Road Surface
  - Low Vegetation
  - Other Ground
  - Unclassified/No Data
  - Uncertain



Figure 5.13

Raster representation of point classification results for tile 2487\_7439.

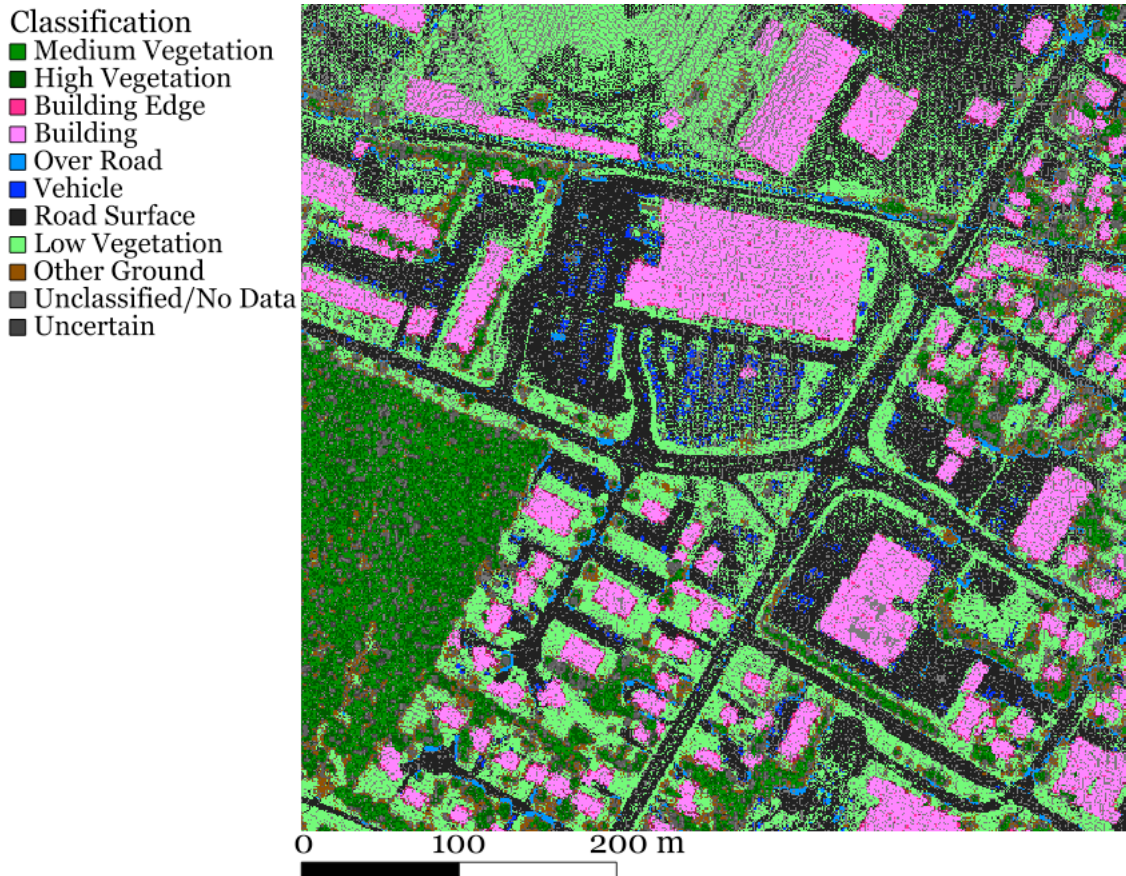


Figure 5.14

Enlarged section of classification results for tile 2487\_7439.

### 5.6.2. Classification Accuracy Assessment

The points in the Fredericton data sets that were obtained for testing were classified as Class 2, 3, or 5 by the data provider yet a visual examination showed that this classification could not be taken as truth. For example, points included in Class 5, "high vegetation," were observed to be building points. The software tools that were available to the author could not produce a truth set large enough (several hundreds of thousands of points) for a rigorous accuracy assessment, either through automatic or manual processes. Therefore, accuracy tests of ground and building classification for three 50 m x 50 m sample areas were



completed. The sample areas were manually classified, classified using the MSPC process up to the building classification stage, and with *LAStools*<sup>™</sup> as a gauge against the performance of a freely available tool. For convenience, these will be referred to as Manual, MSPCb, and LAStools, respectively.

The numerical results of the classification assessment are summarized in Tables 5.3 and 5.4. Overall, MSPCb performed marginally better as compared to Manual than LAStools. In particular, MSPCb performed better with ground classification in terms of both errors of omission (only 8 points versus 71) and errors of commission (222 points versus 386). LAStools was found to be more likely to classify building points as ground (374 points versus 112), whereas MSPCb detected more true building points (1759 points versus 1600) and was otherwise more likely to classify a building point as "other" than as "ground."

Table 5.3  
Ground and building classification accuracy using MSPCb.

	<b>MSPCb other</b>	<b>MSPCb ground</b>	<b>MSPCb building</b>	<b>User's accuracy</b>
<b>Manual other</b>	1122	110	0	<b>91.07%</b>
<b>Manual ground</b>	8	8429	0	<b>99.91%</b>
<b>Manual building</b>	576	112	1759	<b>71.88%</b>
<b>Producer's accuracy</b>	<b>65.77%</b>	<b>97.43%</b>	<b>100.00%</b>	<b>93.35%</b>

Table 5.4  
Ground and building classification accuracy using *LAStools*<sup>TM</sup>.

	<b>LAStools other</b>	<b>LAStools ground</b>	<b>LAStools building</b>	<b>User's accuracy</b>
<b>Manual other</b>	1220	12	0	<b>99.03%</b>
<b>Manual ground</b>	71	8366	0	<b>99.16%</b>
<b>Manual building</b>	393	374	1600	<b>67.60%</b>
<b>Producer's accuracy</b>	<b>72.45%</b>	<b>95.59%</b>	<b>100.00%</b>	<b>92.94%</b>

An examination of where MSPCb fails, illustrated in Figures 5.15 to 5.17, shows that misclassifications occur primarily around building edges, and on roads and in parking lots where vehicles can be found. Applying the remainder of the MSPC process (the "uncertainty", "vegetation", and "road" and "vehicle" classification steps) should improve these results, or at least correct some of the misclassified points, such as vehicle points classified as ground that were all marked as being between 0.3 m and 1 m HAG.

In each of the figures, brown represents ground points, blue represents building points, and green represents vegetation points. (For MSPCb, the vegetation classification is preliminary, as described in Section 5.1, whereas the vegetation classification is final for *LAStools*). The point intensity value was used to modulate the colour in the images. Sample 6606 (Figure 5.16) presents a particular challenge, as it includes a portion of the Science Library on the UNB campus, which is built into the ground. Correct classification of this type of feature depends on how "ground" versus "building" is defined.

The accuracy assessment for all other classes in the MSPC process was performed as a simple visual comparison, due to the challenges noted above in obtaining a suitable truth set. Figures 5.18 to 5.20 contrast the full classification for MSPC against the *LAStools* (limited to ground, building, vegetation, and unclassified classifications) in three samples areas. The colour representations for the main classes are: brown for ground points; red for buildings; shades of green for vegetation with darker green representing higher vegetation; magenta for unclassified points; dark grey for roads; and grey to white for vehicles. Further evidence can be seen of the tendency of *LAStools*<sup>™</sup>, as applied, to fail to find buildings or to misclassify "building" points as "ground" or "vegetation."

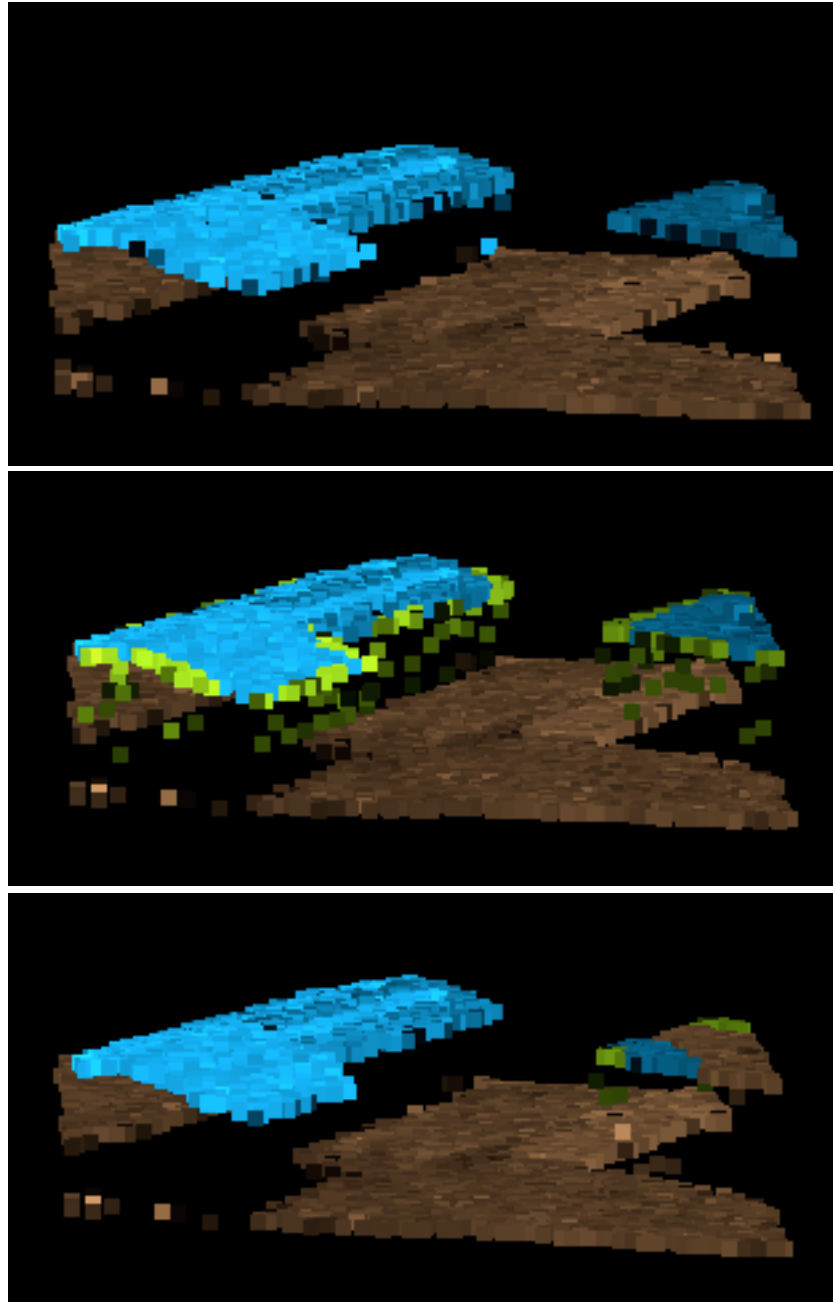


Figure 5.15

Building classification results for Sample 7966. Top: Manual. Middle: MSPCb.  
Bottom: LAStools.

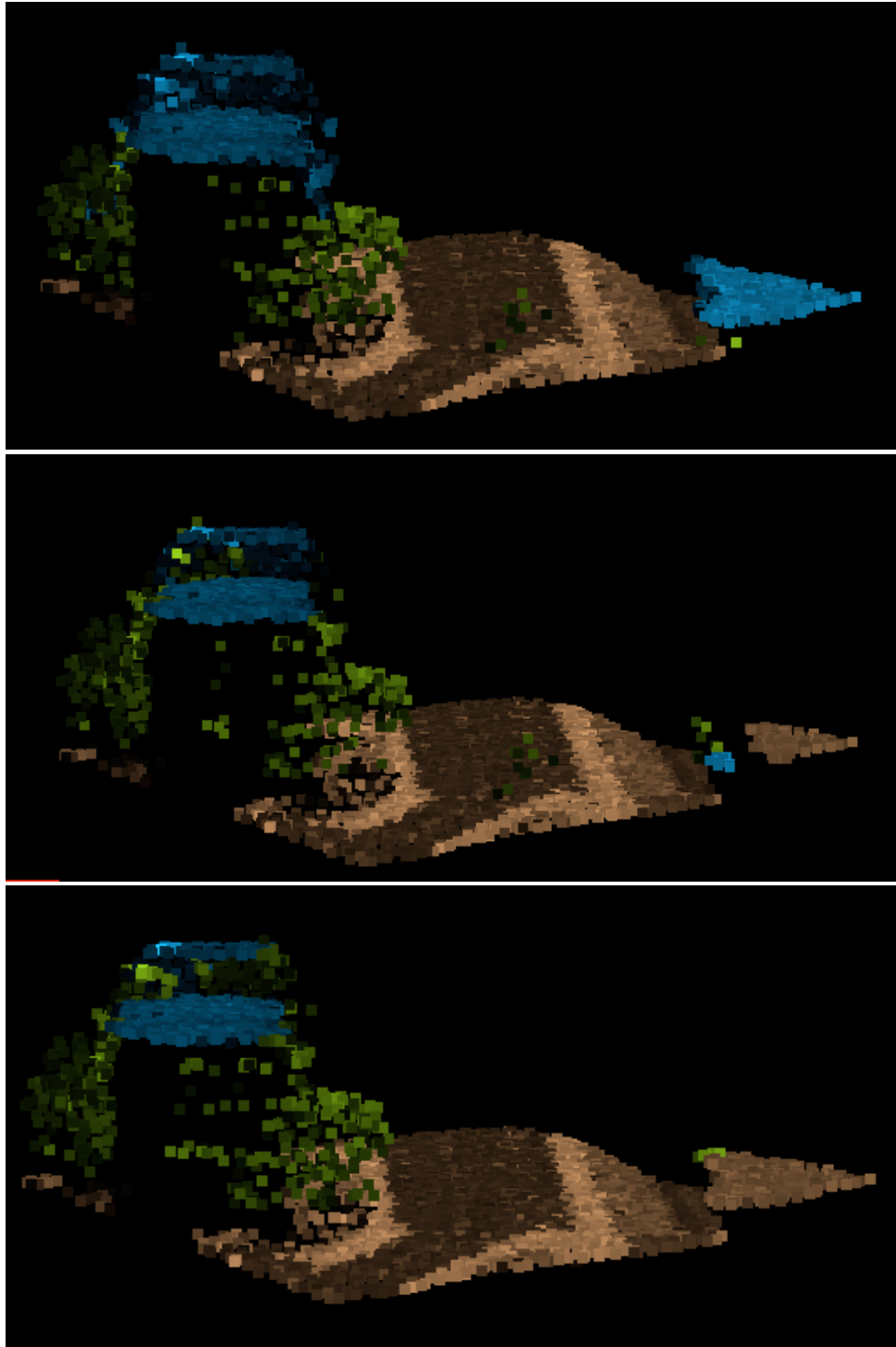


Figure 5.16

Building classification results for Sample 6606. Top: Manual. Middle: MSPCb.  
Bottom: LAStools.

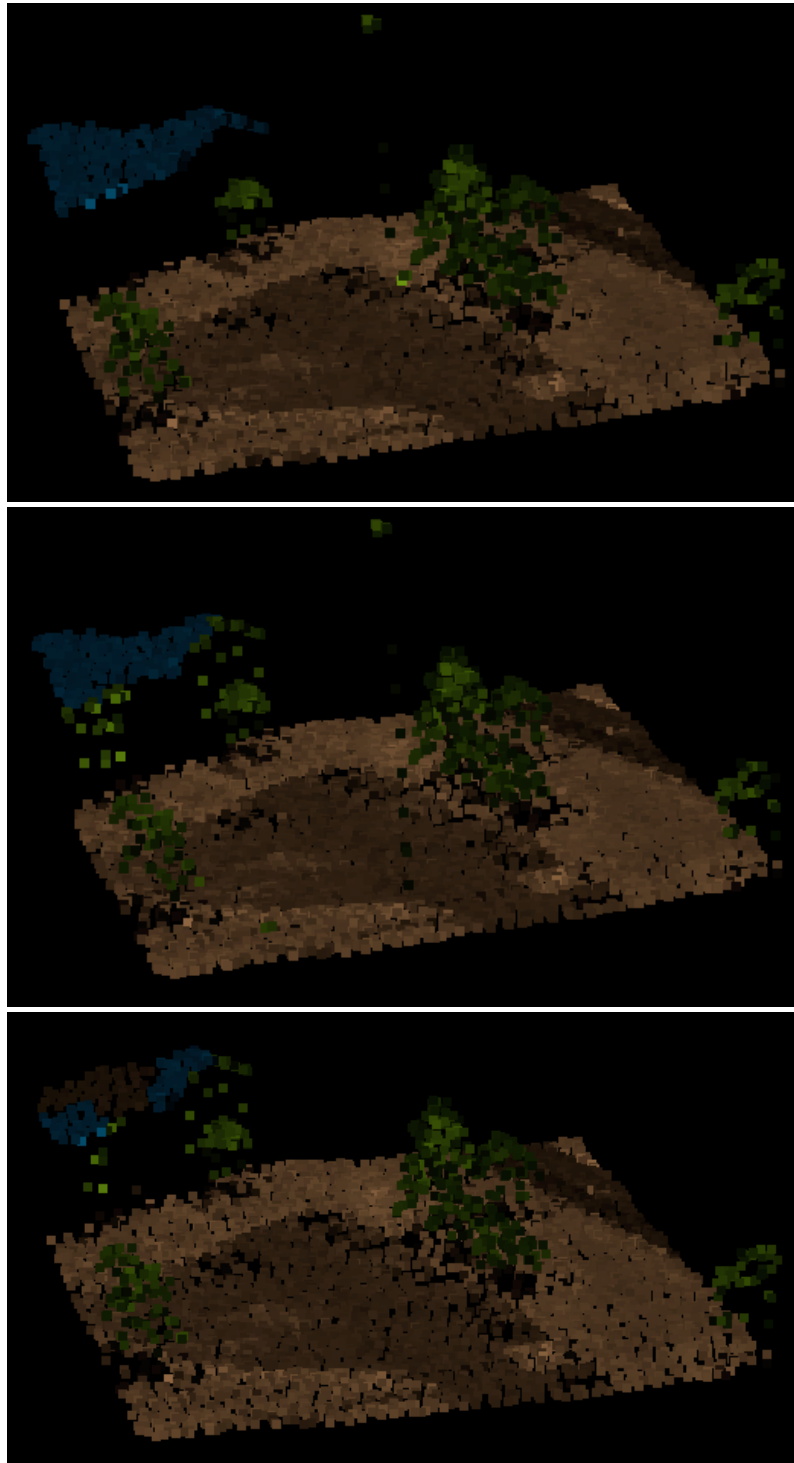


Figure 5.17

Building classification results for Sample 1095. Top: Manual. Middle: MSPCb.  
Bottom: LAStools.

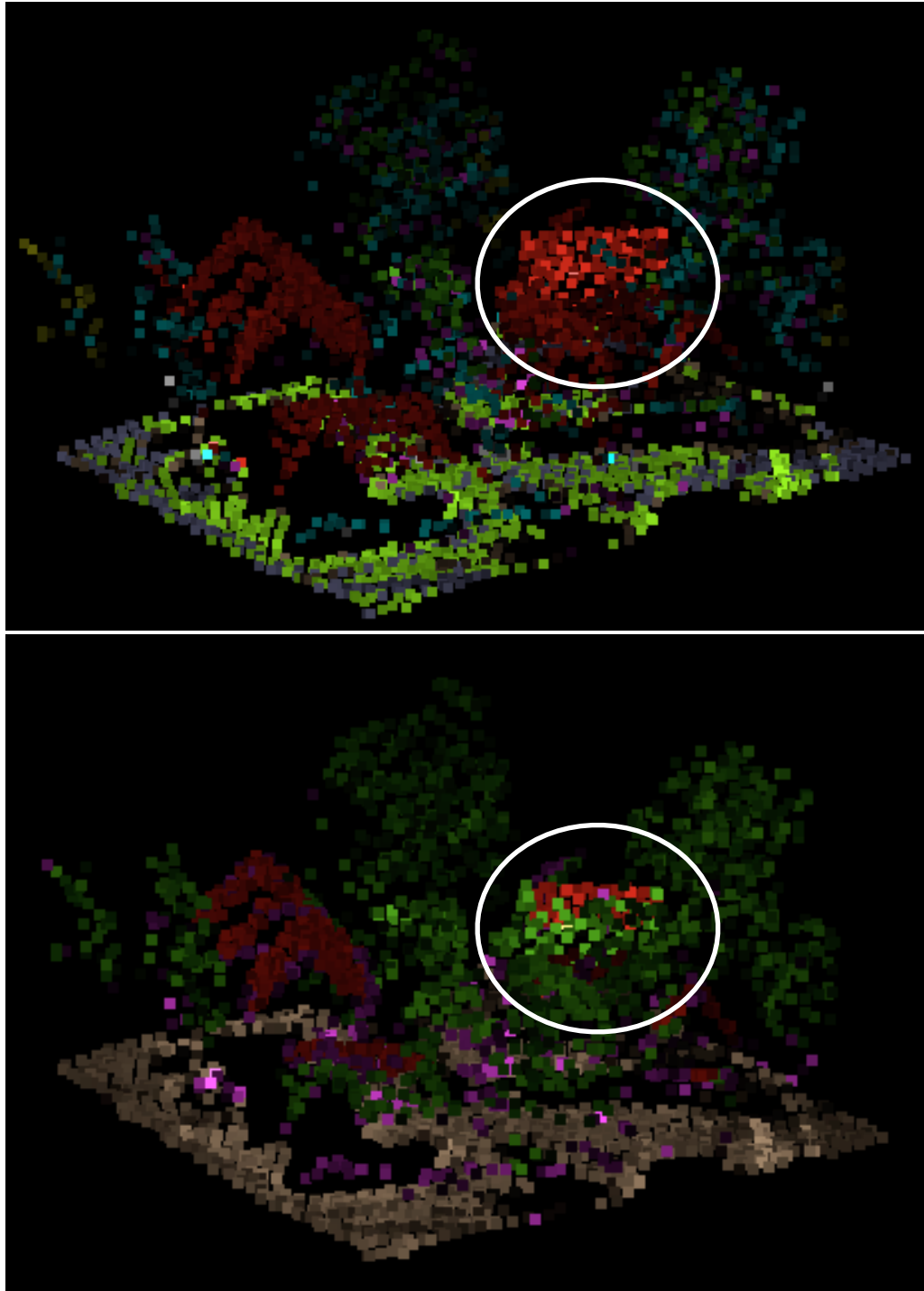


Figure 5.18

Classification results for Sample 3341. Top: Full classification using the MSPC process. Bottom: LAStools. The circled area is an example of roof points classified as vegetation by *LAStools*<sup>™</sup>.

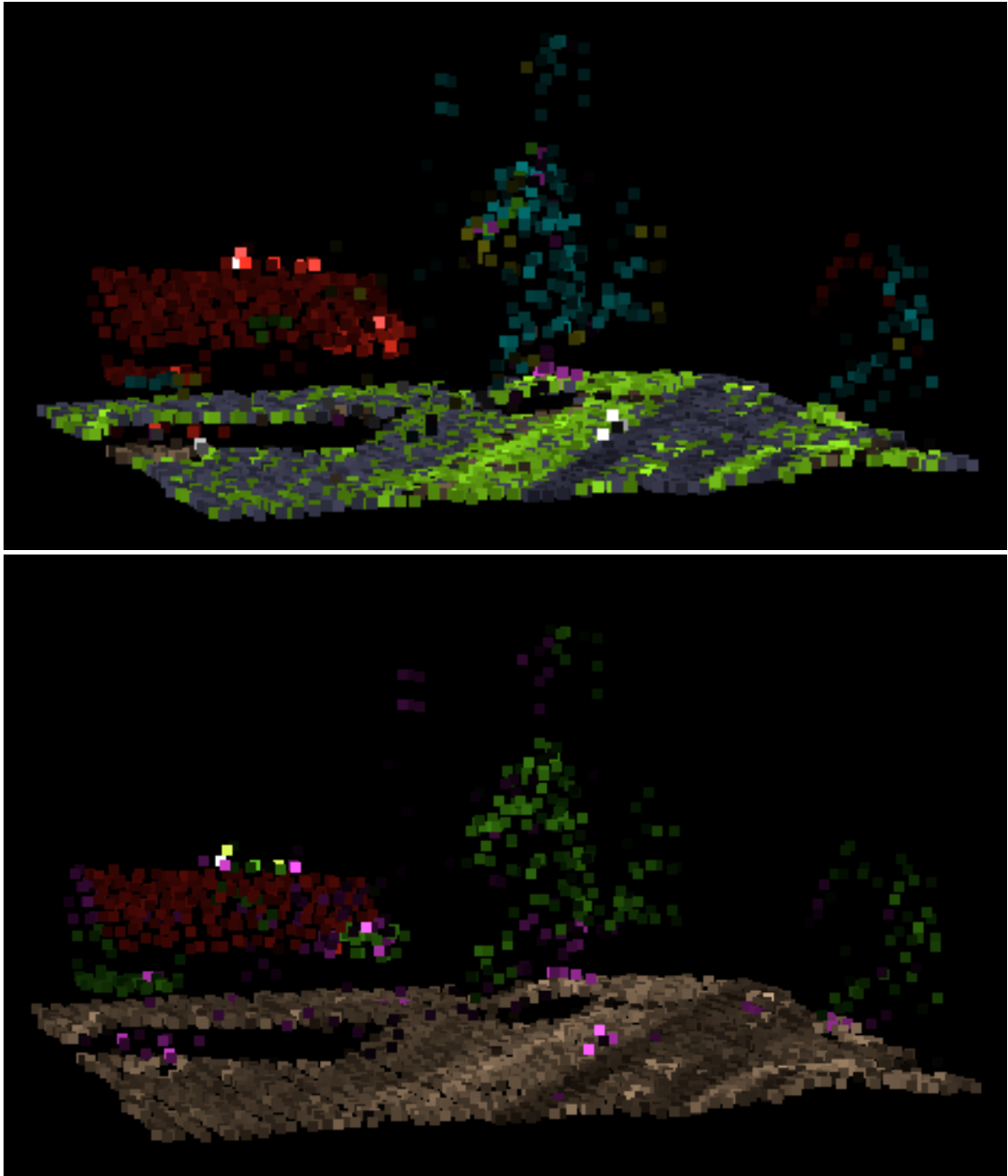


Figure 5.19

Classification results for Sample 3059. Top: Full classification using the MSPC process. Bottom: LAStools.



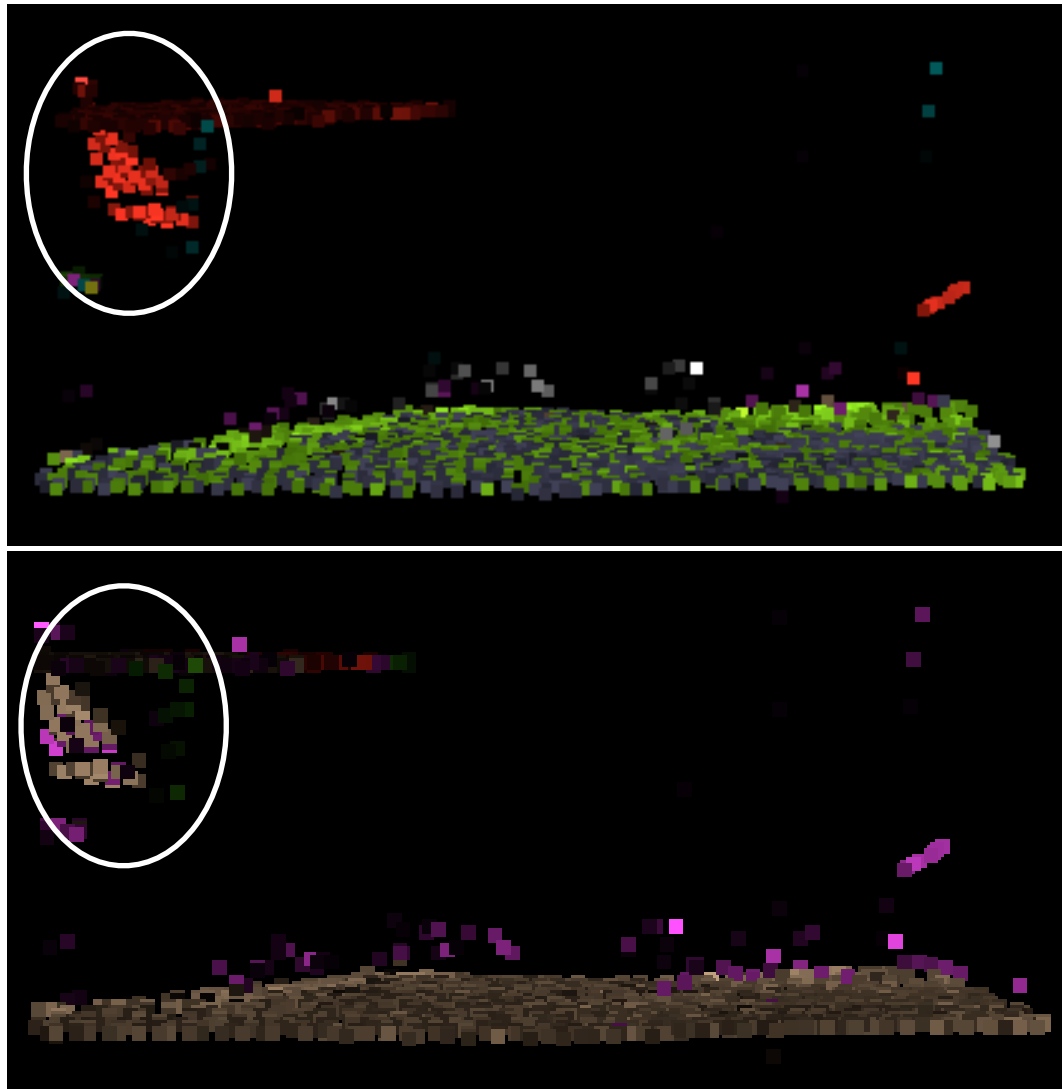


Figure 5.20

Classification results for Sample 2910. Top: Full classification using the MSPC process. Bottom: LAStools. The circled area is an example of roof points classified as ground by *LAStools™*.

## **5.7. SUMMARY OF MSPC PROCESS**

This chapter has described the multi-stage point classification process developed for this thesis and presented results from test areas in Fredericton. Through the seven stages of the MSPC, which builds on the ground point classification from Chapter 4, points are classified as building, high vegetation, medium vegetation, low vegetation, road or other paved surface, vehicle, and other objects above road surface. In the MSPC process, a preference is given to having errors of omission rather than errors of commission and points not meeting the criteria of any class or falling within an area marked as uncertain are left unclassified. This simplifies the process of refining results by, for example, repeating stages of the classification process, or even manually reclassifying points, as focus can be placed determining the correct class for unclassified points rather than correcting misclassification.

Regardless, there will always be limitations to what can be achieved with automated classification using a single LiDAR data set. To achieve more accurate classification results, other data sources are needed. Hence, integration of other data sources in the classification process is discussed in the next chapter.

*"This is a singularly ill-contrived world, but  
not so ill-contrived as all that."*

*~ A.J. Balfour*

## **CHAPTER 6**

### **CLASSIFICATION OF LIDAR DATA USING MULTIPLE DATA SOURCES**

The processes described in Chapters 4 and 5 identify ground points within a point cloud and further classify points as building, high and low vegetation and other classes. Tests of these processes showed few or no errors of commission and, in the case of building points, misclassification as ground only in unusual cases where the building has been built into or under the ground.

With LiDAR as the sole data source, boundaries between objects can be indistinct and the lower the point density, the larger the area of uncertainty between objects. Approximately 25% of the points in the test data set used in Chapter 5 were left unclassified because of this uncertainty. The results could be refined and improved iteratively, using similarity measures derived from the classified points to assign unclassified points to a class and allowing direct operator input in areas of high uncertainty. Another alternative, however, is to integrate data from other sources and make use of the additional information in the classification process.

The following sections explore procedures for modifying and adding to the ground point identification (GPI) and multi-stage point classification (MSPC) processes described in Chapters 4 and 5 to make use of integrated data sets. Different sets of test data are used in this chapter from those used in Chapters 4

and 5 to illustrate particular aspects of the process modifications. Images representing the single source classification results are included where a direct, visual comparison is appropriate. Pseudocode for implementing any necessary modifications to the GPI or MSPC processes can be found in Appendix A.

First, the advantages and limitations of existing commercial options for using other data sources to classify LiDAR point clouds are explored as alternatives to modifying the processes and the code from Chapters 4 and 5 (Section 6.1) then characteristics of different data sets that may affect the quality of integration results are discussed (Section 6.2).

The potential for using a ground surface extracted from a leaf-off LiDAR data set to extract ground from a leaf-on LiDAR data set is examined as an example of using an available ground surface from another source to improve GPI processing time (Section 6.3) and the potential for using feature data to enhance the MSPC process is investigated in three cases (Section 6.4 to 6.6). The first case is using water polygons to separate water points from ground (Section 6.4); the second case is using existing building footprints to supplement building data extracted from the LiDAR point cloud (Section 6.5); and the third case is using existing road centrelines to replace the intensity threshold approach for road extraction (Section 6.6). Finally, the potential for using multi-temporal LiDAR data to detect change over time is explored (Section 6.7).

## **6.1. EXISTING TOOLS**

A number of commercial tools are available for classifying LiDAR points using

other data, including *ArcGIS*<sup>™</sup>, *LP360*<sup>™</sup>, and *MARS*<sup>®</sup> *Explorer*, which are described below and were available to the author during at least part of the research process. Commercial tools offer certain advantages, including user interfaces to help select data and set parameters, that may not be offered by the code tools developed as part of this research but they also have limitations.

The LiDAR handling capabilities introduced in version 10.1 of *ArcGIS*<sup>™</sup> include a tool for classifying points in LAS files using vector feature data [Esri Inc., 2012]. This tool allows buffering around features but does not use z values, which creates the potential for misclassification of points in areas where multiple classes occur in the same planar region but in different vertical spaces.

*LP360*<sup>™</sup> also has a tool to classify points using vector feature data [QCoherent, n.d.], and while it also does not use z values explicitly, height filters that use heights relative to ground elevation or any other base elevation can be applied before classification and so can exclude, for example, trees overhanging roads or water from the classification.

Another example is the *MARS*<sup>®</sup> *Explorer* software from Merrick & Company, which has two raster-based classification tools, one that uses an ENVI classification data set and the other an RGB image. LiDAR points within a specified distance of a pixel with the specified characteristics are reclassified. As with the two examples above, z values are not considered [Merrick & Company, n.d.].

These and other similar tools can greatly simplify and speed up the classification process if they are understood and used correctly but will achieve

low classification accuracy if proper care is not taken to ensure the disparate data sets, whether LiDAR and vector or LiDAR and raster, are matched in terms of feature content and alignment. In addition to the limitations noted, these tools may not be accessible to all users due to cost or other factors and therefore may not be a viable alternative to modifying the processes from Chapter 4 and 5.

## **6.2. ASSESSING DATA INTEGRATION**

Examples of approaches to fusion tend to focus on combining imagery to improve resolution (e.g., multispectral and panchromatic); introducing additional data to improve classification (e.g., LiDAR height, hyperspectral imagery, SAR data); or improving the quality of DEMs. Whatever terminology or techniques are used, the purpose is, as stated in Zhang [2010], "to improve the potential values and interpretation performances of the source data." In Warriner and Mandlbürger [2005], a process is described for adding newer, higher resolution data (from LiDAR) to an existing database that includes a measure of quality, while the work of Papasaïka and Baltsavias [2009] is based on the belief that local quality is an important factor in fusing data. Local quality is equally important when examining the results of fusion and assessing the quality of integration.

In all cases of data integration, it is important to know how the products used in data integration have been generated or derived. Elevation data are generally available as points and the sampling distance and pattern greatly affect the end product in terms of accuracy and resolution. When working with LiDAR data, a

visual representation of the distribution of points, such as the LPD and MRD images described in Sections 3.1.2.1 and 3.1.2.2, can help identify areas where data are sparse and therefore the quality of products may be lower as compared to areas where the data are dense.

Different land covers have different associated errors and limitations: for example, in areas with dense vegetation it is more difficult to find ground points, regardless of the technology used. A representation of land cover types in the area of interest as a land cover map, as described in Section 3.1.2.6, can be used to locate areas where special care or attention may be needed due to the presence of vegetation or other features and may also provide an explanation for any larger errors or differences between data from different sources than were expected.

Intensity images (Section 3.1.2.3) for LiDAR data can also be used to assess local quality as they can indicate possible range bias where substances reflecting a higher percentage of the laser pulse energy appear to be at higher elevations than substances reflecting a lower percentage of the laser pulse energy [Csanyi and Toth, 2007]. Another variation of land cover representation for LiDAR data, a ground-vegetation ratio representation as described in Section 3.1.2.4, can indicate how well the laser pulses were able to penetrate openings in the vegetation. Finally, a representation of the terrain slope can help the user identify areas where the vertical accuracy of LiDAR data may be most affected.

When LiDAR data are to be integrated with other elevation data, such as existing DEMs, any systematic biases in  $z$  must be identified and eliminated

between the data sets. Depending on the nature of the data, raster-to-raster, raster-to-point and/or point-to-point comparisons can be made between elevation data sources to be integrated to determine if any systematic biases exist. Examples of each type of comparison can be found in Appendix C. Although horizontal alignment should also be verified for elevation data integration, if the integration is with a lower resolution DEM there may be insufficient detail to assess the horizontal alignment and make any adjustments.

When sufficiently accurate horizontal data, e.g., accurate road centrelines or building footprints, are available, however, it is possible to check the alignment and make any necessary adjustments. The LiDAR data must have sufficiently high LPD to make a horizontal comparison meaningful: there are never any guarantees that a point will hit a building corner or that a road intersection can be precisely located, but higher LPD provides a greater level of detail and reduces the area of uncertainty. A pixel resolution no lower than 1 m should be used, as lower resolutions place increasing importance on the operator's interpretation of the location of objects. Different information (e.g., intensity or elevation) can be interpolated depending on which best matches the reference data. An example of using an intensity image and road centrelines to correct offsets in data sets can be found in Appendix C.

### **6.3. AUGMENTED GROUND EXTRACTION**

In the MSPC process described in Chapter 5, ground points must be accurately identified and classified before other features can be accurately



classified as the ground surface provides a base layer. The process described in Chapter 4, while successful, may require more processing time than is desired. Processing times will vary depending on processor speed and the data themselves, but as an example, each tile in the Odell Park study area (Section 3.2.1.1) required approximately one- to one-and-a-half hours of processing time, depending on the voxel size used in the pre-classification voxel sorting stage. When the voxel size was 50 m (meaning length, width and height dimensions all 50 m), the sorting stage took an hour or more to complete for each 1 km x 1 km tile, while applying the Point Neighbourhood ground detection technique to the tile, which is the technique most dependent on how spatially adjacent points are organized in a data file, took approximately five minutes. When the voxel size was 100 m, the time for the sorting stage was reduced to fifteen to twenty minutes but the Point Neighbourhood time increased to ten to fifteen minutes.

As a whole, the four square kilometres of the Odell Park study area required four to six hours of processing time, which was acceptable for the purposes of testing the processes developed as part of this research but may be too long in another context. The first and most time-consuming stages of the GPI process (i.e., ground detection techniques) can be bypassed if a DEM or some other initial approximation of the ground surface is available, regardless of its source.

The ground surface approximation is used in place of the output of the surface comparison technique in the modified GPI process. Large differences between the external DEM and the LiDAR ground surface are overcome during the final stage of the GPI process, namely the classification and refinement stage (Section

4.4): in areas where the differences are positive, indicating that the DEM is higher, lower LiDAR points will pull the reference surface down; in areas where the differences are negative, the minimum LiDAR points can provide an initial approximation that can be refined in by through iterations of the process.

An initial approximation from another data source is particularly useful in areas of dense vegetation where it is more difficult to find ground. The CRB data sets (described in Section 3.2.2.1 and in Guo [2011]) were selected to illustrate this concept because little more than three months elapsed between the two surveys and so few differences were expected in terrain or building features. Significant differences were expected in areas of high vegetation, since the first data set was collected in April in leaf-off conditions and the second was collected in July in leaf-on conditions. The rasters in Figure 6.1 were generated by selecting the minimum and maximum z values within each cell. Although both data sets have high point densities, with NPD at 10.27 pts/m<sup>2</sup>, a 1 m resolution was chosen for these rasters to reduce vegetation artifacts in the minimum interpolations. The April interpolation (Figure 6.1a) includes far fewer non-ground minimum elevations than the July interpolation (Figure 6.1c).

The full GPI process described in Chapter 4 was applied to the April data and then the identified ground points were extracted and interpolated to a raster surface, shown in Figure 6.2a. However, instead of applying the entire process to the July data, the extracted April surface was used as the raster input for the July data set in the final GPI stage, the ground point classification and refinement process (Section 4.4). It was assumed that, because the data were collected as

part of the same project, they were accurately aligned both vertically and horizontally. The resulting extracted surface for the July data is shown in Figure 6.2b. Obtaining the same results solely from the July data would have involved far more steps and taken significantly more time: each application of the Point Neighbourhood detection technique to the April data required an hour and a half to complete, but it did not need to be applied to the July data.

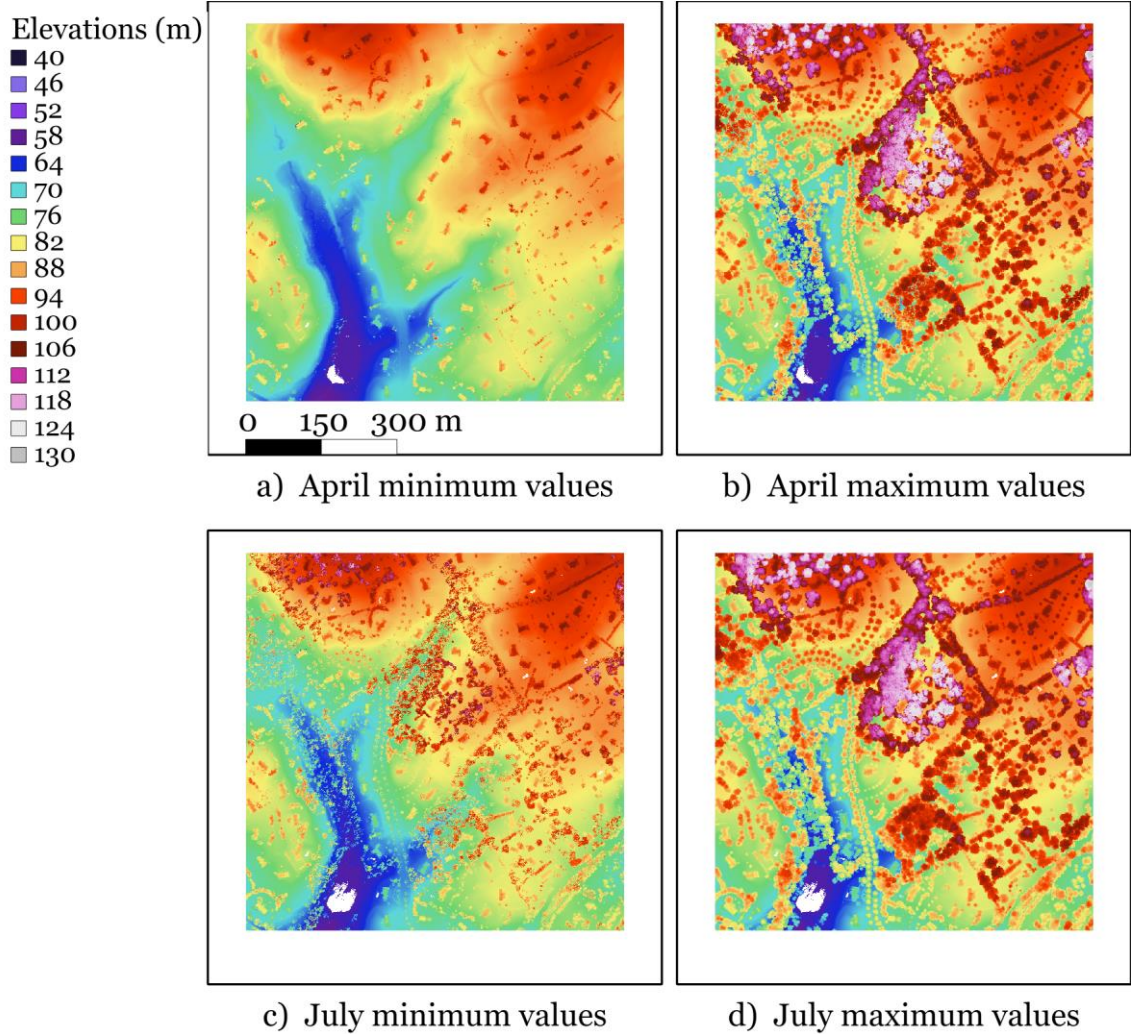


Figure 6.1

Interpolations of data from Christina River Basin, PA: a) April minimum values; b) April maximum values; c) July minimum values; d) July maximum values.

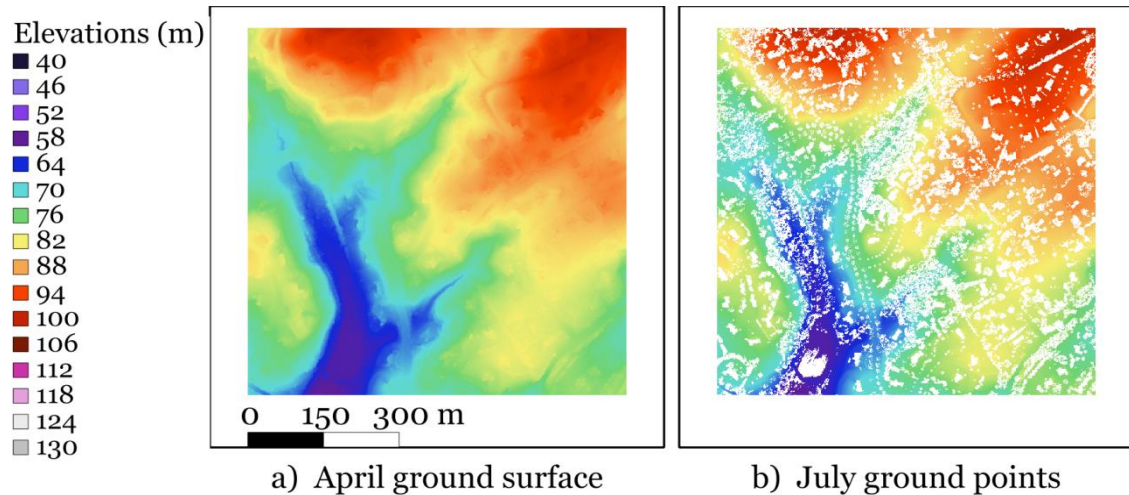


Figure 6.2

Augmented ground extraction: a) ground surface extracted from leaf-off data and b) ground points extracted from leaf-on data using leaf-off surface.

## 6.4. WATER CLASSIFICATION

No attempt was made to classify water points in the MSPC process described in Chapter 5. Classifying water points is a difficult task to automate because of inconsistencies in LiDAR results. Although point returns are not often generated from water bodies, gaps in the data coverage are not necessarily caused by water as there may be other materials present whose reflective and absorption properties similarly prevent sufficient energy from returning to the sensor. For example, black neoprene has a very low reflectivity at the wavelengths typically used in airborne LiDAR systems [Wehr and Lohr, 1999]. When returns are generated, depending on the angle of incidence of the laser and the water depth and clarity, the intensity values can range from near zero to the maximum value recorded. Additional information or prior knowledge of the location of water bodies is therefore needed to classify water points. Water classification can be

applied before the GPI process, if water bodies are clearly separated from all other features, or after the GPI process, if there may be objects that overhang or bisect the water body that may be filtered out using elevation criteria.

If the body of water is flat, and its elevation is known, an elevation threshold can be used to classify any points generated from its surface; however, this approach will not work for water bodies that experience a change of elevation within the LiDAR scene or where multiple flat bodies of water, for example, ponds and swimming pools, occur at different elevations within the scene. The solution that was explored in this research was to use water polygons to define the area where water points may be found. Elevation filtering was used together with the polygons because of the likelihood of having other features, such as vegetation or bridges, overhanging the water. The pseudocode can be found in Appendix A, Section A.2.7.

The LiDAR data set from Ottawa, obtained from GeoDigital International, was selected to illustrate water classification because of the particular challenge posed by the Rideau Canal that bisects the data set. The LiDAR data as provided were simply classified as "ground" and "non-ground," with water points from both the canal and the river included in the ground class, as shown in Figure 6.4. Because the non-ground points seemed to include a large number of points at ground level, the full GPI process was applied to the data set before water classification was attempted using water polygons obtained from Open Data Ottawa.

A concern when using data from different sources is proper alignment. The

NPD for the Ottawa LiDAR data, first returns only, is 3.57 pts/m<sup>2</sup> but from the LPD representation (Appendix B, Figure B.4) there are at least 5 pts/m<sup>2</sup> throughout most of the area, providing detailed information about buildings and other features. This facilitated an assessment and verification of the horizontal alignment of the water polygons with respect to the LiDAR data.

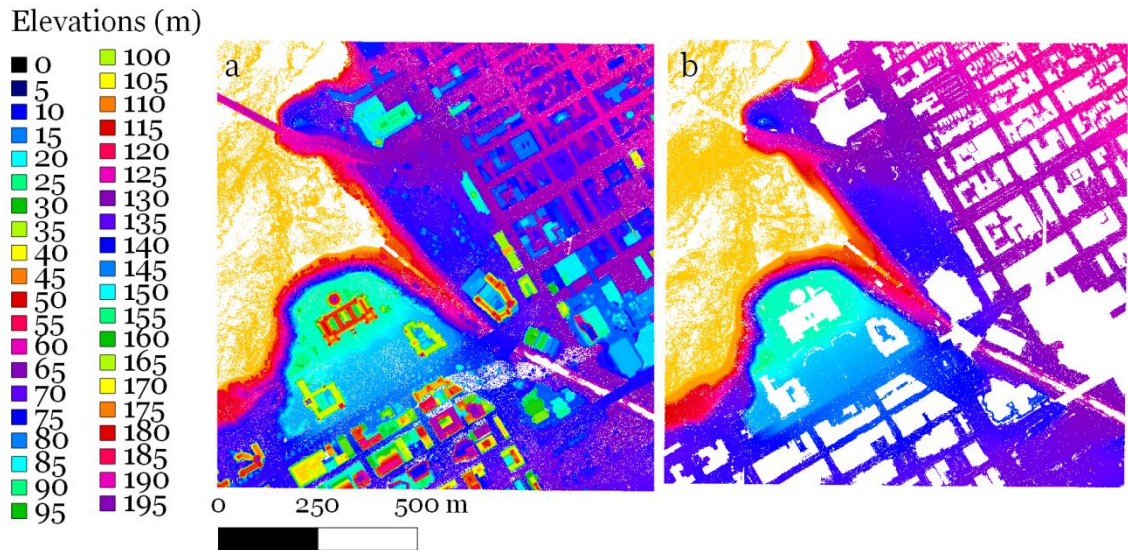


Figure 6.3

Elevation interpolation of Ottawa LiDAR data set as classified by GeoDigital:  
 a) non-ground points and b) ground points.

The scene includes Parliament Hill, which, as can be seen in the point cloud representations in Figure 5.6 and the slope image in Appendix B, Figure B.5, sits high above the water near the edge of a precipice. It also includes a series of locks from the Ottawa River up to the Rideau Canal. While an elevation threshold would have been sufficient to separate points in the Ottawa River from the ground class because they are at the global minimum elevation for the scene, a thresholding approach would not have been successful in classifying the points from the locks or the canal because they are at only locally minimum elevations.

It might be noted that the locks may or may not have contained water at the time the LiDAR data were collected, and so arguably points within the locks may or may not actually be from water. This is another example of the classification of a point being dependent on how one chooses to define the feature. Using the water polygons to classify points removes this ambiguity by defining clear boundaries for the water area, regardless of actual conditions.

The water classification process implemented as part of this research required the use of analysis tools in *QGIS* to first clip the surface extracted from the GPI results to the water polygons before a custom algorithm developed by the author was applied to mark points as water. The surface clipping provided both boundaries for the water area and an elevation filter to ensure points marked as water were both planimetrically and vertically within the identified area. Figure 6.4 illustrates water classification results for the Ottawa LiDAR data.

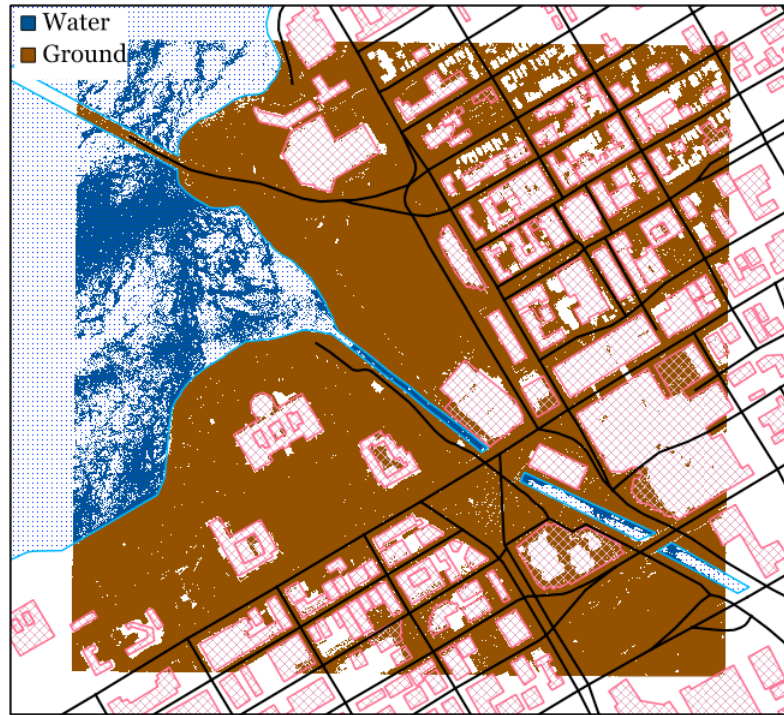


Figure 6.4

Illustration of water classification using polygons, with road and building features overlaid on extracted and interpolated ground and water classes.

## 6.5. BUILDING FOOTPRINTS

Although water levels may change seasonally or year-to-year, water body boundaries do not tend to change significantly over time, and can often be digitized from a raster interpolation of the LiDAR data if necessary for use in point classification. Other types of features will change over time, either individually or as groups of features and the data available from municipalities or other sources may not be current. For example, in the case of building footprints, assuming the LiDAR data are more current, the footprint data may (1) include buildings that were torn down between the time when the footprints



were generated and the time when the LiDAR data were collected; and (2) not include new buildings or building additions that were constructed in that interval.

Building footprints therefore should not be used as the sole basis for building classification. They can, however, provide greater certainty regarding building classification and potentially be very helpful in finding smaller buildings (houses) on tree-lined streets as well as classifying points from buildings with irregular architectural features, such as domes, that might otherwise pose great challenges to any building classification process. The conjugate of using building footprints to classify data is using classified data to update building footprints.

The building classification process described in Section 5.2 requires a building mask infused with elevations. As part of this research, a three-step process was developed to create the building mask needed for the MSPC process from footprints. Because the footprints are in vector format, which is more difficult to work with in code than raster or LAS formats, all three steps are completed in a software package such as *QGIS* or *ArcGIS*. The first step is to verify the horizontal alignment between the building data and the LiDAR data using well defined features present in both data sets and adjust the alignment, if necessary.

The second step uses the mean minimum HAG values derived from the LiDAR data points within each building footprint as value attributes to convert the polygon footprints to a raster. This has the effect of assigning values near or below zero to cells where buildings represented in the footprints do not exist in the LiDAR data. Cells outside of building footprints are null-valued. The final

step is to create a raster where only the cells where the mean minimum HAG value was greater than zero are infused with elevation values from the LiDAR data and all other cells are null-valued, thereby eliminating buildings that no longer exist from the building mask. This approach cannot capture points from new buildings so in the modified MSPC process, preliminary classification (as described in Section 5.1) is performed before the building classification algorithm is applied using the new building mask.

Figure 6.5 and 6.6 illustrate the LiDAR-only and building footprint classification processes. A tile from the 2011 Fredericton data that covers part of the UNB campus was used because it contains examples of buildings missing in one or the other data set. However, the LPD is primarily below 2 pts/m<sup>2</sup>, which is too low to accurately assess horizontal alignment and so greater uncertainty exists around the boundaries of the polygons. Figure 6.5 shows the two building masks: new buildings appear in the LiDAR-only mask (Figure 6.5a), while smaller buildings and those built into the ground appear in the LiDAR plus footprints mask (Figure 6.5b); examples of each case are circled. Figure 6.6 illustrates the benefits of performing a preliminary classification: new buildings can be identified in the classification results because they are still classified as preliminary building points (examples circled).

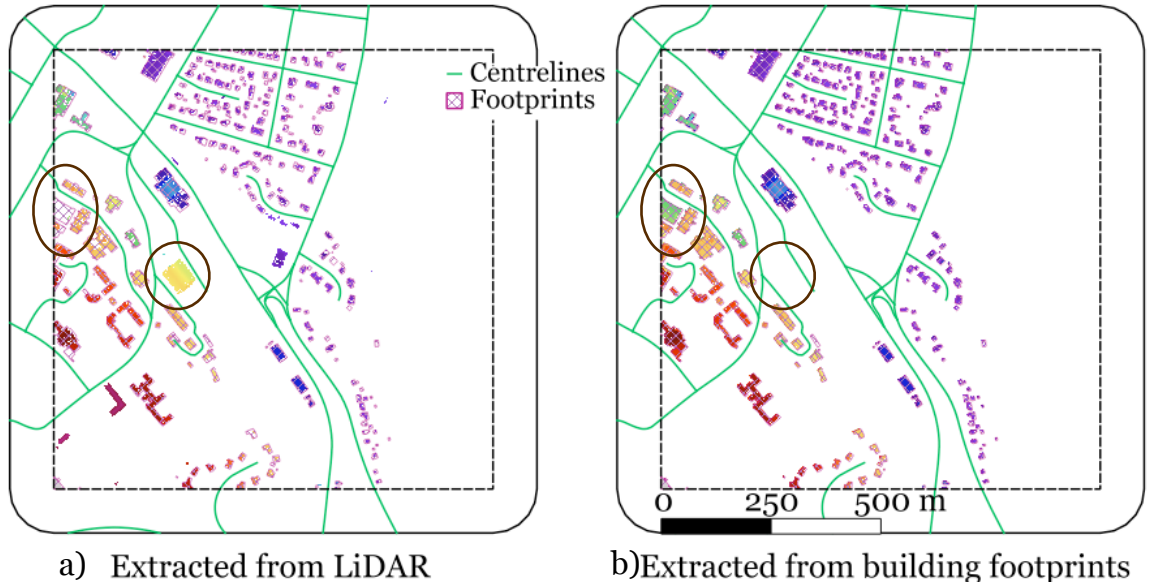


Figure 6.5

Elevation-infused building masks derived from a) LiDAR data and b) footprints.

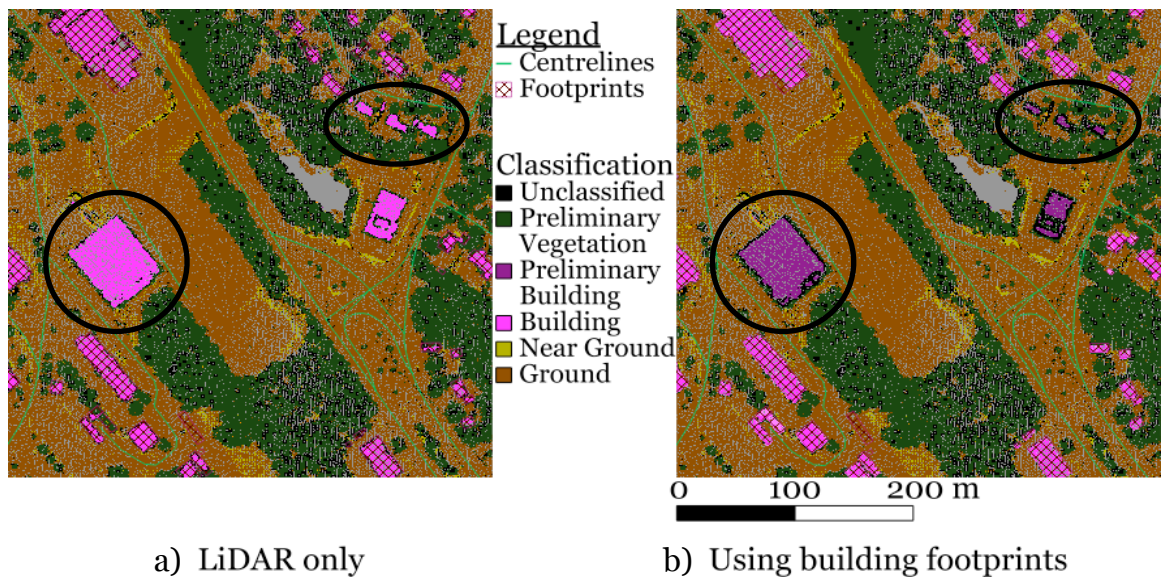


Figure 6.6

Building classification results, using a) LiDAR data only and b) LiDAR data and building footprints.

## 6.6. ROAD CENTRELINES

In the MSPC process, road points are identified by applying an intensity value threshold. Since there are many factors that can affect the recorded intensity of a point return, this is not always a reliable approach. Using polylines from road network data instead can provide more reliable results. In addition, by using polyline data to classify road points, the results will not be affected by the presence of trees overhanging the road, which may cause broken lines when an intensity threshold is used (as described in Section 5.5).

Road polylines need to be buffered before they can be used for classification in the modified MSPC process. Yet, the appropriate choice for a buffer width to capture the road surface on either side of the centerline is not necessarily any easier to determine than the appropriate choice for the intensity threshold. The road centreline data available from the City of Fredericton include a "street class" attribute, which may indicate road width, for example, for freeway road segments in contrast to residential road segments. Such information is not included in the Ottawa centreline data, however, and may not be provided by other municipalities, either.

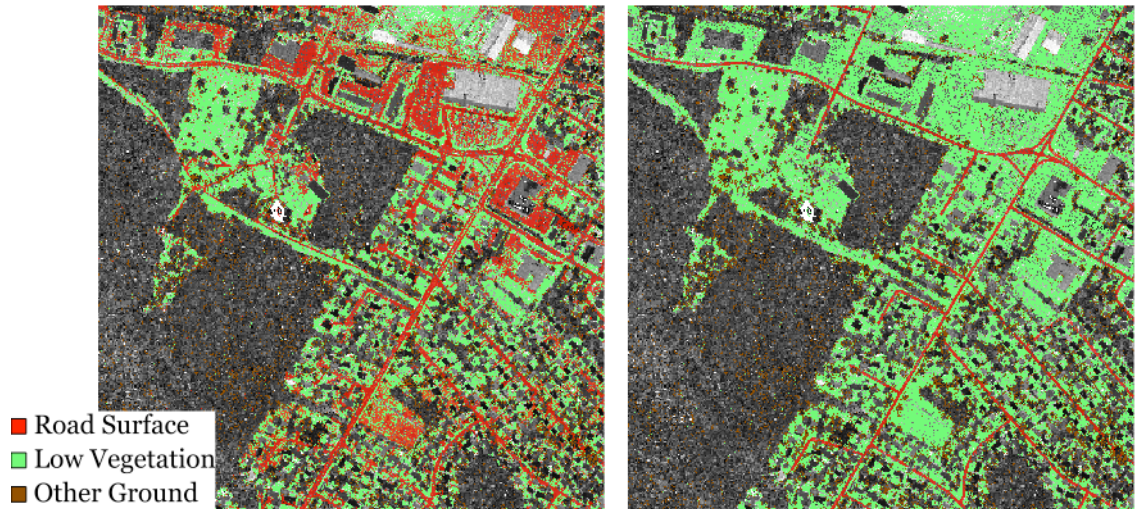
In the absence of more specific road width information, a buffer size is selected that will not exceed the actual road boundaries in most cases. Similarity measures can then be used to improve and refine the results. As part of this research, code was developed to use buffered road polylines to classify road points. Figure 6.7 contrasts the results of the two road identification approaches, namely intensity threshold (as described in Section 5.5) and road centreline

buffer, overlaid on an interpolation of intensity values to provide context. The same data used for the tests in Chapter 5 were used for this illustration.

Since road points are only at ground level, the road classification criteria are applied only to points classified as "ground" in both the intensity threshold and centreline buffer methods with the intent of subdividing this class into "road surface," "low vegetation," and "other ground" (ground point not clearly belonging to either of the other two classes). It can be seen in the images that the intensity threshold method (Figure 6.7a, all three classes included, and 6.7c, road surface points only) classifies more points as road surface, as opposed to low vegetation or other ground, while the road centreline buffer method (Figure 6.7b and 6.7d) produces smoother results, in terms of compact and connected road segments.

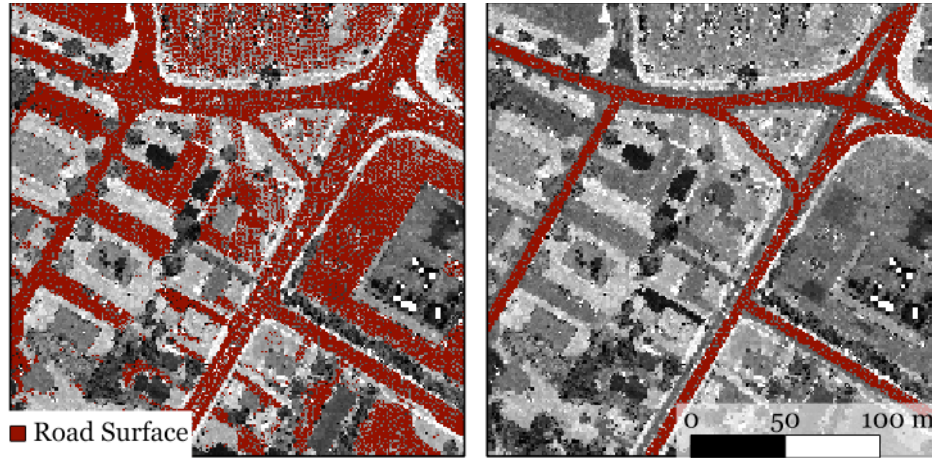
It can also be seen that, compared to the intensity interpolation, if the data sets are not carefully registered and if an appropriate buffer is not chosen, the road centreline buffer may miss classifying true road points. As was the case with the tile used to test building footprints, LPD for this data set was too low to accurately assess the horizontal alignment of the polyline data with respect to the LiDAR data.

Although the road centerline buffer method classifies more points along actual roads, it does not classify any points in other paved areas such as parking lots. This affects classification of vehicles. The vehicle classification approach described in Section 5.5 defined vehicle points as being within the road mask (derived from points classified as "road surface") and 0.3 to 2 m above ground.



a) Based on intensity threshold

b) Based on road centreline buffer



c) Based on intensity threshold

d) Based on road centreline buffer

Figure 6.7

Example of road surface classification results: a) using intensity threshold value of 100, all ground classes; b) using a 3 m road centreline buffer, all ground classes; c) using intensity threshold value of 100, road surface only; and d) using a 3 m road centreline buffer, road surface only.

Using the road centreline buffer approach to classify road surface points largely precludes vehicle point classification because parking lots are not included in the road surface class. To overcome these limitations, and also separate roads from other ground types such as parking lots, trails, and exposed

soil, a combined approach may be used that first applies the intensity threshold method to all points classified as ground and then applies the road centreline buffer method only to points already classified as road surface. Developing such an approach is one of the recommendations for further research.

Other polyline data that may be available include trails and streams. Figure 6.8 illustrates how applying a buffer to these data might help to further refine classification of the ground surface. The same data used to illustrate the modified building classification process was used here because it is an area where the trails and streams may not otherwise be identifiable in the LiDAR data. Each data source and feature type will have its own characteristics that may simplify or complicate point classification. Further research is required to determine if and how such data may be used.

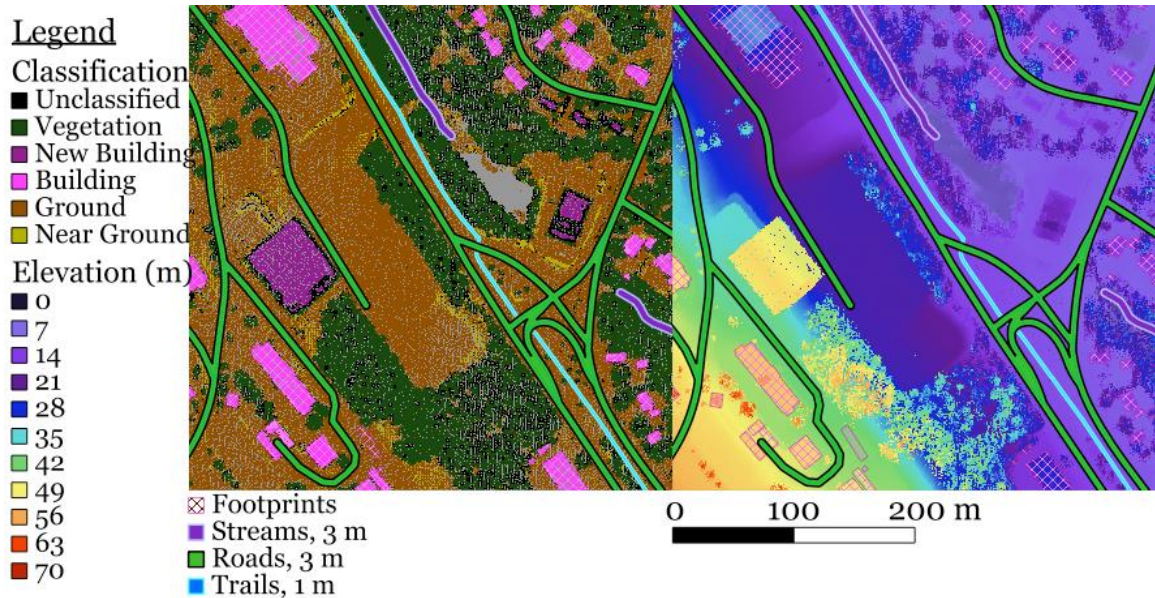


Figure 6.8

Polyline buffers that could be used to classify streams (3 m), roads (3 m) and trails (1 m) overlaid on a) classification results and b) elevation interpolation.

## 6.7. MULTI-TEMPORAL DATA

In addition to other data types, newer LiDAR data sets may be available in areas previously surveyed, as is the case for downtown Fredericton and UNB campus where LiDAR surveys were conducted in 2006, 2007, and 2011. If the older data are already classified, they can be used to simplify classification of new data as described in Section 6.2. Multi-temporal data can also be used to detect changes in terrain or features.

The CRB data used to illustrate augmented ground extraction are examples of multi-temporal LiDAR data, but the short interval between collection of the two data sets limits their utility in detecting change primarily to seasonal leaf-on/leaf-off variations. Figure 6.9 is a difference image generated from the two CRB data sets, with the interpolation of maximum values in the April data subtracted from the interpolation of maximum values in the July data. As expected, most of the differences are positive (July values higher), representing vegetation growth. Where there are large negative differences (April values higher), high vegetation (trees, hedges) was removed or trimmed between April and July. Smaller negative differences may be artifacts of the differences in data collection specifications and of the interpolation method.



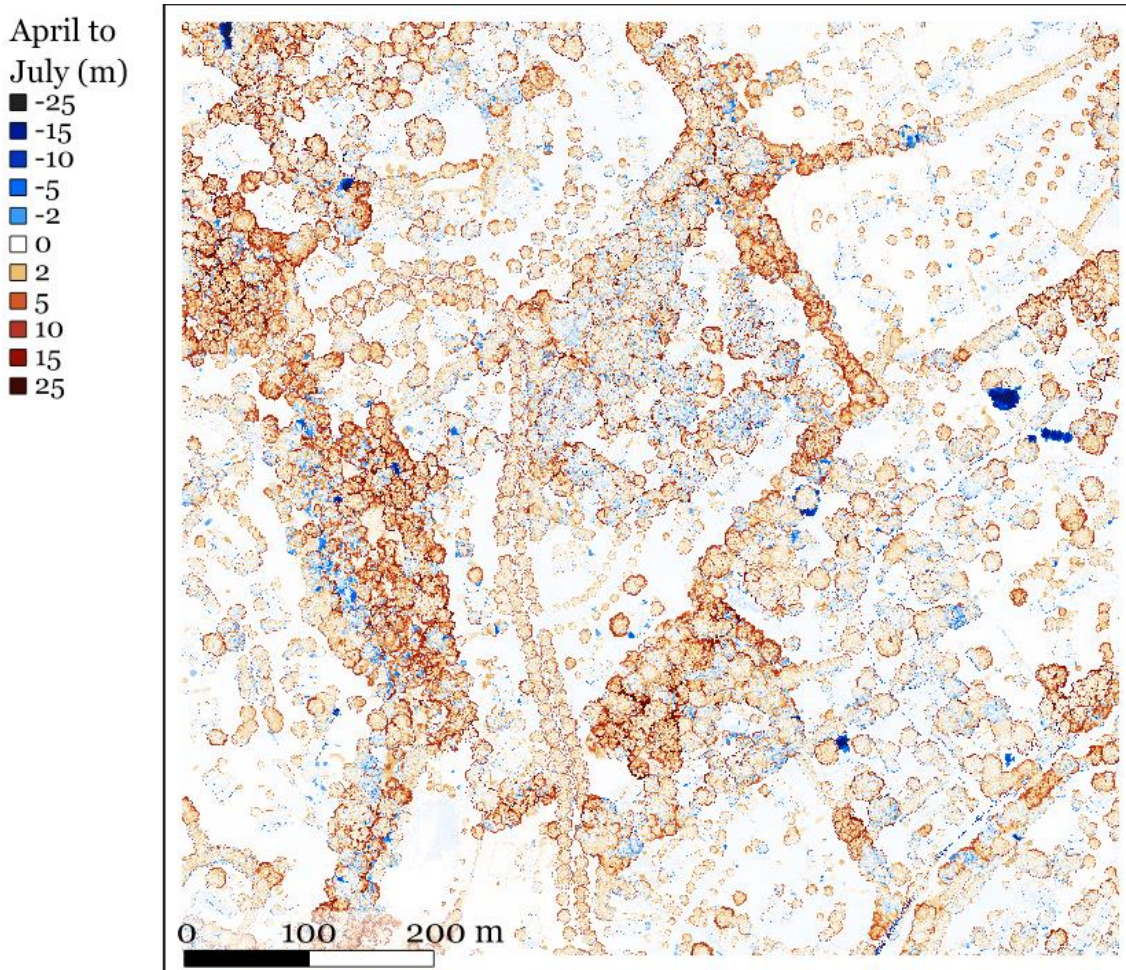


Figure 6.9

Elevation differences, April data subtracted from July data.

The small differences may also be caused by a light snow cover. Snow is a highly reflective material for LiDAR, higher than low vegetation (grass) and in the April data intensity values from the ground are often more than 50 units higher than the corresponding July data and up to 10 cm higher. While the difference in elevation is too small to be conclusive, in comparison the intensity values from rooftops and roads are mostly less than 20 units higher in the April data, which suggests that a more reflective material was present on the ground in April than in July.

Where LiDAR data are collected over the same area at time intervals of a year or more, the possibility arises of using these data to detect medium to large changes in the environment: destruction or construction of buildings and growth or removal of high vegetation. The former has applications in disaster response, facilitating identification of collapsed buildings, while the latter has applications in forestry, aiding in tree volume calculations, or for general monitoring of green spaces.

This potential is illustrated in Figure 6.10 and 6.11 using the Fredericton LiDAR data sets collected in 2006 and 2011. The 2006 survey only covered downtown Fredericton, where the terrain is mostly flat. Both data sets have leaf-on conditions, although the 2006 data were collected in late May and so the vegetation may not be as full as in the 2011 data, which are believed to have been collected in the summer months (exact dates unknown). The figures in Section 6.3 show examples of changes in building features between building footprints and buildings detected in the LiDAR data. In Figure 6.10, differences are noticeable in the elevation interpolations of the two point clouds where, for example, small buildings have been replaced by a larger building (1); a building has been enlarged and high vegetation removed (2); small features and a large tree have been removed (3); and generally trees have grown taller and fuller.

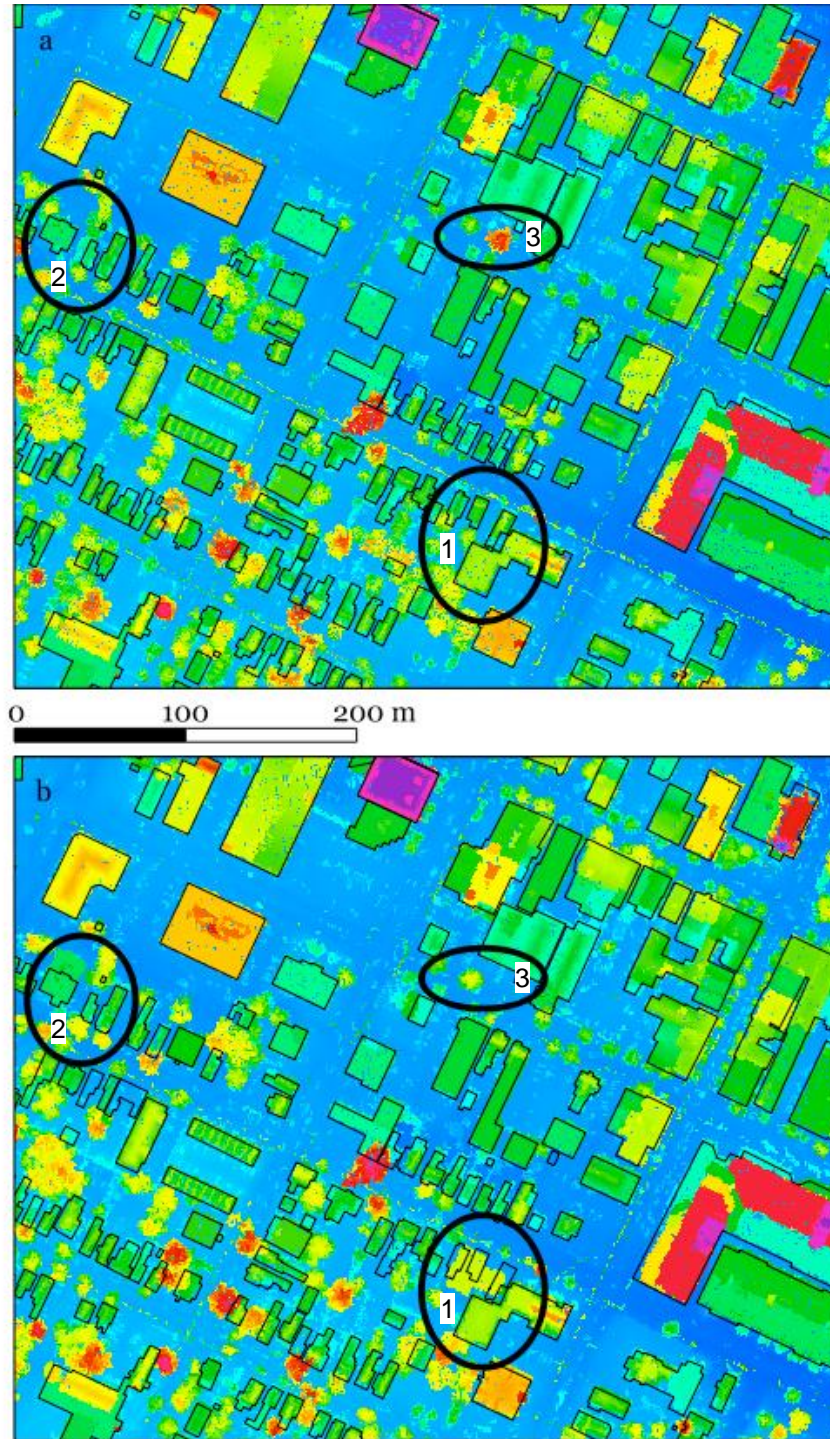
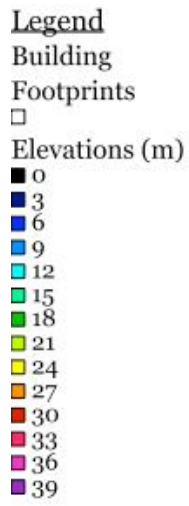


Figure 6.10

a) Sample of 2006 LiDAR data. b) Sample of 2011 data. Some notable differences, such as building construction and destruction and tree removal, are circled.

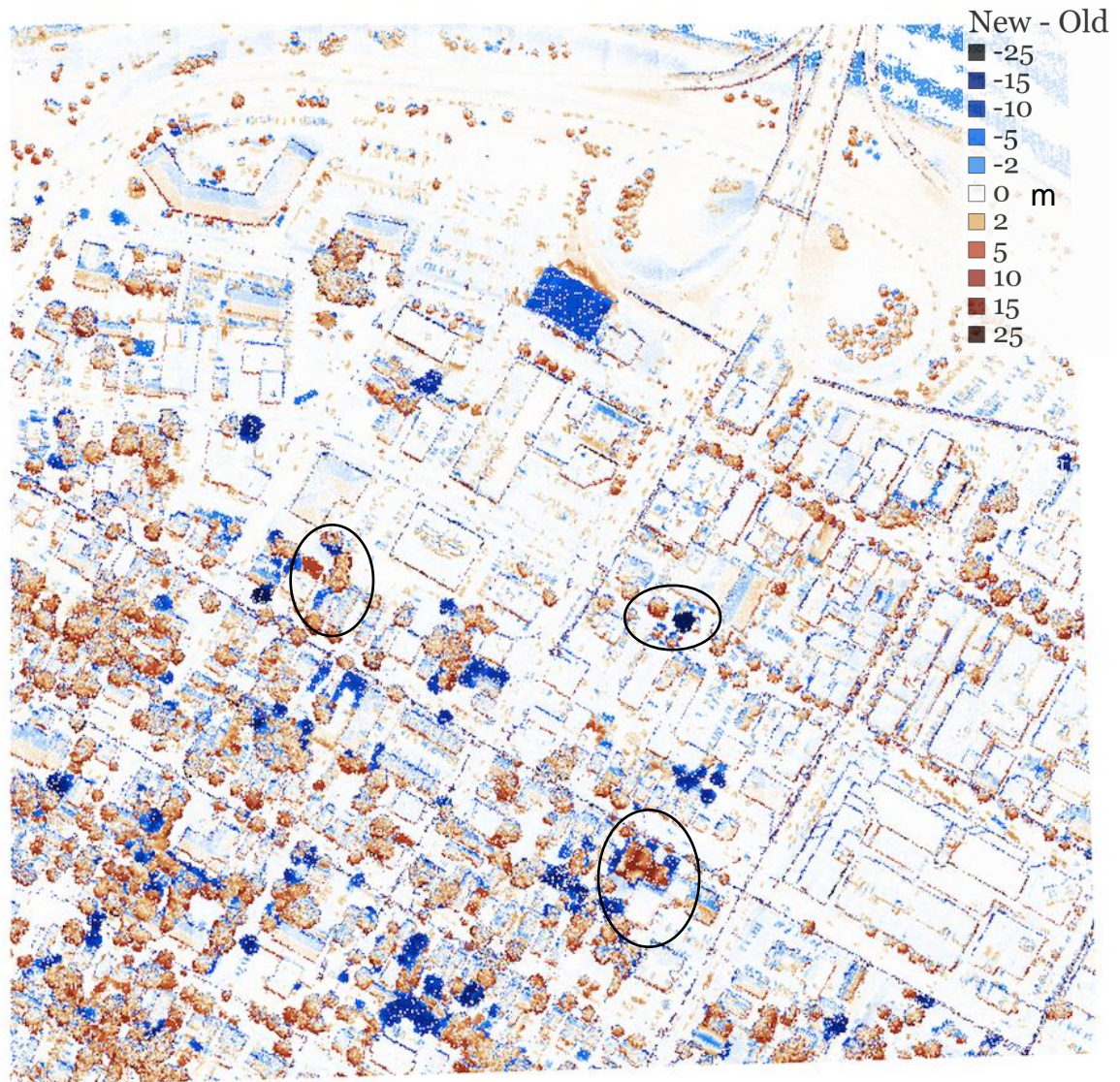


Figure 6.11

Elevation differences, 2006 data subtracted from 2011 data. Circled areas correspond to circled areas in Figure 6.10.

Full classification and comparison of these data sets would provide a comprehensive study of the changes in Fredericton over the five year period. Yet, such a comparison is not straightforward: the 2006 data are in the UTM coordinate system, zone 19 N, and use ellipsoidal heights; the 2011 data are in the New Brunswick stereographic coordinate system and use orthometric

heights. Tools are available to transform data between coordinate systems but extra care must still be taken to ensure the data sets are accurately aligned horizontally.

A greater difficulty with the 2006 data is that they do not appear to be true ellipsoidal heights: after adding the appropriate value for geoid-ellipsoid separation, which is -22.37 m in this study area, there is still a difference of unknown cause amounting to approximately -1.3 m between the surfaces. To generate the image in Figure 6.11, which is a difference image between the 2006 and the 2011 data, the 2006 data were subtracted from the 2011 data and then a constant value of 23.67 was subtracted to account for both the geoid-ellipsoid separation and the unknown bias. In these unbiased results, large negative differences (2006 values higher) correspond to building deconstruction and high vegetation removal; large positive differences (2011 values higher) correspond to building construction and vegetation growth.

## **6.8. SUMMARY OF INTEGRATED CLASSIFICATION**

In this chapter, different approaches were explored for modifying the classification GPI and MSPC processes developed by the author and described in Chapters 4 and 5, to make use of data from other sources. In some cases, such as with water bodies, additional data are necessary because the features to be classified do not have sufficiently distinguishable point characteristics and therefore cannot be reliably classified solely using LiDAR data. In other cases, such as with augmented ground classification, additional data can significantly

reduce processing time.

Additional data may also be complementary to the LiDAR data, such as in the case of road surface classification where neither LiDAR intensity nor road centreline buffers provide truly satisfactory results on their own but combined could possibly offer both visually and numerically accurate results. In all cases, when using data from multiple sources for classification or for comparison, the horizontal and vertical alignment of the data sets must be verified and adjusted as necessary to ensure the classification and analysis results are as accurate as possible.

Where multi-temporal data exist, there is great potential for using them to detect changes over time. The data may be solely LiDAR data sets, collected months or years apart, or disparate data types (LiDAR and vector, LiDAR and raster). This potential can be seen both in the test results for the building classification modification for building footprints and the assessment of the multi-temporal Fredericton LiDAR data, and even in the data sample from the Christina River Basin. More research is needed to determine how change detection can be automated. The following chapter summarizes the author's achievements and proposes areas for future research.

*"One never notices what has been done; one  
can only see what remains to be done."  
~ Marie Curie*

## **CHAPTER 7**

### **CONCLUSION AND RECOMMENDATIONS**

LiDAR is a tool whose importance in remote sensing has been growing since the mid-1990s. In a discussion of current capabilities and community needs for working with LiDAR, Arrowsmith et al. [2008] identify the increase in spatial resolution, and the corresponding ability to analyze terrain features at higher scales, as the primary benefit. Applications of LiDAR elevation data range from the simple (derivation of elevation models, e.g., Kobler et al. [2007]) to the complex (e.g., georegistration of high resolution satellite imagery [Oh et al., 2012]), and include soil moisture mapping (e.g., Southee et al. [2012]), archaeology (e.g., Chase et al. [2011]), and delineation of areas at risk from flooding and sea-level rise (e.g., Webster et al. [2004]; Gesch [2009]). LiDAR point cloud data have also been used for environmental quality assessment (e.g., Garcia-Gutierrez et al. [2011]), urban vegetation detection (e.g., [Höfle et al., 2012]), building change detection (e.g., Champion et al. [2009]), and in numerous other ways.

Yet, non-expert LiDAR users' knowledge and use of the data may be limited by several factors including differing product standards and the availability of suitable processing software. NRCan recently developed a Canadian LiDAR acquisition guidelines document [Natural Resources Canada, 2014] to present standardized criteria for data acquisition and derived products and encourage

data ownership models that permit data sharing but these guidelines cannot be applied retroactively to all existing data sets because some of the required information may be missing or the data may not have been collected in a manner that is compatible with the guidelines. Existing commercial software packages for working with LiDAR data can be cost-prohibitive while free software is often limited to viewers or has been developed for a specific purpose, and the software may require extensive training and familiarity with the tools for users to achieve their desired results.

Making reference to the NRCan guidelines, this thesis addressed the challenges non-expert LiDAR users may have when working with the data by developing a semi-automated, multi-stage point classification framework that does not require expert user input to classify individual points within the point cloud. The stated purposes for developing this framework were: to create a method for processing and interpreting LiDAR data that is simple to use; to create a point classification process that will classify LiDAR data to a desired level of completeness; and to create a process that can incorporate additional data when they are available and can augment single-source LiDAR data. These purposes were met by achieving the following objectives:

1. Develop a ground point identification process that achieves 95% point classification accuracy.
2. Develop a semi-automated multi-stage point classification process to classify points as "building/structure", "medium vegetation" and "high vegetation", and separate ground points into "low vegetation", "road (or



paved) surface", and "other ground". High point classification accuracy for all classes should be visually verifiable and, where adequate truth exists for point classification, numerically as 90% correct or better.

3. Propose and develop measures to assess the quality of data integration results.

4. Develop, implement, and test strategies for integrating disparate data sets into the LiDAR point classification process.

With the exception of data visualization and the application of a few basic GIS functions, particularly vector data manipulation, all of the work carried out as part of this research made use of code developed by the author in the C programming language. The core functionality of the developed code is included as pseudocode in Appendix A. The full code can be found in a repository on Bitbucket<sup>11</sup> at <https://bitbucket.org/kamolins/thesiscode>. The following sections summarize the contributions made by this research and outline areas for future research.

## **7.1. GROUND POINT IDENTIFICATION**

The most significant contribution of this research is the development and implementation of a ground point identification (GPI) process that requires little or no operator input to classify ground points within a LiDAR point cloud. The GPI process consists of three stages, all of which are implemented through code

---

<sup>11</sup> Bitbucket is a code management and collaboration service. Cloud hosting is free for individuals. <https://bitbucket.org/>

developed by the author. In the first stage, four different ground detection techniques, two point-based and two raster-based, are applied to the LiDAR point cloud to identify potential ground points. In the second stage, the outputs from the four ground detection techniques are compared to obtain a ground surface representation and in the final stage, the ground surface is used to classify points as "ground."

None of the ground detection techniques require any expert knowledge to run. Input parameters may be set manually but can also be automated. Tests of the GPI process were conducted on a set of 50 m x 50 m sample areas, representing approximately 1.26% of the total number of points in the 2011 Fredericton test data and a variety of conditions, including under dense forest cover on hilly terrain. The overall accuracy for the GPI process with these samples was 96.78% accuracy as compared to results produced using the *LAStools*<sup>™</sup> *lasground* tool.

The *lasground* tool requires the user to be familiar both with the data and with the parameters of the tool, which means it is not an appropriate tool for non-expert users. It was used to check the results of the GPI process because none of the LiDAR point clouds that were obtained for testing were classified to the degree needed to conduct a rigorous accuracy assessment. Visual inspection of the point data as provided revealed inconsistencies and what could be deemed incompleteness in the ground point classification, with many points at ground level not classified as ground. The data therefore were reprocessed to provide a ground reference at the point level.

Sample areas where the accuracy of the GPI process was lower than the average for the tested samples were found to contain a significant percentage of high vegetation points, conditions under which the *LAStools*<sup>TM</sup> method also seemed to perform relatively poorly. With a manual classification of these samples to correct any remaining errors in the ground reference, the author believes the ground point classification accuracy would have been found to be higher than 97%. The test data were all of mixed urban scenes with varying terrain and areas of high vegetation. While this did provide a variety of conditions in which to test the data, the GPI process may not perform as well in other conditions, for example scenes entirely covered in dense vegetation.

## **7.2. CLASSIFICATION OF SINGLE LIDAR DATA SETS**

The second most important contribution of this research is the development of a multi-stage point classification (MSPC) process that, like the GPI process, does not require the user to have any expert knowledge. There is only one input parameter to set, the intensity threshold, and it is chosen arbitrarily within an identified range. The stages of the MSPC process, after the ground surface is identified, are: preliminary classification, to separate potential building points from potential vegetation points; building point classification; identification of areas of high uncertainty; high vegetation classification; separation of low vegetation and roads or other paved surfaces; and identification of vehicles and other objects above road surfaces.

The NRCan guidelines define "low" and "medium" vegetation based strictly

on height above ground; however, the low vegetation threshold is the same as the FVA, 0.3 m, making it inseparable from ground. Therefore, in the MSPC process, the low vegetation classification was used to distinguish unpaved from paved or road surfaces, which is a class that is not defined in the NRCan guidelines but that is defined in the LAS 1.4 specification. The medium vegetation classification was used in the MSPC process to identify vegetation points that were a distance of between 1 m and 2 m from other vegetation points.

"Vehicles" and "other objects above the road surface" are new classifications defined by the author, as being 0.3 m to 2 m above the road surface and more than 2 m above the road surface, respectively. Vehicles do not belong to any of the standard classes nor do other objects overhanging roads such as power lines or traffic signals, yet these are common features in urban areas and being able to locate them in the point cloud provides a more complete representation of the urban space.

A numerical assessment of the MSPC process only up to the building classification stage was conducted and only with respect to a very small percentage of total points in the test area due to the unavailability of a "true" classification to reference. A small set of points were manually classified for assessment purposes. The assessment revealed that the method developed by the author achieved an overall accuracy of 93.35% – marginally better than the *LAStools*<sup>™</sup> accuracy of 92.94%, though likely not statistically significantly better. Nevertheless, visual inspection revealed that the classification process developed by the author does perform very well and in several instances was

able to classify building points where *LAStools*<sup>™</sup> had failed to do so.

The stages of the MSPC process favour errors of omission over errors of commission. This can result in a significant number of points remaining unclassified, up to 25% or more in testing. This may be considered a severe limitation of the process. However, each stage can be repeated with manually modified parameters to try to reduce the percent of unclassified points. Alternatively, if data are available from other sources, these can be introduced into the MSPC process to add additional spatial context for the point classification.

### **7.3. CLASSIFICATION OF LIDAR DATA USING MULTIPLE DATA SOURCES**

Although a detailed point classification can be achieved with the MSPC process using only a single LiDAR data set, the process can be simplified, refined, and/or improved using data from other sources. The final contribution of the research is an investigation of the integrating data from sources other than the target LiDAR point cloud into the MSPC process.

Many of the measures used in the GPI and MSPC processes, such as local point density, intensity, and ground-vegetation ratio also provide indications of the local quality of the LiDAR data and by extension the quality of integration results. In particular, a low point density means feature boundaries may not be clearly identifiable and therefore data from other sources may not be properly

horizontally aligned to the LiDAR data.

When the additional data include elevation information, proper vertical alignment is also important. While large differences between two elevation data sources may be expected in areas of steep terrain slope and where the ground is obscured by dense vegetation, any systematic elevation biases need to be identified through careful comparison of the data.

The GPI process that was developed by the author, while effective, may be time-consuming. A ground surface derived from other data, for example, from a provincial DTM or an earlier LiDAR point cloud, can be used as a reference ground surface to speed up the process. The best results will be achieved when the reference ground surface has similar properties to the LiDAR point cloud from which ground is being extracted, particularly a similar vertical accuracy, yet even a ground surface with large differences can be used as a reference ground if steps are taken to account for these differences.

The MSPC process developed by the author does not classify water points. This is because of the unpredictability of returns from water. However, if polygon data or land cover maps that delineate the boundaries of water bodies, derived from, for example, satellite imagery, are available, these data can be applied to the results of the GPI process to identify points that are within water bodies and are near the water surface elevation.

The building classification stage can potentially be simplified by deriving the elevation-infused building mask from existing building footprint polygons; however, since the building polygons may not fully correspond to the buildings

captured in the point cloud, they should not be the sole means used to locate building points.

To achieve the best results, the horizontal alignment between the polygons and the point cloud should be carefully assessed and adjusted and steps should be taken when converting the polygons into a building mask to eliminate building shapes from the mask that do not exist in the point cloud. Building classification should always be performed after the preliminary classification stage of the MSPC process, as this will facilitate locating buildings that are in the point cloud but are not in the building polygons. If the LiDAR data are newer, these will be buildings that have been constructed since the polygons were created.

Similarly, road centrelines can be used in the road and low vegetation separation stage. However, if a buffer around the centrelines is used to classify roads instead of an intensity threshold, the resulting low vegetation class will not be entirely vegetation as it will also include parking lots, private lanes, and any other paved surfaces not part of the road network. An approach combining both the centrelines and the intensity threshold is discussed below as a recommendation for future research.

Finally, while not strictly classification, integrated multi-temporal LiDAR data can be used in change detection. Once adjustments have been made to correct any vertical biases or horizontal misalignments, and remaining differences in digital surface models (DSMs) derived from two LiDAR point clouds from the same area surveyed at different times will be an indication of changes that

occurred in the time between the surveys. Changes may include growth or pruning of vegetation; removal of vegetation; and construction or destruction of buildings.

#### **7.4. RECOMMENDATIONS FOR FUTURE WORK**

Although the objectives for the thesis were achieved, no single work can fully explore every possible aspect of the topic being studied. Recommendations for future work include:

- Making more full use of voxels. Using voxels to order LiDAR data may be an effective method of overcoming the unpredictable arrangement of points in a LiDAR data file. The Pixel Connectedness ground extraction method only used voxels to determine and confirm the lowest elevation in the area and to obtain seed pixels. The possibility of extending pixel connectedness to the layers immediately above and below a seed pixel should be explored, as a potential alternative to requiring slope thresholds.
- A point-based comparison technique for ground extraction. The raster-based comparison technique is effective, yet it is subject to the limitations of raster interpolations, namely a loss of information. A point-based comparison could better capture small, local variations in the terrain. The Point Neighbourhood ground extraction method already assigns probabilities to ground points; if the other methods were modified to also assign probabilities, a point-based comparison could calculate an overall certainty value that a point is ground.



- Explore different equations for the Point Neighbourhood ground extraction method. The equations used were selected to assign specific probabilities to points in an ellipsoidal neighbourhood determined by the weights for elevation and planimetric distance from a central point. These equations were found to be effective, yet a more thorough analysis of terrain versus feature relationships may help determine more appropriate equations or parameters.
- Develop a road classification process that utilizes both road centrelines and intensity threshold. In Chapter 6, the results of using only road centreline buffers were compared to the results of using only an intensity threshold. Both approaches have their strengths and weaknesses; combining the two could produce a better result overall. One approach would be to first apply the road centreline buffer method and use the results to determine an appropriate intensity threshold. Another approach would be to first apply the intensity threshold method and then the road centreline buffer. Either approach would separate roads from other ground types such as parking lots, trails, and exposed soil, as well as from low vegetation.
- Improve methods for refining classification results. The process developed by the author was designed to favour errors of omission over errors of commission. This approach leaves a significant percentage of points labelled as "unclassified" or "uncertain" (around 25% for one tested tile). Since the points that are classified should consequently be classified with a high level of certainty, neighbouring points that have similar properties (elevation, intensity, not proximal to other classes) should have a similarly high level of

certainty of belonging to the same class. Some methods to refine classification results were developed and implemented as part of the ground extraction and overall classification process, but these could be further developed.

- Explore the implications of multi-temporal LiDAR data. With the growing prevalence of airborne LiDAR, more data are becoming available and new data are becoming available in areas previously covered by LiDAR surveys, creating the possibility of high resolution, high accuracy monitoring of changes over time. In particular, monitoring of changes that are more difficult to observe and quantify, such as vegetation growth and pruning, may be of interest.

The importance of LiDAR as a tool for gathering elevation and other information has been growing since the mid-1990s. Making reference to the Canadian LiDAR acquisition guidelines document [Natural Resources Canada, 2014], this thesis addressed the challenges non-expert LiDAR users may have when working with LiDAR data by developing a semi-automated, multi-stage point classification framework that does not require expert user input to classify individual points within the point cloud.

## REFERENCES

- Al-Durgham, M., E. Kwak, and A. Habib (2012). "Automatic extraction of building outlines from LiDAR using the minimum bounding rectangle algorithm." *Proceedings of Global Geospatial Conference*. Quebec City, Canada, 14-17 May, 10 pp.
- Alexander, C., K. Tansey, J. Kaduk, D. Holland, and N. J. Tate (2011). "An approach to classification of airborne laser scanning point cloud data in an urban environment." *International Journal of Remote Sensing*, Vol. 32, No. 24, pp. 9151-9169.
- Antonarakis, A. S., K. S. Richards, and J. Brasington (2008). "Object-based land cover classification using airborne LiDAR." *Remote Sensing of Environment*, Vol. 112, No. 6, pp. 2988-2998.
- Arefi, H., M. Hahn, and J. Lindenberger (2003). "LIDAR data classification with remote sensing tools." *Proceedings of the ISPRS Joint Workshop on Challenges in Geospatial Analysis, Integration and Visualization II*. ISPRS, Stuttgart, Germany, 8-9 September, pp. 131-136.
- Apple Dictionary (n.d.). "Classification", "Extraction", Apple, Inc. [Electronic]
- Arrowsmith, J., N. Glenn, C. J. Crosby, and E. Cowgill (2008). "Current capabilities and community needs for software tools and educational resources for use with LiDAR high resolution topography data." *Proceedings of the OpenTopography Meeting*. held in San Diego, California, August. Vol. 8.
- Australian Intergovernmental Committee on Surveying & Mapping (2010). *ICSM LiDAR Acquisition Specifications and Tender Template, Version 1.0*. Elevation Working Group. 34 pp.
- Axelsson, P. (1999). "Processing of laser scanner data - algorithms and applications." *ISPRS Journal of Photogrammetry & Remote Sensing*, Vol. 54, pp. 138-147.
- Ayeni, O. O. (1982). "Optimum sampling for digital terrain models: A trend towards automation." *Photogrammetric Engineering & Remote Sensing*, Vol. 48, No. 11, pp. 1687-1694.

- Baltsavias, E. P. (1999a). "A comparison between photogrammetry and laser scanning." *ISPRS Journal of Photogrammetry & Remote Sensing*, Vol. 54, pp. 83-94.
- Baltsavias, E. P. (1999b). "Airborne laser scanning: Basic relations and formulas." *ISPRS Journal of Photogrammetry & Remote Sensing*, Vol. 54, pp. 199-214.
- Bartels, M., and H. Wei (2006). "Towards DTM generation from LIDAR data in hilly terrain using wavelets." *4th International Workshop on Pattern Recognition in Remote Sensing, in conjunction with International Conference on Pattern Recognition*, pp. 33-36.
- Bartels, M., H. Wei, and J. Ferryman (2006). "Analysis of LIDAR ." *Proceedings of the IEEE . IEEE*, Sydney, Australia, 22-24 November, 6 pp.
- Bewley, R. S., S. Crutchley, and C. Shell (2005). "New light on an ancient landscape: Lidar survey in the Stonehenge World Heritage Site." *Antiquity*, Vol. 79, No. 305, pp. 636-647.
- Briese, C., and N. Pfeifer (2001). "Airborne laser scanning and derivation of digital terrain models." *Proceedings of the Fifth Conference on Optical 3D Measurement Techniques*. Vienna, Austria, 1-3 October, pp. 80-87.
- Brodu, N., and D. Lague (2011). "3D Terrestrial lidar data classification of complex natural scenes using a multi-scale dimensionality criterion: Applications in geomorphology." *ISPRS Journal of Photogrammetry & Remote Sensing*, Vol. 68, pp. 121-134.
- Caceres, J., and K. Slatton (2007). "Improved classification of building infrastructure from airborne lidar data using spin images and fusion with ground-based lidar." *Proceedings of the Urban Remote Sensing Joint Event*. IEEE, Paris, France, 11-13 April, 7 pp.
- Challis, K., C. Carey, M. Kincey, and A. J. Howard (2011). "Assessing the preservation potential of temperate, lowland alluvial sediments." *Journal of Archaeological Science*, Vol. 38, pp. 301-311.
- Champion, N., F. Rottensteiner, L. Matikainen, X. Liang, J. Hyypä, and B. P. Olsen (2009). "A test of automatic building change detection approaches." *International Archives of the Photogrammetry, Remote Sensing and Spatial Information Sciences*, Vol. XXXVIII, Part 3/W4, pp. 145-150.

- Chase, A. F., D. Z. Chase, J. F. Weishampel, J. B. Drake, R. L. Shrestha, K. C. Slatton, J. J. Awe, and W. E. Carter (2011). "Airborne LiDAR, archaeology, and the ancient Maya landscape at Caracol, Belize." *Journal of Archaeological Science*, Vol. 38, pp. 387-398.
- Chehata, N., L. Guo, and C. Mallet (2009). "Airborne lidar feature selection for urban classification using random forests." *International Archives of the Photogrammetry, Remote Sensing and Spatial Information Sciences*, Vol. XXXVIII, Part 3/W8, pp. 207-212.
- Chen, Y., L. Cheng, M. Li, J. Wang, L. Tong, and K. Yang (2014). "Multiscale Grid Method for Detection and Reconstruction of Building Roofs from Airborne LiDAR Data." *IEEE Journal of Selected Topics in Applied Earth Observations and Remote Sensing*, Vol. 7, No. 10, pp. 4081-4094.
- Cho, W., Y. S. Jwa, H. J. Chang, and S. H. Lee (2004). "Pseudo-grid based building extraction using airborne LIDAR data." *International Archives of the Photogrammetry, Remote Sensing and Spatial Information Sciences*, Vol. XXXV, Part B3, pp. 378-381.
- City of Fredericton. (n.d.). "Open Data." [On-line] Accessed 10 January 2015. Retrieved from <http://www.fredericton.ca/en/citygovernment/DataMain.asp>
- Clode, S., F. Rottensteiner, P. Kootsookos, and E. Zelnikar (2007). "Detection and vectorization of roads from lidar data." *Photogrammetric Engineering & Remote Sensing*, Vol. 73, No. 5, pp. 517-535.
- Cook, B. D., P. V. Bolstad, E. Naesset, R. S. Anderson, S. Garrigues, J. T. Morissette, J. Nickeson, and K. J. Davis (2009). "Using LiDAR and quickbird data to model plant production and quantify uncertainties associated with wetland detection and land cover generalizations." *Remote Sensing of Environment*, Vol. 113, pp. 2366-2379.
- Csanyi, N., and C. K. Toth (2007). "Improvement of lidar data accuracy using lidar-specific ground targets." *Photogrammetric Engineering & Remote Sensing*, Vol. 73, No. 4, pp. 385-396.
- Dalponte, M., L. Bruzzone, and D. Gianelle (2008). "Fusion of hyperspectral and LIDAR remote sensing data for classification of complex forest areas." *IEEE Transactions on Geoscience and Remote Sensing*, Vol. 46, No. 5, pp. 1416-1427.

- Demir, N., D. Poli, and E. Baltsavias (2009). "Detection of buildings at airport sites using images & lidar data and a combination of various methods." *International Archives of the Photogrammetry, Remote Sensing and Spatial Information Sciences*, Vol. XXXVIII, Part 3/W4, pp. 71-76.
- Doyle, F. J. (1978). "Digital Terrain Models: An Overview." *Photogrammetric Engineering & Remote Sensing*, Vol. 44, No. 12, pp. 1481-1485.
- Elaksher, A. F., and J. S. Bethel (2002). "Reconstructing 3D buildings from LIDAR data." *International Archives of the Photogrammetry, Remote Sensing and Spatial Information Sciences*, Vol. XXXIV, Part. 3/A, pp. 102-107.
- Esri Inc. (2012). "Set LAS Class Codes Using Features (3D Analyst)." [On-line] Accessed 30 May 2013. Retrieved from ArcGIS Help 10.1:  
<http://resources.arcgis.com/en/help/main/10.1/index.html#//00q90000000n1000000>
- Esri Inc. (2014). "An overview of displaying LAS datasets in ArcGIS." [On-line] Accessed 1 May 2014. Retrieved from  
<http://resources.arcgis.com/en/help/main/10.2/index.html#//015w0000003s0000000>
- Florinsky, I. V. (1998). "Combined analysis of digital terrain models and remotely sensed data in landscape investigations." *Progress in Physical Geography*, Vol. 22, No. 1, pp. 33-60.
- Forlani, G., C. Nardinocchi, M. Scaioni, and P. Zingaretti (2006). "Complete classification of raw LIDAR data and 3D reconstruction of buildings." *Pattern Analysis and Applications*, Vol. 8, No. 4, pp. 357-374.
- Fowler, R. A., A. Samberg, M. J. Flood, and T. J. Greaves (2007). "Topographic and terrestrial lidar." In *Digital Elevation Model Technologies and Applications: The DEM Users Manual*, Ed. Maune, D. F., American Society for Photogrammetry and Remote Sensing, Bethesda, Maryland, pp. 199-252.
- Fowler, R. J., and J. J. Little (1979). "Automatic extraction of irregular network digital terrain models." *ACM SIGGRAPH Computer Graphics*, Vol. 13, No. 2, pp. 199-207.
- Garcia-Gutierrez, J., L. Gonçalves-Seco, and J. C. Riquelme-Santos (2009). "Decision trees on LIDAR to classify land uses and covers." *International*

*Archives of the Photogrammetry, Remote Sensing and Spatial Information Sciences*, Vol. XXXVIII, Part 3/W8, pp. 323-328.

- Garcia-Gutierrez, J., L. Gonçalves-Seco, and J. C. Riquelme-Santos (2011). "Automatic environmental quality assessment for mixed-land zones using lidar and intelligent techniques." *Expert Systems with Applications*, Vol. 38, No. 6, pp. 6805-6813.
- Gesch, D. B. (2009). "Analysis of lidar elevation data for improved identification and delineation of lands vulnerable to sea-level rise." *Journal of Coastal Research*, No. 53, pp. 49-58.
- Goodenough, D., H. Chen, A. Dyk, G. Hobart, and A. Richardson (2008). "Data fusion study between polarimetric SAR, hyperspectral and LIDAR data for forest information." *Proceedings of the IEEE International Geoscience and Remote Sensing Symposium 2008*. Boston, Massachusetts, U.S.A., 6-11 July, pp. 281-284.
- Goulden, T. (2009). *Prediction of error due to terrain slope in LiDAR Observations*. M.Sc.E. thesis, Department of Geodesy and Geomatics Engineering Technical Report No. 265, University of New Brunswick, Fredericton, N.B., Canada. 138 pp.
- Goulden, T., C. Hopkinson, R. Jamieson, and S. Sterling. (2014). "Sensitivity of watershed attributes to spatial resolution and interpolation method of LiDAR DEMs in three distinct landscapes." *Water Resources Research*, Vol. 50, pp. 1908-1927.
- Graham, L. (2012). "The LAS 1.4 specification." *Photogrammetric Engineering & Remote Sensing*, Vol. 78, No. 2, pp. 93-102.
- Guan, H., J. Li, Y. Yu, L. Zhong, and Z. Ji (2014). "DEM generation from lidar data in wooded mountain areas by cross-section-plane analysis." *International Journal of Remote Sensing*, Vol. 35, No. 3, pp. 927-948.
- Guo, L., N. Chehata, C. Mallet, and S. Boukir (2011). "Relevance of airborne lidar and multispectral image data for urban scene classification using random forests." *ISPRS Journal of Photogrammetry & Remote Sensing*, Vol. 66, No. 1, pp. 56-66.
- Guo, Q. (2011). *Critical Zone Observatory LiDAR*. Mapping Project Report for the National Center for Airborne Laser Mapping, Merced, California, U.S.A., 14 January. 34 pp.

- Haala, N., and C. Brenner (1999). "Extraction of buildings and trees in urban environments." *ISPRS Journal of Photogrammetry & Remote Sensing*, Vol. 54, pp. 130-137.
- Haala, N., and V. Walter (1999). "Automatic classification of urban environments for database revision using lidar and color aerial imagery." *International Archives of the Photogrammetry, Remote Sensing and Spatial Information Sciences*, Vol. XXXII, Part 7-4-3 W6, 7 pp.
- Halifax Regional Municipality. (n.d.). LIDAR DEM 5M. *Halifax Regional Municipality Open Data Catalogue*. Accessed 30 May 2013. Retrieved from <https://www.halifaxopendata.ca/Demographics/LIDAR-DEM->
- Heidemann, H. K. (2014). *Lidar Base Specification*. U.S. Geological Survey, National Geospatial Program.
- Hiltz, D. (2012). "Landscape-wide LiDAR mapping of vegetation type by soil moisture regime." *Presentation at the Global*. Quebec City, Canada, 14-17 May.
- Höfle, B., M. Hollaus, and J. Hagenauer (2012). "Urban vegetation detection using radiometrically calibrated small-footprint full-waveform airborne LiDAR data." *ISPRS Journal of Photogrammetry & Remote Sensing*, Vol. 67, pp. 134-147.
- Höfle, B., M. Vetter, N. Pfeifer, G. Mandlbürger, and J. Stötter (2009). "Water surface mapping from airborne laser scanning using signal intensity and elevation data." *Earth Surface Processes and Landforms*, Vol. 34, pp. 1635-1649.
- Hopkinson, C. (2013). Personal communication.
- Hosoi, F., Y. Nakai, and K. Omasa (2013). "3-D voxel-based solid modeling of a broad-leaved tree for accurate volume estimation using portable scanning lidar." *ISPRS Journal of Photogrammetry & Remote Sensing*, Vol. 82, pp. 41-48.
- Hudak, A. T., N. L. Crookston, J. S. Evans, M. J. Falkowski, and A. M. Smith (2006). "Regression modeling and mapping of coniferous forest basal area and tree density from discrete-return lidar and multispectral satellite data." *Canadian Journal of Remote Sensing*, Vol. 32, No. 2, pp. 126-138.
- Idaho LiDAR Consortium. (n.d.). "Free LiDAR Tools." [On-line] Accessed May 1 2014. Retrieved from <http://www.idaholidar.org/tools/free>



- Isenburg, M. (n.d.). "Readme files for LAStools." [On-line] Accessed 30 May 2013. Retrieved from rapidlasso GmbH: <http://rapidlasso.com/lastools/>
- Jwa, Y., G. Sohn, and H. Kim (2009). "Automatic 3D powerline reconstruction using airborne LiDAR data." *International Archives of the Photogrammetry, Remote Sensing and Spatial Information Sciences*, Vol. XXXVIII, Part 3/W8, pp. 105-110.
- Kabolizade, M., H. Ebadi, and S. Ahmadi (2010). "An improved snake model for automatic extraction of buildings from urban aerial images and LiDAR data." *Computers, Environment and Urban Systems*, Vol. 34, pp. 435-441.
- Kada, M., and L. McKinley (2009). "3D building reconstruction from LIDAR based on a cell decomposition approach." *International Archives of the Photogrammetry, Remote Sensing and Spatial Information Sciences*, Vol. XXXVIII, Part 3/W4, pp. 47-52.
- Kim, Y. M., Y. D. Eo, A. J. Chang, and Y. I. Kim (2013). "Generation of a DTM and building detection based on an MPF through integrating airborne lidar data and aerial images." *International Journal of Remote Sensing*, Vol. 34, No. 8, pp. 2947-2968.
- Kobler, A., N. Pfeifer, P. Ogrinc, L. Todorovski, K. Oštir, and S. Džeroski (2007). "Repetitive interpolation: A robust algorithm for DTM generation from aerial laser scanner data in forested terrain." *Remote Sensing of Environment*, Vol. 108, No. 1, pp. 9-23.
- Kraus, K., and N. Pfeifer (1998). "Determination of terrain models in wooded areas with airborne laser scanner data." *ISPRS Journal of Photogrammetry & Remote Sensing*, Vol. 53, pp. 193-203.
- Kraus, K., and N. Pfeifer (2001). "Advanced DTM generation from LIDAR data." *International Archives of the Photogrammetry, Remote Sensing and Spatial Information Sciences*, Vol. XXXIV, Part 3/W4, pp. 23-30.
- Krishnan, S., C. Crosby, V. Nandigam, M. Phan, C. Cowart, C. Baru, and R. Arrowsmith (2011). "OpenTopography: a services oriented architecture for community access to LIDAR topography." *Proceedings of the 2nd International Conference on Computing for Geospatial Research & Applications*. ACM, Washington, D.C., U.S.A., 23-25 May, 7 pp.
- LAS Working Group. (n.d.). "LASer (LAS) File Format Exchange Activities." [On-line] Accessed 30 May 2012. Retrieved from American Society of

Photogrammetry and Remote Sensing:

<http://www.asprs.org/Committee-General/LASer-LAS-File-Format-Exchange-Activities.html>

- Leberl, F., A. Irschara, T. Pock, P. Meixner, M. Gruber, S. Scholz, and A. Wiechert (2010). "Point clouds: Lidar versus 3D vision." *Photogrammetric Engineering & Remote Sensing*, Vol. 76, No. 10, pp. 1123-1134.
- Lehrbass, B., and J. Wang (2012). "Urban tree cover mapping with relief-corrected aerial imagery and lidar." *Photogrammetric Engineering & Remote Sensing*, Vol. 78, No. 5, pp. 473-484.
- Lehto, D. J. (2012a). "Applications of LiDAR data." *Presentation at the LiDAR Technical Session*. CIG, Ottawa, Canada, 22 November.
- Lehto, D. J. (2012b). *Personal communication*. Production Manager, GeoDigital International Inc., Ottawa, Canada, 22 November.
- Li, W., Q. Guo, M. K. Jakubowski, and M. Kelly (2012). "A new method for segmenting individual trees from the lidar point cloud." *Photogrammetric Engineering & Remote Sensing*, Vol. 78, No. 1, pp. 75-84.
- Li, Z. (1994). "A comparative study of the accuracy of digital terrain models (DTMs) based on various data models." *ISPRS Journal of Photogrammetry and Remote Sensing*, Vol. 49, pp. 2-11.
- Lu, W., K. P. Murphy, J. J. Little, A. Sheffer, and H. Fu (2009). "A hybrid conditional random field for estimating the underlying ground surface from airborne LiDAR data." *IEEE Transactions on Geoscience and Remote Sensing*, Vol. 47, No. 8, pp. 2913-2922.
- Ma, Y., C. Wei, T. Hu, R. Wang, and G. Zhou (2015). "Hybrid filtering of Lidar Data based on the Echoes." *2nd IEEE International Conference on Spatial Data Mining and Geographical Knowledge Services*. ICSDM, Fuzhou, China, 8-10 July, pp. 147-151.
- Mallet, C., and F. Bretar (2009). "Full-waveform topographic lidar: State-of-the-art." *ISPRS Journal of Photogrammetry & Remote Sensing*, Vol. 64, No. 1, pp. 1-16.
- Mancini, A., E. Frontoni, and P. Zingaretti (2009). "Automatic extraction of urban objects from multi-source aerial data." *International Archives of*

*the Photogrammetry, Remote Sensing and Spatial Information Sciences*, Vol. XXXVIII, Part 3/W4, pp. 13-18.

- Mao, J., X. Liu, and Q. Zeng (2009). "Building extraction by fusion of LIDAR data and aerial images." *Proceedings of the Urban Remote Sensing Joint Event*. IEEE, Shanghai, China, 20-22 May, pp. 969-973.
- Meng, X., N. Currit, W. Le, and X. Yang (2012). "Detect residential buildings from lidar and aerial photographs through object-oriented land-use classification." *Photogrammetric Engineering & Remote Sensing*, Vol. 78, No. 1, pp. 35-44.
- Merrick & Company. (n.d.). "MARS LiDAR Software." [On-line] Accessed 1 May 2014. Retrieved from <http://www.merrick.com/Geospatial/Software-Products/MARS-Software>
- Merrick & Company. (n.d.). "MARS® Explorer." [On-line] Accessed 30 May 2013. Retrieved from <http://www.merrick.com/Geospatial/Services/MARS-Software>
- Miliaresis, G., and N. Kokkas (2007). "Segmentation and object-based classification for the extraction of the building class from LIDAR DEMs." *Computers & Geosciences*, Vol. 33, No. 8, pp. 1076-1087.
- Miller, C. L., and R. A. Laflamme (1958). *The Digital Terrain*. MIT Photogrammetry Laboratory. 20 pp.
- Mofford, L. (2012). "RE: information about lidar data?" [On-line] Accessed 16 August 2012. To K. Amolins <km.amolins@unb.ca> from <Lori.Mofford@gnb.ca>
- Moosmann, F., O. Pink, and C. Stiller (2009). "Segmentation of 3D lidar data in non-flat urban environments using a local convexity criterion." *Proceedings of the 2009 IEEE Intelligent Vehicles Symposium*. IEEE, Xi'an, China, 3-5 June, pp. 215-220.
- Morsdorf, F., A. Mårell, E. Rigolot, and B. Allgöwer (2009). "A role for airborne laser scanning intensity data in vertical stratification of multilayered ecosystems." *International Archives of the Photogrammetry, Remote Sensing and Spatial Information Sciences*, Vol. XXXVIII, Part 3/W8, pp. 141-146.

- Mosa, A. S., B. Schön, M. Bertolotto, and D. F. Laefer (2012). "Evaluating the benefits of octree-based indexing for lidar data." *Photogrammetric Engineering & Remote Sensing*, Vol. 78, No. 9, pp. 927-934.
- Mouland, C., K. Wen, and J. Ogilvie (2012). "Determining culvert locations and size across bare-earth LiDAR-DEMs, automatically." *Presentation at the Global Geospatial Conference 2012*. Quebec City, Canada, 14-17 May.
- Mumtaz, S. A., and K. Mooney (2009). "A semi-automatic approach to object extraction from a combination of image and laser data." *International Archives of the Photogrammetry, Remote Sensing and Spatial Information Sciences*, Vol. XXXVIII, Part 3/W8, pp. 53-58.
- Musselman, K. N., S. A. Margulis, and N. P. Molotch (2013). "Estimation of solar direct beam transmittance of conifer canopies from airborne LiDAR." *Remote Sensing of Environment*, Vol. 136, No. 9, pp. 402-415.
- Natural Resources Canada (2012). *Canadian LiDAR Acquisition Guideline - Draft*. Mapping Information Branch, Ottawa, Canada.
- Natural Resources Canada (2013). *Canadian Airborne LiDAR Acquisition Guideline - draft*. Mapping Information Branch, Ottawa, Canada.
- Natural Resources Canada (2014). *Canadian Airborne LiDAR Acquisition Guideline*. Mapping Information Branch, Ottawa, Canada.
- Núñez, J., X. Otazu, O. Fors, A. Prades, V. Palà, and R. Arbiol (1999). "Multiresolution-based image fusion with additive wavelet decomposition." *IEEE Transactions on Geoscience and Remote Sensing*, Vol. 37, No. 3, pp. 1204-1211.
- Oh, J., C. Lee, Y. Eo, and J. Bethel (2012). "Automated georegistration of high-resolution satellite imagery using a RPC model with airborne lidar information." *Photogrammetric Engineering & Remote Sensing*, Vol. 78, No. 10, pp. 1045-1056.
- Optech. (n.d.). "ALTM Lidar-Camera Integration." [On-line] Accessed 30 May 2013. Retrieved from ALTM Airborne Laser Terrain Mapper: [http://www.optech.ca/altm\\_dimac.htm](http://www.optech.ca/altm_dimac.htm)
- Papasaïka, H., and E. Baltsavias (2009). "Fusion of lidar and photogrammetric generated digital elevation models." *Proceedings of the ISPRS Hannover Workshop 2009 High-Resolution Earth Imaging for Geospatial Information*.

- Parent, J. R., J. C. Volin, and D. L. Civco. (2015). "A fully-automated approach to land cover mapping with airborne LiDAR and high resolution multispectral imagery in a forested suburban landscape." *ISPRS Journal of Photogrammetry and Remote Sensing*, Vol. 104, pp. 18-29.
- Pegler, K. H. (2001). *An Examination of Alternative Compensation Methods for the Removal of the Ridging Effect from Digital Terrain Model Data Files*. M.Eng. report, Department of Geodesy and Geomatics Engineering Technical Report No. 209, University of New Brunswick, Fredericton, N.B., Canada. 173 pp.
- Petrie, G., and C. K. Toth (2008). "Introduction to laser ranging, profiling, and scanning." In *Topographic laser ranging and scanning: Principles and processing*, Eds. Shan, J., and C. K. Toth, CRC Press, Boca Raton, Florida, U.S.A., pp. 1-18.
- Podobnikar, T. (2005). "Production of integrated digital terrain model from multiple datasets of different quality." *International Journal of Geographical Information Science*, Vol. 19, No. 1, pp. 69-89.
- Podobnikar, T., Z. Stancic, and K. Oštir (2000). "Data integration for the DTM production." *Proceedings of the Workshop on International cooperation and technology transfer*. Ljubljana, Slovenia, 2-5 February, pp. 134-139.
- Polat, N., M. Uysal, and A. S. Toprak (2015). "An investigation of DEM generation process based on LiDAR data filtering, decimation, and interpolation methods for an urban area." *Measurement*, Vol. 75, pp. 50-56.
- QCoherent Software LLC. (n.d.). "Limitless LIDAR." [On-line] Accessed 1 May 2014. Retrieved from <http://www.qcoherent.com>
- QCoherent. (n.d.). "LP360 for ArcGIS™ - Standard Edition." [On-line] Accessed 30 May 2013. Retrieved from <http://www.qcoherent.com/products/standard.html>
- rapidlasso GmbH. (n.d.). "License agreement." [On-line] Accessed 1 May 2014. Retrieved from <http://www.cs.unc.edu/~isenburg/lastools/LICENSE.txt>, <http://rapidlasso.com>
- Reiss, P. (2002). "Combination of LIDAR, digital photogrammetry and terrestrial survey to generate high-quality DEMs." *International Archives of the Photogrammetry, Remote Sensing and Spatial Information Sciences*, Vol. XXXIV, Part 4, pp. 526-531.

- Riley, S. J., S. D. DeGloria, and R. Elliot (1999). "A terrain ruggedness index that quantifies topographic heterogeneity." *Intermountain Journal of Sciences*, Vol. 5, No. 1-4, pp. 23-27.
- Rottensteiner, F., and C. Briese (2002). "A new method for building extraction in urban areas from high-resolution LIDAR data." *International Archives of the Photogrammetry, Remote Sensing*, Vol. XXXIV, Part 3/A, pp. 295-301.
- Rottensteiner, F., J. Trinder, S. Clode, and K. Kubik (2004). "Fusing airborne laser scanner data and aerial imagery for the automatic extraction of buildings in densely built-up areas." *International Archives of the Photogrammetry, Remote Sensing and Spatial Information Sciences*, Vol. XXXV, Part B3, pp. 512-517.
- Saeedi, S., F. Samadzadegan, and N. El-Sheimy (2009). "Object extraction from LIDAR data using an artificial swarm bee colony clustering algorithm." *International Archives of the Photogrammetry, Remote Sensing and Spatial Information Sciences*, Vol. XXXVIII, Part 3/W4, pp. 133-138.
- Salah, M., J. Trinder, A. Shaker, M. Hamed, and A. Elsagheer (2009). "Aerial images and lidar data fusion for automatic feature extraction using the self-organizing map (SOM) classifier." *International Archives of the Photogrammetry, Remote Sensing and Spatial Information Sciences*, Vol. XXXVIII, Part 3/W8, pp. 317-322.
- Samadzadegan, F., M. Hahn, and B. Bigdeli (2009a). "Automatic road extraction from LIDAR data based on classifier fusion." *Proceedings of the Urban Remote Sensing Joint Event*. IEEE, Shanghai, China, 20-22 May, 6 pp.
- Samadzadegan, F., T. Schenk, and F. T. Mahmoudi (2009b). "A multi-agent method for automatic building recognition based on the fusion of lidar range and intensity data." *Proceedings of the Urban Remote Sensing Joint Event*. IEEE, Shanghai, China, 20-22 May, 6 pp.
- Schickler, W., and A. Thorpe (2001). "Surface estimation based on LIDAR." *Proceedings of the ASPRS Annual Conference*. St. Louis, Missouri, 23-27 April, pp. 1-11.
- Schindler, K., H. Papasaika-Hanusch, S. Schütz, and E. Baltsavias (2011). "Improving wide-area DEMs through data fusion-chances and limits." *Proceedings of the 53rd Photogrammetric Week*. Institute for

Photogrammetry, University of Stuttgart, Stuttgart, Germany, 5-9 September, pp. 3-14.

- Service New Brunswick (2002). "New Brunswick Control Monument Database Information." [On-line] Accessed 30 May 2013. Retrieved from <https://www.pxw1.snb.ca/snb7001/e/2000/2920e.asp>
- Service New Brunswick (2010). "Digital Topographic Data Base – 1998 (DTDB) - Information." [On-line] Accessed 30 May 2013. Retrieved from SNB Geographic Data & Maps: [http://www.snb.ca/gdam-igec/e/2900e\\_1c\\_i.asp](http://www.snb.ca/gdam-igec/e/2900e_1c_i.asp)
- Shan, J., and A. Sampath (2005). "Urban DEM generation from raw lidar data: A labeling algorithm and its performance." *Photogrammetric Engineering & Remote Sensing*, Vol. 71, No. 2, pp. 217-226.
- Sheng, Y. (2008). "Quantifying the size of a lidar footprint: A set of generalized equations." *IEEE Geoscience and Remote Sensing Letters*, Vol. 5, No. 3, pp. 419-422.
- Shepard, D. (1968). "A two-dimensional interpolation function for irregularly-spaced data." *Proceedings of the 1968 23rd ACM National Conference (ACM '68)*. Las Vegas, Nevada, 27-29 August, pp. 517-524. doi:<http://dx.doi.org/10.1145/800186.810616>
- Sithole, G. (2001). "Filtering of laser altimetry data using a slope adaptive filter." *International Archives of the Photogrammetry, Remote Sensing and Spatial Information Sciences*, Vol. XXXIV, Part 3/W4, pp. 203-210.
- Sithole, G., and G. Vosselman. (2003). "Automatic structure detection in a point-cloud of an urban landscape." *Proceedings of the 2nd GRSS/ISPRS Joint Workshop on Remote Sensing and Data Fusion over Urban Areas*. IEEE and ISPRS, Berlin, Germany, 22-23 May, pp. 67-71.
- Sithole, G., and G. Vosselman. (2004). "Experimental comparison of filter algorithms for bare-Earth extraction from airborne laser scanning point clouds." *ISPRS Journal of Photogrammetry & Remote Sensing*, Vol. 59, pp. 85-101.
- Song, J., S. Han, K. Yu, and Y. Kim (2002). "Assessing the possibility of land-cover classification using LiDAR intensity data." *International Archives of the Photogrammetry, Remote Sensing and Spatial Information Sciences*, Vol. XXIV, Part 3/B, pp. 259-262.

- Southee, F. M., P. M. Treltz, and N. A. Scott (2012). "Application lidar terrain surfaces for soil moisture modeling." *Photogrammetric Engineering & Remote Sensing*, Vol. 78, No. 12, pp. 1241-1251.
- Stoker, J. (2009). "Volumetric visualization of multiple-return lidar data: Using voxels." *Photogrammetric Engineering & Remote Sensing*, Vol. 75, No. 2, pp. 109-112.
- Stoker, J. (2010). "Making lidar more photogenic: Creating band combinations from lidar information." *Photogrammetric Engineering & Remote Sensing*, Vol. 76, No. 3, pp. 216-220.
- Syed, S., P. Dare, and S. Jones (2005). "Automatic classification of land cover features with high resolution imagery and lidar data: An object-oriented approach." *Proceedings of the Spatial Sciences Institute Biennial Conference*. Spatial Sciences Institute, Melbourne, Australia, 14-16 September, pp. 512-522.
- Terrasolid Oy. (n.d.). "Terrasolid software: Software for processing LiDAR point clouds and images." [On-line] Accessed 1 May 2014. Retrieved from <http://www.terrasolid.com/home.php>
- US Geological Survey (2010). *Lidar Guidelines and Base Specification, Version 13 (Draft)*. National Geospatial Program. 18 pp.
- US National Research Council (2007). *Elevation Data for Floodplain Mapping*. Committee on Floodplain Mapping Technologies, The National Academies Press, Washington, D.C., U.S.A.
- Voss, M. (2008). "Seasonal effect on tree species classification in an urban environment using hyperspectral data, LiDAR, and an object-oriented approach." *Sensors*, Vol. 8, No. 5, pp. 3020-3036.
- Vu, T. T., F. Yamazaki, and M. Matsuoka (2009). "Multi-scale solution for building extraction from LiDAR and image data." *International Journal of Applied Earth Observations and Geoinformation*, Vol. 11, No. 4, pp. 281-289.
- Wang, C., and N. F. Glenn (2009). "Integrating LiDAR intensity and elevation data for terrain characterization in a forested area." *IEEE Geoscience and Remote Sensing Letters*, Vol. 6, No. 3, pp. 463-466.
- Wang, C., M. Menenti, M. Stoll, A. Feola, E. Belluco, and M. Marani (2009). "Separation of ground and low vegetation signatures in LiDAR



- measurements of salt-marsh environments." *IEEE Transactions on Geoscience and Remote Sensing*, Vol. 47, No. 7, pp. 2014-2023.
- Warriner, T., and G. Mandlbürger (2005). "Generating a new high resolution DTM product from various data sources." *Proceedings of the 50th Photogrammetric Week*. Institute for Photogrammetry, University of Stuttgart, Stuttgart, Germany, 5-9 September, pp. 197-206.
- Webster, T. L., D. L. Forbes, S. Dickie, and R. Shreenan (2004). "Using topographic lidar to map flood risk from storm-surge events for Charlottetown, Prince Edward Island, Canada." *Canadian Journal of Remote Sensing*, Vol. 30, No. 1, pp. 64-76.
- Wehr, A., and U. Lohr (1999). "Airborne laser scanning -- an introduction and overview." *ISPRS Journal of Photogrammetry & Remote Sensing*, Vol. 54, No. 2-3, pp. 68-82.
- Wittner, E., T. Reitz, and C. McCabe (2013). "Creating, managing and utilizing a 3D Virtual City." *Presentation at the Esri International Developer Summit*. Palm Springs, California, U.S.A., 25-28 March.
- Wu, H., C. Lui, Y. Zhang, and W. Sun (2009). "Water feature extraction from aerial-image fused with airborne LIDAR data." *Proceedings of the Urban Remote Sensing Joint Event*. IEEE, Shanghai, China, 20-22 May, pp. 919-925.
- Yao, W., S. Hinz, and U. Stilla (2009). "Object extraction based on 3D-segmentation of LiDAR data by combining mean shift with normalized cuts: Two examples from urban areas." *Proceedings of the Urban Remote Sensing Joint Event*. IEEE, Shanghai, China, 20-22 May, pp. 1216-1221.
- Yoon, C., K. Kim, J. Shin, H. Lee, and C. Hwang (2006). "Hierarchical land-use classification using optical imagery and LiDAR data." *Proceedings of the IEEE International Geoscience and Remote Sensing Symposium 2006*. Denver, Colorado, U.S.A., 31 July - 4 August, pp. 2746-2749.
- Yoon, J., J. Shin, and K. Lee (2008). "Land cover characteristics of airborne LiDAR intensity data: A case study." *IEEE Geoscience and Remote Sensing Letters*, Vol. 5, No. 4, pp. 801-805.
- Yu, B., H. Liu, L. Zhang, and J. Wu (2009b). "An object-based two-stage method for a detailed classification of urban landscape components by integrating airborne LiDAR and color infrared image data: A case study of downtown

- Houston." *Proceedings of the Urban Remote Sensing Joint Event*. IEEE, Shanghai, China, 20-22 May, pp. 450-457.
- Yu, Z., C. Xu, J. Liu, O. C. Au, and X. Tang (2011). "Automatic object segmentation from large scale 3D urban point clouds through manifold embedded mode seeking." *Proceedings of the 19th ACM international conference on Multimedia*. ACM, Scottsdale, Arizona, U.S.A, 28 November - 1 December, pp. 1297-1300.
- Yuan, F., J. Zhang, L. Zhang, and J. Gao (2009). "Urban DEM generation from airborne lidar data." *Proceedings of the Urban Remote Sensing Joint Event*. IEEE, Shanghai, China, 20-22 May, pp. 1041-1045.
- Zhang, H., Y. Zhang, J. Liu, and S. Ji (2009). "Automatic Building Detection Using Airborne LIDAR Data." *Proceedings of the 2009 International Forum on Information Technology and .* IEEE, Chengdu, China, 15-17 May, pp. 668-671.
- Zhang, J. (2010). "Multi-source remote sensing data fusion: Status and trends." *International Journal of Image and Data Fusion*, Vol. 1, No. 1, pp. 5-24.
- Zhang, K., S. Chen, D. Whitman, M. Shyu, J. Yan, and C. Zhang (2003). "A progressive morphological filter for removing nonground measurements from airborne LIDAR data." *IEEE Transactions on Geoscience and Remote Sensing*, Vol. 41, No. 4, pp. 872-882.
- Zhou, M., B. Xia, G. Su, L. Tang, and C. Li (2009). "A classification method for building detection based on LiDAR point clouds." *Proceedings of the Urban Remote Sensing Joint Event*. IEEE, Shanghai, China, 20-22 May, pp. 828-831.
- Zhou, W. (2013). "An object-based approach for urban land cover classification: Integrating LiDAR height and intensity data." *IEEE Geoscience and Remote Sensing Letters*, Vol. 10, No. 4, pp. 928-931.
- Zinger, S., M. Nikolova, M. Roux, and H. Maître (2002). "3D resampling for airborne laser data of urban areas." *International Archives of the Photogrammetry, Remote Sensing and Spatial Information Sciences*, Vol. XXXIV, Part 3/A, pp. 418-423.

## **APPENDIX A**

### **PSEUDOCODE FOR GPI AND MSPC IMPLEMENTATION**

## A.1. GROUND POINT IDENTIFICATION PROCESS

This section contains key code developed to implement the GPI process described in Chapter 4. Common functions, such as opening files, allocating memory, and reading data from files, have been omitted due to space considerations and the code has been rendered as pseudocode for readability.

Full code files can be found at <https://bitbucket.org/kamolins/thesiscode>.

### A.1.1. Pixel Connectedness

Starts at lowest value pixels, as specified by a set of ground seed pixels, and applies an angle threshold to add connected pixels to the ground surface.

Input

- *in\_grid*: initial potential ground surface, generated from lowest point in each cell (elevation raster)
- *seed\_grid*: set of ground seed pixels (raster where seed pixel cells have value 1 and all other cells have value 0);
- *angle*: slope threshold (scalar, in degrees)

Output *out\_grid*: ground surface (elevation raster)

Intermediate data *ref\_grid*: used for holding and transferring values

```
// Step 1: Initialize intermediate grid using seed
pixel raster
for each (row i, col j)
  if (seed_grid[i][j] == 1)
    ref_grid[i][j] = 1
  else
    ref_grid[i][j] = no data

// Step 2: Transfer elevations for seed pixels to
```

```

    output surface
    for each (row i, col j)
        if (ref_grid[i][j] == 1)
            out_grid[i][j] = in_grid[i][j]
        else
            out_grid[i][j] = no data

// Step 3: Iterative process. Check all neighbouring
// (8-connected) pixels to every seed pixel for
// connected ground. Mark connected pixels and
// transfer elevations to output surface. Repeat
// until no new pixels are marked.
mark = 1
while (mark > 0)
    mark = 0 // reset counter
    for each (row i, col j)
        if (ref_grid[i][j] == 1)
            for each (-1 <= k <=1, -1 <= l <= 1)
                xy_dist = cellsize *  $\sqrt{k^2 + l^2}$ 
                z_dist = in_grid[i+k][j+l] - in_grid[i][j]

                if (z_dist/xy_dist < angle)
                    ref_grid[i+k][j+l] = 1
                    out_grid[i+k][j+l] = in_grid[i+k][j+l]
                    mark++ // increment counter

// clear cells marked in previous iteration
ref_grid[i][j] = 0

```

### A.1.2. Point Neighbourhood

Starts with three ground seed pixels selected by percentile from start of point file sorted by elevation and assigns probability of other points being ground based on Euclidean distance.

#### Input

- *in\_pts*: point cloud sorted into voxel bins (LAS file)
- *per<sub>1</sub>*, *per<sub>2</sub>*, *per<sub>3</sub>*: percentiles from start of point file at which to locate ground seed points (scalars)

- *eq*: type of equation (See Section 4.2.2)

Output *out\_pts*: point cloud with added probabilities (LAS file)

Intermediate data *seed\_pts*: used for holding probable ground points

```
// Step 1: Locate ground seed points
for i in (1,2,3)
    fseek(in_pts, peri * size(point) + size(header))
    pi = fread(point)
    while (pi not last return)
        pi = fread(point)
        pi.user_data = 100
        fwrite(seed_pts, pi)

refX = p1.x
refY = p1.y
refZ = p1.z
count = 3

// Step 2: First iteration, using p1 as reference to
// calculate initial probability for each last
// return point in file. Keep any points with
// probabilities greater than 50% as new seed
// points. Mark non-last return points as such so
// can be skipped later.
for each (p in in_pts)
    if (p is last return)
        delta_d = √((p.x - refX)2 + (p.y - refY)2)
        delta_z = | p.z - refZ |

        if(eq is Eq. 4.2)
            prob = 100 - 25 * (delta_z + delta_d/2)2

        if(eq is Eq. 4.3)
            if((delta_d/3 + delta_z) <= 2)
                prob = (5.0*(delta_z + delta_d/3) - 10.0)2
            else
                prob = 0 // tamp out rising quad

        if(eq is Eq. 4.1)
            prob = 100 - 50 * (delta_z + delta_d/2)

        p.user_data = prob

    if(prob >= 50 ){
```

```

        fwrite(seed_pts,p)
        count++

    else
        p.user_data = 'm'; // mark it as multi

// Step 3: Iterative process. Test points in 2 m
// spherical neighbourhood of remaining seed points,
// including those added in first iteration. Keep
// any points with probabilities greater than 50% as
// new seed points.
i = 2
while(i < count){
    refX = seed_pts[i].x
    refY = seed_pts[i].y
    refZ = seed_pts[i].z

    for each (p in in_pts)
        if (p within 2 m neighbourhood of seed_pts[i]
and p.point_data != 'm')
            delta_d =  $\sqrt{(p.x - refX)^2 + (p.y - refY)^2}$ 
            delta_z = | p.z - refZ |

            if(eq is Eq. 4.2)
                prob = 100 - 25 * (delta_z + delta_d/2)2

            if(eq is Eq. 4.3)
                if((delta_d/3 + delta_z )<= 2)
                    prob = (5.0*(delta_z + delta_d/3)-10.0)2
                else
                    prob = 0

            if(eq is Eq. 4.1)
                prob = 100 - 50 * (delta_z + delta_d/2)

            if(prob > p.user_data)
                p.user_data = prob

            if(prob >= 50)
                // (additional logic is used in actual code
to avoid duplicate seed points)
                fwrite(seed_pts,p)
                count++

for each (p in in_pts)
    fwrite(p, out_pts)

```

### A.1.3. Wavelet Detail Mask

Part 1: Applies a 5x5 B3 cubic spline wavelet filter to interpolated elevation raster to generate an approximation image and a detail image containing the information removed from the original image.

#### Input

- *in\_grid*: initial potential ground surface, generated from lowest point in each cell (elevation raster)
- *res*: dyadic power setting the effective resolution of the approximation with respect to the resolution of the original (scalar)

#### Output

- *out\_grid\_A*: approximation of input surface (raster)
- *out\_grid\_D*: details removed from the input surface (raster)

Intermediate data *a\_sum*: accumulated sum as filter applied

```
filter[5][5] = {
    {1,4,6,4,1},
    {4,16,24,16,4},
    {6,24,36,24,6},
    {4,16,24,16,4},
    {1,4,6,4,1}
}
divisor = 256.0

// Apply filter
for each (row i, col j)
    for each (1 <= k <=5, 1 <= l <= 5)
        a_sum += in_grid[i+res*(k-2)][j+res*(l-2)]*filter[k][l]

    out_grid_A[i][j] = a_sum / divisor
    out_grid_D[i][j] = in_grid[i][j] -
    out_grid_A[i][j]
```



Part 2: Applies a mask created from the detail image to the original potential ground surface. Mask is based on detail values: where the detail value is greater than a set threshold, the potential ground surface will be masked.

Input

- *in\_grid*: initial potential ground surface, generated from lowest point in each cell (elevation raster)
- *mask\_grid*: either the wavelet detail image along with a threshold or the equivalent image generated, e.g., in another software package, where 1 represents a masked cell and 0 represents an unmasked cell.

Output *out\_grid*: ground surface (elevation raster)

```
for each (row i, col j)
  if (mask_grid[i][j] == 1)
    out_grid[i][j] = no_data
  else
    out_grid[i][j] = in_grid[i][j]
```

#### **A.1.4. Preliminary Ground**

Uses a reference ground surface, determined through other means (e.g., by applying the Pixel Connectedness method) to classify points as ground based on the height difference from the reference ground surface. The allowable height difference is 1 m, to account for potentially poor accuracy for the reference surface, and so this is a preliminary classification only.

The full code includes options to reset all point classification to 0; to check points previously classified as ground against the reference surface; to split points above the reference surface into two classes (0 to 0.3 m and 0.3 to 1 m above) and mark points between 1 and 2 m below the reference surface; and

allow points up to 10 m below the reference surface to pull it down.

Input

- *in\_pts*: point cloud (LAS file)
- *ref\_grid*: reference ground surface (elevation raster)

Output *out\_pts*: point cloud with ground classified (LAS file; ground is class 2)

Intermediate data *hag*: height above ground value

```
for each (p in in_pts)
  if (p is last return)
    hag = p.z - ref_grid[p.x, p.y]
    if (|hag| <= 1)
      p.class = 2
  fwrite(p, out_pts)
```

#### **A.1.5. Surface comparison technique**

Compares values from six surfaces to find likely ground surface values. For cells where three or more surfaces have data, the standard deviation of the values is calculated. If the standard deviation is less than 0.6, the ground surface value for the cell is calculated as the average of the input values.

Input *in\_grid[n]*, n from 1 to 6: ground surfaces to compare (raster). Output from point-based methods must be interpolated to grid at same resolution as other surfaces.

Output

- *count\_grid*: counts of how many input surfaces have data in each cell (raster)
- *sd\_grid*: standard deviation for input surface values (raster)

- *avg\_grid*: average of input surface values, output ground surface (elevation raster)

Intermediate data *sum\_grid*: sum of values from input surfaces

```
// Step 1: Count the number of input surfaces that
// have data in each cell
for each (row i, col j)
  for (n from 1 to 6)
    if(in_grid[n][i][j] != no data)
      count_grid[i][j]++
      sum_grid[i][j] += in_grid[n][i][j]

// Step 2: Calculate average and standard deviation
avg_grid[i][j] = sum_grid[i][j]/count_grid[i][j]
for (n from 1 to 6)
  sd_grid[i][j] += (in_grid[n][i][j] -
  avg_grid[i][j])2/count_grid[i][j]

// Step 3: Apply criteria
if (count_grid[i][j] < 3 or st_dev[i][j] >= 0.6)
  avg_grid[i][j] = no data
```

## **A.2. MULTI-STAGE POINT CLASSIFICATION**

This section contains key code developed to implement the MSPC process described in Chapter 5, plus water classification described in Chapter 6. Common functions, such as opening files, allocating memory, and reading data from files, have been omitted due to space considerations and the code has been rendered as pseudo-code for readability. Full code files can be found at <https://bitbucket.org/kamolins/thesiscode>.

Table A.1  
Classification Codes used in MSPC

Name	Code	Stage
Ground	2	0
Potential medium vegetation	14	1
Potential high vegetation	15	1
Potential building	16	1
Building	6	2
Non-building within building area (temporary, for stage 2 only)	13	2
Non-ground within area of uncertainty	0	3
Mixed neighbourhood (not classified)	1	4
High vegetation	5	4
Medium vegetation	4	4
Low vegetation	3	5
Road surface	11	5
Vehicle	10	6
Other object above road	13	6
Water	9	-

### **A.2.1. Preliminary Classification**

Uses a mask derived using TRI or MMM and a DEM derived from points classified as ground to classify points as potential medium or high vegetation and as potential building.

To create the TRI mask, first TRI is calculated for a 1 m resolution DSM. A threshold is then applied, to mark pixels with TRI values below 5 as flat and all other pixels as rough. The results are cleaned to remove isolated points, and finally a count is made for each pixel of how many surrounding pixels are flat.

The MMM mask is a combination of MRD, MaxMin, and mHAG. First, cells with MRD 0, MaxMin less than 1, and mHAG greater than one are marked. As

for the TRI mask, the results are cleaned to remove isolated points, then any marked cells not touching any unmarked cells are assigned a value of 2.

In both cases, the steps before cleaning and creating the final mask were performed using QGIS but could be implemented in code.

#### Input

- *in\_pts*: point cloud with ground classified (LAS file)
- *mask\_grid*: integer values derived from TRI or MMM. A value of 0 indicates a rough area. In the MMM mask, a value of 2 indicates a flat area above ground. In the TRI mask, the value is the number of eight connected pixels that are flat.
- *mode*: type of mask. Either TRI or MMM.
- *ground\_grid*: surface interpolated from ground points (raster)

Output *out\_pts*: point cloud with added preliminary classifications (LAS file; ground is class 2; preliminary classifications as below)

```
for each (p in in_pts)
  // skip if classified as ground or noise

  row = floor(p.y - in_pts.y_min)/cellsize
  col = floor(p.x - in_pts.x_min)/cellsize
  hag = p.z - ground_grid[row][col]

  if (mask_grid[row][col] == 0)
    if (0.3 <= hag < 2)
      p.class = 14 // temporary class for medium
vegetation
    if (hag >= 2)
      p.class = 15 // temporary class for high
vegetation
  else
    if (mode is MMM)
      if (hag > 2 and mask_grid[row][col] == 2)
```

```

        p.class = 16 // temporary class for
potential building
        if (mode is TRI)
            if (hag > 2 and mask_grid[row][col] > 6 and p
is last return)
                p.class = 16

fwrite(p, out_pts)

```

### A.2.2. Building Classification

Classifies points as building based on a mask infused with elevation values, derived from points identified as potential building points or from building footprints.

Input

- *in\_pts*: point cloud with ground, and potential medium and high vegetation and potential building classified (LAS file; ground is class 2; potential classes as in previous section)
- *mask\_grid*: building mask derived from points identified as potential building, with infused height. Cells that are not potentially buildings have a value of 0.
- *ground\_grid*: surface interpolated from ground points (raster)

Output *out\_pts*: point cloud with ground and buildings classified (LAS file). Points in temporary class can be target of refinement process, or simply reassigned to "not classified."

```

for each (p in in_pts)
    // skip if classified as ground or noise

    row = floor(p.y - in_pts.y_min)/cellsize
    col = floor(p.x - in_pts.x_min)/cellsize
    hag = p.z - ground_grid[row][col]

```

```

bdiff = p.z - mask_grid[row][col]

if (mask_grid[row][col] > 0)
  if (bdiff < 1 and hag > 2)
    p.class = 6

  else
    p.class = 13 // temporary class

fwrite(p, out_pts)

```

### A.2.3. Uncertainty

Part 1: Calculates the ratio of ground points, vegetation points and other points within a window.

Input

- *in\_pts*: point cloud with ground, building, and potential medium and high vegetation classified (LAS file)
- *w*: size of window, in pixels, for calculating the ratio
- *cellsize*: resolution, in m, for output grid

Output *out\_grid*: surface representing ground vegetation ratio (raster)

Intermediate data

- *g\_grid*: used for holding count of ground points in window
- *v\_grid*: used for holding count of vegetation points in window
- *t\_grid*: used for holding total count of ground in window
- *max\_t*: highest number of points within any window

```

// Step 1: Count the ground, vegetation, and total
// points in each window
for each (p in in_pts)
  // skip if classified as noise

  row = floor(p.y - in_pts.y_min)/cellsize

```

```

col = floor(p.x - in_pts.x_min)/cellsize

for each (-w <= k <= w, -w <= l <= w)
  if (p.class == 2)
    g_grid[row+k][col+l]++
  if (p.class == 14 or p.class == 15)
    v_grid[row+k][col+l]++

    t_grid[row+k][col+l]++
    if (t_grid[row+k][col+l] > max_t)
      max_t = t_grid[row+k][col+l]

// Step 2: Calculate ratios and output to 3-band
image
for each (row i, col j)
  out_grid[R][i][j] = g_grid[i][j]/t_grid[i][j]
  out_grid[G][i][j] = v_grid[i][j]/t_grid[i][j]
  out_grid[B][i][j] = t_grid[i][j]/max_t

```

**Part 2:** Resets to "unclassified" any non-ground points within an area marked as uncertain.

#### Input

- *in\_pts*: point cloud with ground, building, and potential medium and high vegetation classified (LAS file)
- *mask\_grid*: uncertainty mask derived from ground-vegetation ratio. Has a value of 1 where at least 10% of points in the window are ground points and at least 10% are vegetation points.

Output *out\_pts*: point cloud with uncertainty points removed from preliminary classes (LAS file)

```

for each (p in in_pts)
  // skip if classified as ground or noise

  row = floor(p.y - in_pts.y_min)/cellsize
  col = floor(p.x - in_pts.x_min)/cellsize

  if (mask_grid[row][col] == 1)

```



```

p.class = 0

fwrite(p, out_pts)

```

#### A.2.4. High Vegetation

Classifies points that were potential high vegetation as high vegetation based on proximity to other high vegetation points.

Input *in\_pts*: point cloud with ground, building, and potential medium and high vegetation classified (LAS file)

Output *out\_pts*: point cloud with high vegetation added (LAS file)

Intermediate data

- *neighbour*: count of points within spherical neighbourhood
- *sameC*: count of points of same class within spherical neighbourhood

```

// Step 1: Count points within 2m sphere, and points
// of the same class within the sphere
for each (p in in_pts)
  refX = p.x
  refY = p.y
  refZ = p.z
  refC = p.class
  neighbour = 0
  sameC = 0

  for each (q in in_pts and  $\sqrt{(q.x - refX)^2 + (q.y - refY)^2 + (q.z - refZ)^2} < 2$ )
    neighbour++
    if (refC == q.class)
      sameC++

  if (sameC/neighbour < 0.5)
    p.class = 1

// Step 2: Reassign potential high vegetation points
// within 1 m of other potential high vegetation
// points to high vegetation class

```

```

for each (p in in_pts)
  if (p.class == 14)
    p.class = 4

    for each (q in in_pts)
      if (p.class == q.class == 15)
        distance =  $\sqrt{(q.x - refX)^2 + (q.y - refY)^2 + (q.z - refZ)^2}$ 
        if (distance < 1)
          p.class = 5
        if (1 <= distance < 2)
          p.class = 4

fwrite(p, out_pts)

```

### A.2.5. Roads and Low Vegetation

Classifies ground points that are single returns as low vegetation if the intensity value is above the specified threshold, and as road surface if below threshold.

#### Input

- *in\_pts*: point cloud with ground, building, medium vegetation, and high vegetation classified (LAS file)
- *threshold*: intensity value selected to divide roads (low intensity) from vegetation (high intensity)

Output *out\_pts*: point cloud with ground split in to road, low vegetation, or other (LAS file)

```

for each (p in in_pts)
  if (p.class == 2 and p is single return)
    if (p.i > threshold)
      p.class = 3
    else
      p.class = 11

fwrite(p, out_pts)

```

### A.2.6. Object Above Roads

Classifies points within areas identified as roads/paved surfaces and are above ground as vehicles (0.3 m to 2 m above) or other object (more than 2 m above). The same cleaning is applied to the road mask as for TRI and MMM masks to remove isolated pixels.

Input

- *in\_pts*: point cloud with ground, building, medium vegetation, high vegetation, low vegetation and roads classified (LAS file)
- *mask\_grid*: paved surface mask derived from points classified as road or paved surface (raster). Cells that are part of a paved area have a value of 2.
- *ground\_grid*: surface interpolated from ground points (raster)

Output *out\_pts*: point cloud with vehicles and other objects above road added (LAS file)

```
for each (p in in_pts)
  row = floor(p.y - in_pts.y_min)/cellsize
  col = floor(p.x - in_pts.x_min)/cellsize
  hag = p.z - ground_grid[row][col]

  if (mask_grid[row][col] == 2)
    if (0.3 <= hag < 2)
      p.class = 10
    if (2 <= hag)
      p.class = 13

  fwrite(p, out_pts)
```

### A.2.7. Water Classification

Classifies points a water (class 9) using a mask derived from a water boundary

polygon and ground elevation.

Input

- *in\_pts*: point cloud (LAS file)
- *mask\_grid*: water area mask derived from water polygons (raster)
- *ground\_grid*: surface interpolated from ground points (raster)

Output *out\_pts*: point cloud with water points classified(LAS file)

```
for each (p in in_pts)
  row = floor(p.y - in_pts.y_min)/cellsize
  col = floor(p.x - in_pts.x_min)/cellsize
  hag = p.z - ground_grid[row][col]

  if (mask_grid[row][col] != 0)
    if (hag < 0.5)
      p.class = 9

fwrite(p, out_pts)
```

### **A.3. UTILITY SCRIPTS**

This section contains additional script tools that were used in the GPI and MSPC processes to prepare mask, ground surfaces, etc. Common functions, such as opening files, allocating memory, and reading data from files, have been omitted due to space considerations and code has been rendered as pseudo-code for readability. Full code files can be found at <https://bitbucket.org/kamolins/thesiscode>.

### A.3.1. Fill

Fills gaps in a raster so that surface appears continuous.

Input

- *in\_grid*: surface to be filled (raster)
- *mode*: method to calculate fill value. Can be average, minimum, or maximum.
- *num\_iter*: optional, maximum number of iterations

Output: *out\_grid*: filled surface (raster)

Intermediate data

- *empty*: count of cells that have no data
- *changed*: count of cells filled during the current iteration
- *iter*: current iteration number
- *mode\_value*: calculated value for empty cell

```
// Set loop conditions
num_iter = 200 or input limit
empty = rows * cols
changed = rows * cols

while (empty > 0 and (changed > rows*cols/100/100
|| iter < num_iter))
  empty = 0
  changed = 0

  for each (row i, col j)
    if (in_grid[i][j] == no data)
      neighbour = 0
      for (-1 <= k <= 1, -1 <= l <= 1)
        if (in_grid[i+k][j+l] != no data)
          neighbour++
          mode_value = ... (depends on mode)

      if (neighbour > 2)
        out_grid[i][j] = mode_value
```

```

        changed++
    else
        out_grid[i][j] = no data
        empty++

    else
        out_grid[i][j] = in_grid[i][j]

    iter++

```

### A.3.2. Grid

Interpolates LAS point data to a grid.

Input

- *in\_pts*: point cloud (LAS file)
- *cellsize*: grid resolution
- *mode*: method to calculate interpolation. Options: average elevation; average intensity; IDW (elevation); average elevation of points in one class only; average elevation of points in one flight line; local point density; multiple return density; minimum; maximum; count number points of specific classes in cell; user data.
- *search\_area*: criteria for selecting points to aggregate. See Section 3.1.1. and Figure 3.1.

Output: *out\_grid*: interpolated surface (raster)

Intermediate data: varies, depending on mode

```

for each (p in in_pts)
    // skip if doesn't match mode criteria, e.g.,
    // specified class, return number

    row = floor(p.y - in_pts.y_min)/cellsize
    col = floor(p.x - in_pts.x_min)/cellsize

```

```

count[row][col]++

if average elevation mode
    temp[row][col] += p.z

if average intensity mode
    temp[row][col] += p.i

if IDW mode
    distance =  $\sqrt{(x_{col} - p.x)^2 + (y_{row} - p.y)^2}$ 
    temp[row][col] += p.z/distancep

if minimum mode
    if (p.z < temp[row][col]) temp[row][col] = p.z

if maximum mode
    if (p.z > temp[row][col]) temp[row][col] = p.z

for each (row i, col j)
    if average mode
        out_grid[i][j] = temp[i][j]/count[i][j]

    if LPD or MRD mode
        out_grid[i][j] = count[i][j]/cellsize/cellsize

    for all other modes
        out_grid[i][j] = temp[i][j]

```

### A.3.3. Clean

Removes salt and pepper noise from masks and images.

Input

- *in\_grid*: image to be cleaned (raster).
- *mode*: cleaning process: regular (0, 2, optional 1) or count (0-8)
- *threshold*: if count mode, threshold for counting a connected pixel

Output *out\_grid*: cleaned image (raster)

Intermediate data *count*

```

for each (row i, col j)

```

```
if (regular mode)
  for each (-1 <= k <= 1, -1 <= l <= 1)
    if (input_grid[i+k][j+l] >= 1)
      count++

  if (count >= 6)
    out_grid[i][j] = 2
  if (count <= 2)
    out_grid[i][j] = 0

  if (2 < count < 6 and want marked)
    out_grid[i][j] = 1

if (count mode)
  for each (-1 <= k <= 1, -1 <= l <= 1)
    if (input_grid[i+k][j+l] >= threshold)
      count++

out_grid[i][j] = count
```



**APPENDIX B**

**ADDITIONAL IMAGES**

## B.1. MEASURE ILLUSTRATIONS

This section contains examples of the measures described in Section 3.1.

### B.1.1. Height Measures

Figure B.1 illustrates the process of obtaining a HAG image. A HAG value can also be calculated for individual points. For mHAG, both the DSM and the DEM are derived from the minimum values in each cell.

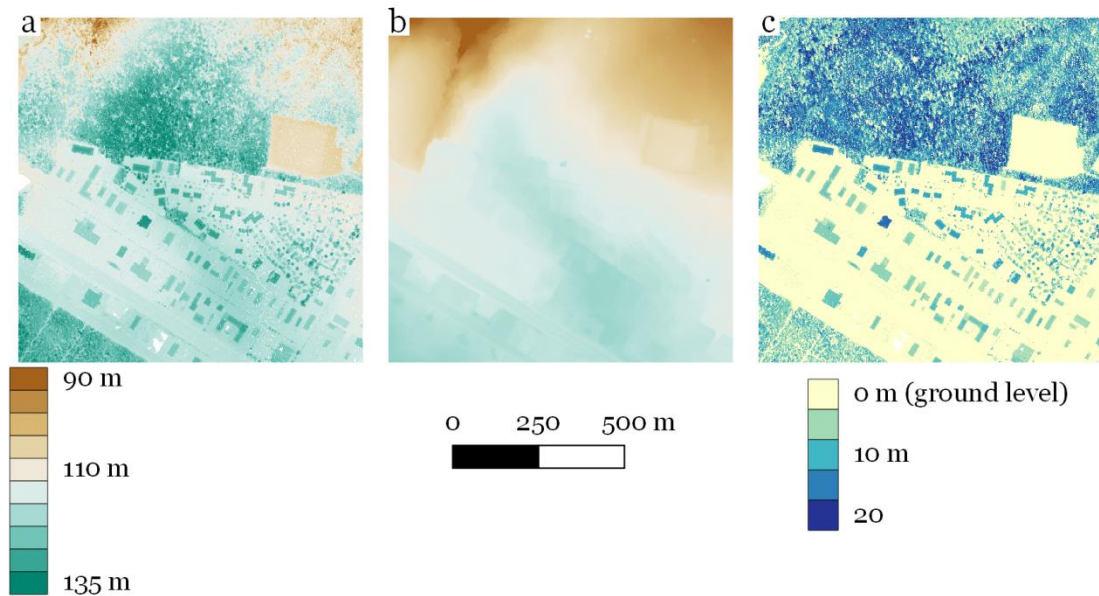


Figure B.1

Sample height above ground surface. a) DSM b) DEM c) Difference between DSM and DEM.

Figure B.2 illustrates the MaxMin measure. It is very similar to HAG, but uses actual minimum values for the lower surface rather than a derived DEM. Figure B.3 is of the terrain ruggedness index. The raster resolution is 1 m and the TRI values in the range of 0 to 20. Figures B.3b and B.3c show the effect of choosing different values as the threshold for roughness: 1.0 and 1.5, respectively.

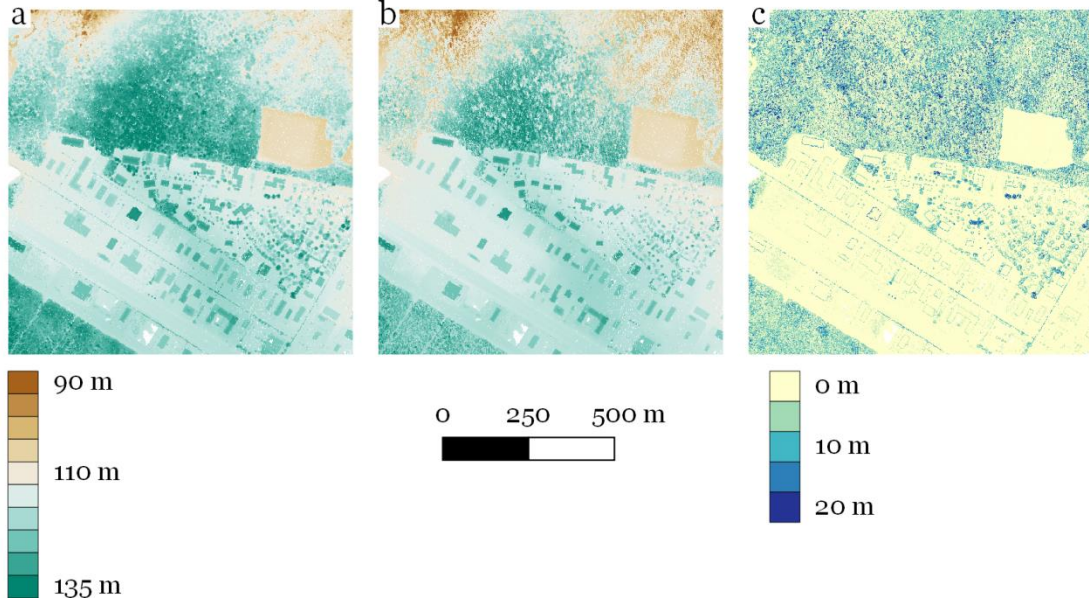


Figure B.2

Sample maximum minus minimum surface. a) Maximum values b) minimum values c) Difference between maximum and minimum.

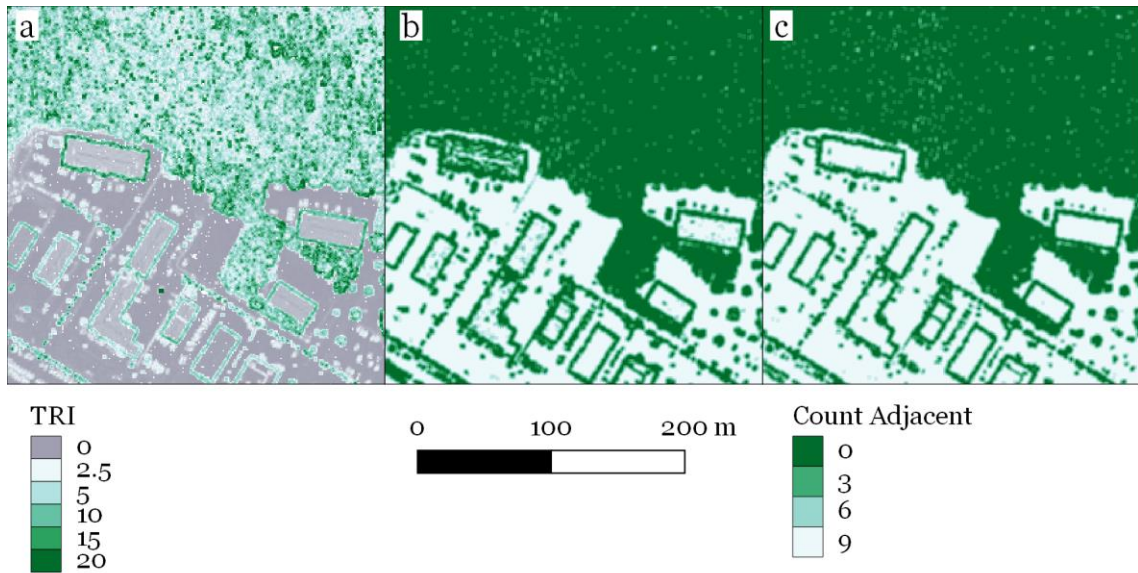


Figure B.3

a) Sample terrain ruggedness index and two masks from TRI: count of adjacent pixels with TRI less than b) 1.0 and c) 1.5.

### B.1.2. Non-Height Measures

Figures B.4 and B.5 illustrate local point density and slope, and are also included to further illustrate water point classification example in Section 6.4. Most cells appear to have a local point density of at least 5 pts/m<sup>2</sup> and the terrain primarily has slopes less than 15 ° except along the river's edge.

Figure B.6 illustrates multiple return density, in which only the non-single, non-first returns are counted.

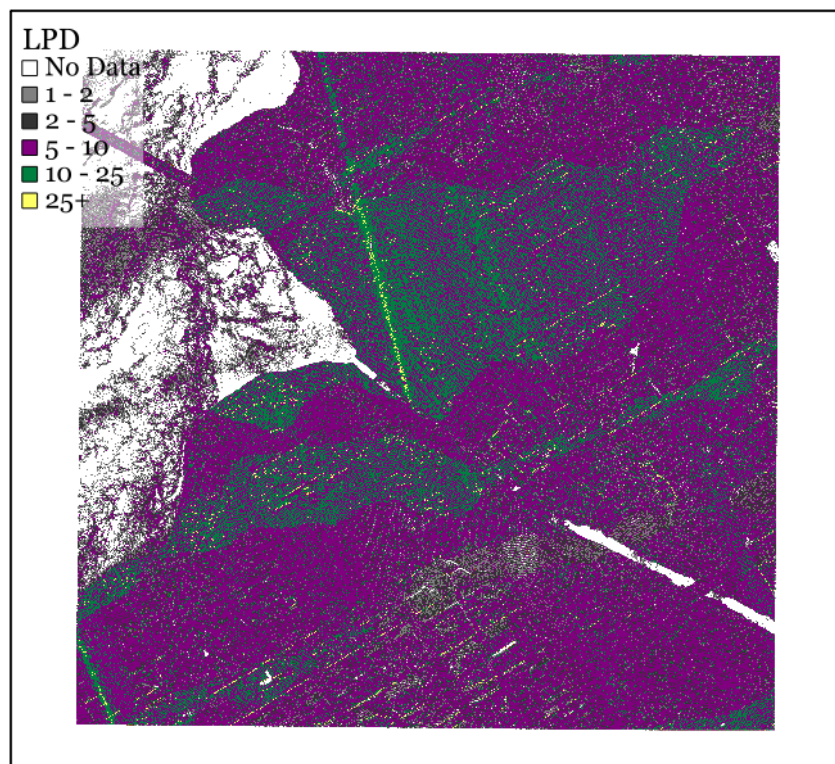


Figure B.4

Sample local point density image from Ottawa data.

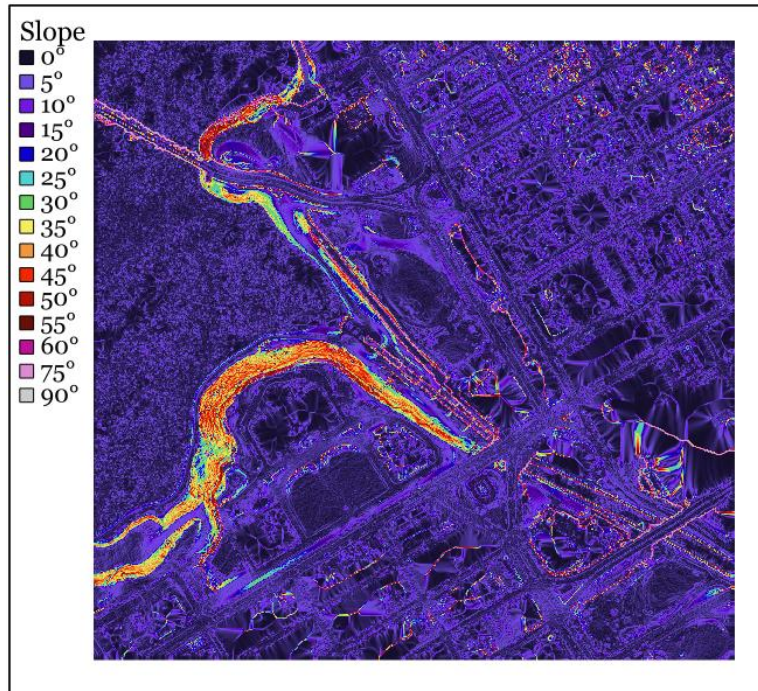


Figure B.5  
Sample terrain slope representation for Ottawa data.

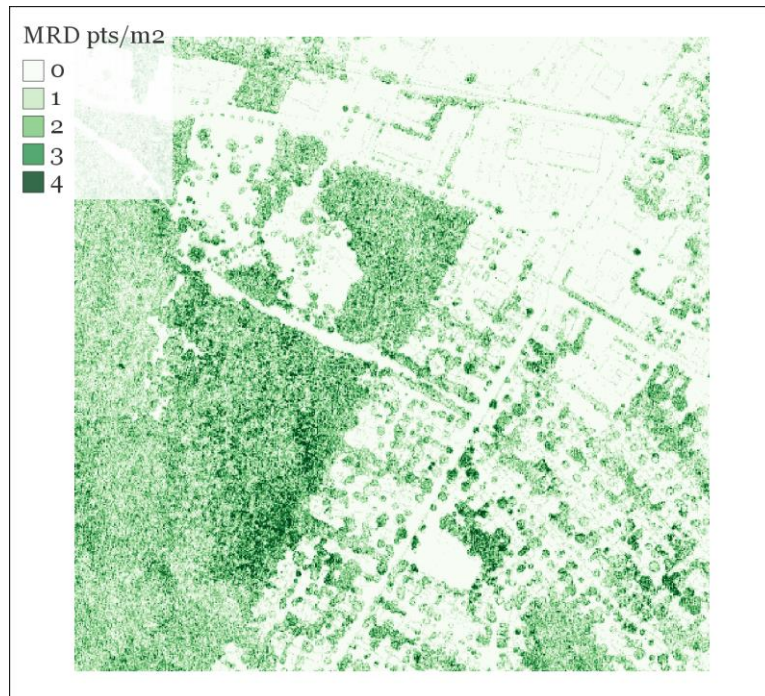


Figure B.6  
Sample multiple return density.

Figure B.7 is an example of an intensity image. The upper portion of the image includes the St. John River. For the most part, no returns were generated from the water but the points that were generated have intensity values through almost the full range of values recorded for the area.



Figure B.7  
Sample intensity image.

Figure B.8 is an example of a land cover map. Only ground, building and vegetation points have been classified, and not points at the boundaries between feature types.



Figure B.8

Example of a land cover map derived from LiDAR data showing ground, buildings, and high vegetation.

## B.2. GPI OUTPUT SAMPLES

This section contains sample output from the GPI process. Figure B.9 shows the set of ground detection results detailed in Section 4.3 as inputs to the surface comparison technique for testing: a) Pixel Connectedness using a  $10^\circ$  threshold and b) a  $15^\circ$  threshold; c) Point Neighbourhood using the negative quadratic equation and d) the linear equation; e) Preliminary Ground Points, filled; and f) Wavelet Detail Mask using a threshold of  $\pm 0.15$ .

Figure B.10 shows the two measures calculated during the surface comparison technique output and the final output. In this implementation, the wavelet detail mask was allowed to override the count criterion (Figure B.10a) since the threshold used for the mask left a sparse surface and any parts of that surface that are not part of the ground will be counteracted by the standard deviation criteria (Figure B.10b) with the inclusion of a filled surface.

Figure B.11 shows the raster products of two iterations of the ground point classification and refinement stage. The initial input surface, Figure B.11a, is the output from the comparison technique and has a 5 m resolution. Figure B.11b is the same surface but with gaps filled. Figures B.11c and B.11d are the surface/filled surface pair resulting from classifying points as ground based on Figure B.11b. Because the surface after is being interpolated from points and not based on a raster, the resolution could be increased to 2 m. Similarly, Figures B.11e and B.11f (output of second iteration) are the surface/filled surface pair resulting from classifying ground points based on Figure B.11d.



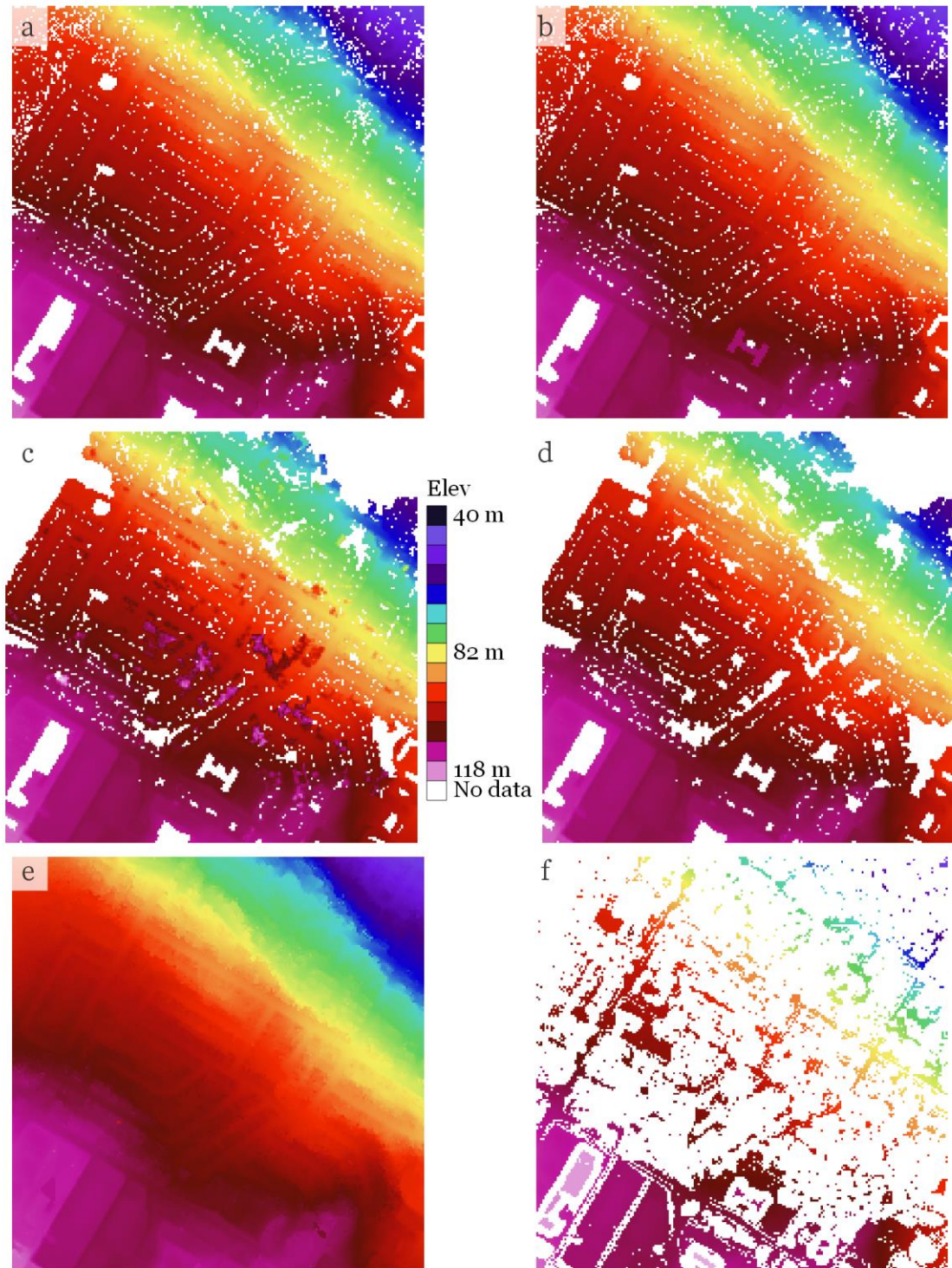


Figure B.9

Results from ground detection techniques: a) Pixel Connectedness,  $10^\circ$ ; b) Pixel Connectedness,  $15^\circ$ ; c) Point Neighbourhood, negative quadratic equation; d) Point Neighbourhood, linear equation; e) Preliminary Ground Points, filled; e) Wavelet Detail Mask, threshold  $\pm 0.15$ .

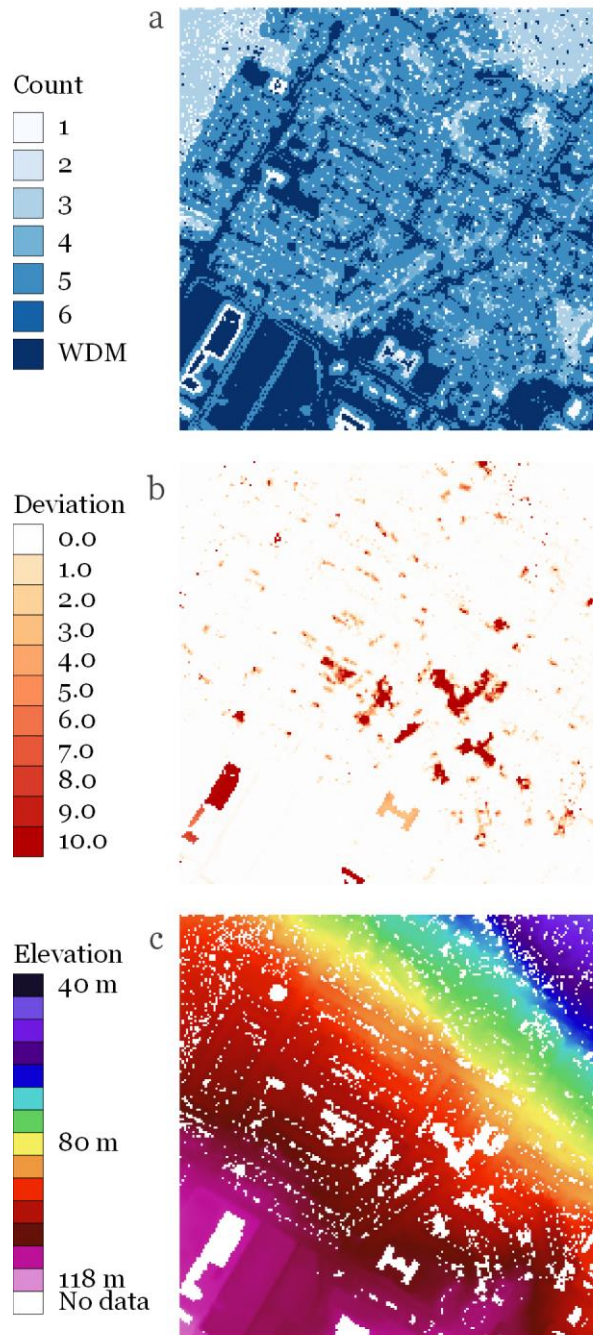


Figure B.10

Results from an application of the surface comparison technique using the surfaces in Figure B.9. a) Count criterion; b) standard deviation criterion; and c) output surface, the average of input surfaces where criteria are met.

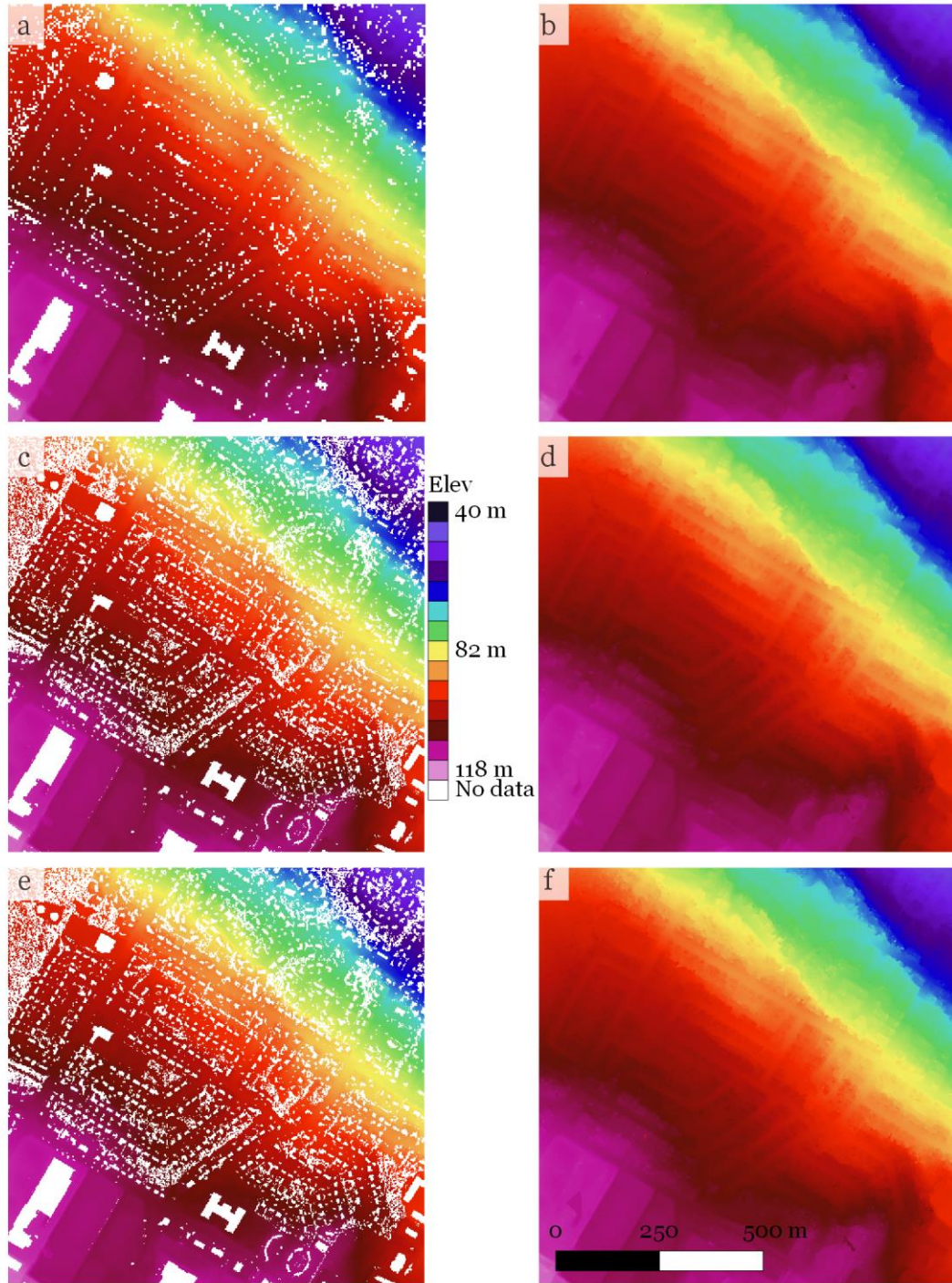


Figure B.11

Raster products from two iterations of the ground point classification and refinement process. a) Initial input, 5 m resolution; b) filled input; c) interpolation of ground points classified in first iteration, 2 m resolution; d) filled interpolation, input to second iteration; e) interpolation of points classified in second iteration; and f) filled surface.

**APPENDIX C**  
**INTEGRATION ASSESSMENTS**

## C.1. RASTER-TO-RASTER

Figure C.1 is an example of a raster-to-raster comparison between interpolations of filtered data set from SNB DTDB98 and the 2011 LiDAR data in the Odell Park sample area. Figure C.2 shows an enlarged area from the upper-left corner of C.1. There do not seem to be any systematic biases but there are three "problem types," meaning large differences between surfaces in the comparison:

1. Connected areas where the LiDAR surface is above the SNB surface (smooth blue areas).
2. Disjoint areas where the LiDAR surface is above the SNB surface (rough blue areas).
3. Disjoining areas where the LiDAR surface is below the SNB surface (rough red areas).

The likely explanation for Type 1 is that between the time the SNB points were collected and the LiDAR points were generated, the terrain was filled and/or levelled and (in some cases) a building constructed. For Type 2, there are no direct comparisons between the LiDAR points and the SNB points. The data characteristics suggest that it is the SNB interpolation that is in error. For Type 3, clusters of LiDAR points indicate a lower surface, suggesting the laser was able to penetrate through to the bottom of a narrow ravine which is not captured in the SNB data.

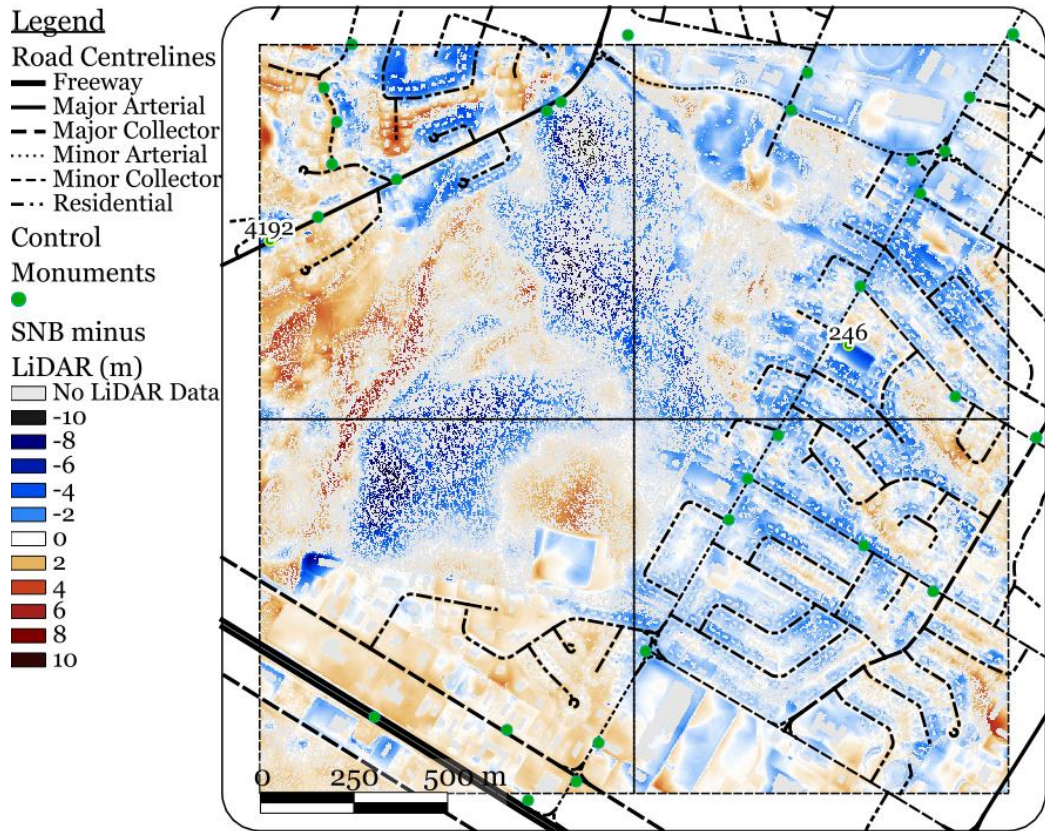


Figure C.1

Result of subtracting LiDAR elevations from SNB elevations. Orange/red means SNB values are higher; blue means LiDAR values are higher.

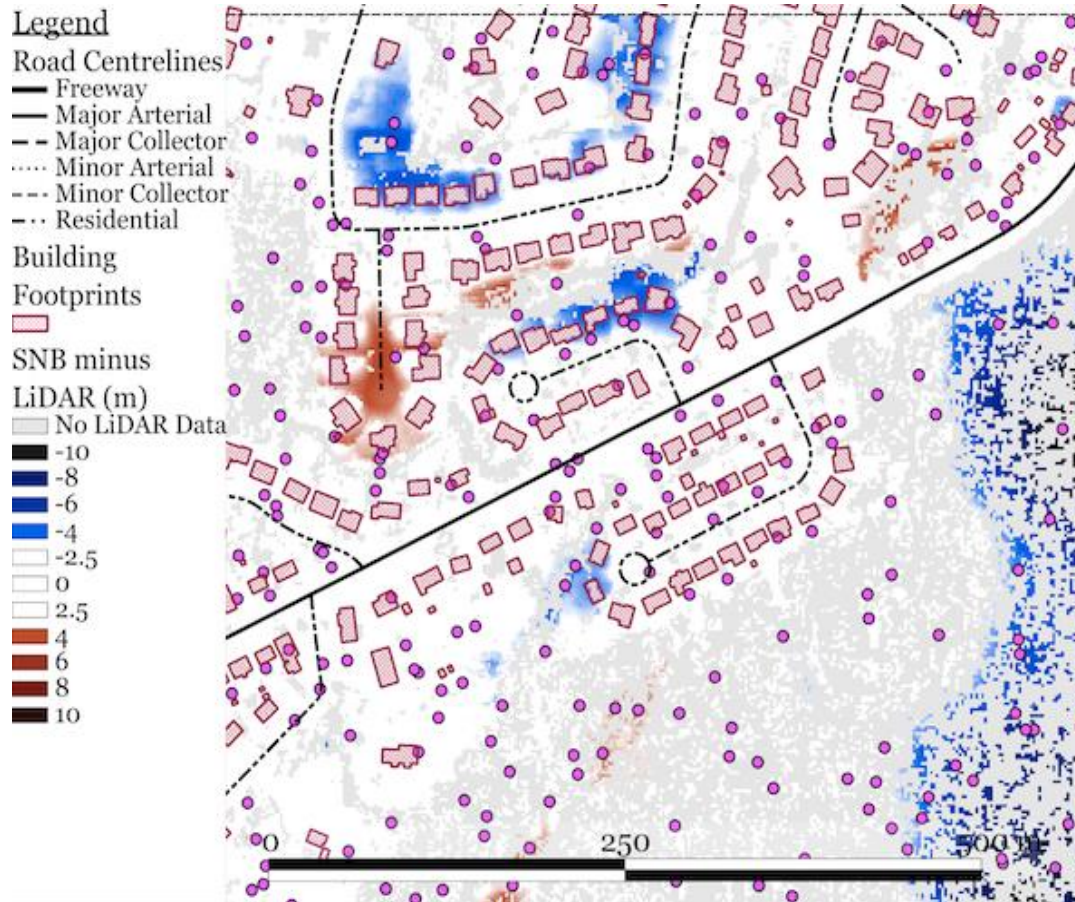


Figure C.2

Close-up of from Figure C.1, with building footprints and SNB points added.

## **C.2. RASTER-TO-POINT**

A software tool was used to determine the elevations of each interpolated surface (LiDAR, SNB, and CoF) at 27 control monument locations within the Odell Park case study area. The errors between the control and the interpolations were then calculated by subtracting the surface elevations from the control elevations. Table C.1 contains the calculated differences. Differences greater than 0.3 are highlighted.

The error for the LiDAR data is greater than 0.3 m for only two monuments and one of these, Monument 7027, was destroyed before the LiDAR data were collected. When this monument is removed from consideration, the RMSE for the LiDAR data is 0.15 m. This suggests that the LiDAR data is accurate with respect to control, however accuracy may be lower in other areas and particularly on sloped terrain and under dense vegetation.



Table C.1  
 Summary of differences for surface elevation subtracted from monument elevation. \* indicates no LiDAR data in corresponding cell, ° indicates a destroyed monument.

Monument	LiDAR (m)	SNBf (m)	CoF (m)
6294	-0.313	-1.768	-0.977
4192	-0.283	2.652	0.002
4310	-0.232	0.754	-0.240
7028	-0.215	1.128	-0.037
6295	-0.166	-1.241	-0.884
7131*	-0.157	1.050	-0.524
4178	-0.135	0.183	0.916
7128	-0.133	1.392	0.052
6296	-0.111	-1.634	-0.434
23727	-0.103	0.416	-0.621
7026	-0.096	0.012	-0.312
7126	-0.078	-0.710	-0.535
4305	-0.066	0.804	-0.103
4308	-0.059	1.025	-0.320
4311	-0.033	-0.183	0.391
23726	-0.026	-0.525	-0.335
7133	-0.022	0.660	-0.710
7130	-0.021	-0.374	-0.441
7127	0.018	0.763	-0.294
4309	0.049	0.065	0.023
6293	0.078	-0.353	-0.434
23744	0.086	-1.018	-0.161
4307	0.156	0.631	0.1914
246	0.2029	4.2705	1.7376
23743	0.242	-0.540	-0.108
4300*	0.244	1.883	0.3124
7027°	0.7195	1.5599	0.1027
Mean	-0.017	0.404	-0.139
RMSE	0.204	1.288	0.541
RMSE°	0.147	1.292	0.549

### C.3. POINT-TO-POINT

As a final assessment of the LiDAR accuracy, a point-to-point comparison was conducted around each of the control monuments in the Odell Park study area. Figure C.3 and Table C.2 show the assessment around the destroyed monument, Monument 7027. Figure C.4 and Table C.3 show the assessment around Monument 7127, which is on sloped terrain. The first three columns in each table give the coordinates of the LiDAR point. The next column gives the planimetric distance ( $d$ ) to the control monument, in  $10^{-3}$  m. Points within 1 m of the control monument are indicated with bold font and points within 0.5 m of the control monument also have a green cell background. The fifth column gives the height difference ( $\Delta z$ ), in m. Points within 0.3 m of the control monument elevation are indicated with bold font and points within 0.15 m of the control monument elevation also have a green cell background. The final column indicates whether or not the LiDAR point is a ground point.

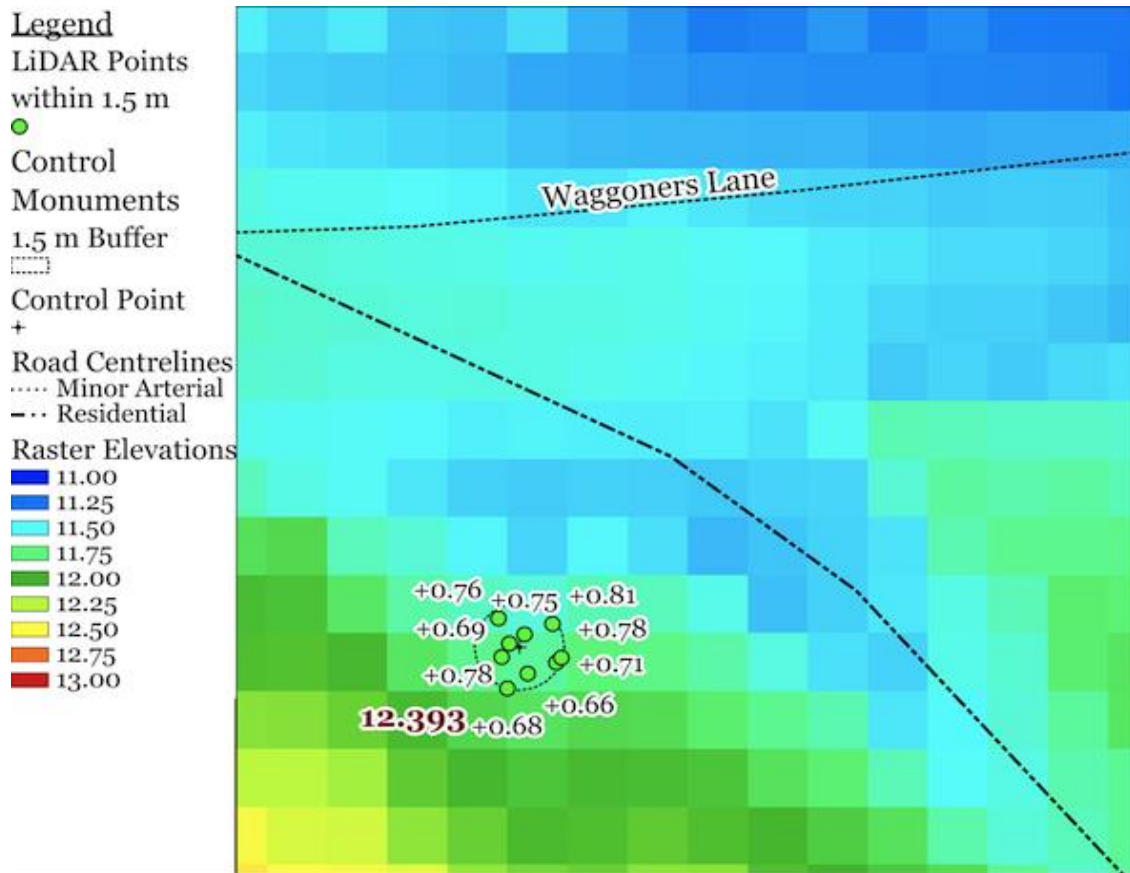


Figure C.3

LiDAR points within 1.5 m of Monument 7027 (destroyed) and their errors.

Table C.2

LiDAR points around Monument 7027

X (m)	Y (m)	Z (m)	d (10 <sup>-3</sup> m)	Δz (m)	ground point
2487741.68	7439691.61	11.735	<b>9625</b>	0.658	1
2487740.99	7439691.10	11.714	14934	0.679	1
2487740.81	7439692.19	11.705	<b>6831</b>	0.688	1
2487742.62	7439692.01	11.686	13278	0.707	1
2487741.56	7439692.97	11.645	<b>4578</b>	0.748	1
2487740.69	7439693.51	11.631	12093	0.762	1
2487742.80	7439692.17	11.617	14405	0.776	1
2487741.05	7439692.66	11.612	<b>3724</b>	0.781	1
2487742.50	7439693.33	11.581	13535	0.812	1

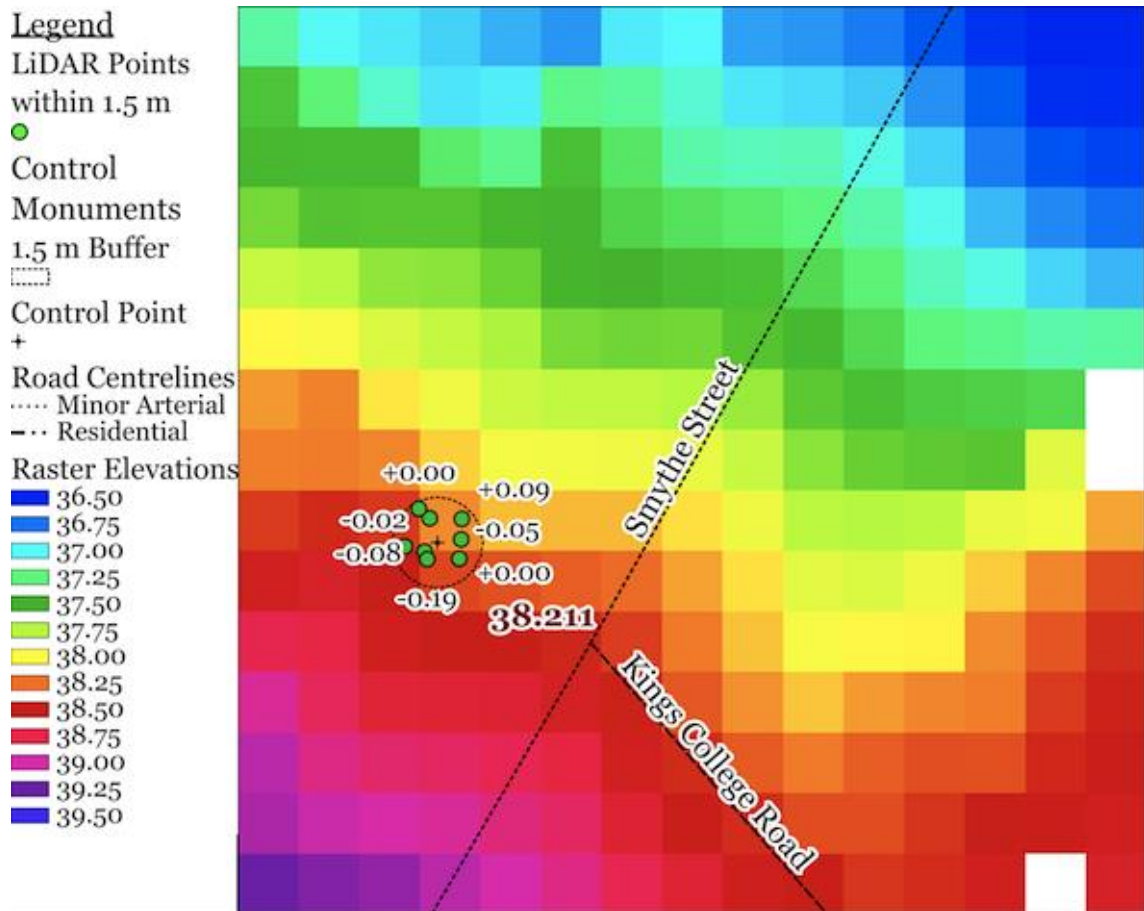


Figure C.4  
LiDAR points within 1.5 m of Monument 7127 and their errors.

Table C.3  
LiDAR points around Monument 7127

X (m)	Y (m)	Z (m)	d (10 <sup>-3</sup> m)	$\Delta z$ (m)	ground point
2487600.49	7439357.16	38.413	11040	<b>-0.202</b>	1
2487601.25	7439356.73	38.403	<b>6358</b>	<b>-0.192</b>	1
2487601.16	7439356.97	38.292	<b>5249</b>	<b>-0.081</b>	1
2487602.30	7439356.74	38.257	<b>8885</b>	<b>-0.046</b>	1
2487601.33	7439358.08	38.229	<b>8506</b>	<b>-0.018</b>	1
2487600.98	7439358.40	38.209	12841	<b>0.002</b>	1
2487602.37	7439357.38	38.206	<b>7832</b>	<b>0.005</b>	1
2487602.38	7439358.07	38.124	11232	<b>0.087</b>	1

## C.4. HORIZONTAL ADJUSTMENT

A proper assessment of horizontal alignment between two data sources can only be conducted when the data are sufficiently detailed to allow common features to be identified in both. For LiDAR data, or other point elevation data, this means an NPD of at least 1 pt/m<sup>2</sup>, preferably more. In Figure C.5, horizontal offsets can be observed between road centerlines and building footprints, and the LiDAR intensity image. The NPD of the LiDAR data is high enough that, for example, street intersections and building corners can be clearly located and used in georeferencing.

In FigureC.6, a transformation has been applied to the LiDAR-derived image to bring it in alignment with the vector data. However, the transformation was only applied to the image product, not the actual LiDAR points.

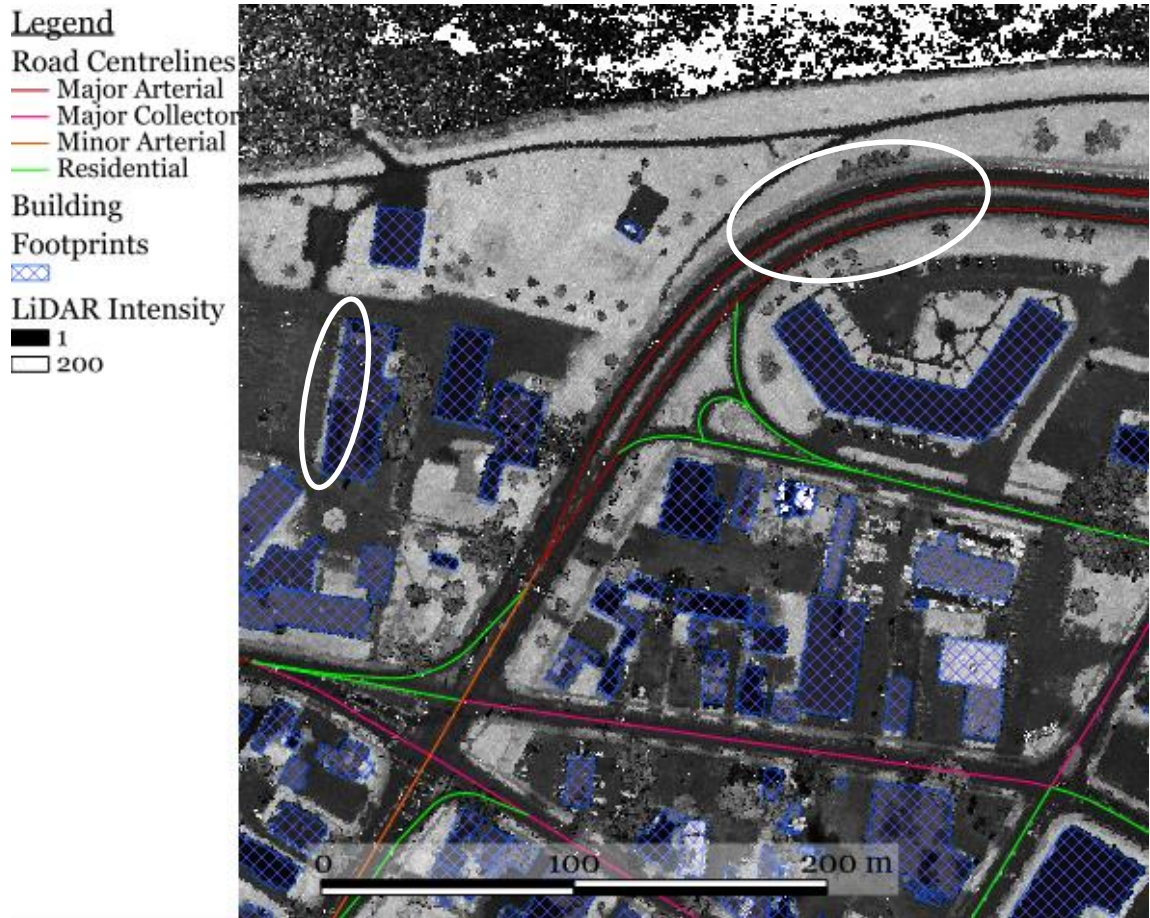


Figure C.5

Observed horizontal offsets between a LiDAR-derived image and vector data sets.

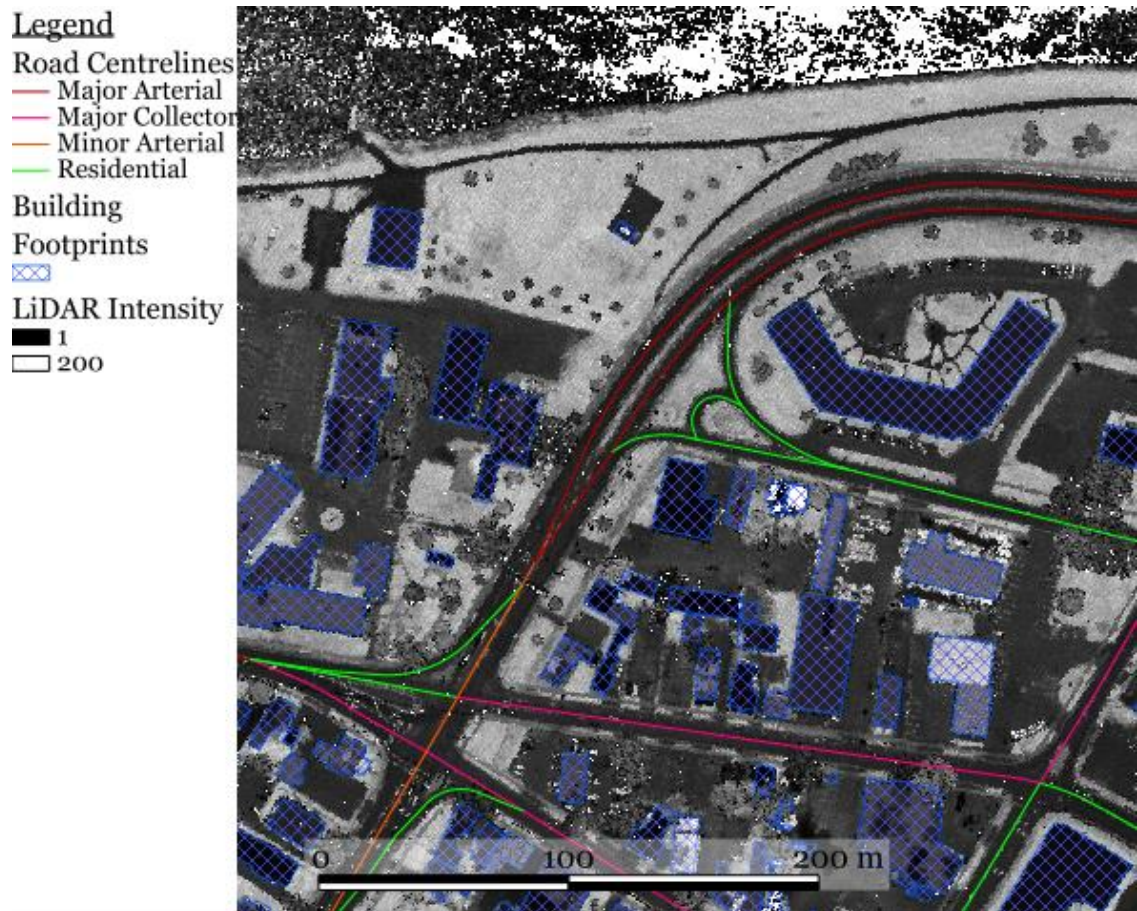


Figure C.6

Improved horizontal alignment can be observed after a transformation is applied to the LiDAR-derived image.

## Curriculum Vitae

Candidate's full name: Krista Marija Amolins

Universities attended (with dates and degrees obtained):

Queen's University, B.Sc.E., 2004

Queen's University, B.A., 2005

University of New Brunswick, M.Sc.E., 2008

Publications:

Amolins, K., Y. Zhang, and P. Dare (2007). "Wavelet based image fusion techniques – An introduction, review and comparison." *ISPRS Journal of Photogrammetry and Remote Sensing*, Vol. 62, No. 4, pp. 249-263.

Amolins, K. (2008). "Incorporating obstructions in GDOP mapping through the use of LiDAR data." *Proceedings of the 21st International Technical Meeting of the Satellite Division of The Institute of Navigation (ION GNSS 2008)*. ION, Savannah, Georgia, U.S.A., 16-19 September, pp. 1631-1640.

Brooks, R., T. Nelson, K. Amolins, G.B. Hall (2015). "Semi-automated building footprint extraction from orthophotos." *Geomatica*, Vol. 69, No. 2, pp. 231-244.

Conference Presentations:

Amolins, K., Y. Zhang, and P. Dare (2008). "Classification of LiDAR data using standard deviation of elevation and characteristic point features." *Proceedings of the IEEE International Geoscience and Remote Sensing Symposium 2008 (IGARSS 2008)*. Boston, Massachusetts, U.S.A., 6-11 July, Vol. 2, pp. 871-874.

Amolins, K., D. Coleman, Y. Zhang, and P. Dare (2011). "Mapping solar potential obstructions using LiDAR data." *Proceedings of the ASPRS 2011 Annual Conference*. ASPRS, Milwaukee, Wisconsin, U.S.A., 1-5 May.